2006-01-10

Engineering of Substrate Surface for the synthesis of Ultra-Thin Composite Pd and Pd-Cu Membranes for H2 Separation

Federico Guazzone
Worcester Polytechnic Institute

Engineering of Substrate Surface for the Synthesis of Ultra-Thin Composite Pd and Pd-Cu Membranes for H_2 Separation

by

Federico Guazzone

A PhD thesis

Submitted to the faculty of the

Worcester Polytechnic Institute

In fulfillment of the requirements for the

Degree of Doctor of Philosophy

In Chemical Engineering

by

December 2005

APPROVED:

Dr. Yi Hua Ma, Advisor	Dr. David DiBiasio, Interim Head of Department
Dr. Nikolaos K. Kazantzis, Committee Member	
Dr. Satya Shivkumar, Committee Member	

To my family

Acknowledgements

I would like to express my sincere gratitude to my advisor Prof. Yi Hua Ma for the time he spent explaining to me physical concepts and the time he awarded me to understand them. The assimilation of a concept needs reasoning and a lot of maturation and I am thankful to Prof. Ma in understanding and respecting these maturation times in all of his students. The models, concepts and ideas exposed in this thesis are the fruit of many Saturday after-noon conversations that Prof. Ma and I had during the four years of my PhD work at Worcester Polytechnic Institute. I hope he enjoyed, as much as I did, all those fruitful scientific conversations. I particularly appreciated the freedom Prof. Ma accorded to all of us in our research. I am very grateful to the committee members Prof. Nikolaos Kazantzis and Prof. Satya Shivkumar for their suggestions and valuable comments.

I also would like to thank Dr. Erik Engwall and Dr. Ivan Mardilovich for giving me the valuable technical and experimental knowledge a student needs at the beginning of his PhD to build new set-ups and conceive new experiments for his research. I would like to thank Jack Ferraro and Doug White for the great help they provided in building the experimental set-ups used during my research years. I also would like to thank Engin, Raj, Alpna, Natalie, Mike, Diana and Ceylan for the scientific and philosophical conversations that made this experience worthwhile and most of all, enjoyable.

I particularly would like to thank Dr. Andrew Payzant and Dr. Scott Speakman at the High Temperature Materials Laboratory in Oak Ridge National Laboratories for making my visits to html so fruitful. Larry Walker and Tom Geer are also acknowledged for their expertise in microscopic techniques and sample preparation for electron microscopy. The important physical concepts learnt at the html were determinant for my research.

Sincere appreciation is expressed to the Shell team, especially Dr. Andreas Matzakos, for all meetings rich in science, technique and ideas. The financial and technical support for this project from Shell International Exploration and Production, Inc. and Shell Hydrogen is sincerely acknowledged.

Appreciation is expressed to the entire Chemical Engineering Department and staff for making my research a rewarding experience and Diana Johnson for her great talents in finding the old, but very interesting, publications that I needed.

I believe that leaving my country and coming to this new land to pursue a doctoral degree would have been hardly possible without Majo's and Erik's friendship. I express my sincere gratitude to Majo, Diana, Luis and Prof. Ma to support me and help me during the interesting time it took to write the thesis.

I dedicate this work to my family, which was always there, in the very good times as well as in the difficult times.

Abstract

This work describes a new technique to prepare ultra-thin composite Pd–Porous Metal (PM) membranes for H_2 separation. This technique consists of the gradual smoothing of the PM support's surface with several layers of pre-activated alumina particles of different sizes. The deposition of coarse, fine and ultra-fine alumina particles resulted in the narrowing of the PM support's surface pore size distribution. The surface smoothness achieved after the grading of the PM support's surface allowed for the preparation of gas tight Pd layers as thin as 5.6μm. The Pd layers were very uniform due to the presence of the grade layer and strongly attached to the support.

Composite Pd membranes prepared on graded supports showed H_2 permeance as high as 50 $m^3/(m^2\ h\ bar^{0.5})$ at 500ºC and ideal selectivities (H_2/He) as high as 27000. Moreover, the H_2 permeance and ideal selectivity were stable over 1100 hr at 500ºC in H_2 atmosphere. Composite Pd-Cu membranes showed H_2 permeance as high as 30 $m^3/(m^2\ h\ bar^{0.5})$ at 450ºC and ideal selectivities (H_2/He) as high as 900. The H_2 permeance and ideal selectivity of Pd-Cu membranes were stable over 500 hr at 450ºC in H_2 atmosphere. The long-term H_2 permeance and ideal selectivity stability of all composite Pd and Pd-Cu membranes represents a breakthrough in composite Pd membrane synthesis.

Executive summary

The analysis carried along this dissertation provides a thorough understanding of a new technology available for the preparation of composite Pd and Pd alloy membranes on Porous Metal (PM) supports. This new technique consists of the gradual smoothing of the PM support's surface with several layers of pre-activated alumina particles of different sizes. The deposition of coarse, fine and ultra-fine alumina particles resulted in the narrowing of the PM support's surface pore size distribution. The surface smoothness achieved after the grading of the PM support's surface allowed for the preparation of gas tight Pd layers as thin as 5.6μm. The Pd layers were very uniform due to the presence of the grade layer and strongly attached to the support. SEM investigations of the Pd-engineered supports interface revealed that the grade layer was only located at the pores mouth. Composite Pd membranes prepared on graded supports showed H_2 permeance as high as 50 $m^3/(m^2\ h\ bar^{0.5})$ at 500ºC and ideal selectivities (H_2/He) as high as 27000. Moreover, the H_2 permeance and ideal selectivity were stable over 1100 hr at 500ºC in H_2 atmosphere. Composite Pd-Cu membranes showed H_2 permeance as high as 30 $m^3/(m^2\ h\ bar^{0.5})$ at 450ºC and ideal selectivities (H_2/He) as high as 900. The H_2 permeance and ideal selectivity of Pd-Cu membranes were stable over 500 hr at 450ºC in H_2 atmosphere. The long-term H_2 permeance and ideal selectivity stability of all composite Pd and Pd-Cu membranes represents a breakthrough in composite Pd membrane synthesis.

The alloying of Pd-Cu bi-layers and the ordering transformation taking place in PdCu alloys were studied by means of High temperature X-Ray Diffraction (HTXRD) analysis. Experimental results showed that alloying of Pd-Cu bi-layers occurred by the diffusion of Cu into Pd. Also, it was found that the ordering fcc to bcc transformation taking place in PdCu alloys did not rely on the diffusion of metallic elements to occur i.e. the ordering transformation was a diffusionless transformation.

This study also focused on the elucidation of the intermetallic diffusion phenomenon encountered in composite Pd-Porous Stainless Steel (PSS) membranes. By measuring the kinetics at which the H_2 flux declined at every temperature, two mechanisms were identified: (1) the first one occurring at low temperatures (<500ºC) and attributed to the diffusion of Fe through the grain boundaries of Pd and, (2) the second one occurring at high temperatures (>500ºC) attributed to the diffusion of Fe through the lattice of Pd.

The thermal stresses arising from the mismatch in the coefficient of thermal expansion between the Pd film and the support were determined by means of x-ray diffraction. The results indicated that the release of stresses began to occur at temperatures close to 400ºC. Also, the release of stresses took place with a visible sintering of Pd clusters within the thin Pd film. The stresses due to the absorption of H_2 were also studied and modeled. It was estimated that the maximum compressive stress under which these composite Pd membranes were during H_2 characterization was equal to 260 MPa.

Finally, the mechanism leading to selectivity decline was studied. Although composite Pd membranes showed high selectivities (H_2/He) values (>10000 at temp. <400ºC), their selectivity slowly declined at 450 and 500ºC. The energy the system needed to lead to the

growth of leaks was equal to 237 $kJmol^{-1}$, which closely matched the activation energy of sintering.

Table of contents

List of figures

List of tables

1 Introduction

The fossil energy reserves, mostly oil and methane, that we have been burning for years are expected to reach a production peak in the middle of the 21st century (Bartlett, 2000; Campbell and Laherrere, 1998; Duncan and Youngquist, 1999; Edwards, 1997; IEA, 1997). When the oil and methane production peaks, it will initially perturb prices, changing the world economy in a drastic manner. Coal reserves are still important worldwide. For instance, the United States of America's coal reserves are thought to last for 250 years, although we all know, burning coal will certainly lead, even with the cleanest coal technologies, to large amounts of CO_2 released to the atmosphere.

Soon, a new source of energy will have to be found. There exists the alternative to synthetically manufacture fuels via coal gasification followed by Fischer-Trops synthesis to produce highly branched hydrocarbons. Although gasification may be coupled with very attractive carbon sequestration technologies, the overall process is not secure enough. Carbon sequestration consists of trapping the CO_2 by pumping it in liquid form into deep oceans or by pressurizing old oil reservoirs (tertiary oil recover) with it. Yet, questions on the fate of the trapped CO_2 after years still remain. To guarantee the safe continuity of our civilization and development, it is imperative to decrease the fast rate of burning fossil fuels and coal, in order to limit the amount of CO_2 released into the atmosphere. Therefore, both for urgent environmental safety and acknowledging the economic

impact of a diminishing reserve of fossil fuels a new and clean source of energy needs to be found.

One of the most attractive alternatives for energy production is the oxidation of H_2 with air. This chemical reaction releases large amounts of energy with only H_2O as by-product. Therefore H_2 would be one of the cleanest sources of energy. In fact, H_2 is an energy carrier and not an energy source. Indeed, H_2 is not naturally available as oil but has to be produced by splitting the H-C bonds in hydrocarbons or the H-O bonds in water or alcohols, which requires large amounts of energy.

H_2 is nowadays produced at low cost mainly from the steam reforming of methane. H_2 is essentially used (two thirds of the world production) for the production of ammonia, which is the main chemical for the synthesis of fertilizers. Secondly, H_2 is used in the petrochemical industry for the refining of sour crude oils and in the semiconductor industry during sputtering processes. Finally, a small amount is used as chemical for the hydrogenation of edible oils and a very small amount as fuel in the rocket industry. The first use of H_2 is particularly important, since fertilizers are a crucial component of today's large scale agricultural industry, and the absence of it could result in a widespread hunger. Hence, the sustainability of the 7 billion humans on Earth is indirectly related to the production of H_2, which is still ensured by the presence of CH_4.

If a shortage of fossil fuels exists, humankind may need to choose nuclear energy to solve the global energy and food problems. Indeed, nuclear energy can be used to produce electricity, which can be used for the production of H_2. H_2 can be used for the production of fertilizers and as energy carrier in transportation vehicles by means of the fuel cells. Nuclear energy is very safe and clean although waste management poses seri-

ous problems. Moreover, the sad accident occurred in Chernobyl and all the terrible consequences that people are still witnessing in the disaster area are still in our minds. Humankind is indeed reluctant to use nuclear energy for all its power needs. Hoping that one day we will be able to capture solar, wind and other unlimited energy sources with economically viable technologies to break water molecules by electrolysis and produce H_2 for food and energy needs, the safe (compared to nuclear) and short-term solution for H_2 production is the improvement of the steam reforming of hydrocarbons process to make it more economical and environmental friendly. H_2 production from steam reforming of hydrocarbons coupled with membrane technology is indeed the preliminary step towards a carbon free energy economy.

A more efficient process to convert fossil fuels into H_2 is by using a Pd based membrane reactor, where the steam reforming reaction and the separation process (with a Pd based composite membrane) are carried out in the same vessel. Di-atomic hydrogen, H_2, has the unique ability to dissociate on the catalytic surface of Pd to form H atoms that can readily diffuse through the Pd bulk. Since no other gas molecule can pass through the Pd or Pd-alloy films, an infinite selectivity for H_2 separation is possible. Therefore, in theory, composite Pd and Pd-alloy membranes are infinitely selective to H_2. Also, Pd membranes are of preference to extract the H_2 from the reactant mixture due to their high mechanical and thermal stability. Combining the reaction and the separation in the same unit operation allows the use of lower temperature (500ºC), which represents a saving in energy, higher yields due to the removing of H_2 during reaction, pure H_2 and high pressure CO_2 that would be suitable for sequestration.

The prospect of higher yields H_2 production has sparked academic and industrial interests. The production of H_2 from hydrocarbons steam reforming in Pd based membrane reactors has been proven to work in laboratory scale reactors. Research on hydrocarbon steam reforming in Pd based membrane reactors has been carried out in Taiwan (Lin et al., 1998; Lin and Rei, 2000, 2001), Japan (Itoh et al., 2002; Itoh et al., 2003; Kikuchi, 2000; Kikuchi et al., 2000; Shirasaki et al., 1997) and United States of America (Matzakos et al., 2003; Wellington et al., 2003). Mathematical models on Pd-based membrane reactors have also been developed (Marigliano et al., 2003). Steam reforming and/or partial oxidation of carbonaceous compounds were carried out in membrane reactors using essentially Pd (Galuszka et al., 1998; Kikuchi, 2000; Lin and Rei, 2001), Pd-Ag alloys (Wieland et al., 2002), and PdCu alloys (Han et al., 2002; Wieland et al., 2002) composite membranes or foils for H_2 separation.

Pd alloys are preferred over pure Pd since Pd undergoes a phase transformation (α to β) when exposed to H_2 at temperatures lower than 300°C and high H_2 pressures. This phenomenon, called 'H_2 embrittlement', is due to the lattice parameter of the β phase being larger than that of the α phase. Indeed, stresses are induced during the nucleation of the β phase leading to distortions in the dense composite membrane or foil. Therefore, multiple H_2 absorption/desorption cycles at room temperature induce series of α to β and β to α transformations leading to the deformation or cracking of the Pd membrane. Alloying Pd with other metals such as Au, Ag, Cu, Fe, Ce and Y decreases the critical temperature above which no α to β transformation occurs. Thus, Pd alloys can undergo H_2 absorption/desorption cycles at lower temperatures than 300°C without failure due to H_2 embrittlement. Moreover, some alloys have even greater H_2 permeability than pure

Pd. Examples of high H_2 permeability alloys are: $Pd_{77}Ag_{23}$[1], $Pd_{60}Cu_{40}$, $Pd_{90}Y_{10}$, $Pd_{80}Au_{20}$ and others. Ternary alloys also showed, in special cases, greater H_2 permeability than pure Pd. Examples are: $Pd_{93.5}Ru_{0.5}In_{6.0}$ and $Pd_{80}Ag_{19}Rh_1$ having respectively a H_2 permeability of 2.8 and 2.6 the H_2 permeability of pure Pd (Gryaznov, 2000). Furthermore, some alloys such as Pd-Cu and Pd-Au showed resistance in H_2S containing feed streams, which make them very attractive for H_2 separation from coal gases.

Laboratory scale reformers include thin Pd and Pd alloy foils (cold rolled) or thin composite Pd or Pd alloy membranes (Pd deposited on a porous substrate) as H_2 separators. It is not yet clear which technology will prevail in industrial Pd based membranes steam reformers, although, due to their easy manufacturing on tubular supports, composite Pd membranes may be chosen in the future. Indeed, tubular geometry, compared to planar geometry, is generally easier to adopt for industrial applications.

High H_2 flux membranes can be achieved by depositing a thin film (<10μm) of Pd or Pd alloy on top of a porous substrate to give the necessary mechanical strength to the thin metallic layer. Vycor glass, ceramics and Porous Metals (PM) can be used as porous substrates. PM substrates have great chances to be implemented in industrial application due to their easy handling and mechanical properties. However, the main drawback of PM supports is that at high temperatures the metallic elements of the support (Fe, Ni and Cr) diffuse into the Pd layer, thereby decreasing the H_2 permeability of the composite membrane. This phenomenon, called "intermetallic diffusion" is not encountered in ceramics. Yet, ceramics supports are too brittle and difficult to connect to metal parts for industrial applications. Several methods can be used for the deposition of Pd on porous substrates,

[1] All subscripts in weight percent.

however, four methods are widely used: Chemical Vapor Deposition (CVD), sputtering, electrodeposition and electroless deposition. Electroless deposition has the advantage over the others of being inexpensive, easy to put in practice and the Pd deposits can be very uniform on complex shapes. Depositing Pd alloys with electroless or electrodeposition is a challenge. If a Pd alloy membrane is desired, the "coating and diffusion" technique is applied. This technique consists of the sequential electroless deposition of the two metals in two distinctive layers followed by heat-treatment at high temperatures. The resulting membranes show a composition gradient across the thickness unless very high temperatures are used (>650ºC). Sputtering techniques are more suited for composite Pd alloy membranes preparation.

Generally, composite Pd membranes are prepared at temperature and pressure conditions different from the ones they will be used in a membrane reactor. Moreover, fresh thin films are characterized by remaining "intrinsic" stresses and a large surface energy due to the fine-grain structure (build up of energy) that are automatically released at high temperatures. Therefore, at the reaction temperature of 500ºC, composite Pd membranes undergo a series of structural transformations that lead to several problems such as H_2 permeance loss and H_2 selectivity decrease over time.

The main objective of this research was to understand the fundamental principles involved in the synthesis, H_2 transport mechanism, mechanical and chemical stability of very-thin (<10μm) composite Pd and Pd alloy membranes prepared by the electroless deposition method on PM supports. The effects of surface roughness of the porous support on the thin Pd film thickness and the thin Pd film morphology were elucidated. The effects of gas transport properties of the porous support, H_2 diffusion through defects and

the catalytic activity of the Pd surface on the permeation mechanism of H_2 was also studied. The intermetallic diffusion phenomenon was investigated in a wide range of temperatures to understand the diffusion mechanism of Fe, Cr and Ni elements of the metal support into the Pd layer. In addition, the 'extrinsic" stresses on the Pd film due to the film/substrate mechanical interaction at high temperatures were studied. Finally, large efforts were invested in the understanding of the microstructure and microstructure changes at high temperatures of the thin Pd film constitutive of the composite Pd membrane. Specially, a detailed study on the kinetics of leak formation was undertaken.

In summary, the specific objectives were to:

(1) Understand the H_2 diffusion mechanism through composite nanocrystalline Pd membranes.

(2) Understand the effect of Pd surface catalytic activity, defects and porous support resistance on the mechanism of H_2 permeation.

(3) Understand the diffusion mechanism of the metal elements in the porous support (Fe, Cr and Ni) into the Pd layer in order to limit or inhibit the diffusion of these elements into the Pd layer.

(4) Understand how the surface roughness and morphology of the porous support affect the structure and the thickness of the dense Pd layer.

(5) Understand how the surface of porous metal supports can be modified to facilitate the formation of thin membranes.

(6) Understand how "extrinsic" and "intrinsic" stresses affect the long-term mechanical stability of the Pd thin film structure.

(7) Understand the mechanism of leak formation and leak growth in composite Pd membranes by studying the kinetics of leak growth over time at high temperatures in thin composite Pd membranes.

(8) Develop ways to avoid the formation of leaks and/or limit their growth.

2 Literature review

2.1 Pd and Pd-alloys systems

Several materials have the ability to permeate only H_2 although Pd has been the most studied system since the end of the 19th century (Graham, 1869a). The thermodynamics of the Pd-H system were studied in detail at cryogenic temperatures (Mitacek and Aston, 1963), at high pressures and high temperatures (Levine and Weale, 1960) as well as moderate temperatures and pressures (Frieske and Wicke, 1973; Gillespie and Galstaun, 1936; Gillespie and Hall, 1926; Wicke and Nernst, 1964). Figure 2-1 shows the pressure concentration isotherms (*p-n* isotherms) for the Pd-H system (Shu et al., 1991). The data plotted in Figure 2-1 were reported by Frieske and Wicke (1973) and Wicke and Nersnt (1964). In Figure 2-1, the H_2 solubility, n (=H/Pd), which is the ratio of H atoms absorbed per Pd atom is given as a function of the H_2 partial pressure, P_{H2}. The Pd-H system exhibits a miscibility gap region where two phases, α and β, both having a face centered cubic (fcc) crystalline structure, coexist at temperatures below 300°C. The miscibility gap is characterized by pressure invariance isotherms. For every isotherm, $P^{0.5}{}_{H2}$ initially increases linearly with n (see inset Figure 2-1). At n(H/Pd)=α_{max}, which is the maximum H_2 solubility in the α phase for a particular isotherm, $P^{0.5}{}_{H2}$ reaches a plateau (invariance in pressure) and the β phase, with a minimum H_2 concentration n(H/Pd)=β_{min}, nucleates.

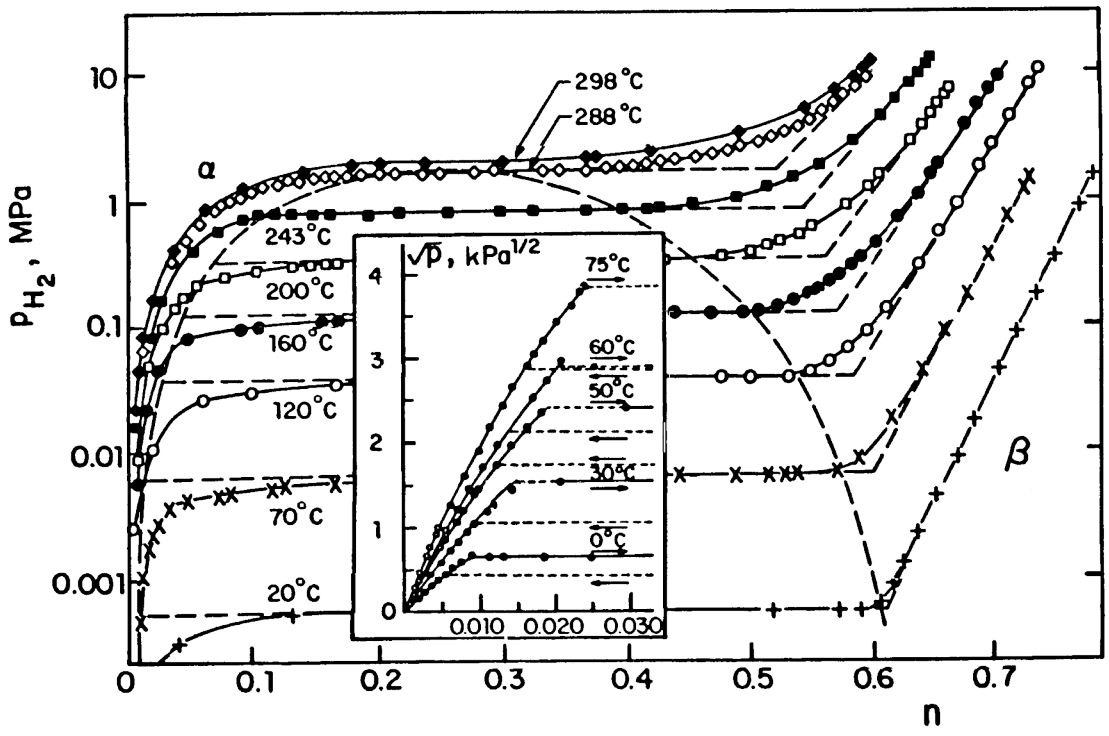

Figure 2-1 Pd-H phase diagram (Shu et al., 1991). Data from Frieske and Wicke (1973). Inset data[1] from Wicke and Nersnt (1964)

[1] In the original review by Sue et al. (1991) the y-axis values were 10, 20, 30 etc. It appeared that these numbers were mistaken and correct values are: 1, 2, 3 etc. The correction was made based on the original article by Wicke and Nernst (1964).

During the α to β transformation, the H_2 content of the α phase (α_{max}) and the H_2 content of the β phase (β_{min}) do not change, only the relative proportions of the α and the β phase does. The β phase, PdH_2, has a lattice parameter somewhat larger than that of the α phase, therefore, when the β phase nucleates within the α phase matrix, distortions appear in the metal. The modifications in shape and microstructure that occur in a Pd foil after several α→β→α transformations are denoted as "H_2 embrittlement" (Lewis, 1967). The H_2 separation properties of Pd foils that underwent several α→β→α transformations are poor due to the large numbers of microcracks. Therefore, in all H_2 purification systems based on Pd membrane technology, care is taken not to exceed the maximum H_2 concentration n(H/Pd)=α_{max} of the α phase above which the β phase nucleates. The maximum H_2 concentration n(H/Pd)=α_{max} is reached at a given H_2 pressure P_{max}, which depends on temperature according to Equation (2-1) (Gillespie and Galstaun, 1936).

$$\log(P_{max}) = 4.6018 - \frac{1877.82}{T} \qquad (2\text{-}1)$$

where P_{max} is in atm and T in K. At a temperature equal to 295.3ºC and a pressure equal to 19.87 atm a critical solution is reached (Gillespie and Galstaun, 1936) so that at temperatures above 300ºC, the α→β transformation no longer occurs. Alloying Pd with other metals decreases the temperature of the critical solution making Pd alloys less prone to H_2 embrittlement.

The Pd-Ag system is probably the most studied Pd alloy since it was found that Pd-Ag alloys absorb more H_2 than does pure Pd (Graham, 1869b). Pd-Ag alloys with more than 20 wt%[1] Ag did not show signs of distortion after thirty cycles of heating and cooling in

[1] wt% = weight percentage

H_2 atmosphere at atmospheric pressure (Hunter, 1960). The great mechanical stability of this alloy to withstand temperature cycling, when pure Pd would have distorted, was understood when *p-n(H/Pd)* absorptions isotherms at 50°C were taken for several Pd-Ag alloys and showed no pressure invariance regions (or miscibility gap) for Pd-Ag alloys having more than 20 wt% Ag (Brodowsky and Poeschel, 1965). Thus, by increasing the amount of silver, the α-β miscibility gap was depressed to lower temperatures. Even small percentages of Ag, 5 to 10 at%[1], led to the decrease of the critical temperature below which the α→β transformation occurs (Fazle Kibria and Sakamoto, 2000). In addition, the Pd-Ag alloy with 27 wt% Ag had higher H_2 permeability than pure Pd (Hunter, 1960).

The permeability coefficient, *Q*, is the product of the H_2 diffusion coefficient, *D*, and the H_2 solubility, *S*. For almost all Pd systems, *D* decreases in the presence of alloying elements and it is particularly true for Ag. However, *S* is largely increases when the Ag content is about 30 wt% Ag (Holleck, 1970; Sieverts et al., 1915). Therefore, an optimal Ag composition for the highest H_2 permeability exists between 20 and 40 wt% Ag. The highest permeability for the Pd-Ag alloys was measured for a composition of 27 wt% Ag (McKinley, 1969) and also for a composition of 23 wt% Ag (Holleck, 1970). The H_2 permeability of the $Pd_{77}Ag_{23}$ alloy is believed to reach 1.7 times the H_2 permeability of pure Pd.

Alloying Pd with Cu also decreases the critical temperature of the miscibility gap, although little work has been done on the Pd-Cu system. This is due to the fact that at the optimum Cu concentration, 40 wt% Cu, the permeability of the alloy is only 1.1 times the

[1] at% = atomic percentage

permeability of pure Pd (McKinley, 1967). The $Pd_{60}Cu_{40}$ alloy does not undergo any α to β transformation even at room temperature since its *p-n(H/Pd)* isotherm at 25°C does not show any invariance in pressure (Karpova and Tverdovskii, 1959). Therefore, Pd-Cu is one of the most robust systems available for H_2 purification. Yet, at temperatures higher than 400°C, the $Pd_{60}Cu_{40}$ alloy loses its ordered bcc structure (β phase[1]), which has a high H_2 permeability, and transforms into a disordered fcc phase (α phase[2]), which has a low permeability (Subramanian and Laughlin, 1991). The H_2 flux of the $Pd_{60}Cu_{40}$ alloy was experimentally observed to decline during the α to β phase transformation that occurred at 400ºC (McKinley, 1967). Since Pd-Cu alloys lose their high H_2 permeance structure above temperatures ranging from 400 to 600°C depending on the copper content, Pd-Cu membranes are suitable for low temperatures H_2 purification applications. Indeed, the ordered β CuPd phase has the highest H_2 permeability at low temperatures among all metal-hydrides systems. Recently, the possibility of having H_2 permeance stability of Pd-Cu alloys in atmospheres containing H_2S triggered considerable amounts of studies on the Pd-Cu alloys membrane preparation and characterization (Hoang et al., 2004; Nam and Lee, 2001; Roa et al., 2003), Pd-Cu alloy oxidation (Roa and Way, 2005) and Pd-Cu alloys permeability calculations and estimations (Kamakoti et al., 2005; Kamakoti and Sholl, 2003). More interestingly the α phase, with low H_2 permeability, appeared to be more stable than the β phase in the presence of H_2/H_2S mixtures (Morreale et al., 2004). Therefore, a compromise needs to be found between H_2S poisoning stability and H_2 permeance.

[1] Not to confuse with high H content Pd hydrides, also named β phase.
[2] Not to confuse with low H content Pd hydrides, also named α phase.

Many other metal alloys have been studied beside Pd-Ag and Pd-Cu alloys. The Pd-Au system showed higher H_2 permeabilities than pure Pd although the experimental results of different research groups differed somehow (Gryaznov, 2000; McKinley, 1967). Pd/Ce and Pd/Y alloys showed very high H_2 permeabilities and very good mechanical properties (Farr and Harris, 1973; Fort et al., 1975). The H_2 fluxes of the Pd-Au, Pd-Ce and Pd-Y systems at 350°C and 20.4 atm for 25 μm thick membranes were reviewed and are shown in Figure 2-2 (Knapton, 1977). It is important to note in this figure the large increase in H_2 flux, up to 3.7 times that of pure Pd, with small amounts of Y.

Figure 2-3 shows the Pd alloy permeance at 500ºC over the pure Pd permeance with Ag, Au, Pt and Rh alloying elements as a function of the amount of the alloying element (Gryaznov, 2000). Comparing Figure 2-2 with Figure 2-3, a large difference in H_2 permeability for the Pd-Au system can be observed between McKinley's work and Gryaznov's work. Indeed, everything being the same, Gryaznov found that the Pd-Au system, with Au compositions ranging from 5 to 20 wt%, showed H_2 permeances equal to twice the H_2 permeance of pure Pd. On the other hand, according to McKinley, the Pd-Au system, with Au composition ranging from 5 to 20 wt%, hardly reached the performances of pure Pd.

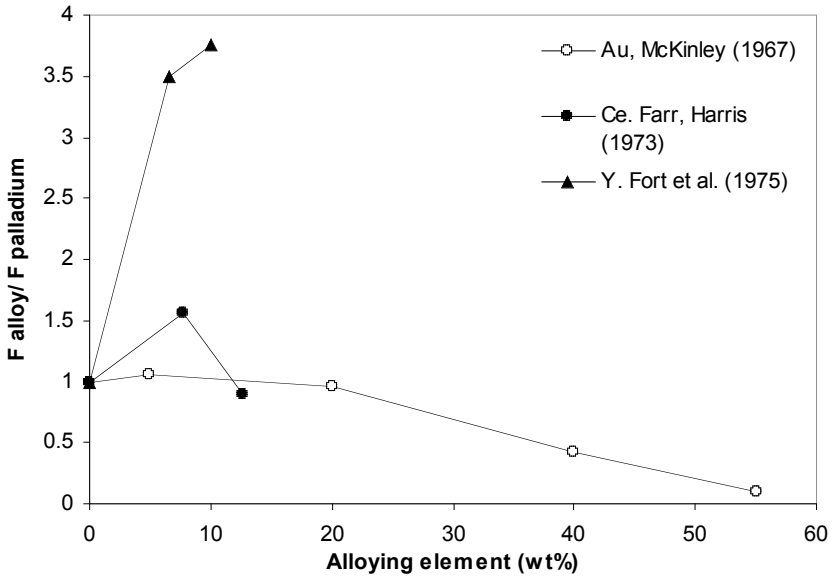

Figure 2-2 H_2 flux ratio of Pd-Au, Pd-Ce and Pd-Y alloy

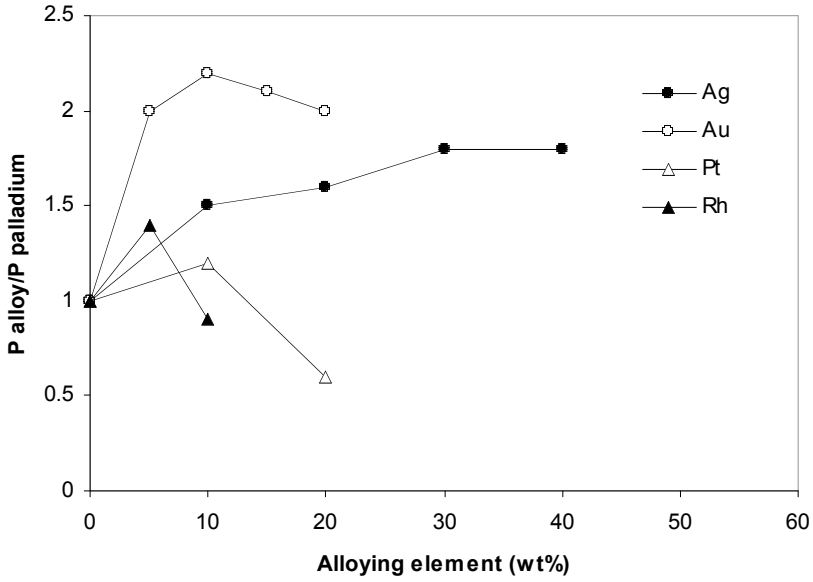

Figure 2-3 H_2 permeance ratio of Pd-Ag, Pd-Au, Pd-Pt and Pd-Rh measured by Gryaznov (2000)

Ternary alloys were also studied (Gryaznov, 2000). The $Pd_{93.5}Ru_{0.5}In_{6.0}$ showed a ratio of H_2 permeability over pure Pd of 2.8 and the $Pd_{80}Ag_{19}Rh_1$ system showed a ratio of 2.6. Since binary and ternary alloys discussed in the present section were mainly arc-melted under Ar, cooled to room temperature and rolled into thin foils, their composition was uniform and data obtained were in general very reliable.

2.2 Methods of Pd deposition onto porous substrates

The H_2 permeability of all Pd alloys described in Section 2.1 was measured with foils. Interesting works showed that wrapping a porous support with a Pd or Pd-alloy foil was technically possible, and led to very high conversion factors when used in Catalytic Membrane Reactors (CMR) (Tosti, 2003; Tosti et al., 2002; Tosti et al., 2000). However, thinner composite Pd and Pd alloy membranes can be prepared by deposition of a thinner layer than that of foils, which is usually around 20μm, on a porous substrate. Four methods are commonly used for composite Pd and Pd alloy synthesis on porous substrates. These are:

- Chemical Vapor Deposition (CVD) is the reduction or decomposition of a volatile compound of the coating material upon a heated surface. CVD allows depositing coatings of most refractory metals while other techniques are unsuccessful. CVD leads to pure and thin layers on small substrates. However the procedures are tedious and nearly impossible for industrial purposes. Metal-Organic Chemical Vapor Deposition (MOCVD) differs from CVD in that only high purity organo-metallic compounds are used. CVD was used by many researchers (Jun and Lee, 2000).

- Sputter techniques: magnetron sputtering deposition is achieved by applying a high voltage across a low-pressure gas (usually argon at about 5 mtorr) to create a "plasma," which consists of electrons and gas ions in a high-energy state. During sputtering, energized plasma ions strike a "target," composed of the desired coating material (pure Pd or a Pd alloy), and cause atoms from that target to be ejected with enough energy to travel to, and bond with, the porous substrate. A powerful magnet is used to confine the "glow discharge" plasma to the region closest to the target plate. A similar technique, Electron Beam (e-beam) evaporation can be used for Pd and Pd-alloy deposition. In e-beam evaporation the porous substrate is placed in a high vacuum chamber at a desired temperature with a crucible containing the material to be deposited. An electron beam is aimed at the material in the crucible causing it to evaporate and condense on all exposed surfaces in the vacuum chamber and substrate. Several crucibles, with different compounds (or metals), are available in the same chamber and switching crucibles leads to the evaporation and condensation of different compounds. Ion-Beam (i-beam) evaporation is essentially the same as e-beam but using argon ions instead of electrons. Magnetron sputtering, e-beam evaporation and ion beam evaporation, which are called physical vapor deposition (PVD), are generally applied when depositing alloys. The main drawback of sputtering techniques is that sputtering chambers have a confined space and coating of large supports for large scale high purity H_2 production is almost impossible. CVD and sputtering techniques offers the very attractive advantage that they allow for the support to be heated during deposi-

tion, which in turn allows for the possibility of controlling the film microstructure (Dirks, 1977; Thornton, 1974; Zhao and Xiong, 1999). The microstructure of the Pd thin film is a determinant parameter in long-term composite membrane stability, since the microstructure changes as the composite Pd membrane is exposed to reactions conditions (Roa and Way, 2005; She, 2000).

- Electrodeposition of metals involves the movement of positive metallic ions towards the cathode to be reduced and finally be incorporated in the metallic growing film. The film thickness depends on the electrolyte used, temperature, pH and mainly on current density and time. Variants of electrodeposition are vacuum electrodeposition, where vacuum is applied at the cathode, and pulsed electrodeposition where the electrical potential is varied over time (pulsed) to improve the uniformity of the deposition. Vacuum electrodeposition led to thinner and more selective films than electrodeposition (Nam and Lee, 2000; Nam et al., 1999).
- Electroless deposition is the reduction of metastable metallic salt complexes by a reducing agent on a target surface. It has been widely used for Pd membrane synthesis. This is due to the low cost, easy procedures and simplicity of the needed equipment. The advantage of the electroless deposition over the electrodeposition is that substrates do not have to be conductive and one can cover the surface of complicated shapes uniformly where electrodeposition tends to cover “hills” with a thicker layer while letting “valleys” poorly covered. The main draw back of electroless (and electrodeposition) deposition is that the deposition of alloys represents a challenge since co-deposition of two metals is

difficult. In general, when a Pd-alloy is desired, the two metals are deposited sequentially and heat-treated at high temperatures to obtain the alloy. Such process was denoted as coating and diffusion technique (Uemiya et al., 1991b; Uemiya et al., 1991c).

2.3 Electroless deposition of Pd and Pd alloys coatings

The following section describes the electroless deposition method due to its relevance to the understanding of the morphology, microstructure and properties of composite Pd membranes prepared in this study.

2.3.1 Activation of the substrate

Prior to electroless deposition, the porous substrates need to be activated. The activation process can be achieved using sequential dipping in $SnCl_2$-HCl (1 g/l, pH: 2) and $PdCl_2$-HCl (1 g/l, pH: 2) solutions. Sn^{2+} reduces Pd^{2+} by the following equation leading to the deposition of active Pd nuclei on the surface of the substrate. The size of the deposited nuclei (5.5 nm) was determined by considering the Binding Energy (BE) shift of the Pd $3d_{5/2}$ peak (Takasu et al., 1978).

$$Sn^{2+} + Pd^{2+} \rightarrow Sn^{4+} + Pd^{0}$$

This activation method has been widely used when electroless plating was applied. Moreover a wide range of substrates, including plastics and metals, can be activated. High resolution XPS scans of the Sn $3d_{5/2}$ and Pd $3d_{5/2}$ peaks were conducted after sensitizing (dip in the $SnCl_2$ solution), activation (dip in the $PdCl_2$ solution), thorough washing with DI water and finally Cu deposition of fly-ash particles (Shukla et al., 2001). Shukla et al. (2001) found that $SnCl_2$ was present on the surface just after sensitizing indicating

the good adhesion of Sn^{2+} ions on the surface of fly-ash particles. After activation, $SnCl_4$, $PdCl_2$ and Pd^0 were found on the surface confirming the reaction step leading to Pd nuclei. The DI water cleaning step led to $Sn(OH)_4$, PdO, $PdCl_2$ and Pd^0 indicating that Sn^{4+} and Cl^- ions remained on the surface even after the washing step. After the Cu deposition step, Sn^{4+} and Cl^- were neither detected on the surface of the Cu deposit nor underneath the coating using EDX analysis on a cross section of a particle. However, element composition less than 1 wt% can not be detected by EDX, therefore, traces of Sn^{4+} and Cl^- could still remain underneath the Cu coating. The absence of Cl^- and Sn^{4+} impurities after Cu plating was attributed to the dissolution of $Sn(OH)_4$ and $PdCl_2$ by the alkaline Cu plating solution.

Paglieri et al. (1999) compared the long term stability of membranes activated with the usual Sn-Pd procedure and the long term stability of membranes activated by a new activation method. The new method consisted of the deposition of $Pd(O_2CCH_3)_2$ on the surface to be plated and burnt off the organic fraction by heat treatment. They noticed that membranes activated with $Pd(O_2CCH_3)_2$ were more stable over time than those activated by Sn-Pd procedure. Therefore, they attributed the lack of long term stability showed by Pd membranes activated with Sn-Pd procedure, to Sn^{4+} impurities trapped between the palladium layer and the support. UV-light was also used to reduce $PdCl_2$ or Pd-acetate on porous substrate and avoid Sn contamination (Wu et al., 2000; Zhang et al., 1997). Pd nuclei obtain by UV-light reduction were as small as 2 nm (Lafferty et al., 1997).

A new trend in the past 10 years consisted of applying an activated layer on the support, which decreases the number of synthesis steps and the amount of raw materials.

Ceramic supports were activated with Pd(II)-modified boehmite sol gel. After calcination and reduction under H_2 at 500°C, Pd nuclei were obtained on the substrates (Li et al., 1996; Zhao et al., 1998). ZrO_2 sols were also doped with Pd nuclei, cast on Porous Stainless Steel (PSS) substrates to form a smooth activated surface for the deposition of Pd (Gao et al., 2005).

2.3.2 The chemistry of Pd deposition

A palladium plating bath includes: a palladium ion source ($PdCl_2$, $Pd(NH_3)_4Cl_2$, $Pd(NH_3)(NO_3)_2$, $Pd(NH_3)_4Br_2$), a complexant (ethylenediamine tetra acetic acid (EDTA), ethylenediamine (EDA), ammonia (NH_3)), a reducing agent (hydrazine (NH_2-NH_2), sodium hypophosphite ($NaH_2PO_2 \cdot H_2O$), Trimethylamine borane), stabilizers and accelerators.

The first hypophosphite based Pd plating bath had EDTA and EDA as the complexing agents to stabilize the solution (Sergienko, 1968). More stable baths were developed using NH_3 as the complexing agent and hypophosphite as the reducing agent (Pearlstein and Weightman, 1969). The plating bath stability was further improved by adding small amounts of thiosulfate ($Na_2S_2O_3 \cdot 5H_2O$) into Pearlstein and Weightman's bath (Zayats et al., 1973). Other hypophosphite based baths were used for corrosion protection in nuclear plants and chemical industries (Mizumoto et al., 1986; Vereshchinskii et al., 1973). The main drawback of hypophosphite based Pd baths is that phosphorous is included in Pd coating, thereby affecting the H_2 permeability of the membrane (Hough et al., 1981; Pearlstein and Weightman, 1969). Moreover, when removing substrates from plating bath, cracking appeared in the palladium layer due to H_2 gas production during plating (Cheng and Yeung, 2001; Pearlstein and Weightman, 1969). In fact, H_2 was produced

and adsorbed by the Pd layer when using hypophosphite. At the plating temperatures of 60-70°C, the β phase nucleated leading to distortions and cracking of the Pd layer.

The use of hydrazine as a reducing agent did not lead to the formation of H_2 but N_2, which avoided the cracking of the freshly deposited Pd film (Rhoda, 1959b; 1959a). Rhoda's plating bath stability was further improved by the addition of thiourea as the stabilizer (Kawagoshi, 1977). Formaldehyde was used to deposit Pd with strong acidic baths (Abys, 1964). Indeed, Pd is not a very good catalyst for formaldehyde oxidation at high pH (Ohno et al., 1985) yet it is at low pH. It was reported that $Pd(NH_3)(NO_3)_2$ led to a better Pd conversion than $Pd(NH_3)_4Cl_2$ and that pH should be between 9 and 11 for better solution stability (Keuler et al., 1977). Also, EDTA to Pd molar ratios between 20:1 and 40:1 and T> 65°C resulted in palladium salt conversion levels greater than 80 percent (Keuler et al., 1977).

Over the years electroless Pd plating baths and deposition conditions reached a common standard with small variations. Plating baths and deposition conditions are listed in Table 2.1.

Table 2.1 Pd plating bath and plating conditions commonly reported in the literature

Pd ion source	$Pd(NH_3)_4Cl_2 \cdot H_2O$, g/l	4–5
	or	
	$Pd(NH_3)(NO_3)_2$, g/l	0.35–15
Complexant, stabilizer	$Na_2EDTA \cdot 2H_2O$ g/l	40-80
Buffer, stabilizer	NH_4OH (28%), ml/l	200-650
Reducing agent	H_2NNH_2 (1 M), ml/l	4–10
pH		9–11.5
Temperature (°C)		50-70

In order to prepare a composite Pd membrane by the electroless deposition method the activated porous support is immersed in a Pd plating bath with the chemical composition

and at the conditions listed in Table 2.1. The reduction of Pd complexes, which depends on the composition of the bath, occurs at the surface of the activated support leading to a Pd deposit.

2.4 Composite Pd and Pd alloy membranes

This section describes the different types of supports onto which Pd is deposited by any of the techniques described in Section 2.2. In addition, a review on different composite Pd and Pd alloy membranes and their properties is given.

2.4.1 Supports and diffusion barriers used for metal composite membranes

The deposition of Pd, or any other H_2 permeable metal, onto a porous substrate forms a Pd or Pd alloy composite membrane. Vycor glass, porous metals (stainless steel, hastelloy, inconel) and ceramics (Al_2O_3, silica, TiO_2, zeolites) can all be used as porous substrates. Three important support properties have significant influences on the general performance of the Pd or Pd alloy membrane. These are: the nature (or chemical composition) of the support, porosity and pore size distribution at the surface.

The chemical composition of the support mainly affects the long term stability of the membrane. The use of metallic supports like Porous Stainless Steel (PSS) and Porous Hastelloy (PH) leads to intermetallic diffusion at high temperatures (usually above 300°C) unless a diffusion barrier is formed between the metallic support and the thin Pd film. Intermetallic diffusion is the migration of Fe, Cr, Ni and other elements from the support into the Pd layer, thereby affecting the H_2 permeation properties of the membrane. This problem is not encountered when using ceramics or Vycor glass.

Mostly oxides (including thin ceramic layers) have been used as intermetallic diffusion barriers. The passive film that naturally forms on Fe-Cr alloys is usually less than 50nm thick (Collins, 1998) yet does not protect against intermetallic diffusion at high temperatures and the treatment of the support is necessary before Pd deposition. Heat treatment of stainless steel at temperatures above 400°C led to an oxide layer that increases Pd membrane stability to over 6000 hr at 350°C (Ma et al., 1998). When the oxidation of 316L PSS supports was performed at temperatures lower than 400ºC H_2 permeance was found to decline (Guazzone et al., 2004). Oxides formed on 316L SS at temperatures equal or higher than 800ºC were found to be thick, 5-7μm, and consisting of a Cr rich oxide on top of a Fe rich oxide (Ma et al., 2004).

γ-Al_2O_3 was also widely used as intermetallic diffusion barrier (Nam and Lee, 2001; Yepes et al.). Nam and Lee (2001) covered a PSS disk first with nickel powder to obtain a smoother surface. After sintering under high vacuum at 800°C for 5 hr, they applied a thin γ-Al_2O_3 layer by the sol gel method. Two layers of Pd and two layers of Cu were sequentially deposited. The structure was then annealed to obtain an homogeneous Pd-Cu membrane. Long term H_2 flux stability was tested at 500°C for 960 hr and no H_2 flux decline was observed. Jun et al (2000) applied the same nickel powder on PSS disks but did not use γ-Al_2O_3. The Pd-Ni alloy membrane deposited on this Ni(powder)/PSS smooth support did exhibit more than 80% H_2 flux decline over a long period at 500°C (Jun and Lee, 2000). More recently, Yepes et al. (2005) obtained Pd-Ag membranes prepared by the coating and diffusion technique on PSS supports modified with γ-Al_2O_3. They proved with EDX techniques the absence of intermetallic diffusion although their H_2 permeance

was fairly low and equaled to 19 $m^3/(m^2\ h\ bar^{0.5})$ at 500ºC. The low H_2 permeability was in fact due to a relatively thick Pd-Ag layer of 16μm.

TiN layers with thicknesses ranging from 0.1 to 5μm, formed by sputter deposition inhibited the diffusion of Fe into the Pd-Ag dense film up to temperatures close to 700ºC (Shu et al., 1996). Recently, the TiN layer was also found to slightly improve the separation properties of Pd-Tin-PSS membranes (Nam and Lee, 2005). Nam and Lee (2005) prepared a Pd-Tin-PSS membranes with a submicron thickness having a H_2 permeance of around 52 $m^3/(m^2\ h\ bar^{0.5})$ and a selectivity of 4600 (H_2/N_2) at 450ºC. Both H_2 permeance and ideal selectivity were stable for over 40 days at 450ºC in H_2 atmosphere. The H_2 permeance was relatively high compared to other composite Pd membranes in the literature although very low for a composite Pd membrane having a submicron thickness. The low H_2 permeance was due to the large support resistance after deposition of the TiN layer. The rate at which intermetallic diffusion occurs in composite Pd membranes prepared on Porous Metallic (PM) supports was shown to be faster in H_2 atmosphere than in He atmosphere (Edlund and McCarthy, 1995).

The second important parameter, which is crucial for H_2 flux, is the support porosity or void fraction. Gas flow through porous media can be modeled using the Ergun equation, Equation (2-2)

$$\frac{\Delta P}{L} = \frac{150\mu(1-\varepsilon)u_0}{\varepsilon^3 d_p^2} + \frac{1.75(1-\varepsilon)\rho u_0^2}{\varepsilon^3 d_p} \qquad (2\text{-}2)$$

With ΔP the pressure drop, L the length of the porous media, μ the gas viscosity, ε the porosity or void fraction, u_0 the gas superficial velocity, d_p the particles diameter and ρ the gas density. For porous tubes, Equation (2-2) is valid if the thickness of the wall is

negligible when compared to the radius of the tube. For a given pressure drop, ΔP, the gas flow through the porous support can be increased if ε tends to 1 i.e. with high porosities. Therefore, high porosity supports are suitable for high H_2 flux. The limit for porosity is set by mechanical properties of the support. Porous supports with low porosity lead to composite Pd membranes with low H_2 permeance due to large mass transfer resistance within the supports. Vycor glass and ceramic supports have low inert gas permeances. The presence of mass transfer within the porous support has the effect of lowering the activation energy for H_2 permeation (Wang et al., 2004)

The maximum pore size on the surface of the support is the third crucial parameter (Ma et al., 2001). Ma et al. (2001) deposited a thin Pd layer on three PSS samples characterized by different grades: 0.1, 0.2 and 0.5 μm. Mercury intrusion analysis showed that: the lowest grade included the smallest maximum pore size on the surface and the highest grade included the largest maximum pore size on the surface. The Pd thickness needed to obtain a He tight membrane was shown to be approximately three times the diameter of the largest pore for the three membranes.

2.4.2 Asymmetric supports

In order to combine small pores on the surface and high porosity asymmetric supports can be used. An asymmetric support is a high porosity support covered by a second layer characterized by a small average pore size and a narrow pore size distribution. Thin Pd films of a few microns (Jayaraman and Lin, 1995; Li et al., 1996; Li et al., 1993; Uemiya et al., 1991b) were deposited on asymmetric γ-Al_2O_3/α-Al_2O_3 supports due to their small pore size on the surface (50-200 nm) and showed high H_2 flux due to low mass transfer resistance (support's pore size: 4–10 μm). Ni particles/PSS (Jun and Lee, 2000), γ-

Al_2O_3/Ni particles/PSS (Nam and Lee, 2001), ZrO_2/PSS (Wang et al., 2004) are also examples of asymmetric supports. Hence, it appears that the current trend is to modify by in-house techniques the bare porous support in such a way that a very smooth surface is achieved for the deposition of Pd.

Physical methods were also used to modify the surface of porous metal supports (Jemaa et al., 1996; She, 2000). Jemaa et al. (1996) obtained composite Pd membranes as thin as 6 μm on 0.5 μm grade PSS supports after shot peening the bare surface with 100μm in diameter Fe particles. However, they reported a H_2 permeance of 11.3 $m^3/(m^2\ h\ bar^{0.5})$ at 400ºC, which is low for a 6 μm thick membrane. No reason was given for such a low H_2 permeability. She (2000) obtained thin (20 μm) composite Pd membranes on 0.5 μm grade PSS supports by brushing the bare support with a metallic brush.

Wang et al. (2004) modified a 0.2 μm grade PSS support (Mott Corporation) with zirconium oxide. ZrO_2 was deposited from a colloidal solution by pulling a vacuum in the inside of the tube for 1 hr. After removing the excess ZrO_2 with water, the support was calcined at 300ºC for 2 hr. The ZrO_2 colloid-deposition and calcination procedure was repeated several times before activation and Pd deposition. A 10 μm thick Pd membrane was obtained after electroless deposition. The 10 μm composite Pd membrane on the ZrO_2/PSS modified support showed a H_2 permeance of 32.2 $m^3/(m^2\ h\ bar^{0.5})$ with a low selectivity (H_2/Ar) equal to 156. No reasons were reported for such a low selectivity.

PSS supports have recently been modified with SiO_2 colloid suspensions (Su et al., 2005), $Al(OH)_3$ and CeO_2 colloids (Tong et al., 2005a; Tong et al., 2005b; Tong et al., 2005c). Su et al. (2005) achieved H_2 permeabilities as high as 50 $m^3/(m^2\ h\ bar^{0.5})$ at 500ºC and ideal separation factors (H_2/N_2) of 300-450 on SiO_2 modified PSS supports.

The high fluxes were due to the thinness of the Pd layers, 2-6 μm, achieved on modified supports. Tong et al. (2005) achieved H_2 permeances ranging between 50-60 $m^3/(m^2\ h\ bar^{0.5})$ at 500ºC on modified PSS supports. Their composite Pd membrane was 6 μm thick. Unfortunately, none of the above-cited researchers carried out long-term H_2 permeance stability tests in order to elucidate the long-term H_2 permeance and ideal selectivity of their composite Pd membranes.

2.4.3 The use of an external driving force during deposition

Osmotic pressure carried the Pd complexes present in the plating solution deeper into the large pores of the substrate (Souleimanova et al., 2000; Souleimanova et al., 2002; Souleimanova et al., 2001; Yeung et al., 1995). Hence, the preferential deposition of Pd in deep "valleys" (large pores) resulted in the selective blocking of big defects. The small pores were then covered with a thin Pd layer producing a highly H_2 permeable membrane. Li et al. (1998) used electroless plating coupled with osmosis to prepare a 10 μm composite Pd membrane, with a low H_2 permeability of $18.7 \cdot 10^{-5}$ m^3 $m/(m^2\ h\ bar^{0.5})$ at 480ºC and a selectivity (H_2/N_2) in the range 1200-1600. Souleimanova et al. (2001) studied the effect of osmotic pressure on Pd particle size and showed that the particle size decreased when the osmotic pressure was increased and consequently, the Pd surface was smoother. The H_2 permeability of composite Pd membranes prepared with osmotic pressure was found to be higher (although by only 1.5 m^3 $m/(m^2\ h\ bar^{0.5})$) than the H_2 permeability of composite membranes prepared without osmotic pressure (Souleimanova et al., 2002), which was explained by the fact that finer Pd agglomerates were obtained at higher osmotic pressures. Souleimanova et al. (2002) also reported better mechanical stability under temperature cycling for membranes prepared by electroless plating and

osmosis on PSS. Furthermore, Pd went deeper in the PSS support increasing the adhesion of the membranes to the support.

It should be noted that membranes prepared with electroless plating coupled with osmosis had a lower permeability than membranes prepared with electroless plating. This was due to the fact that in membranes prepared using the electroless plating method coupled with osmosis, the thickness of the Pd layer was thicker than the determined value since Pd was forced into the pores.

2.5 The microstructure of Pd thin films from electroless deposition

The microstructure of composite Pd membranes was not extensively studied. It has been widely accepted that the fresh Pd layers deposited with electroless deposited method included very small Pd grains in the order of 10 nm (Li and Cheng, 1996; Souleimanova et al., 2002). Due to the presence of N_2 bubbles at the surface of the layer during plating, some microporosity was incorporated within the deposit (Yang et al., 2001). Also due to the low temperature (around 60ºC) at which electroless deposition method is carried out Pd columnar grains are expected (Müller, 1985). In fact, very little is known on the microstructure of Pd deposits besides grain size and microstrains. Pd films are suspected to have microporosity although no EXAFS studies were carried out to measure the size of microvoids in electroless Pd deposits (Babanov et al., 1997). Porosity and pore size can also be measured by Small Angle Neutrons Scattering (SANS) (Sanders et al., 1998).

Several researchers reported a possible effect of Pd grain size on H_2 permeance and their conclusions are varied. Some thought that small grains enhanced H_2 permeance (Bryden and Ying, 2002; Yan et al., 1994) while others believed that large crystallites led to high H_2 permeation (Li et al., 1998; McCool and Lin, 2001). The basis of the first

thought being "small crystallites lead to high H_2 fluxes" is the fact that for many metallurgical systems grain boundary diffusion is characterized by an activation energy lower than the activation energy of bulk diffusion by a factor of two. Using Quasielastic Neutron Scattering (QENS), H_2 diffusion was shown to be rapid within the grain boundaries in nanocrystalline palladium (Janßen et al., 1997). Also, at 20°C the H_2 diffusion coefficient of nano-Pd sample at low H_2 concentrations was lower than H_2 diffusion coefficient at low H_2 concentrations in Pd single crystal due to the trapping of H_2 atoms in high energy sites of the grain boundaries (Mütschele and Kirchheim, 1987). Once all these high energy sites in the grain boundaries have been filled (this occurred at higher concentrations) the diffusion coefficient of H_2 in nano-Pd became larger than the H_2 diffusion coefficient in single Pd crystals (Mütschele and Kirchheim, 1987). Finally at even higher H_2 concentrations the diffusion coefficient of H_2 in the nano-Pd starts to decrease due to H-H interactions inside the grain boundaries. Moreover, several researches found an increase in H_2 solubility in nanocrystalline Pd (Eastman et al.; Mütschele and Kirchheim, 1987; Wolf et al., 1994) that might contribute to an increase in H_2 permeability. The second thought being "large grains enhance H_2 permeation" is based on the fact that grain boundaries are seen as gaps where, to go from one grain to the other, H_2 needs to desorb and recombine on the surface of the first grain, travel as molecule through the boundary, readsorb and dissociate on the surface of the second grain and finally diffused in the lattice of the second grain. The effect of Pd grain size on H_2 permeability in composite Pd membranes is still unclear.

2.6 Leaks in composite Pd and Pd alloys membranes

At the present, a number of composite Pd membranes have been prepared by many researchers on Al_2O_3 supports, Vycor glass and PM supports. Many composite Pd membranes showed high H_2 permeance and good chemical stability. Indeed, even for composite Pd membranes on PM supports, new technologies decreased to a large extent the problems posed by intermetallic diffusion. However, leak stability over time is an issue that have not received too much attention but arises in all Pd composite membranes.

Leaks can form in composite Pd membranes due to "H_2 embrittlement". Originally, the term "H_2 embrittlement" was used to describe the shape, size and structure modifications (deformations) of freestanding Pd samples after several $\alpha-\beta-\alpha$ transformations (Lewis, 1967). β phase nucleation will not occur if care is taken to keep the conditions of the membrane in the stability region of the α phase, which is relatively easy to perform by adequately controlling the temperature and pressure. Therefore the α to β transformation poses little problem.

Reasons for leak formation and leak growth are in fact microstrains and stress release. Indeed, microstrains are present in fresh (or "green") membranes and are due to imperfections between Pd grain boundaries (Li and Cheng, 1996). Microstrains are released upon heating of the sample (Murakami, 1991). Stresses are denoted as intrinsic (Floro et al., 2001; Koch, 1994; Rajamani et al., 2002) when the causes of the formation of the stress are related to the material itself. Stresses caused by external factors are denoted as extrinsic. Extrinsic stresses are mostly due to thermal expansion coefficient mismatch between the film and the support (Murakami, 1991; Vook and Witt, 1965; Witt and Vook, 1968). Intrinsic and extrinsic stresses lead to either the expansion or contraction of

the Pd lattice parameter. The fundamental difference between microstrains and stresses is that microstrains are located at the Pd grain boundaries or at the external shell of Pd grains (Reimann and Wurschum, 1997), while stresses are due to contraction or expansion of the unit cell. When enough energy is given to the system, microstrains and stresses are relaxed and the structural changes that occur during stress relaxation (Floro et al., 2001) may play an important role in leak formation and leak growth.

The absorption of H_2 in a composite Pd membrane also leads to compressive extrinsic stresses denoted as H_2 stresses. The magnitude of compressive stresses after H_2 absorption depends on the H_2 loading n(H/Pd). Indeed, H_2 loading leads to the expansion of the Pd film (Baranowski et al., 1971). However, since the film is attached to the support, its expansion will be limited and compressive stresses will arise. Therefore, if the H_2 pressure is cycled at any temperature below 300ºC and, between a low pressure and a high pressure such that the miscibility gap boundary is closely approached, structural changes (dislocations, microcracks) may occur in the membrane after many cycles due to the repeated tensile/compressive stresses in the Pd layer.

Cycling H_2 pressure can have a degrading effect on composite Pd membranes (Checchetto et al., 2004). Checchetto et al. (2004) studied a 4 μm thick Pd/polycarbonate coated PSS at 100ºC and H_2 pressures ranging from 10 mbar to 195 mbar. They studied the mechanical stability of the composite membrane by switching 10 times H_2 and N_2 at 100ºC and a pressure difference of 100 mbar. They reported cracks on the Pd coating and attributed those cracks to $\alpha \rightarrow \beta \rightarrow \alpha$ phase transformations. However, at 100ºC, 200 mbar are needed to trigger the β phase nucleation. Therefore, switching gases at 100ºC and a pressure of 100 mbar was safe. However, what caused the membrane to fail were the re-

peated "extrinsic" tensile/compressive stresses. Also, the membrane may have failed during H_2 testing when the pressure was raised up to 195 mbar. Indeed, 195 mbar was very close to or even higher than the maximum pressure allowed at 100ºC. Nam and Lee (2001) studied the mechanical stability of a 2 μm PdCu/γ-Al_2O_3 coated PSS membrane by switching 18 times at 450ºC H_2 and N_2 atmospheres at a pressure difference of 0.7 bar. The total mechanical stability experiment lasted for 40 days. Nam and Lee (2001) reported no degradation of separation properties of the thin film. Tong et al. (2005) also cycled 40 times at 500ºC between H_2 (ΔP = 1 bar) and Ar atmosphere a 6 μm thick composite Pd $Al(OH)_3$-modified PSS membrane without seeing any deterioration in the separation properties of the membrane.

In many cases, pinholes were found on the surface of composite Pd membranes after characterization. These pinholes were attributed to the oxidation and reduction during membrane testing of some localized regions in the Pd layer and/or localized regions in the PSS support (Lee et al., 2003). Paglieri et al. (1999) suspected Sn impurities from the activation layer to be responsible for pinhole formation. Pinhole formation is far from being understood.

The lack of understanding in the leak formation and growth is partially due to the time it requires to follow a composite Pd membrane at different temperatures over a long period of time. Works in the literature only reported leak and selectivity data at one temperature from the measurement of a single leak rate. The difficulty in understanding the leak behavior of Pd composite membranes is also due to the complexity of different type of membranes studied where the dense layer could be Pd or Pd alloy, the intermediate layer could be an oxide formed in-situ or an oxide formed by the sol gel technique

and the support may be glass, Al_2O_3 or porous metals. A study on the role that stresses and stress release play on the leak formation is needed.

3 Experimental set-up and procedures

3.1 Composite Pd membranes synthesis

3.1.1 Porous metal supports

Two types of support geometries were used in this study: plates and cylindrical supports. The Porous Metal (PM) plates 1 cm ×1.5 cm were made out of 316L Stainless Steel, C22 Hastelloy or α-alumina (denoted as PSS plates, PH plates and α-Al_2O_3 plates). The Porous metal cylindrical supports were made out of 316L Stainless Steel or Hastelloy, with either 1.27 cm or 2.54 cm OD, variable length (2.54, 5.08 and 15.24 cm) and also denoted as PSS supports and PH supports. All porous metal supports were available in 0.1, 0.2 and 0.5 μm grade. The grade of a support is defined as follows: a support with a 0.5 μm grade rejects 95% of particles larger than 0.5μm in diameter.

PSS and PH plates were made by cutting a 100 cm^2 porous metal sheet into pieces of 1 to 1.5 cm^2. A small hole was drilled in a corner of the PSS and PH plates to hang them from hooks for activation and plating procedures. Cylindrical porous metal supports for composite Pd membranes were prepared by welding to one end of the PSS or PH tube a blind cap and welding a non-porous metal tube to the other end. A typical porous metal support for the fabrication of composite Pd membranes is shown in Figure 3.1.

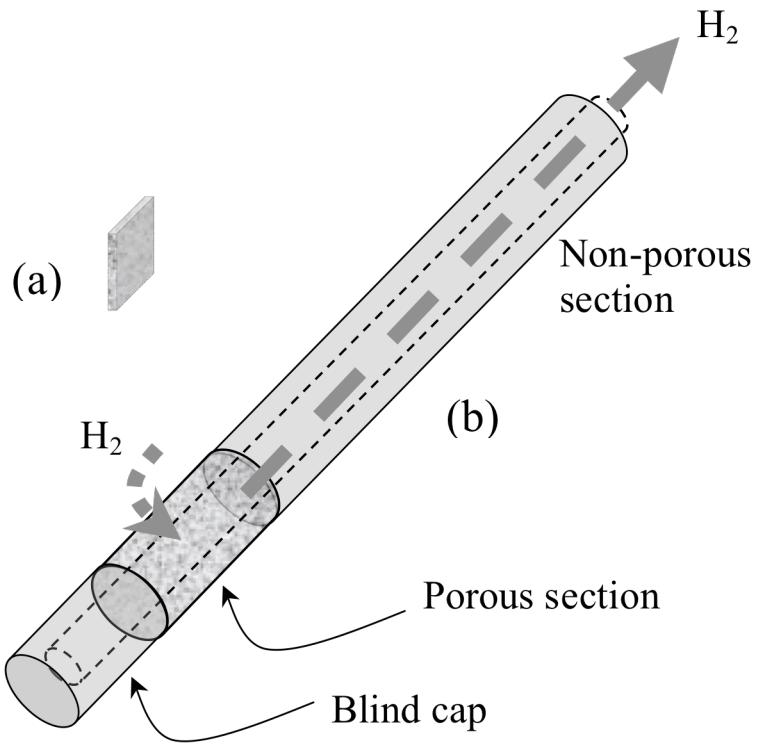

Figure 3-1 (a) PSS, PH or Al_2O_3 plate. (b) Assembly of a blind cap, porous metal tube and non-porous metal tube

The weld nugget between the blind cap and the porous metal tube was denoted as the "lower weld" and the weld nugget between the porous metal tube and the non-porous metal tube was denoted as the "upper weld". All porous metal plates and porous metal supports were purchased from Mott Corporation, Farmington, CT.

All PM supports were cleaned before oxidation, activation and Pd electroless deposition. The following cleaning procedure was used for every sample: 30 to 60 min. immersion in an alkaline solution (45 g/l NaOH, 65 g/l Na_2CO_3, 45g/l $Na_3PO_4 \cdot 12H_2O$), including 5ml/l of a saturated solution of industrial detergent, for dirt and grease removal. The samples were then thoroughly washed with De-Ionized Water (DI water) to remove the alkaline solution trapped in the pores of the supports. A strip of pH paper was stuck on the surface of the samples to check the acidity of the water remaining within the pores. The DI water cleaning step was repeated until the pH paper indicated 7. The last step involved a 10 min immersion in isopropanol (IPA) to hasten the drying of the supports. All the cleaning steps were carried out in an ultrasonic bath at 60°C. The supports were finally dried at 120°C overnight. After cleaning, the supports were oxidized in stagnant air at the desired temperature (10 to 12 hr at 400-600ºC for PSS supports and 12 hr at 700ºC for PH supports) to produce an oxide layer to prevent intermetallic diffusion. The mass of the bare support was measured before and after oxidation prior to any Pd plating. After oxidation, the He flux of the porous support was measured at different pressures in order to determine the initial He permeance.

3.1.2 Grading porous metal supports

After oxidation, the surface of most of the porous metal supports was smoothed by sequentially depositing coarse, fine and very fine pre-activated Al_2O_3 particles with

intermediate short Pd deposition to consolidate the powder. The process of making the surface of the porous metal support smoother was denoted as "grading" and is similar to the process yielding to asymmetric Al_2O_3 supports, where layers with different pore size are deposited by the sol gel process. The following grading procedure describes the steps followed for the grading of the support of membrane C01-F09. Any variation from this procedure was described when it occurred.

Three different mixtures of powders were prepared as described below.

Powder Mixture 1 included 65 wt% Al_2O_3 with an average particle size of 1 μm (Alfa Aesar); 30 wt% Al_2O_3 with an average particle size of 5 μm (Beuhler, Ltd.), and 5 wt% Al_2O_3 with an average particle size of 3 μm (Beuhler, Ltd.).

Powder Mixture 2 included 60 wt% Al_2O_3 with an average particle size of 0.3 μm (Alfa Aesar); 30 wt% Al_2O_3 with an average particle size of 3 μm (Beuhler, Ltd.), and 10 wt% Al_2O_3 with an average particle size of 1 μm (Alfa Aesar).

Powder Mixture 3 included 60 wt% Al_2O_3 with an average particle size of 0.01-0.02 μm (Alfa Aesar); 30 wt% Al_2O_3 with an average particle size of 1 μm (Alfa Aesar), and 10 wt% Al_2O_3 with an average particle size of 0.3 μm (Alfa Aesar).

Each powder was placed in a separate 500 ml cylinder containing 250 ml of aqueous $SnCl_2$ solution (1 g/l, pH=2). This step of sensitizing the powder was performed in an ultrasonic bath at 60ºC for 10 minutes. After 10 minutes, 250 ml of aqueous $PdCl_2$ solution (0.1 g/l, pH=2) were added into the cylinder already containing the aqueous $SnCl_2$ solution and Al_2O_3 powder. The resulting slurry, with a total volume of about 500 ml, became brown instantly. The slurry was placed in an ultrasonic bath at 60ºC for 10 minutes. The resulting surface activated powder was then filtered from the slurry by using one filter

paper (WHATMAN® GF/F type) for every 50 ml of slurry. The filter cakes were dried at 120ºC for 2 hr.

The fine and very fine mixtures of Al_2O_3 powders (*i.e.*, Powder Mixtures 2 and 3) were activated separately following the procedure described above. The coarse powder (*i.e.*, Powder Mixture 1) was not activated to avoid subsequent deposition of Pd too deep into the pore system of the PSS support.

The oxidized PSS support was placed for 1 minute in a 200 ml water slurry at pH 2 that contained 0.5 g of Powder Mixture 1. A vacuum was applied to the tube side of the support and an Al_2O_3 cake easily formed on the support.

Pd adhesion to the support is increased by the presence of anchoring sites. Anchoring sites, such as the tips of the substrate particles (*e.g.*, the tips of 316L SS particles[1] forming the PSS support), should not be covered by the Al_2O_3 powder for good adhesion between the Pd membrane and the support. To expose the anchoring sites, the extra Al_2O_3 cake was removed by gloved hand while gently rinsing with distilled water. The vacuum in the tube side was maintained during the removal of the extra Al_2O_3. Al_2O_3 remained inside the pores mouth of the porous support.

Following the deposition of Powder Mixture 1, the support was immersed for 1 minute in a 200 ml water slurry that contained 0.5 g of pre-activated Powder Mixture 2 while a vacuum was applied to the tube side of the support. Again, extra Al_2O_3 cake was removed carefully by gloved hand as described above. After deposition of the pre-activated Powder Mixture 2, the support was placed in 140 ml of Pd plating solution for 5 minutes of Pd plating (with no vacuum applied to the tube side) to glue the Al_2O_3 particles. Fol-

[1] The anchoring sites or tips of 316L SS (or PH) particles are shown in Figure 6-3, page 144

lowing the deposition of Powder Mixture 2, the support was immersed in a 200 ml water slurry that contained 0.5 g of pre-activated Powder Mixture 3 for 1 minute while a vacuum was applied to the tube side of the support. Again, extra Al_2O_3 cake was removed carefully by gloved hand. After the deposition of the pre-activated Powder Mixture 3, the support was immersed in 140 ml of Pd plating solution for 5 minutes of Pd plating (with no vacuum applied to the tube side). This process produced a graded support. The graded support was dried overnight at 120ºC and weighed. Also, the He leak at different pressures was measured in order to determine the He permeance after the grading step.

3.1.3 Support activation

Through out this study, the activation process was performed using sequential dipping in $SnCl_2$-HCl (1 g/l, pH 2) and $PdCl_2$-HCl (0.1 g/l, pH 2) solutions. Tin chloride dihydrate ($SnCl_2 \cdot 2H_2O$, 98% ACS) and Pd chloride ($PdCl_2$, 99.9%, metal basis, Assay) used for the preparation of the activation solutions, were purchased from Aldrich and Alfa Aesar respectively. The preparation of $SnCl_2$ solution consisted of putting 1 ml of HCl 10 mol/l (30%) into 10 - 20 ml of Di water, adding 1 g of $SnCl_2 \cdot 2H_2O$, shaking and finally adding Di water up to 1 l. The preparation of $PdCl_2$ solution consisted of putting 1 ml of HCl 10 mol/l (30wt%) into 100 ml of Di water, adding 0.1 g of $PdCl_2$, heating the solution to 60-80ºC until complete dissolution of the $PdCl_2$ salt and finally adding Di water up to 1 l. The $PdCl_2$ solution could be stored for long periods of time (months), on the other hand, $SnCl_2$ solution had always to be prepared just before the activation since aging of the $SnCl_2$ solution led to polymeric substances within the solution (Reva and Vorob'eva, 2002).

3.1.4 Pd plating solution

The Pd plating solution included $Pd(NH_3)_4Cl_2 \cdot H_2O$ as the Pd source, Na_2EDTA as the complexing agent, NH_3OH as the buffer and NH_2-NH_2 (hydrazine) as the reducing agent. The Pd plating bath did not include any accelerator or stabilizer to keep the chemistry simple. The bath composition used for Pd deposition is listed in Table 3-1.

Table 3-1 Pd plating bath and deposition conditions for membrane preparation

$Pd(NH_3)_4Cl_2 \cdot H_2O$	4 g/l	99.9% (metal basis), Alfa Aesar
$Na_2EDTA\ 2H_2O$	40.1 g/l	99+%, Aldrich
NH_4OH	198 (ml/l)	28wt%, Merck
H_2NNH_2 (1 M)	5.7 ml/l	99 wt%, Aldrich
pH	10-11	
Temperature	60°C	

One liter of the Pd plating solution was prepared by first, adding 198 ml of ammonium hydroxide to 200 ml of Di water. Secondly, 4 g of $Pd(NH_3)_4Cl_2\ H_2O$ were added and the solution was shaken until complete dissolution of the Pd salt. 40.1 g of Na_2EDTA were added in a third step and the solution was stirred for 20-30 min until complete dissolution of the Na_2EDTA. Finally, Di water was added to the total volume of one liter. Pd plating solutions were prepared 24 hr before use to let the system reach an equilibrium state. Hydrazine was added into the plating solution right before the activated support was immersed in the plating bath. Even though Pd plating solutions could be stored for long periods of time, Pd plating solutions not older than 1-2 weeks were used for the preparation of composite Pd membranes.

3.1.5 Pd deposition on activated substrates

Pd deposition was carried out by immersing the activated support into the Pd plating bath for 90 minutes at 60ºC. After 90 minutes of Pd plating, the support was placed in Di water at the same temperature (60ºC) and let cool to room temperature. The plating solution was changed in the plating cell, hydrazine was added to the new plating solution and the support was reintroduced in the plating bath after a short rinsing of the plated surface with Di water. Sessions of 90 minutes Pd plating were carried out 2 to 4 times after activation. After Pd deposition, the support was thoroughly rinsed with Di water and let dry overnight at 120ºC. The Pd plating rate ranged from 0.5 μm/h to 3 μm/h and was mainly dependent on the ratio of the volume of Pd plating solution over the activated surface. For example, the simultaneous deposition of Pd onto four small plates (3 cm^2 per plate) was performed in a 100 ml beaker with 70 ml of plating solution ($R_{vol/surf}$ = 5.8 ml/cm^2) at a plating rate of around 2 μm/hr. Composite Pd membranes with a porous surface of 120 cm^2 were plated in a 500ml graduate cylinder with 400 ml of Pd plating solution ($R_{vol/surf}$ = 3.3 ml/cm^2) at a plating rate of around 1 μm/h. The activation-plating procedure was repeated until the composite Pd membrane became dense. The composite Pd membrane was assumed dense when the He permeance was lower than 10^{-4} $m^3/(m^2\ h\ bar)$ at room temperature and at a pressure difference of 1 bar. During the plating procedure, vacuum was created in the tube side of the membrane using an aspirator when the He permeance of the membrane reached 1 $m^3/(m^2\ h\ bar)$ in order to easily block the last remaining large pores.

The thickness of the Pd thin film was determined by the gravimetric method i.e. weight gain of the sample divided by the product of the plated surface area and the metal

density. Gravimetric methods gave an average thickness value for the membrane generally in good agreement with the thicknesses determined by SEM pictures. Table 3-2 summarizes all the membranes prepared for this study.

Table 3-2 List of all membranes studied in this work

Membrane	Support type (μm-alloy)	Area (cm^2)	Ox.Temp (ºC)	Support grade layer	Pd thickness Gravimetric (μm)	Pd thickness SEM (μm)
C01-F03	0.1-PSS	8.4	400	No	32	37
C01-F04	0.1-PSS	8.4	none	No	28	28
C01-F05	0.1-PSS	8.4	500	No	33	Not determined
C01-F06	0.1-PSS	23	600	No	19	21
C01-F07	0.1-PSS	23	500	No	23	24
C01-F08	0.1-PSS	23	500	Yes	15	19-24
C01-F09	0.1-PSS	23	500	Yes	14	14-15
C01-F11a	0.1-PSS	23	500	Yes	10	Not determined
C01-F11b	C01-F11	23	500	Yes	13	17
C02-F01	0.2-PSS	23	500	No	37	Not determined
C02-F03	0.2-PSS	23	500	No	37	Not determined
Ma-32	0.1 medium-PH	120	700	Yes	7.7	Not determined
Ma-32b	Ma-32	120	-	Yes	10	Not determined
Ma-32c	Ma-32b	120	-	Yes	12	12-14
Ma-34	0.1 coarse-PH	120	700	Yes	4	Not determined
Ma-34b	Ma-34	120	-	Yes	8	9.4
Ma-41	0.1 coarse-PH	120	700	Yes	10	Not determined
Ma-42	0.1 medium-PH	120	700	Yes	5.6	Not determined

3.2 The determination of H_2 permeance in composite Pd membranes

3.2.1 H_2 permeation set-up

The H_2 permeation characterization of the composite Pd membranes with small H_2 permeable surface (8.4 and 23 cm^2) was performed in a "small" unit. The H_2 permeation characterization of composite Pd membranes with large H_2 permeable surface (120 cm^2) was performed in a "large" unit. The only differences between the "small" and the "large" units were the size of the furnaces, the size of the ballast volumes and the range of H_2 and He digital mass flow meters. However, the functionality and layout of both units was the same and is shown schematically in Figure 3-2.

The permeation set-ups consisted of a tube furnace and a stainless steel reactor where the membrane was housed in a shell-and-tube arrangement and sealed with stainless steel and graphite ferrules. The temperature was monitored in the tube side of the membrane and controlled by a separate J type thermocouple located on the outside wall of the stainless steel reactor for safety purposes. A temperature controller (Eurotherm type 2116) was used to control the temperature at the reactor wall and adjusted to have the desired temperature at the tube side. A Type 600A MKS pressure transducer was used to measure the pressure in the tube side and a second transducer, type 727A MKS, was placed at the shell side to monitor the H_2 inlet pressure. Inert gas flow rates (leaks) through the membrane were measured with a digital mass flow meters with 10 ("small" unit) or 50 ("large" unit) sccm[1] range (MKS M10MB model), specially calibrated for He.

[1] sccm= standard cm^3 per minute

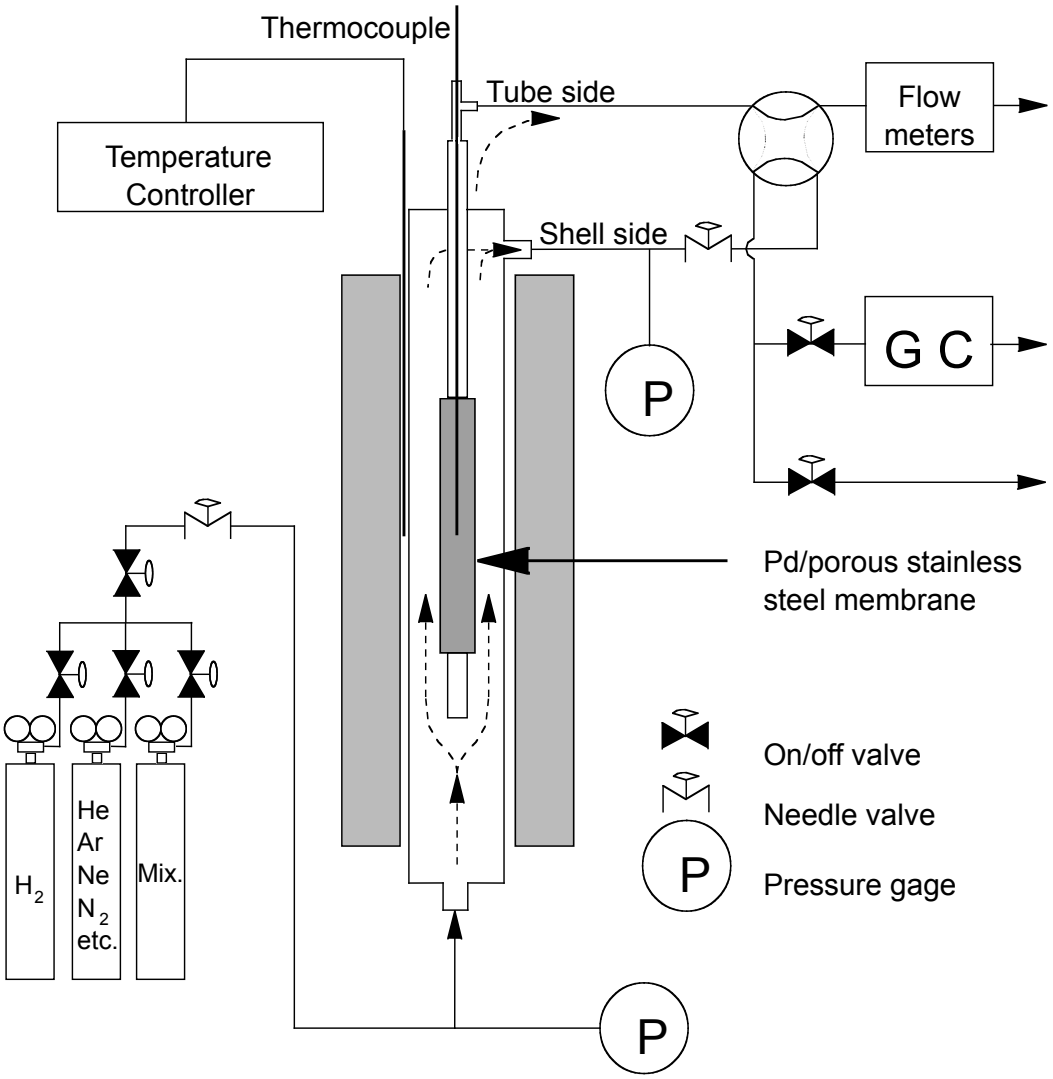

Figure 3-2 H_2 permeation set-up

When the leaks were measured with other gases such as Ar or N_2 bubble flow meters with different ranges were used. The H_2 flux was measured using a second digital mass flow meter with 200, 500 and 1000 sccm range in the "small" unit and 5000 or 20000 sccm range (MKS M10MB model) in the "large" unit. All H_2 digital mass flow meters were specially calibrated for H_2 gas. All parameters, tube temperature, pressures and flows were logged continuously into a computer using a TBX-68T Terminal block (National Instruments) data acquisition box and NI 4351 high precision voltage meter (National Instruments). Ballast volumes (500 ml to 6000 ml depending on the permeation unit) in the inlet side permitted a gradual change of the composition of the gas to be purged (He to H_2 or H_2 to He). A He sweep line was also used at the tube side of the membrane to keep at all times the H_2 partial pressure at the tube side lower than the H_2 partial pressure at the shell side while changing from H_2 to He. Therefore, the tube-side purge avoided any back flow of H_2 from the tube side to the shell side while changing from H_2 to He. Any small amount of H_2 back flow might cause the membrane to fail. All membranes were tested using Ultra High Purity (UHP) H_2 gas purchased from Aimtek Inc., Auburn, MA.

3.2.2 Typical characterization procedure for a composite Pd membrane

The general characterization procedure of a composite Pd membrane involved:

(1) The heating of the membrane in He atmosphere (P_{shell}=2 bar) from room temperature to 250ºC at a rate of 1ºC/min. A small tube purge (10-40 sccm) was also established to remove water vapor from the tube side. At 250ºC the tube purge was stopped.

(2) The measurement of the leak (He, Ar and N_2) at 250ºC at several different pressures.

(3) The introduction of H_2 at 250ºC and a pressure of 2 bar.

(4) A dwell time in H_2 atmosphere ranging from 1 to 4-5 days during which the H_2 pressure difference was kept equal to 1 bar (2:1). During the dwell time, the H_2 permeance was determined 1 to 3 times. For each time the H_2 permeance was determined, the H_2 flux was measured at 10-15 different pressures within the 1-4.4 bar pressure interval at the shell. The permeate pressure was always kept equal to atmosphere.

(5) The switching from H_2 to He at 250ºC to measure the leak (He) at 250ºC. Typically, the He leak after the H_2 test at 250ºC was different from the He leak before the H_2 test. The He leak was measured at 5-10 different pressures.

(6) The switching in atmosphere from He to H_2 at 250ºC.

(7) A dwell time of 5 hr[1] to reach the previous H_2 permeance at 250ºC.

(8) The change in temperature from 250 to 300ºC at a rate of 1ºC/min or slower in H_2 atmosphere.

(9) Steps (3), (4), (5), (6), (7) and (8) were repeated at 300, 350, 400, 450 and 500ºC.

(10) The membrane was cooled from 500ºC to 250ºC in H_2 atmosphere.

(10) The atmosphere change at 250ºC from H_2 to He and the cool down from 250ºC to room temperature at a rate of 1ºC/min.

All membranes studied in this work were characterized according to the above-described procedure. However, some steps, such as measuring the He leak or the H_2 per-

[1] hr = hours

meance at a given temperature, were omitted for some membranes. For instance, some membranes were tested at temperatures higher than 500ºC. For some membranes, the He leak at a given temperature was measured 4 to 5 times in order to measure the rate at which the He leak increased as a function of time at a given temperature. Also, for some membranes (Ma-32b/41) H_2 permeance was monitored for times longer than 4-5 days to study the long-term stability of the composite Pd membranes prepared in this study.

3.2.3 The determination of H_2 permeance

The H_2 permeance was determined by three different methods. The first method was based on the measurement of a single H_2 flux at a given pressure difference. H_2 permeance, F_{H2}, was estimated by dividing the single H_2 flux, J_{H2}, by the difference of the square root of the high pressure, $P^{0.5}{}_{shell}$, and the low pressure side, $P^{0.5}{}_{tube}$, as shown in Equation (3-1).

$$J_{H_2} = F_{H2} \cdot (P_{shell}^{0.5} - P_{tube}^{0.5}) \qquad (3\text{-}1)$$

F_{H2} was only used to follow the permeance as a function of time, which in fact corresponded to follow H_2 flux as a function of time during dwell times. F_{H2} was particularly used to determine the activation energy for H_2 permeation by monitoring H_2 flux as the temperature was changed, which is explained in Section 3.2.4.

The second method to determine the H_2 permeance was based on the measurement of H_2 flux at 10-15 different pressure differences (ΔP=0.2-3.5 bar). The 10-15 J_{H2} values were plotted as a function of $\Delta(P^{0.5})$ and the data (J_{H2}, $\Delta(P^{0.5})$) were then fitted with a linear regression assuming the n-exponent equal to 0.5 using Equation (3-2).

$$J_{H_2} = F_{0.5} \cdot (P_{shell}^{0.5} - P_{tube}^{0.5}) \qquad (3\text{-}2)$$

The H_2 permeance determined assuming Sieverts' law was denoted as $F_{0.5}$.

Finally, the third method was based on the measurement of H_2 flux at 10-15 different pressure differences (ΔP=0.2-3.5 bar). The 10-15 (J_{H2}, P_{shell}, P_{tube}) data points were then fitted with a non-linear regression given by Equation (3-3). Hence, the experimental data were fitted with the F_n and the n-exponent parameters.

$$J_{H_2} = F_n \cdot (P_{shell}^{n-\exp onent} - P_{tube}^{n-\exp onent}) \quad (3\text{-}3)$$

The H_2 permeance determined assuming P^n dependence of the H_2 flux was denoted as F_n. The regression of the experimental data (linear and non-linear) was performed by the least squares method, i.e. minimizing the Sum of the Squares of the Residuals (SSR) shown in Equation (3-4).

$$SSR = \sum_{i=1}^{N} (J_{H2,\exp}^{i} - F_{0.5,n} \cdot ((P_{shell,\exp}^{i})^n - (P_{tube,\exp}^{i})^n)^2 \quad (3\text{-}4)$$

The subscript "*exp"* in Equation (3-4) stands for experimental.

3.2.4 Determination of the activation energy for H_2 permeance

Two different methods were used to determine the activation energy for H_2 permeation through composite Pd-PM membranes:

(1) Determining the steady state values of H_2 permeance, $F_{0.5}$, at all temperatures (250, 300, 350, 400, 450 and 500ºC) after allowing the membrane to dwell in H_2 atmosphere for long times, 20 to 100 hr. Experimental values were then plotted in an Arrhenius plot ($Ln(F_{0.5})$, 1/T) and fitted with a straight line.

(2) Measuring the H_2 flux, J_{H2}, as a function of temperature while changing temperature at a very slow rate of 1°C/min. During the temperature change the pressure difference was kept constant and equal to 1 bar (2:1). Temperature changes were

performed by increments of 50ºC. Since the logging data terminal box was set to log all system parameters every 3 minutes, a total of 16 experimental (J_{H2}, Temp.) points were collected for every temperature change. Experimental values were then plotted in an Arrhenius plot ($Ln(J_{H2})$, 1/T) or ($Ln(F_{H2}=J_{H2}/(\sqrt{2}-1))$, 1/T) and fitted with a straight line.

3.3 Leaks in composite Pd membranes

3.3.1 Leak measurements and ideal separation factor

Leaks in composite Pd membranes were most of the times measured with He. N_2 and Ar were used for only specific experiments, which are detailed in their respective sections. The measurement of the He leak consisted of determining the He permeance. Hence, at any given temperature, the He flow was measured at the following pressure differences: 1, 1.5, 2, 2.5, 3 and 3.5 bar. The permeate side pressure was always kept at the atmospheric conditions. The He permeance was then determined by fitting the (He flux, ΔP) experimental points with Equation (3-5)

$$J_{He} = He_{permeance} \cdot \Delta P \qquad (3\text{-}5)$$

where J_{He} is the He flux in $m^3/(m^2\ h)$, $He_{permeance}$ is the permeance of the He leak in $m^3/(m^2\ h\ bar)$ and ΔP the pressure difference in bar. The ideal separation factor, denoted as selectivity, was defined by the ratio of the H_2 flux and the He flux at the same pressure difference. Since, the H_2 flux was proportional to $\Delta(P^{0.5})$ and the He flux was proportional to ΔP, the selectivity value depended on the pressure considered. In this work, all reported selectivities were determined at a pressure difference of one bar according to Equation (3-6).

$$Selectivity = \left(\frac{J_{H_2}}{J_{He}}\right)_{\Delta P=1} = \frac{F_{0.5}\cdot(\sqrt{2}-\sqrt{1})}{He_{permeance}} \quad (3\text{-}6)$$

In addition, the experimental data (J_{He}, ΔP) was plotted in the form (J_{He}, P_{ave}), where P_{ave} was the average transmembrane pressure equal to (P_{shell}+P_{tube})/2. Plotting (J_{He}, P_{ave}) allowed for the determination of the average pinhole[1] diameter, the total pinhole surface and the total number of pinholes. The calculations leading to pinhole diameter, total pinhole surface and number of pinholes are described in Chapter 10, Section 10.3.1.

[1] Pinholes: defects with the shape of a little hole that form in the dense Pd layer of a composite Pd membrane at high temperatures. The size and formation of these features are discussed in Chapter 10

3.3.2 Leak distribution along the membrane length

The distribution of leaks in large membranes (15 cm long, 2.54 cm OD, area=120cm^2) was studied by means of a "rising water test". The set-up, shown in Figure 3-3, and concepts used for this experiment were kindly transmitted from the research team at Shell International Exploration and Production, Inc., Huston, TX. The composite Pd membrane was housed in a Plexiglas shell and sealed with rubber O rings. A scale, divided in cm, was printed on the wall of the Plexiglas tube. The membrane was placed in such a position that the lower weld matched with the "zero" mark of the printed scale. A water reservoir was placed at a higher level than the plastic cell and connected via Tygon® tubing to the plastic cell. A on/off valve (valve A) allowed the admission of water to the plastic cell.

A pressurized He tank was connected to the plastic cell via stainless steel tubing and a 3-way valve (valve B) such that the inlet of the 3-way valve was connected to the plastic cell, the first outlet of the valve B was connect to the He tank and the second outlet of valve B was open to the atmosphere.

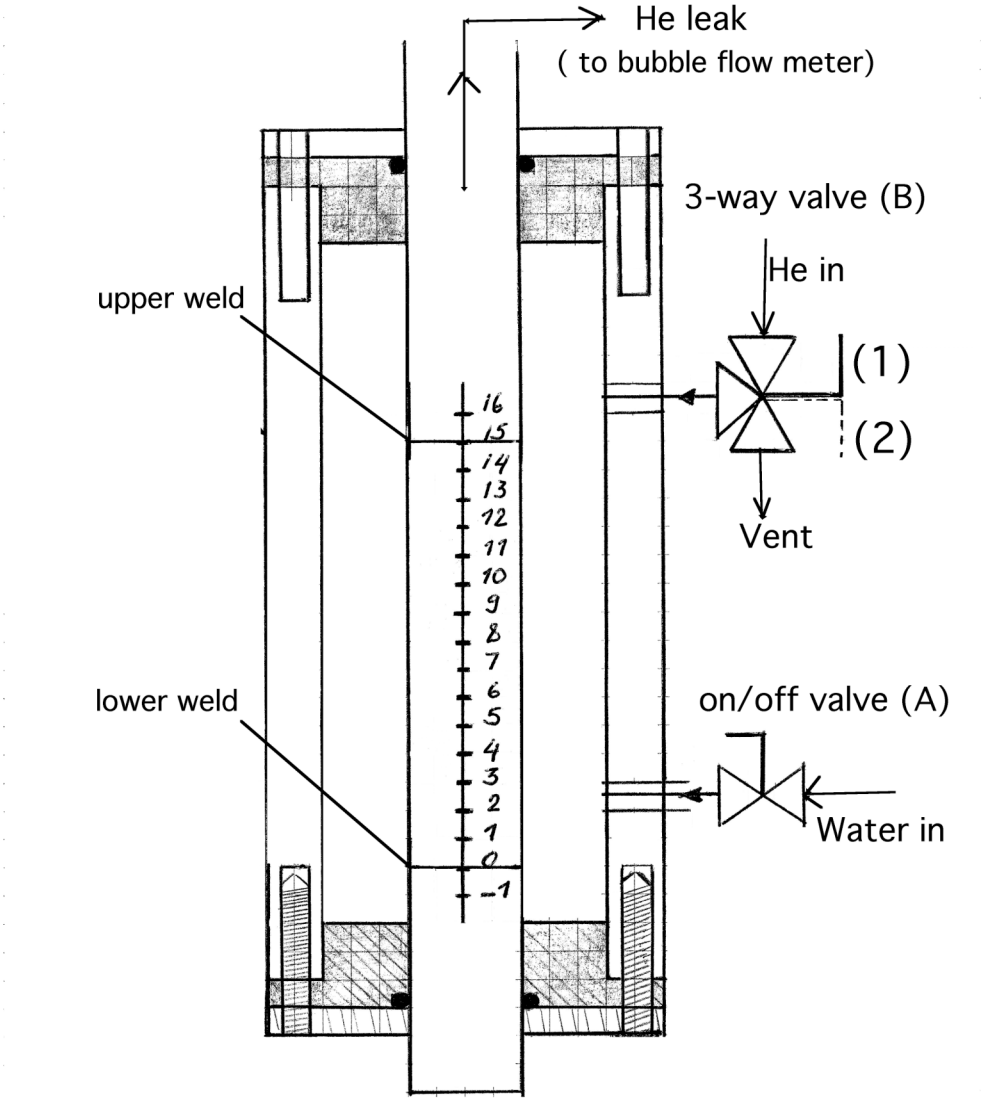

Figure 3-3 "Rising water test" apparatus (Shell International Exploration and Production, Inc.)

The leak distribution along the composite Pd membrane was determined as follows:

(1) At atmospheric pressure (3-way valve B in position 2), the on/off water valve (valve A) was opened to let water flow into the Plexiglas shell until the water meniscus reached the "-1" mark. At the "-1" mark the on/off valve A was closed.

(2) He was then introduced into the shell by switching the 3-way valve (valve B) to position 1. The He leak was measured with a bubble flow meter at a given pressure difference. Since the water was at the "-1" mark, the first leak measurement corresponded to the total leak of the membrane.

(3) The pressure in the shell was then released by switching the 3-way valve to position 2 and the water level was increased up to the "0" cm mark by opening the on/off water valve A. At the "0" mark the leak equaled the leak at the "-1" mark, however, sometimes, due to capillary forces water flowed above the lower weld and clogged some cracks and defects in the welding area resulting in a lower He leak. The leak at "-1" ensured the true total leak of the membrane.

(5) He was reintroduced into the shell and the He leak of the membrane was measured.

The procedure was repeated until the water level reached the last mark where the He leak was zero.

3.4 Microstructure characterization methods

3.4.1 Scanning Electron Microscope (SEM)

Surface characterization was performed using an Amray 1610 Turbo Scanning Electron Microscope (SEM) coupled with Energy Dispersion X-Ray (EDX) capabilities (Princeton Gamma-Tech Instruments Inc., Rocky Hill, NJ). The EDX detector was

equipped with a beryllium window allowing the detection of light elements. Atom and weight concentration profiles were determined with the Spirit software (Princeton Gamma-Tech Instruments Inc., Rocky Hill, NJ).

Elemental composition (line-scans) was performed at an acceleration potential of 10, 15 or 20 kV, 39 mm working distance, 33º tilt and a 5-10 minutes dwell time. The spatial resolution increased as the accelerating voltage was decreased and equaled 0.3 μm at 15 kV. Most of the elemental composition analysis were performed at 15 kV.

3.4.2 X-ray diffraction (XRD) techniques

XRD was used to investigate the microstructure (grain size and strains), "intrinsic" and "extrinsic" stresses in electrolessly deposited Pd coatings. Also, time dependent processes such as nucleation, phase growth and alloying in Pd-Cu alloys were studied using a time resolved X-ray diffractometer. Hence, three X-ray diffractometers were used for the analysis of thin Pd deposits. A Rigaku Geigerflex located at Worcester Polytechnic Institute (WPI), a PANalytical X'Pert Pro MPD located at Oak Ridge National Laboratories (ORNL) and a time resolved High Temperature XRD also located at ORNL. The PANalytical X'Pert Pro MPD and the High Temperature X-ray diffractometers located at ORNL site were used for macro-stresses measurements and strain release in Pd films and monitoring of phase transformations in Pd-Cu alloys respectively. The Rigaku diffractometer located at WPI was mainly used for grain size-strain measurements and general phase characterization.

XRD techniques and theory, grain size, strain and stress calculations were covered in detail by several researchers (Cullity and Stock, 2001; Klug et al., 1954). A brief theory

on strain-size and stress determination is given in Chapter 9, although, the reader is encouraged to consider Cullity and Klug manuals for a complete understanding.

3.4.2.1 Time resolved phase transformations, High Temperature X-Ray Diffraction

High-Temperature X-Ray Diffraction (HTXRD) was used as a major technique allowing the real-time monitoring of microstructure and phase transformations with respect to temperature and time. The time resolved HTXRD, with copper radiation ($\lambda CuK\alpha$=1.540598Å), was composed of a Scintag PAD X vertical θ/θ goniometer, a Buehler HDK 2.3 furnace and a mBraun linear position sensitive detector (LPSD). The data were collected in a multichannel analyzer (MCA) with the active area of the detector defined by about 500 channels at a resolution of 0.02º/channel corresponding to an angular range of 10º 2θ window. The data from the MCA were downloaded to the computer in 2 sec allowing fast data collection. For instance, a perfect well defined Pd XRD pattern could be taken in just 2 minutes while an hr would have been needed to collect the same Pd XRD pattern on the Rigaku Gegerflex diffractometer. The programmed heating/cooling procedure was controlled precisely and flexibly (heating and cooling rates up to 300ºC/min) through a computer using a thin Pt/10%Rh heater strip[1] and a Pt/Pt-13%Rh thermocouple welded to the Pt/10%Rh heater strip. When thin films on top of the thick substrates were studied, for instance, Pd thin films on 2 mm thick α Al_2O_3 substrates, a second Pt/10%Rh heating strip bent around the sample was used to better control the temperature and overcome the temperature gradient within the substrate.

[1] The heater strip was also the sample holder.

However, the presence of such heater did not permit a pyrometric temperature measurement of the thin film on the substrate. Therefore, temperature calibration of the furnace was performed by correlating the temperature given by the thermocouple and the real temperature deduced from the lattice parameter of silver powder placed on an uncoated $\alpha-Al_2O_3$ substrate. The Ag lattice parameter was measured at four different temperatures in the 200-800ºC temperature range (Touloukian et al., 1977). The calibrating line, thermocouple temperature vs. real temperature shown in Figure 3-4, was then obtained in He atmosphere. A difference in temperature, not larger than 50ºC, was observed between the Pd thin film and the Pt-Rh heater strip due to the low thermal diffusion coefficient of α-Al_2O_3 substrate. To avoid Pd or Cu oxidation He was flowed through a high temperature Ta strips purifier to avoid oxygen contamination.

The atmosphere in the stainless-steel sample chamber could be tailored with various gases (inert, oxidative, or reductive) for specific experimental needs. Data acquisition and analysis were performed using DMS-NT software (Scintag, Inc., Cupertino, California) and Jade 6 software (Materials Data, Inc., Livermore, California).

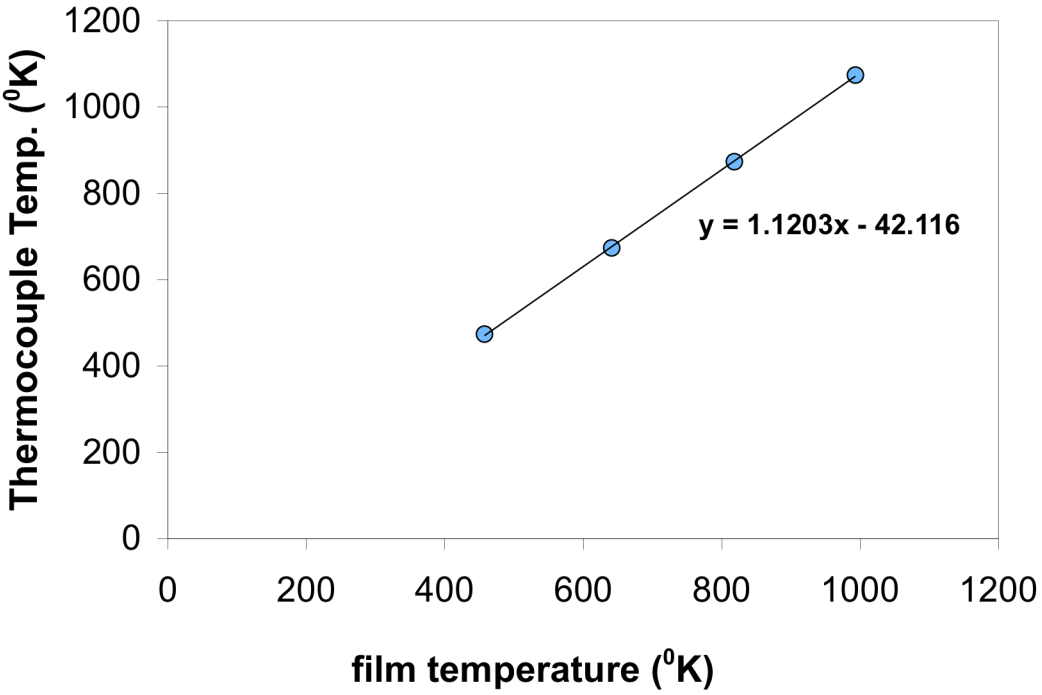

Figure 3-4 Temperature calibration curve when using a surround heater.

4 H_2 permeation through Pd films

4.1 Introduction

It is of great importance to understand the fundamentals of H_2 permeation through a freestanding Pd film (or foil) before studying the H_2 permeation through composite Pd membranes. The H_2 permeation mechanism through thin Pd films involves: the dissociation of H_2 to H atoms at the surface of the Pd film, the diffusion of the H atoms across the Pd layer and the recombination of H atoms into H_2 at the opposite surface. Such a diffusion mechanism is denoted as "solution-diffusion" mechanism since H_2 permeates through Pd by forming a PdH alloy. Each of the above-described steps could be the rate-limiting step for H_2 permeation through the Pd foil. The activation energy for H_2 desorption is given by Equation (4-1).

$$E_d = E_a - \Delta_r H \tag{4-1}$$

where E_d and E_a are the activation energy for H_2 desorption and H_2 absorption respectively. $\Delta_r H$ is the heat of the H_2 absorption reaction. The dissociative absorption of H_2 is a slightly activated process, therefore, $E_d \approx -\Delta_r H$ and at low temperatures, the associative desorption of H_2 is the rate-limiting step for H_2 permeation. The Temperature Programmed Desorption (TPD) of H_2 from Pd/γ-Al_2O_3 showed three desorption peaks (Ragaini et al., 1994). The first desorption peak was attributed to the H dissolved in the bulk and the activation energy for H desorption was found to be 50.2 kJ mol^{-1}. The two

other peaks corresponded to a weakly chemisorbed H specie and a strongly bound H specie respectively. The activation energy for the weakly and the strongly bound H species was 85.7 and 92-133 kJ mol^{-1} respectively (Ragaini et al., 1994). The temperature at which the desorption peak of the strongly bound H specie occurs was found to be equal to 150ºC (Kurman et al., 1990; Ragaini et al., 1994) and 77ºC (Farias et al., 1997). Hence at temperatures higher than 150ºC, when both absorption/desorption are at the thermodynamic equilibrium ($r_{absorption}=r_{desorption}$), the H diffusion through the bulk of Pd is the rate-limiting step for hydrogen permeation. However, if the Pd film thickness is very small, the diffusion of H atoms across the Pd film is very fast and the H_2 desorption becomes the rate-limiting step even though both absorption/desorption are at the thermodynamic equilibrium. The model for the H_2 permeation through Pd foils developed by Ward and Dao, (1999), proved that for a Pd foil with a clean surface, the H diffusion through the Pd bulk was the rate-limiting step at temperatures higher than 300ºC even for membranes with thicknesses approaching 1μm. They also proved that the desorption of H_2 is the rate-limiting step at low temperatures and that absorption is the rate-limiting step only at very low H_2 partial pressures (<<1 bar) or in the case of severe surface contamination.

When the diffusion of H atoms through the Pd bulk is the rate limiting step, Fick's first law is assumed, and the H_2 flux permeating through the Pd foil is proportional to the difference in the amount of H dissolved at the high pressure side of the membrane and the amount of H dissolved at the low pressure side of the membrane. In order to determine the concentration of H dissolved in the Pd, a relation between H_2 pressure in the gas phase and the H dissolved in the Pd bulk needs to be used. At very low H_2 pressures, the

relation between H_2 pressure and H dissolved in the Pd, n(H/Pd), is given by Equation (4-2) (Sieverts et al., 1915).

$$P_{H_2}^{0.5} = K(T) \cdot n(H/Pd) \qquad (4\text{-}2)$$

where P_{H2} is the H_2 pressure, K(T) is a proportionality constant named as Sieverts' constant and n(H/Pd) is the H concentration in the Pd bulk. Therefore, at low H_2 pressures, the H_2 flux, J_{H2}, is proportional to ($P^{0.5}{}_1$- $P^{0.5}{}_2$), with P_1 the high H_2 pressure and P_2 the low H_2 pressure. Since Equation (4-2) is only valid at low pressures, deviations from Sieverts' law (the H_2 pressure exponent ≠0.5) can occur at high H_2 pressures. For instance, at 250ºC, the H_2 absorption isothermal ($P^{0.5}$, *n(H/Pd)*) is linear at low pressures, 0–ca. 0.5 bar but starts to curve as the miscibility gap is approached, i.e. P_{H2} > 1 bar (Gillespie and Galstaun, 1936). Therefore, in the 1.1-2 bar pressure range, the H_2 flux, J_{H2}, is proportional to ($P^{\text{n-exponent}}{}_1$- $P^{\text{n-exponent}}{}_2$) with n-exponent >0.5. The permeation of H_2 through thick Pd foils (100 μm) was studied by Morreale et al. (2003) at very high pressures, and the n-exponents were calculated based on permeation data from four pressure ranges (1.01-1.75, 1.01-7.75, 1.0-16.00, 1.01-26.00 bar). They reported an increase in the n-exponent from 0.53 (the limit value) to 0.65 as the pressure range was increased. Unfortunately, Morreale et al. (2003) did not report the temperature at which the reported n-exponents vs. pressure range were determined and it would be difficult to compare their experimental values with other reported values. Deviations from Sieverts' law also occur in thin Pd foils when the Pd foil is defective and allows for the passage of other gases and when the surface of the Pd foil has low activity for the dissociation of H_2, which happens when contaminants are adsorbed on the surface.

In this chapter, the fundamentals of H_2 absorption in Pd are described. The equation relating H_2 pressure and temperature with H_2 dissolved in Pd is established and the equation of H_2 permeation through Pd is derived. The influence of leakages and low catalytic activity of the surface on the permeation mechanism of H_2 properties are described in Chapter 5.

4.2 Results and discussion

4.2.1 H_2 concentration in Pd: n(H/Pd)

The concentration of H_2 in Pd is usually denoted as "n" and has the units of mol H/mol Pd. The H_2 concentration in Pd, "n", was denoted as n(H/Pd) in this entire thesis. This section aimed at understanding and establishing the relation between P_{H2} and n(H/Pd) for the α phase at temperatures between 250 and 500ºC. The Pd-H phase diagram, inset in Figure 2-1, shows linear absorption isotherms ($P^{0.5}$ as a function of H loading, n(H/Pd)) in a narrow range of pressure for a given temperature. Figure 4-1 shows the absorption isotherms, $P^{0.5}{}_{H2}$ as a function of n(H/Pd), at 250, 290 and 310ºC reported by Gillespie and Galstaun (1936). For the three isotherms pictured in Figure 4-1 and for H_2 pressures higher than 5 bar (=2.23 $bar^{0.5}$), the relation $P^{0.5}$ as a function of H_2 loading, n(H/Pd), is not linear and Equation (4-2) is not valid. The relation between $P^{0.5}{}_{H2}$ and n(H/Pd) is better described by Equation (4-3)

$$P_{H_2}^{n-\exp onent} = K'(T) \cdot n(H/Pd) \qquad (4\text{-}3)$$

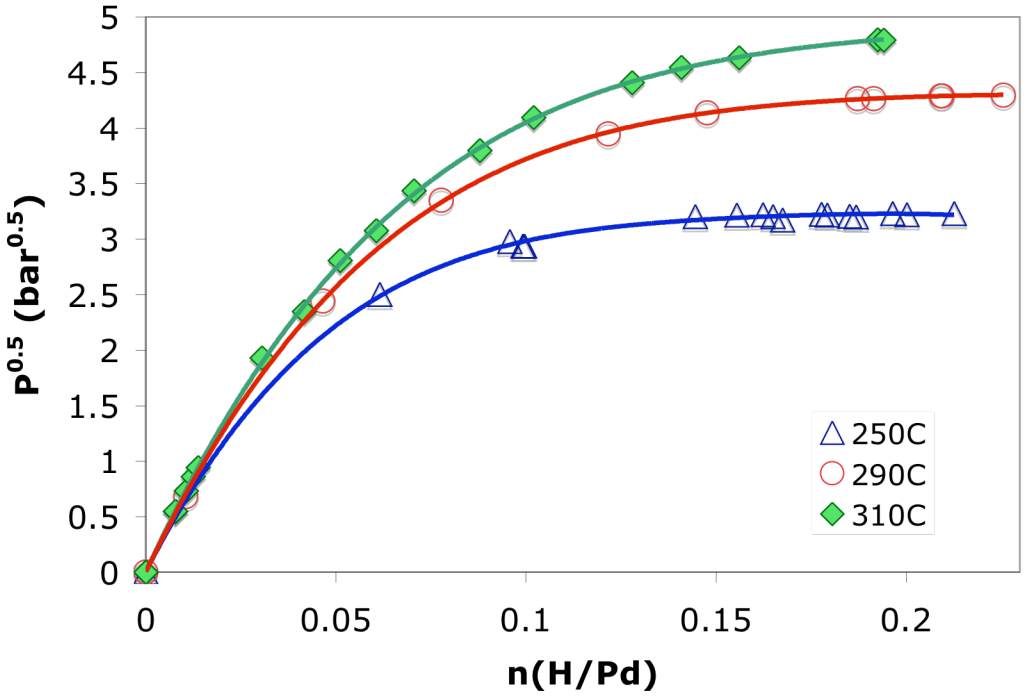

Figure 4-1 $P^{0.5}$ vs. n(H/Pd) data from Gillespie and Galstaun (1936). The experimental data were fitted with a 4^{th} order polynomial function (solid lines)

The H_2 partial pressure exponent is usually called "n" or "n-value" in the literature, yet, in this thesis the H_2 partial pressure exponent will be denoted as n-exponent in order not to confuse it with the H content, n(H/Pd). The experimental data reported by Gillespie and Galstaun (1936) were used to calculate the n-exponent as a function of pressure for the 250, 290 and 310ºC isotherms in Figure 4-1. The n-exponents were calculated by first plotting the raw data (P_{H2} vs. n(H/Pd) of the original publication) in the ($P^{0.5}{}_{H2}$, n(H/Pd)) form for the three isotherms as shown in Figure 4-1. For each isotherm, the ($P^{0.5}{}_{H2}$ vs. n(H/Pd)) experimental points were fitted with a 4^{th} order polynomial function also seen in Figure 4-1.

The 4^{th} order polynomial function was used for the interpolation of the experimental data points between 0 and 0.1 n(H/Pd) at a step of 0.005 n(H/Pd). In order to determine the n-exponent as a function of pressure, the interpolated ($P^{0.5}{}_{H2}$ vs. n(H/Pd)) data were fitted with Equation (4-3) for several 0-n(H/Pd) intervals with n(H/Pd) as high as 0.1. Each 0-n(H/Pd) interval within which the interpolated data ($P^{0.5}{}_{H2}$ vs. n(H/Pd)) were fitted with Equation (4-3) corresponded to a 0-max. pressure interval. For instance, as seen in Figure 4-1, the 0-0.1n(H/Pd) interval corresponded to the 0-8.6 bar (=2.93 $bar^{0.5}$) pressure interval at 250ºC and 0-16.8 bar (=4.8 $bar^{0.5}$) pressure interval at 310ºC. Figure 4-2 shows the n-exponent values calculated for the 250, 290 and 310ºC isotherms as a function of the 0-max. pressure interval. The n-exponent increased as higher values of max. pressure were considered. That is, depending on the pressure range at which the H_2 flux is measured, J_{H2} is proportional to ($P^{0.5}{}_1$- $P^{0.5}{}_2$) at low pressures, for e.g. 1-2 bar, or J_{H2} is proportional to ($P^{0.6}{}_1$- $P^{0.6}{}_2$) in the 1-3.5 bar at 250ºC.

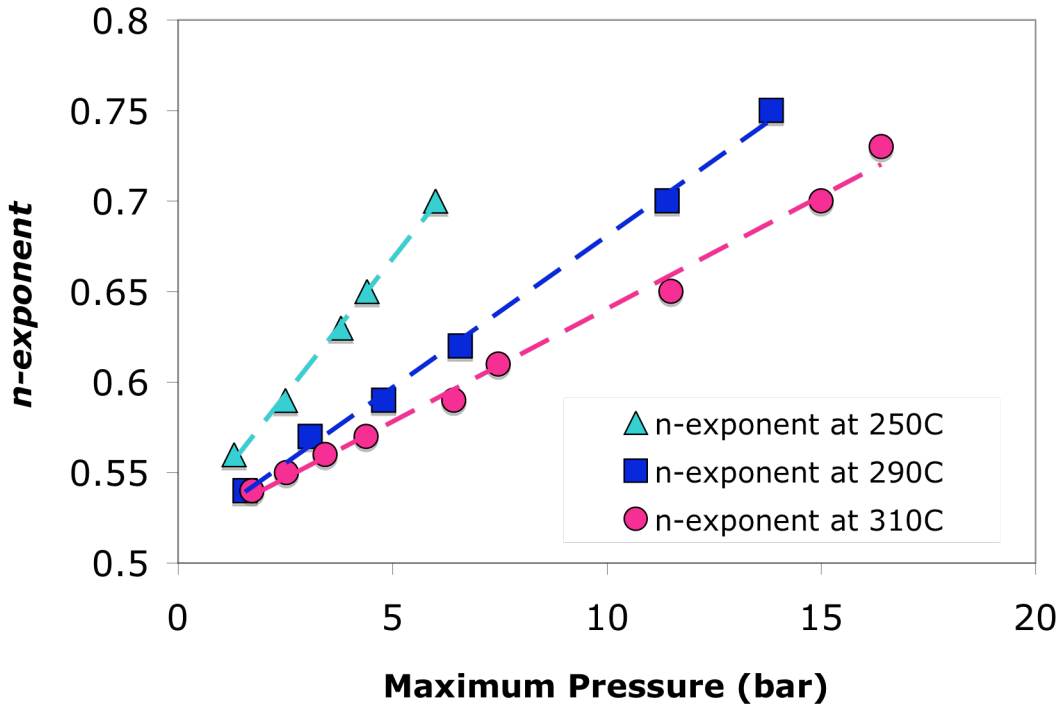

Figure 4-2 n-exponent as a function of maximum pressure for the 250, 290 and 310°C isotherms

The changes in the n-exponent due to the H_2 pressure range at which the H_2 flux is measured are denoted "pressure effects".

4.2.2 The permeation mechanism of H_2 through Pd foils

This section aimed at the establishment of the equation governing H_2 flux through Pd foils. H_2 permeation through Pd involves seven steps depicted in Figure 4-3: (1) H_2 diffusion from the bulk gas to the vicinity of the Pd surface, (2) dissociative adsorption onto the surface, (3) migration of atomic H on the surface into the bulk metal, (4) diffusion through the Pd lattice, (5) transition from the bulk metal to the surface on the permeate side, (6) associative desorption leading to H_2 molecules and (7) diffusion from the surface into the bulk gas. In the absence of external mass transfer, steps (1) and (7) can be neglected. In the case where steps (2)-(3) and (5)-(6) are at thermodynamic equilibrium, which is the case at temperatures higher than 150ºC, and for thick Pd foils (>1 μm), the H diffusion through the Pd lattice, step (4), is the rate-limiting step.

The H_2 flux is then given by Fick's first law, Equation (4-4).

$$J_{H_2} = \frac{D_H}{L_{Pd}}(n(H/Pd)_1 - n(H/Pd)_2) \qquad (4\text{-}4)$$

where J_{H2} is the H_2 flux in $m^3 \cdot m^{-2}\ h^{-1}$, D_H the H diffusivity through Pd in $m^2 \cdot h^{-1}$, L_{Pd} the thickness of the Pd layer in *m* and $n(H/Pd)_1$ and $n(H/Pd)_2$ the H concentrations at the high pressure side and at the low pressure side.

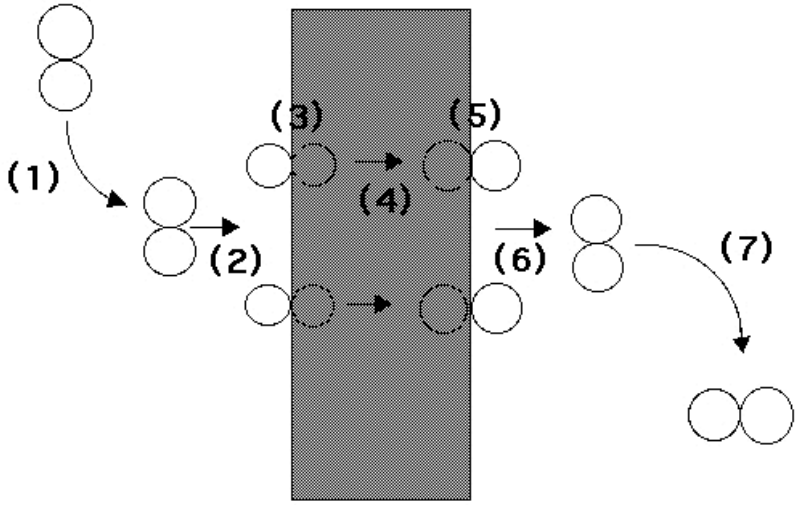

Figure 4-3 H_2 permeation through a freestanding Pd film

Substituting $n(H/Pd)_1$ and $n(H/Pd)_2$ in Equation (4-4) with the expression given in Equation (4-3) leads, after re-ordering, to Equation (4-5).

$$J_{H_2} = \frac{D_H(T) \cdot S_H(T)}{L_{Pd}} (P_1^{n-\exponent} - P_2^{n-\exponent}) \quad (4\text{-}5)$$

In Equation (4-5), S_H(T)=1/K'(T) is the H_2 solubility in the Pd lattice in $\cdot Pa^{-n\text{-}exponent}$. The product $D_H \cdot S_H$ is called H_2 permeability ($m^3\ m\ m^{-2} \cdot h^{-1} \cdot bar^{-n\text{-}exponent}$) and is the magnitude used to compare the H_2 permeation properties of different membranes. The H_2 permeability is temperature dependent via the H_2 diffusion coefficient, following the Arrhenius Equation (4-6), and via the solubility S_H, Equation (4-7)

$$D_H(T) = D_0 \cdot Exp(-\frac{E_{diff}}{R \cdot T}) \quad (4\text{-}6)$$

$$S_H(T) = S_0 \cdot Exp(\frac{\Delta_r H}{R \cdot T}) \quad (4\text{-}7)$$

In Equation (4-6) E_{diff} is the activation energy for H diffusion in $J \cdot mol^{-1}$, R the universal gas constant in $J \cdot mol^{-1} \cdot K^{-1}$ and T the absolute temperature in K. In Equation (4-7), $\Delta_r H$ is the enthalpy of absorption of H_2 in Pd in $J \cdot mol^{-1}$ *H.*

Combining Equations (4-5), (4-6) and (4-7), results in Equation (4-8)

$$J_{H_2} = \frac{Q_0}{L} e^{-\frac{E_p}{RT}} \cdot (P_1^{n-\exponent} - P_2^{n-\exponent}) \quad (4\text{-}8)$$

with

$$Q_0 = D_0 \cdot S_0$$
$$E_p = E_{diff} + \Delta_r H$$

where, E_p is the activation energy of H_2 permeation through Pd in $J \cdot mol^{-1}$. The H_2 flux is further written in terms of H_2 permeability, Q(T) as shown in Equation (4-9)

$$J_{H_2} = \frac{Q(T)}{L_{Pd}} (P_1^{n-\exponent} - P_2^{n-\exponent}) \quad (4\text{-}9)$$

The H_2 permeance is defined as $Q(T)/L_{Pd}$ and is the most important characteristic determined in a Pd foil or a composite Pd membranes. The H_2 permeance is determined as described in Section 3.2.3. Depending on the pressure range used for the determination of the H_2 permeance, "pressure effects" have a large or small contribution to the n-exponent (see Figure 4-2).

4.2.3 The H_2 permeability of clean Pd

The H_2 permeability of the α phase of Pd, given by Equation (4-10), was measured by several researchers on thick Pd foils. Table 4-1 lists the values of Q_0 and E_p reported by Balovnev (1974), Davis (1954), Koffler et al. (1969), Toda (1958), Morreale et al. (2003) and Howard et al. (2004). This section aimed at the establishment of an average value for the H_2 permeability of Pd considering as basis the raw data provided by the above-mentioned authors.

$$Q(T) = Q_0 \cdot e^{\frac{-Ep}{RT}} \tag{4-10}$$

Table 4-1 H_2 permeability for Pd measured in Pd foils in previous works

Q_0 $m \cdot m^3/(m^2\text{-}h\text{-}bar^{0.5})$	Ep kJ/mol	Temp. range ^0C	Press. range bar	Reference
9.821E-03	18.56	200-700	$2.6 \cdot 10^{-5}$-1	(Davis, 1954)
4.396E-03	13.46	170-290	0.047-0.83	(Toda, 1958)
5.612E-03	15.65	27 to 436	$4 \cdot 10^{-7}$-$6.7 \cdot 10^{-5}$	(Koffler et al., 1969)
6.547E-03	15.47	100 to 620	$3 \cdot 10^{-10}$-$6.7 \cdot 10^{-7}$	(Balovnev, 1974)
4.896E-03	13.81	350-900	1-27.6	(Morreale et al., 2003)
2.831E-03	12.97	350-900	1-27	(Howard et al., 2004)

For the determination of the H_2 permeability of Pd, all researchers listed in Table 4-1 considered the n-exponent factor equal to 0.5. In fact, Balovnev (1974), Davis (1954), Koffler et al. (1969) and Toda (1958) experimentally showed that at very low pressures

(see Table 4-1) the H_2 flux was given by Sieverts' law. The average value and the standard deviation for the H_2 permeability of Pd was calculated using the data in Table 4-1 as follows: (1) The Pd H_2 permeability was calculated at 200, 300, 350, 400, 450, 500 and 550ºC using Equation (4-10) and replacing Q_0 and E_p with the numerical values listed in Table 4-1 (six permeabilities values were calculated at each temperature). (2) At each temperature, the average of the six Pd H_2 permeabilities was calculated as well as the standard deviation. The natural logarithm of the averaged Pd H_2 permeability was then plotted as a function of 1/T in order to determine the Q_o and E_p of the average Pd H_2 permeability.

Figure 4-4 shows the calculated Pd H_2 permeability, using the raw data from works listed in Table 4-1, as well as the computed average Pd H_2 permeability, plotted in a logarithmic scale as a function of 1/T. The Pd H_2 permeability reported by authors in Table 4-1, equaled the calculated average Pd H_2 permeability within an error of 30%. Figure 4-5 shows the natural logarithm of the average Pd H_2 permeability, as well as the natural logarithm of the calculated Pd H_2 permeability, plotted as a function of 1/T.

The linear regression performed on the ln(average H_2 permeability) vs. 1/T data led to the expression of the average Pd H_2 permeability, Equation (4-11), that will be considered for the remaining of the thesis to be the Pd H_2 permeability of a Pd foil.

$$Q(T) = Q_0 \cdot e^{\frac{-Ep}{R \cdot T}} = 0.00533 \cdot e^{\frac{-14900}{R \cdot T}} \pm 0.3 \cdot 0.00533 \cdot e^{\frac{-14900}{R \cdot T}} \qquad (4\text{-}11)$$

Hence, the average Pd H_2 permeability pre-exponential factor, Q_0, was determined to be equal to 0.0053 $m^3 \cdot m/(m^2\ h\ bar^{0.5})$ and the activation energy for the average Pd H_2 permeability, E_p, was determined to be equal to 14.9 $kJmol^{-1}$.

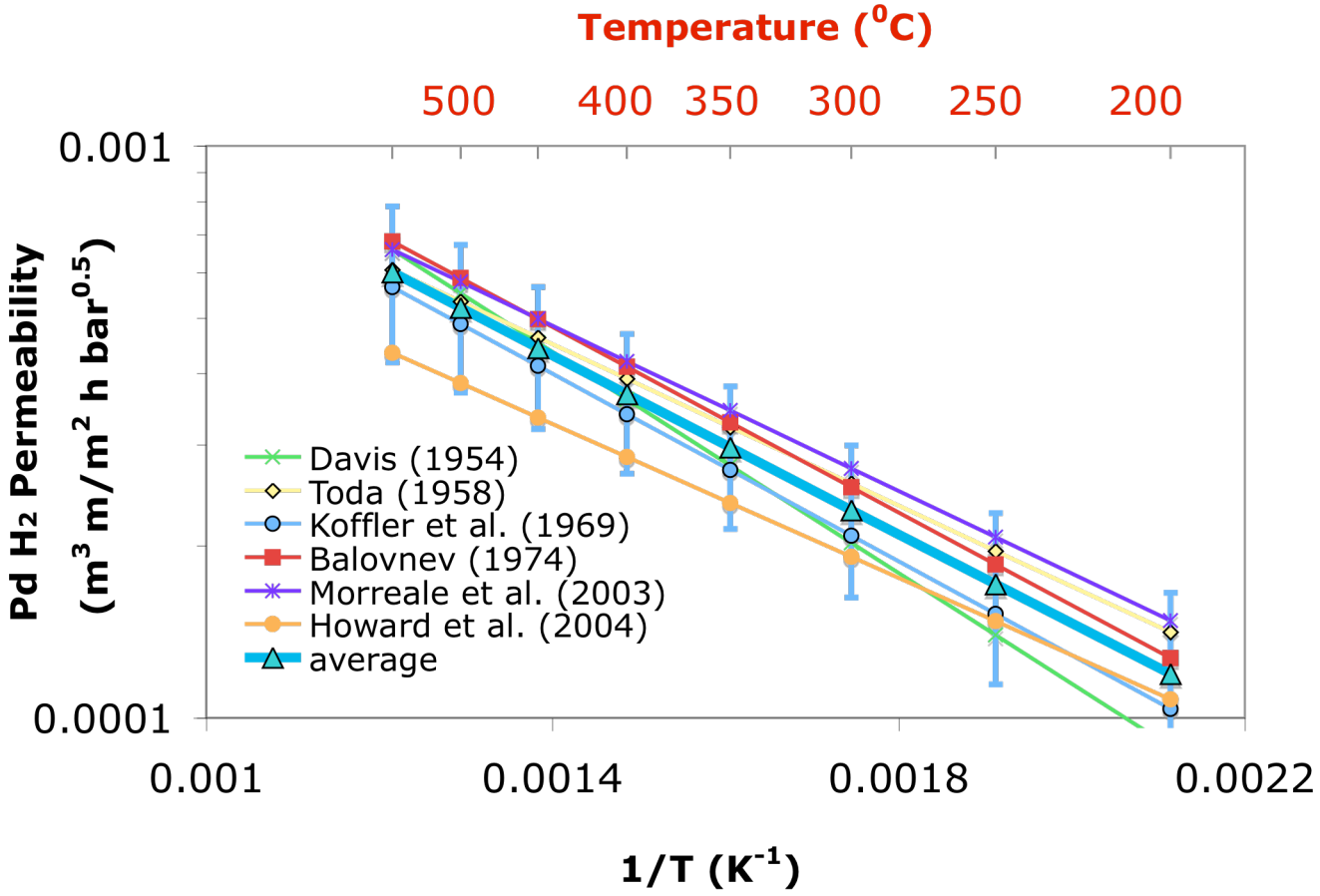

Figure 4-4 Pd H_2 permeability vs. 1/T for all references in Table 4-1

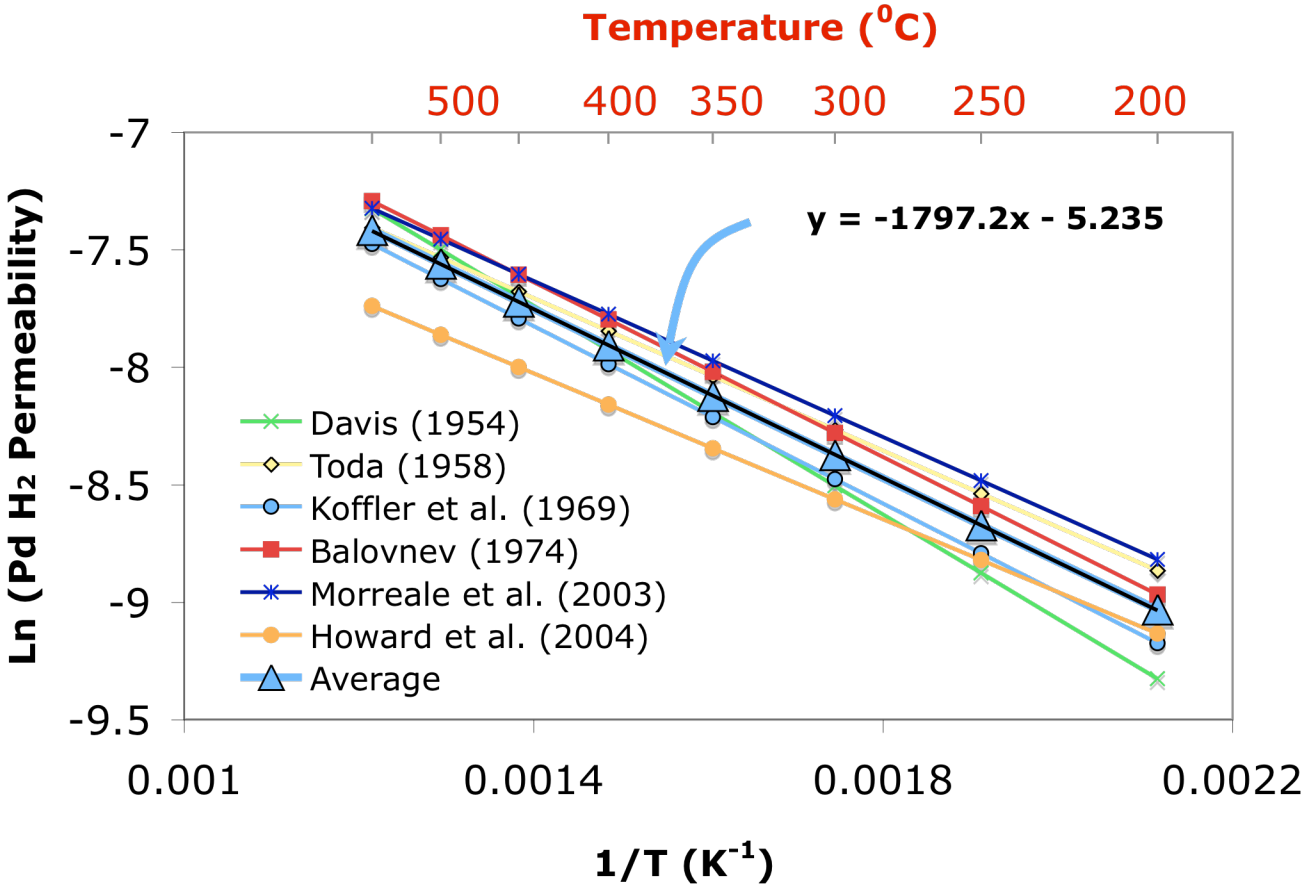

Figure 4-5 Ln(H_2 permeability) vs. 1/T for all references in Table 4-1

5 H_2 permeation through composite Pd membranes

5.1 Introduction

It has been largely accepted that H_2 flux through Pd films (foils and supported membranes) is governed by Equation (4-8).

$$J_{H_2} = \frac{Q_0 \cdot e^{-\frac{E_p}{R \cdot T}}}{L_{Pd}} \cdot (P_1^{n-\exponent} - P_2^{n-\exponent}) \qquad (4\text{-}8)$$

As already described in Chapter 4, H_2 permeation mechanism through a freestanding Pd film is a complex process involving several steps. The presence of a porous substrate on the low pressure side of this Pd film adds a degree of complexity, since H_2 also needs to flow through the porous media. Factors leading to deviations from Sieverts' law were already listed and are: the thickness of the Pd film when lower than 1 μm (Ward and Dao, 1999), surface poisoning, the presence of leaks, the presence of mass transfer resistance within the porous support and high H_2 pressures ("pressure effects"). All these factors alter the parameters in Equation (4-8) that can be determined from the measurement of H_2 flux as a function of pressure and temperature. These parameters are: the H_2 permeance F, the H_2 pressure exponent n-exponent and the activation energy for H_2 permeation E_P.

Surface poisoning, which is the adsorption of contaminants such as C, CO, CO_2 or hydrocarbons on the Pd surface, leads to a decrease in the adsorption rate of H_2. If the poisoning is too severe, reactions at the surface become the rate-limiting step for the H_2

permeation. Air oxidation at 300-450ºC was used for the removal of adsorbed CO, CO_2, methylcyclohexane (MCH), sulfur and chlorine in Pd-Ag membranes (Ali et al., 1994; Keuler and Lorenzen, 2002; Tosti et al., 2002). In some cases, an increase in H_2 permeance was observed (Ali et al., 1994) and was attributed to surface morphology changes. Auger spectroscopy of Pd thin foils was performed before and after air oxidation at 300ºC for 5 min (Yamakawa et al., 2003) and showed that carbon impurities (60at% on the surface) were removed as CO_2. Another important effect of air oxidation is the roughening of the Pd surface by the formation of a nano-structured oxide (Aggarwal et al., 2000; Han et al., 2004; Roa et al., 2003). An increase in surface area up to 50% was measured by Han et al. (2004) in Pd single crystals after exposure in oxygen at 600K, 1-150 torr for 10 min. Therefore, the overall effect of air oxidation resulted in a cleaner and rougher surface, which led to a highly activated Pd surface after reduction in H_2 atmosphere. The catalytic surface of Pd-6wt% Ru was modified by boiling in CCl_4, rinsing with HCl and annealing in H_2 at 700-800ºC, the H_2 permeance of the tube was enhanced by a factor of 2 and was attributed to the formation of an active porous layer due to the dissolution of the alloy components (Roshan et al., 1983). The H_2 permeability of Pd at low temperatures was also enhanced by the deposition of a thin layer (200 Å) of Pd black from glow discharges (Radzhabov et al., 1980). In both works (Radzhabov et al., 1980; Roshan et al., 1983) the increase in H_2 permeability was attributed to the increase of H dissolved in the inlet side of the membrane.

The H_2 flux through defects (cracks and/or pinholes in the Pd film), which is denoted as leaks, occurs via a mixed Knudsen-viscous mechanism (slip-flow) (Mardilovich et al., 1998). Therefore, the H_2 flux through defects can be expressed by the sum of a term pro-

portional to the pressure difference (Knudsen flow) and a term proportional to the square of the pressure (viscous flow). Hence, in a composite Pd membranes having large leaks the pressure exponent n-exponent will be higher than 0.5. Moreover, Knudsen-viscous mechanism is characterized by the activation energy of gas diffusion, which is lower compared to the activation energy of solution diffusion. Therefore, if large leaks are present, the activation energy for H_2 permeation will be lower than 12-20 kJ/mol (see Table 4-1).

Mass transfer within the porous support adds another resistance to the overall H_2 permeation mechanism. If L_{Pd} is thin enough and the porous support does not have a high inert gas permeance, which is the case in supports having a low porosity, the pressure drop within the porous support is high and the H_2 diffusion within the porous media becomes the rate-limiting step for the H_2 permeation. If H_2 diffusion through the porous media is the rate-limiting step, the pressure exponent n-exponent is higher than 0.5 and the activation energy for H_2 permeation decreases.

The primary objective of the models and experiments described in this chapter was to investigate the factors affecting the mechanism of H_2 permeance through composite Pd membranes. The effects of leaks and mass transfer within the porous support were modeled to determine the conditions under which the H_2 permeation mechanism would be strongly affected by leaks or mass transfer. The relation between the Pd surface activity and the n-exponent was also studied.

5.2 Theory

5.2.1 The model of mass transfer within the porous support

The model described in this section has the aim of estimating to what extent and in what manner mass transfer resistance within the support influences on the H_2 permeation, the H_2 pressure n-exponent and the activation energy for H_2 permeation E_p. The thickness of the thin Pd film was always negligible compared to the outside diameter (OD) of the support, therefore, the mass transfer equations were written in a planar geometry. A sketch of a composite Pd/substrate structure is given in Figure 5-1.

The H_2 flux through the dense Pd layer, J_1, is given by Sieverts' law, Equation (5-1).

$$J_1 = \frac{Q(T)}{L_{Pd}} \cdot (P_1^{0.5} - P_2^{0.5}) \tag{5-1}$$

with $Q(T)$ the H_2 permeability in $m^3/(m^2\ h\ bar^{0.5})$ at the temperature T, L_{Pd} the membrane thickness and P_1 and P_2 the high and low H_2 pressure. The average Pd H_2 permeability $Q(T)$ was estimated in Section 4.2.3 and is given by Equation (4-11).

$$Q(T) = Q_0 \cdot e^{\frac{-Ep}{R \cdot T}} = 0.00533 \cdot e^{\frac{-14900}{R \cdot T}} \tag{4-11}$$

The H_2 flux through the porous support, J_2, was given by the dusty-gas model as shown in Equation (5-2). This approach was also undertaken to study the mass transport in asymmetric alumina membranes (Thomas et al., 2001).

$$\begin{aligned} J_2 &= [\alpha_{H_2}(T) + \beta_{H_2}(T) \cdot (\frac{P_2 + P_3}{2})] \cdot (P_2 - P_3) \\ &= [\frac{2}{6}\sqrt{\frac{8}{\pi}} \frac{\varepsilon \mu_k d}{L_{subs}\sqrt{RTM_{H_2}}} + \frac{1}{32} \frac{\varepsilon \mu_v d^2}{L_{subs}\eta_{H_2} RT} \cdot (\frac{P_2 + P_3}{2})] \cdot (P_2 - P_3) \end{aligned} \tag{5-2}$$

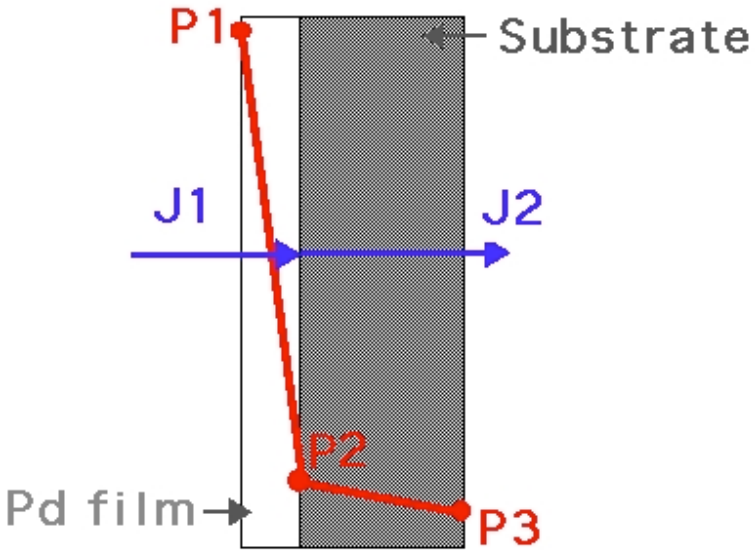

Figure 5-1 Scheme of a composite Pd-porous substrate structure.

The $\alpha_{H2}(T)$ and $\beta_{H2}(T)$ parameters were determined from He permeation measurements at room temperature (T=293K). The He flux of the bare support, without the Pd coating, was measured at 5-10 different pressures P_1 after the grading step or after the oxidation step. The permeate pressure, P_2, was kept at atmospheric conditions. The raw data (J_{He}, P_1) were then plotted in the ($J_{He}/(P_1-P_{atm})$, $(P_1+P_{atm})/2$) form and fitted with Equation (5-2) to finally obtain $\alpha_{He}(293)$ and $\beta_{He}(293)$. Figure 5-2 shows the experimental data ($J_{He}/(\Delta P)$, P_{ave}) collected after the grading of C01-F11a/b membrane' s support as an example. It was also possible to measure $\alpha_{H2}(293)$ and $\beta_{H2}(293)$, and even $\alpha_{H2}(T)$ and $\beta_{H2}(T)$ at different temperatures. However, the measurement of $\alpha_{H2}(T)$ and $\beta_{H2}(T)$ required to place the bare support in a reactor, which implied the same safety procedures as when characterizing membranes. Therefore, for simplicity reasons $\alpha_{H2}(T)$ and $\beta_{H2}(T)$ were determined using $\alpha_{He}(293)$ and $\beta_{He}(293)$.

$\alpha_{H2}(T)$ and $\beta_{H2}(T)$ were readily calculated from $\alpha_{He}(293)$ and $\beta_{He}(293)$ by substituting M_{He} and η_{He} in the expression of α_{He} and β_{He} parameters using Equation (5-3).

$$\begin{aligned} J_2 &= [\alpha_{H_2}(T) + \beta_{H_2}(T)\frac{P_2 + P_3}{2}]\cdot(P_2 - P_3) \\ &= [\alpha_{He}(293)\cdot\sqrt{\frac{293}{T}}\sqrt{\frac{M_{H_e}}{M_{H_2}}} + \beta_{He}(293)\cdot\frac{293}{T}\frac{\eta_{He}(293)}{\eta_{He}(T)}\frac{\eta_{He}(T)}{\eta_{H_2}(T)}(\frac{P_2 + P_3}{2})]\cdot(P_2 - P_3) \end{aligned} \quad (5\text{-}3)$$

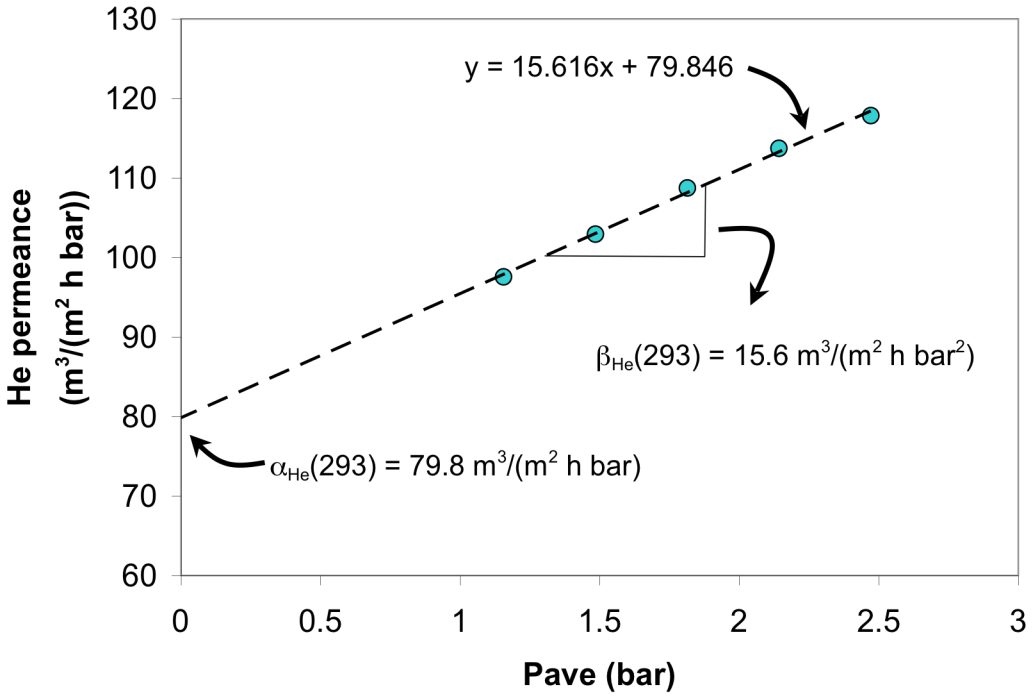

Figure 5-2 He permeance vs. P_{ave} for the graded support of C01-F11a/11b membranes

The ratio η_{He}/η_{H2} was taken to be equal to 2.29, which was the average ratio of the He viscosity over the H_2 viscosity in the 20-500ºC temperature range. At steady state J_1 equals to J_2 leading to Equation (5-4).

$$\frac{Q(T)}{L_{Pd}} \cdot (P_1^{0.5} - P_2^{0.5}) = [\alpha_{H_2}(T) + \beta_{H_2}(T) \cdot (\frac{P_2 + P_3}{2})] \cdot (P_2 - P_3) \qquad (5\text{-}4)$$

The calculations were performed as follows. (1) L_{Pd}, known from gravimetric measurements or SEM micrographs, and the temperature T were set, (2) a given H_2 pressure value ranging within the 0-5 bar was given to P_1, (3) P_3 was kept equal to 1 bar, (4) P_2, the only unknown in Equation (5-4), was solved numerically and, (5) the H_2 flux was then computed using either Equation (5-1) or Equation (5-2). For each temperature T, ten H_2 fluxes were computed at the following P_1 pressures: 1.2, 1.5, 2, 2.5, 3, 3.5, 4, 4.5, 5 and 5.5 bar. The computed data (J_{H2}, P_1, P_3) were then fitted with Equation (3-2) to determine $F_{0.5}$ and with Equation (3-3) to determine the F_n and the n-exponent.

$$J_{H_2} = F_{0.5} \cdot (P_1^{0.5} - P_3^{0.5}) \qquad (3\text{-}2)$$

$$J_{H_2} = F_n \cdot (P_1^{n-\exponent} - P_3^{n-\exponent}) \qquad (3\text{-}3)$$

Mass transfer limitations arise when the H_2 flux through the Pd layer is too large compared to the H_2 flow the support can convey without large pressure drops. That is, a parameter, ξ, that compares the resistance for the H_2 flux through the Pd layer and the resistance for the H_2 flux through the porous support, gives information on the presence of mass transfer effects in a composite Pd membrane. ξ was defined by the ratio of the resistance of H_2 flux through the Pd layer (ΔP=1 bar, $\Delta P^{0.5}$=0.4142 $bar^{0.5}$) over the resistance of the H_2 flux through the support (ΔP=1 bar, P_{ave}=1.5 bar) both estimated from H_2 fluxes at 250ºC and ΔP=1 bar (2:1). ξ_{250} is given by Equation (5-5).

$$\xi_{250} = \frac{R_{Pd}}{R_{\sup port}} = \frac{\left(\frac{1}{J_{H_2,Pd}}\right)_{\Delta P=1,250C}}{\left(\frac{1}{J_{H_2,\sup port}}\right)_{\Delta P=1,250C}} = \frac{[\alpha_{H_2}(T) + \beta_{H_2}(T)\frac{P_1+P_2}{2}]\cdot(P_1-P_2)}{\frac{Q(T)}{L_{Pd}}\cdot(P_1^{0.5}-P_2^{0.5})}$$

$$with,\ \ T = 523\cdot K,\ \ P_1 = 2\cdot bar,\ \ P_2 = 1bar \qquad (5\text{-}5)$$

$$\xi_{250} = \frac{[\alpha_{He}(293)\cdot\sqrt{\frac{293}{523}}\sqrt{\frac{M_{He}}{M_{H_2}}} + \beta_{He}(293)\cdot\frac{293}{523}\frac{\eta_{He}(293)}{\eta_{He}(523)}\frac{\eta_{He}(523)}{\eta_{H_2}(523)}(\frac{3}{2})]\cdot 1}{\frac{Q(523)}{L_{Pd}}\cdot(\sqrt{2}-1)}$$

5.2.2 The leak model

In a composite Pd membrane, H_2 diffuses through the lattice of palladium, along the Pd grain boundaries and also along the defects within the thin Pd layer. Figure 5-3, shows the diffusion of H through the Pd lattice according to a "solution diffusion" mechanism and the diffusion of molecular hydrogen (H_2) along defects in a Pd thin film.

The flow of H_2 through defects can lead to the overestimation of the H_2 that permeates through the "solution diffusion" mechanism. This section describes a model that provides the basis for the establishment of the minimum selectivity (H_2/He) a composite Pd membrane should have in order to consider the effects of leaks on the H_2 permeating according to the "solution diffusion" mechanism negligible. The minimum selectivity is determined is Section 5.4.2.

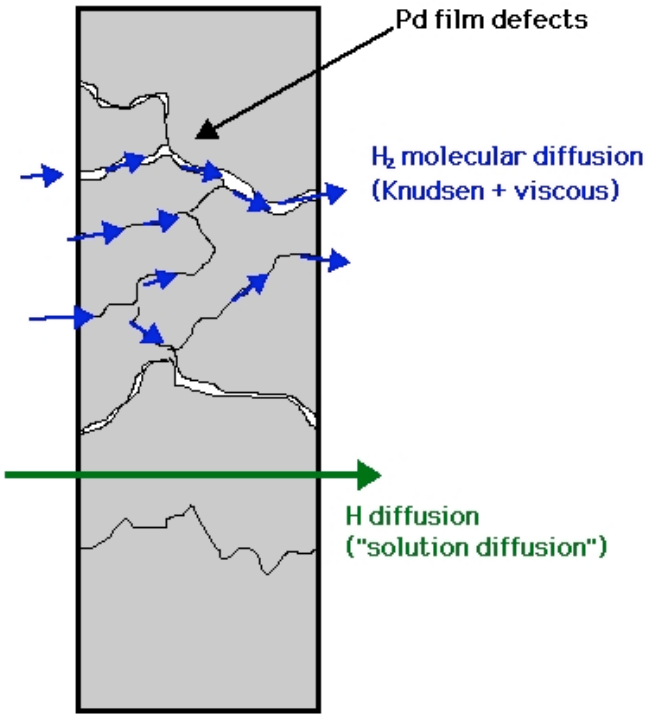

Figure 5-3 The diffusion of H through Pd lattice ("solution diffusion") and the diffusion of H_2 through defects

The total H_2 flux permeating through the Pd foil, shown in Figure 5-3, is equal to the sum of the H_2 permeating according to the "solution diffusion" mechanism and the H_2 permeating along the defects. The model is based on the following assumptions:

- The H_2 flux permeating according to the "solution diffusion" mechanism is independent on the selectivity value. The H_2 permeance of the freestanding Pd foil is set equal to 10 $m^3/(m^2\ h\ bar^{0.5})$. The H_2 flux permeating through the Pd lattice follows Sieverts' law.
- Molecular H_2 diffuses through the defects according to a mixed Knudsen-viscous mechanism. The amount of H_2 flowing through defects was estimated from the flow of He (the He leak) diffusing through the defects. The same approach was taken by Mardilovich et al. (1998) to describe inert gas flow through composite Pd membranes with defects.

The calculations were performed according to the following procedure:

(1) A selectivity value, which was assumed to be determined at a ΔP=1bar (2:1), was set.

(2) The He flux, J_{He}, at a ΔP=1bar (2:1) was calculated according to equation (5-6).

$$J_{He} = \frac{F_{0.5} \cdot \Delta P^{0.5}}{Selectivity} \qquad (5\text{-}6)$$

In Equation (5-6), $\Delta P^{0.5}$ stands for $P^{0.5}_{shell} - P^{0.5}_{tube}$. For the calculations, P_{shell} was set to 2 bar and P_{tube} was set to 1 bar. As already mentioned, the H_2 permeance of the freestanding Pd foil, $F_{0.5}$, was set equal to 10 $m^3/(m^2\ h\ bar^{0.5})$.

(3) The He flux, J_{He}, was equal to the sum of a Knudsen, α, and a viscous, $\beta \cdot P_{ave}$, contribution according to Equation (5-7).

$$J_{He} = [\alpha \cdot + \beta \cdot P_{ave}](\Delta P) \quad (5\text{-}7)$$

An r value was set to calculate α and β. Indeed, in order to calculate α and β the contribution of the Knudsen flow to the overall leak had to be set. Therefore, r values ranging from 0 (leak dominated by viscous flow) to 1 (leak dominated by Knudsen flow) were assumed for the calculations. α, β and r are given by Equation (5-8).

$$r = \frac{\alpha}{\alpha + \beta \cdot P_{ave}}$$
$$\alpha = r \cdot \frac{J_{He}}{\Delta P} \quad (5\text{-}8)$$
$$\beta = \frac{J_{He}}{\Delta P} \cdot \frac{(1-r)}{P_{ave}}$$

where ΔP and P_{ave} are the pressure difference and average pressure at which the He leak was assumed (ΔP=1 bar and P_{ave}=1.5 were used in the calculations).

(4) the total H_2 flux (the sum of the H_2 flowing through defects and the H_2 flowing through the Pd lattice) was estimated at several P_{shell} values in the 0.2-4.5 bar pressure range according to Equation (5-9). P_{tube} was always set to 1 bar.

$$J_{H2} = F_{0.5} \cdot (\Delta P^{0.5}) + [\alpha \cdot \sqrt{\frac{M_{He}}{M_{H2}}} \cdot + \beta \cdot \frac{\eta_{He}}{\eta_{H2}} \cdot P_{ave}](\Delta P) \quad (5\text{-}9)$$

In Equations (5-9), the H_2 flux is the sum of a solution diffusion term, a Knudsen term and viscous term. All pressures in Equation (5-9) are H_2 partial pressures. For the sake of simplicity, the coefficient (η_{He}/η_{H2}) was assumed to be 2.29, which was the average ratio of the He viscosity over the H_2 viscosity in the 250-500ºC temperature range.

Figure 5-4 shows as example the calculated J_{H2} for r = 0 and a selectivity value of 40. At high pressures, the calculated J_{H2} (r=0, selectivity=40) deviates significantly from the J_{H2} this hypothetical Pd film would show at infinite selectivity i.e. for the calculated J_{H2} with selectivity=∞. The same type of data was computed for r=0, 0.2, 0.4, 0.6, 0.8 and 1 and selectivity=10, 20, 30, 40, 50, 100, 200, 300 and 400.

All computed (H_2 flux, P_{shell}) data were then fitted with Equation (3-2) to determine H_2 permeance assuming Sieverts' law ($F_{0.5}$), and also with Equation (3-3) to determine H_2 permeance (F_n) and the n-exponent as described in Section 3.2.3.

5.3 Experimental

Membranes C01-F03/4/5/7 were prepared on non-graded supports following the preparation procedure described in the experimental Chapter 3. Membranes C01-F08, C01-F011, C01-F011b, Ma-32, Ma-32b, Ma-34b, Ma-41 and Ma-42 were prepared on "graded" supports.

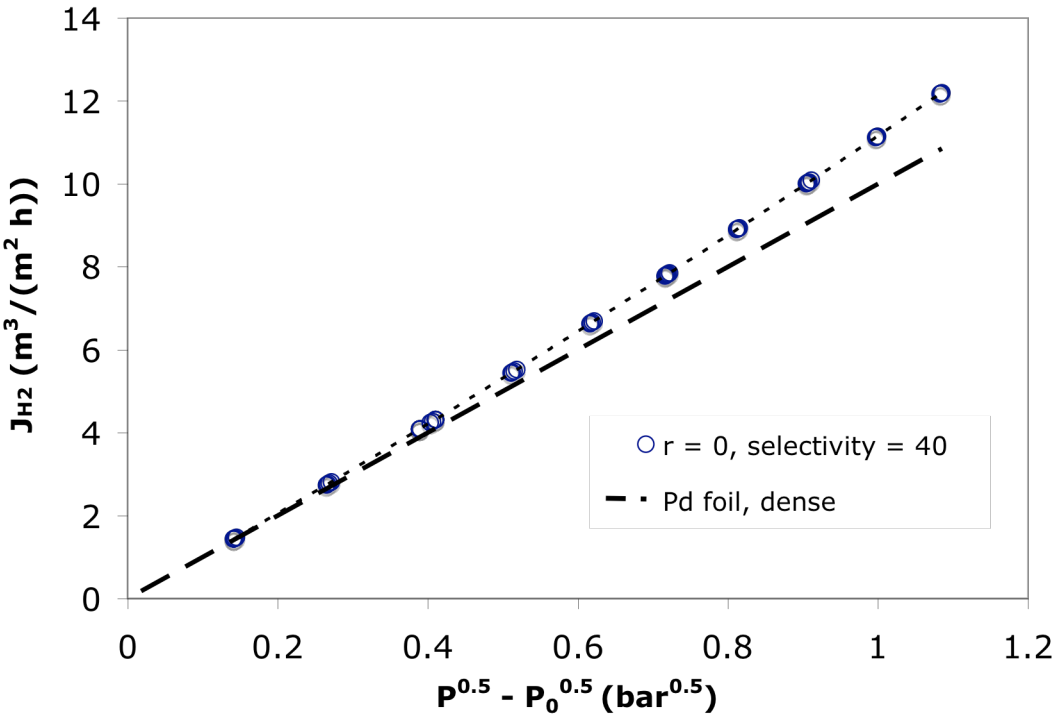

Figure 5-4 Calculated J_{H2} as function of ($P^{0.5}$-$P^{0.5}{}_0$) with r=0 and selectivity =40 (open circles) and selectivity =∞ (dashed line).

The graded supports were synthesized according to the experimental protocol described in Section 3.1.2. For membranes Ma-32, Ma-32b, Ma-34b and Ma-42 only the mass transfer within their porous supports was studied in order to provide sufficient proof for the mass transfer model presented in Section 5.2.1. The particular structure and H_2 permeation properties of membranes Ma-32, Ma-32b, Ma-34b and Ma-42 will be discussed in great detail in Chapter 6.

5.4 Results and discussion

5.4.1 The relevance of the n-exponent in this work

This section aims at understanding the relevance of the n-exponent. As an example, the experimental results from composite Pd membrane C01-F03 are shown.

Figure 5-5 shows the H_2 flux at 300ºC for membrane C01-F03 as a function of the Sieverts' driving force ($P^{0.5}_1$- $P^{0.5}_2$). The H_2 permeance at 300ºC, assuming that the Sieverts' law was followed, was 6.83 $m^3/(m^2\ h\ bar^{0.5})$. Residuals ($H_{2\ exp\ flux} - H_{2\ calc\ flux}$) are also plotted as a function of the Sieverts' driving force in Figure 5-5 (squares) and showed a distinctive polynomial trend. The same trend was found at all temperatures at which all membranes were tested, indicating that the Sieverts' law was not followed and that the pressure exponent was different from 0.5. The H_2 permeance had therefore to be determined by adjusting the n-exponent (Equation (3-3)). Adjusting the n-exponent resulted in a H_2 permeance equal to 5.0 $m^3/(m^2\ h\ bar^{0.63})$ and an n-exponent equal to 0.63. The residuals (crosses in Figure 5-5) lie very close to the value of zero indicating a better fit.

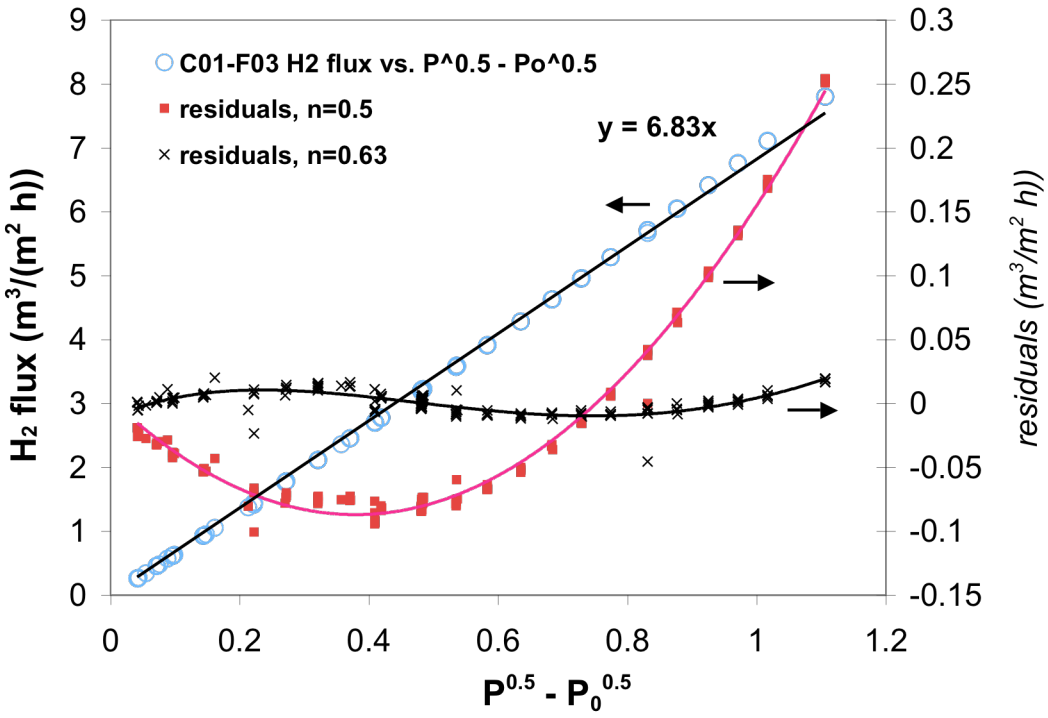

Figure 5-5 H_2 flux and residuals as a function of $P^{0.5}$-$P^{0.5}{}_0$ at 300ºC for membrane C01-F03.

The natural logarithm of the H_2 permeance of membrane C01-F03, calculated by both methods (linear fit with n=0.5 and non-linear regression to determine *n-exponent* and F_n), is plotted in Figure 5-6 as a function of 1/T. The slight decrease of the permeance above 325ºC was due to intermetallic diffusion. Figure 5-6 shows two temperature regions: the 250-400ºC temperature interval, which was characterized by a fast decrease in the n-exponent and a second temperature window 400-500ºC, which was characterized by a rather constant n-exponent.

The n-exponent of membrane C01-F03 decreased as the temperature was increased. At 250ºC the n-exponent was equal to 0.66 and decreased to 0.55 at 400ºC. The n-exponents within the 250-400ºC temperature range were higher than the n-exponents predicted by calculations performed on the experimental isotherms (see Figure 4-1 and Figure 4-2). The high n-exponents measured for C01-F03 were due to the adsorption of impurities on the Pd surface, thereby decreasing the rate of H_2 absorption/desorption reactions. The n-exponents of C01-F03 decreased as temperature was increased following the trend predicted by the calculations on the Pd-H phase diagram (see Figure 4-2). At temperatures higher than 400ºC the pressure exponent of C01-F03 was very close to 0.5 as shown in Figure 5-6. It is interesting to note that the pressure effects (the increase in the n-exponent due to the determination of the H_2 permeance in the 0-4.5 bar pressure range) vanished at a temperature higher than 350ºC, which was in agreement with the predictions of Ward and Dao (1999).

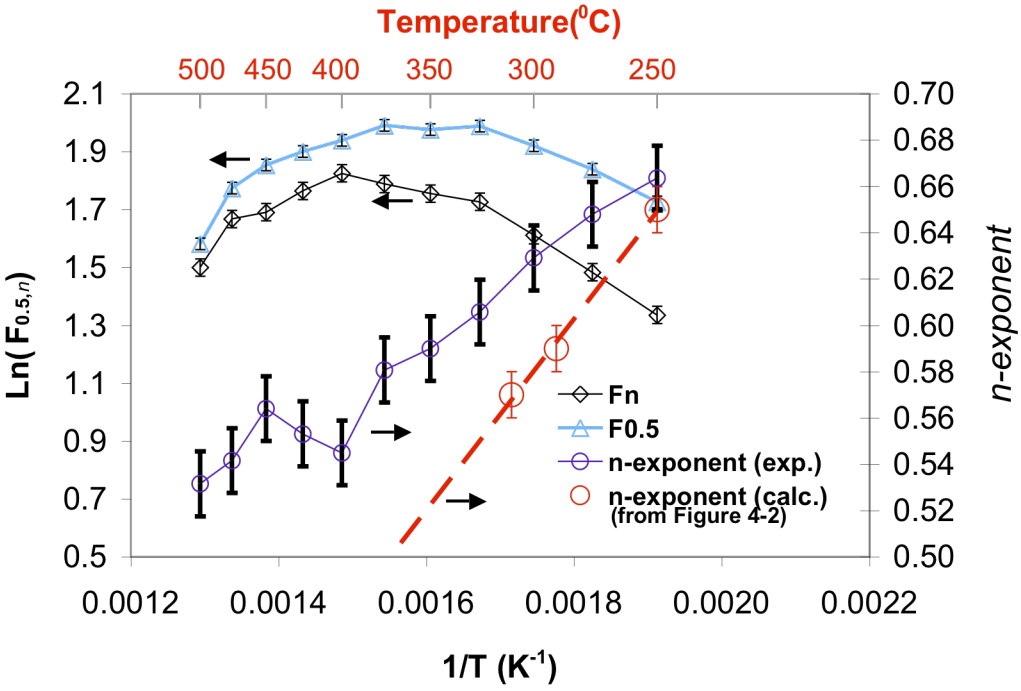

Figure 5-6 Ln(F_n), Ln($F_{0.5}$) and n-exponent for membrane C01-F03 as a function of 1/T.

The decrease of the n-exponent seen for membrane C01-F03 in the 250-400ºC temperature range has also been reported by several authors. Decreasing n-exponents from 0.62 at 450ºC to 0.55 at 600ºC were reported by Collins and Way (1993) on composite Pd-Al_2O_3 membranes. The decrease in n-exponent was attributed to the removal of surface contaminants present on the fresh surface of the membrane. However, n-exponents reported by Collins and Way (1993), were higher than n-exponents seen in membrane C01-F03 at 450ºC. The difference in n-exponents was due to the wider pressure range considered by them (up to 27 bar).

Deviations from the Sieverts' law at temperatures lower than 400ºC (see Figure 5-6) were mainly attributed to the non-linear H_2 absorption isotherms (high H_2 pressure effects) and secondly to the poor catalytic properties of the Pd surface due to the presence of contaminants adsorbed on the surface. The contaminant adsorbed on the surface of fresh composite Pd membranes come form the plating bath, which contains EDTA and ammonia. Theoretically the n-exponent should have been equal to 0.5 (Sieverts' law) at 500ºC however, imperfections formed at high temperatures leading to Knudsen and viscous flow. Indeed, the selectivity (H_2/He) of membrane C01-F03 was just above 100 at the end of the characterization. Indeed, Section 5.4.2 shows that the n-exponent is higher than 0.5 in membranes having selectivities lower than 300. Membranes C01-F03/4/5, which were proven to have no mass transfer limitations (see Section 5.4.3.2), had n-exponent values around 0.6 at 250ºC and around 0.53 at 500ºC. Hence the n-exponent value decreased as temperature was increased for all composite Pd membranes characterized in this study.

It is important to acknowledge the fact that the n-exponent value is slightly different form 0.5 and that the n-exponent is a decreasing function of the temperature. Although, in order to be able to compare the H_2 permeance of all membranes, and also, in order to be able to determine the activation energy for H_2 permeation in any temperature range, Sieverts' law is required to be assumed. The assumption of Sieverts' law is valid since the experimental n-exponents were very close to 0.5. Moreover, all composite Pd membranes prepared in this work had dense Pd layers thicker than 5 μm, were tested at temperatures higher than 250ºC and feed H_2 pressures higher than 1 bar. Therefore, the rate-limiting step for H_2 permeation was the H diffusion through Pd bulk according to calculations performed by Ward and Dao (1999). From this point in the thesis, the H_2 permeance of any composite Pd membrane will be determined assuming the H_2 flux is proportional to $(P^{0.5}-P^{0.5}{}_0)$ and $F_{0.5}$ will be determined fitting $(J_{H2}, (P^{0.5}-P^{0.5}{}_0))$ data with Equation (3-2). Also, the n-exponent, which was always calculated for verification purposes, was used as a tool to understand if any other effect such as leakages, mass transfer resistance within the support or surface activity, had a strong influence on the H_2 permeation mechanism. For all composite Pd membranes prepared in this work, H diffusion through the Pd bulk was the rate-limiting step for hydrogen permeation in the absence of mass transfer, leakages and clean surfaces.

5.4.2 The effects of leaks on H_2 flux

This section aimed at the establishment of the minimum selectivity a composite Pd membrane should have in order to consider the effects of leaks on the determination of the H_2 permeating according to the "solution diffusion" mechanism negligible. The results obtained from the He leak model in Section 5.2.2 are discussed.

Figure 5-7(a) shows the H_2 permeation F_n as a function of selectivity (H_2/He at ΔP=1bar, see Equation (5-6)) for r values ranging between 0 and 1 for the hypothetical Pd foil of Section 5.2.2. Figure 5-7(b) shows the n-exponents as a function of selectivity (H_2/He at ΔP=1bar) for the same r values. The presence of leaks led to the increase of the H_2 pressure exponent. The area between r=0 and r=1 curves can be denoted as the leak envelope and for any experimental point (n-exponent, selectivity) lying in such an envelope its n-exponent is essentially explained by the leak of the membrane. For example, from Figure 5-7(b) the n-exponent of a composite Pd membrane with a selectivity of 300 and r=0 is 0.52. An n-exponent of 0.52 is considered to be equal to 0.5, since n-exponents were determined with a precision of 0.02. Therefore, it can be concluded that when the selectivity of a membrane is above 300, leaks do not have any significant effect on either H_2 permeance or n-exponent. In other words, if n>0.50 and the selectivity is higher than 300 the reasons for n>0.5 are due to factors other than defects.

From the measurement of the He permeance in all membranes and at many temperatures, it was found that r was never lower than 0.6. If we now consider r equal to 0.6, the necessary selectivity to make the n-exponent increase by 0.02 units (0.02 was the precision achieved in the determination of the n-exponent) was around 150-200 as seen in Figure 5-7(b). Therefore, the effects of leaks in a composite Pd membrane with a selectivity of 200 or higher were considered as negligible on the n-exponent and the H_2 permeance $F_{0.5}$.

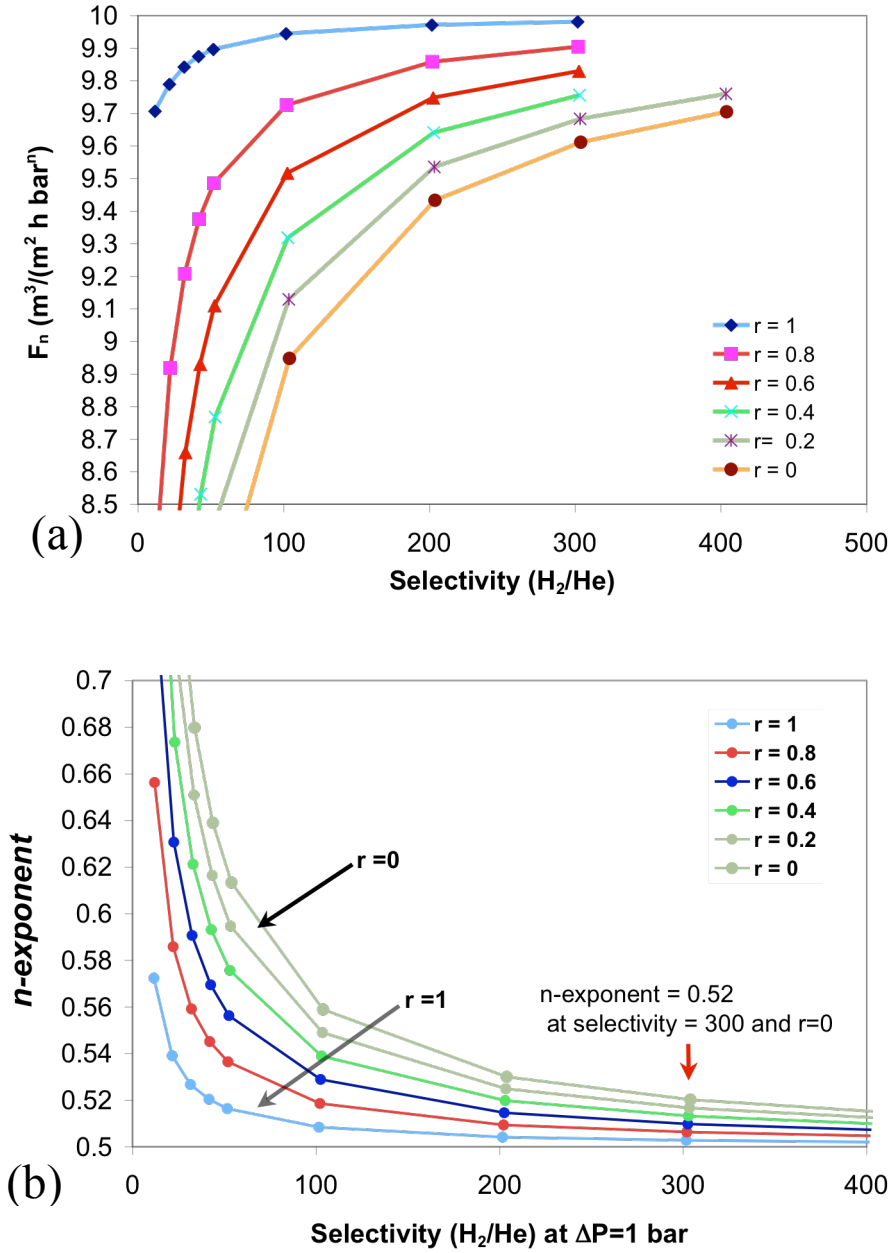

Figure 5-7 (a) F_n vs. selectivity (b) n-exponent vs. selectivity for different r ratios

Figure 5-8 shows the H_2 permeance of the Pd film in Section 5.2.2 one would measure ($J/(P_1^{0.5}-P_3^{0.5})$) assuming Sieverts' law is valid (n=0.5) for different values of r.

As expected the presence of leaks led to an overestimation of the real H_2 permeance (10 $m^3/(m^2\ h\ bar^{0.5})$). For a membrane having a selectivity of 200 and a leak with a Knudsen contribution equal to or higher than 0.6, the computed overestimation in H_2 permeance was only equal to 1.3% of the film's true H_2 permeance. The H_2 permeance was measured within a precision of 2%, which was higher than the computed increase in H_2 permeance due to the leak. Hence, as already stated, leaks did not have significant effects on the measurement of H_2 permeance and n-exponent when the selectivity was over 200 measured at ΔP=1 bar (2:1).

In order to understand the effect of membrane defects on the H_2 permeation and also to validate the n-exponent/selectivity model, two composite Pd membranes, C02-F01 and C02-F03, with large defects were studied. Their initial He leak at 250ºC just before the H_2 introduction was high and equaled $2.95\cdot10^{-3}$ $m^3/(m^2\ h\ bar)$ for C02-F01 and $1.06\cdot10^{-3}$ $m^3/(m^2\ h\ bar)$ for C02-F03. The He leak and selectivity were determined at each temperature after changing from H_2 to He. Two measurements of the He leak were performed at each temperature separated by 24 hr. The calculated n-exponents and selectivities as a function of temperature are plotted in Figure 5-9 for both membranes. As expected, the membrane having the larger defects (large He leak) showed higher n-exponents at any given temperature.

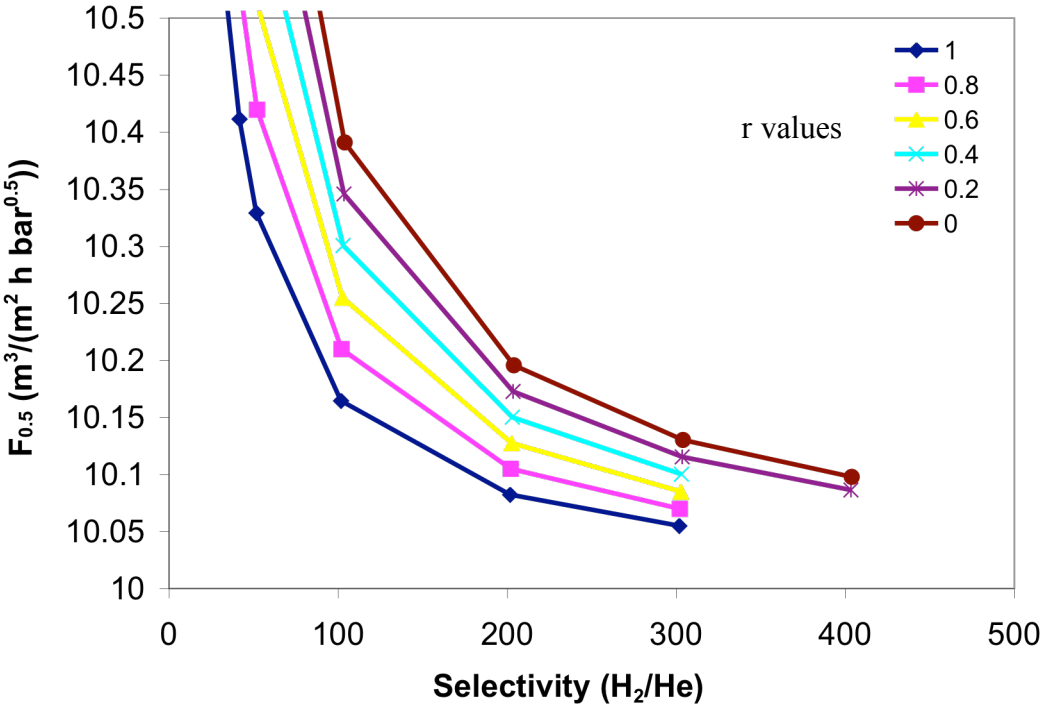

Figure 5-8 $F_{0.5}$ vs. selectivity for different values of r

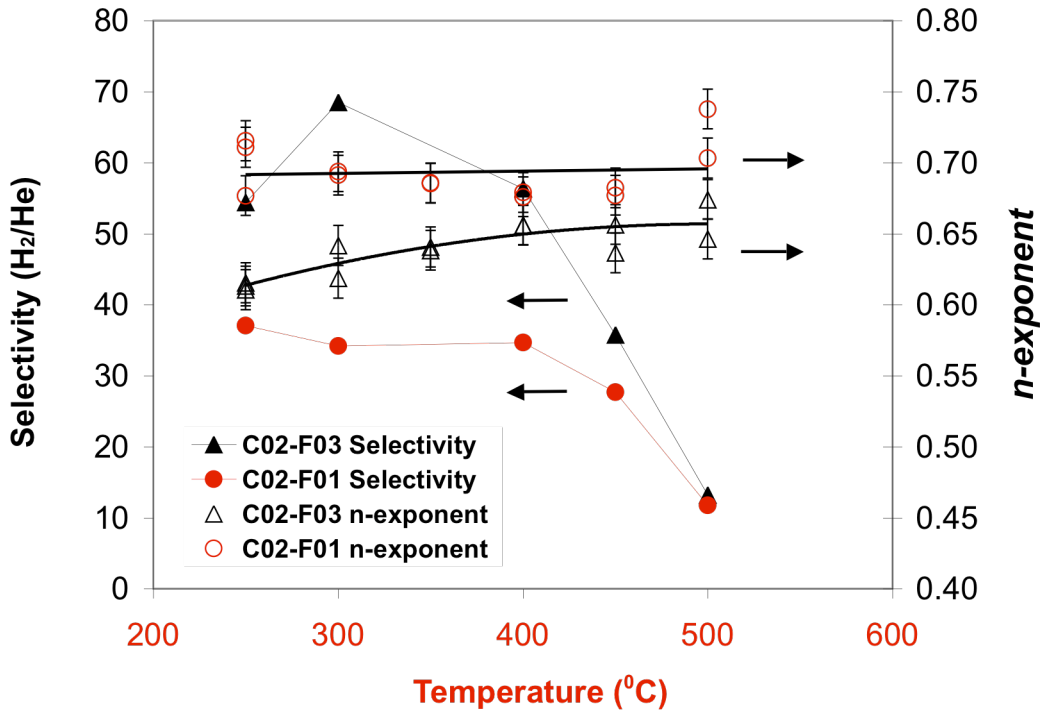

Figure 5-9 Selectivity and n-exponent vs. temperature for C02-F01 and C02-F03 membranes

The n-exponent of membrane C02-F03 increased rather slowly with increasing temperature from 0.61 at 250ºC to 0.66 at 450ºC. The n-exponent of membrane C02-F01 remained constant from 250ºC to 450ºC (0.68-0.70) and increased afterwards up to 0.74 at 500ºC. Interestingly, the n-exponent at 500ºC increased by 0.03 units between the first and second measurement for both membranes (24 hr interval) indicating the rapid growth of the He leak at 500ºC.

Figure 5-10 shows the n-exponent as a function of the selectivity for membranes C02-F01 and C02-F03. Each experimental point corresponds to the temperature shown next to the point. It can be seen that all experimental data points lie very close or within the leak envelope. When selectivities reached 10-20 the higher n-exponents were attributed to large defects in the Pd layer.

5.4.3 The effects of mass transfer resistance in the support on H_2 flux

5.4.3.1 Modeling the H_2 mass transfer within the porous metal support

It was rather difficult to determine from the characteristics of a given membrane (H_2 permeation, H_2 pressure exponent, activation energy for H_2 permeation) if the mass transfer resistance across the porous support accounted for a large portion of the total resistance for H_2 permeation. That difficulty in assessing the possible contribution of mass transfer resistance to the overall resistance was due to the small variations that the mass transfer resistance induced on the H_2 permeance, activation energy for H_2 permeation and n-exponent.

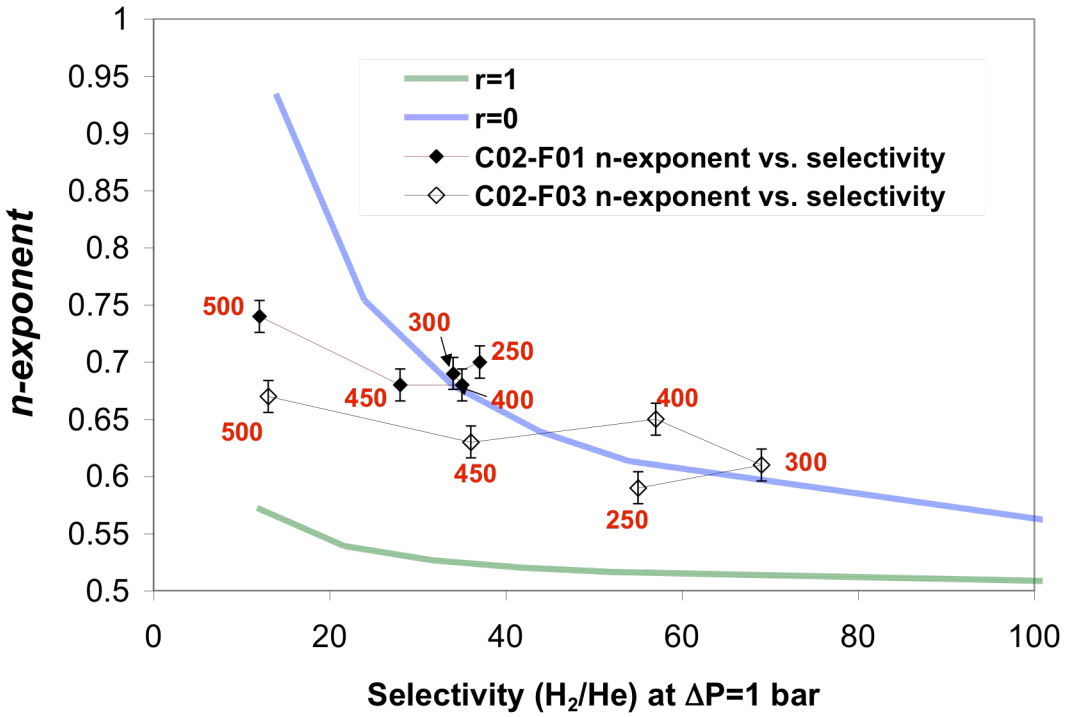

Figure 5-10 n-exponent as a function of selectivity for C02-F01 and C02-F03 membranes

Looking at the absolute values of the H_2 permeance, n-exponent and activation energy for H_2 permeation in a composite Pd membrane did not give sufficient information on the mechanism of the H_2 permeation. However, looking at the variations of the n-exponent and the variations of the activation energy for H_2 permeation with increasing temperature indicated the presence of mass transfer resistance within the support. Indeed, as temperature increases, the H_2 flux across the Pd layer increases and since the pressure drop across the porous support increases with the flux, the mass transfers resistance becomes larger at higher temperatures. Therefore, as the temperature is increased, the activation energy determined within 50ºC temperatures windows (as explained in Section 3.2.4) should decrease and the n-exponent should increase.

As an example, the H_2 permeance and E_p of membrane C01-F11b were calculated using the mass transfer model described in Section 5.2.1 with the following numerical values for LPd, $\alpha_{He}(293)$ and $\beta_{He}(293)$ that were experimentally measured.

$$L_{Pd} = 17 \cdot \mu m$$
$$\alpha(293) = 28 \cdot m^3/(m^2 \cdot h \cdot bar)$$
$$\beta(293) = 21 \cdot m^3/(m^2 \cdot h \cdot bar^2)$$

C01-F11b thickness was determined from SEM micrographs, $\alpha_{He}(293)$ and $\beta_{He}(293)$ were carefully measured after grading the support with Pd pre-activated Al_2O_3 particles. C01-F11b was a perfect example to validate the mass transfer model since no H_2 flux decline was seen at temperatures equal to or lower than 500ºC (no intermetallic diffusion). Also, leaks did not have any effect on H_2 flux since the He leak of C01-F11b at 500ºC was $2.63 \cdot 10^{-3}$ $m^3/(m^2\ h\ bar)$, which corresponded to a selectivity (H_2/He) over 400 at all temperatures.

The calculated values of $F_{0.5}$, E_p and n-exponents were compared with the experimental values obtained for C01-F11b membrane. It is important to keep in mind that none of the parameters in the model described in Section 5.2.1 were fitted to match the experimental data of membrane C01-F11b.

Figure 5-11(a) shows the experimental and predicted H_2 permeance assuming Sieverts' law ($F_{0.5}$). The model underestimated the experimental $F_{0.5}$ values by 1-2 $m^3/(m^2 h bar^{0.5})$ at all temperatures, which was due to the fact that H_2 also permeated through the grade Al_2O_3-Pd layer by the solution-diffusion mechanism. Figure 5-11(b) shows the experimental and predicted Arrhenius plots based on $F_{0.5}$. The overall activation energies within the 250-500ºC temperature range, experimental and predicted, were considered as equal with a value close to 12.5 kJ mol^{-1}. It is important to notice that the activation energy for H_2 diffusion through freestanding Pd foil was set to 14.9 kJ mol^{-1} (see Equation (4-11)) for the calculations and that the activation energy for H_2 permeation through the composite Pd membrane was calculated to be 12.7 $kJmol^{-1}$ and measured to be 12.2 kJ mol^{-1}. The difference between the predicted and measured value was within the measurement errors. Therefore, as predicted, the mass transfer resistance within the porous media led to a decrease in the activation energy for H_2 permeation. The decrease in E_p was equal to 3 kJ mol^{-1} for the particular case of C01-F11b. Figure 5-12 shows the experimental and predicted n-exponents. n-exponents are not predicted or measured to elucidate the mechanism of H_2 permeation but just as a tool to verify, how far a membrane can deviate from Sieverts' law.

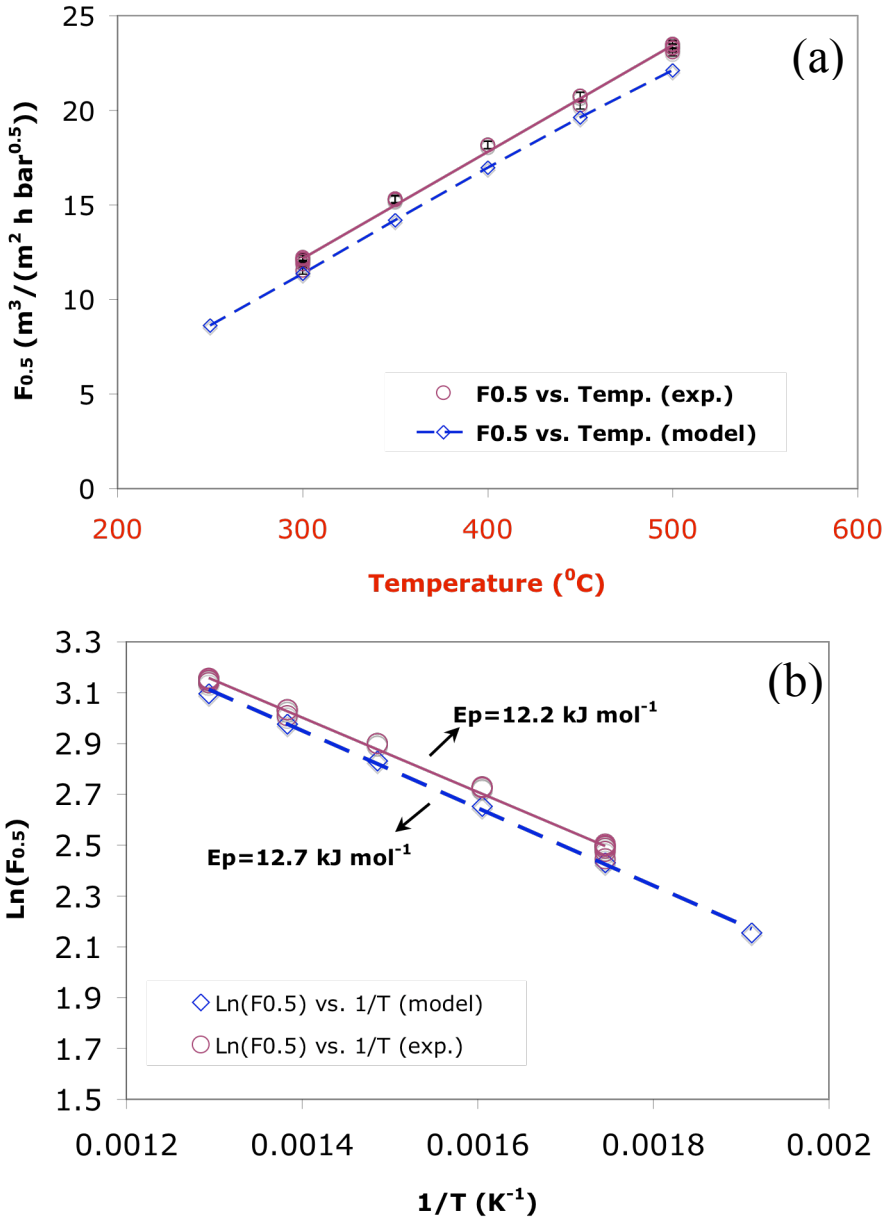

Figure 5-11 (a) Calculated and experimental H_2 permeance $F_{0.5}$. (b) Calculated and experimental activation energy based on $F_{0.5}$ values (250-500°C)

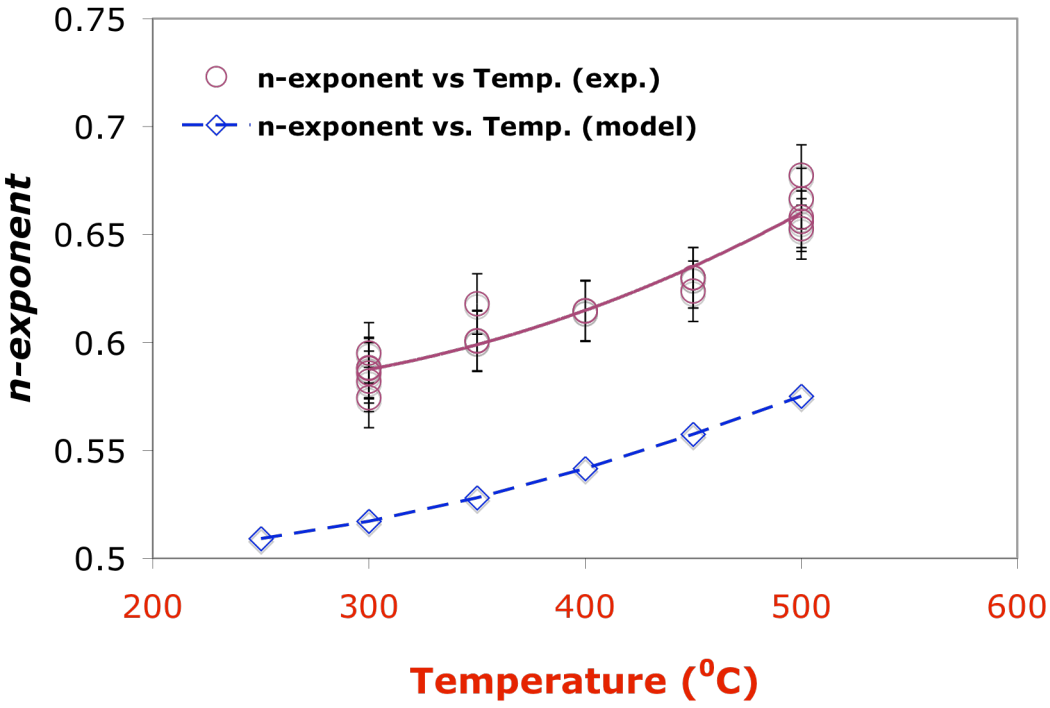

Figure 5-12 Calculated and experimental n-exponents

The model correctly predicted the trend shown by the experimental n-exponent as a function of temperature, yet, the experimental value also included other effects. That is, at higher temperatures, mass transfer resistance prevails and the n-exponent increases from 0.5 to higher values.

Figure 5-13 shows the predicted and experimental Ep for H_2 permeation values determined in small temperature intervals (250-300ºC, 300-350ºC, 350-400ºC, 400-450ºC and 450-500ºC). The E_p for H_2 differed by a maximum of 1 kJ mol^{-1} and, which is very important, in both cases the E_p decreased from a value close to 13.5 kJ mol^{-1} to a value close to 11.1 kJ mol^{-1} in agreement with the fact that at higher temperatures mass transfer within the porous support became more important. As temperature increased, the H_2 flux increased and the pressure drop across the porous support also increased, leading to higher flux resistances within the support at high temperatures.

Therefore, as already stated, the only consideration of absolute values of the H_2 permeance, activation energy and n-exponent, did not give enough information on the presence of mass transfer resistance in the porous support. However, the variations in E_p and n-exponent as temperature was increased, was a powerful indicator of the presence of mass transfer resistance in the porous support.

5.4.3.2 The prediction of mass transfer resistance in composite Pd membranes

This section aimed at the theoretical calculation of $(F_{0.5,\ foil}-F_{0.5,comp})/(F_{0.5,\ foil})$, the n-exponent and the $E_{p(450-500)}$ as a function of ξ_{250}.

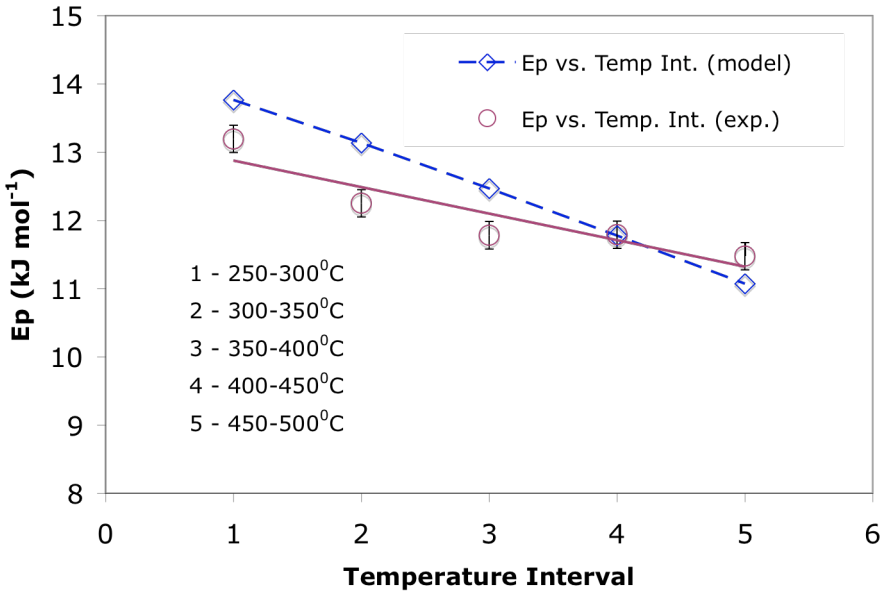

Figure 5-13 Calculated and experimental Ep changes with temperature

Having the dimensionless number ξ_{250} to compare the resistance for the H_2 flux within the Pd film and the resistance within the porous support at 250ºC under a pressure difference of 1 bar (2:1), it was possible to estimate the effect of mass transfer on the H_2 permeance, the E_p and the n-exponent for all membranes listed in Table 5-1. Table 5-1 lists the experimental He permeance parameters $\alpha_{He}(293)$ and $\beta_{He}(293)$ of the supports, the Pd thin film thickness, the determined ξ_{250} parameter and the activation energy for H_2 permeance experimentally determined in the 450-500ºC temperature interval, $E_{p(450\text{-}500)}$, for most of the membranes studied throughout this work.

The calculations were performed by setting hypothetical values of $\alpha(293)$ equal to 70 $m^3/(m^2\ h\ bar)$ and $\beta(293)$ equal to 52 $m^3/(m^2\ h\ bar^2)$ to a given porous support and decreasing the thickness of the Pd layer on that support, thereby changing the ξ_{250} parameter. The thickness of the Pd dense film, L_{Pd}, was varied between 57 and 3.8 μm so that ξ_{250} varied between 150 and 10. For each value of ξ_{250} the permeance assuming Sieverts' law, $F_{0.5}$ at 500ºC, the E_p within the 450-500ºC temperature range and the n-exponent at 500ºC were calculated using the model in Section 5.2.1 (500ºC is the temperature at which mass transfer resistance has the biggest contribution). Figure 5-14 shows the calculated n-exponents and $(F_{0.5,\ foil}\text{-}F_{0.5,comp})/(F_{0.5,\ foil})$ (percentage of the H_2 permeance of a freestanding Pd film), both at 500ºC, as a function of ξ_{250}. It is interesting to note that even for a large value of ξ_{250} (ξ_{250}>100), the composite Pd membrane only allows 93% of the freestanding Pd film H_2 permeance to pass. For ξ_{250} values higher than 100 the increase in n-exponent (0.5056) was very small.

Table 5-1 Support characteristics, Pd film thickness, ξ_{250} parameter and $Ep_{450-500}$ for all membranes in this chapter

Membrane name	Support grade (μm)	Graded	α[(a)] ($m^3/(m^2\ h\ bar)$	β[(a)] $m^3/(m^2\ h\ bar^2)$	L (Gravimetric) (μm)	L (SEM) (μm)	ξ_{250}	$Ep_{(450-500)}$ ($kJ\ mol^{-1}$)
C01-F03	0.1-PSS	No	98	73	32	37	134	n.a.[(b)]
C01-F04	0.1-PSS	No	82	62	28	Not determined	86	n. a.[(b)]
C01-F05	0.1-PSS	No	83	62	33	Not determined	102	n.a.[(b)]
C01-F07	0.1-PSS	No	100	81	23	24	92	n.a.[(b)]
C01-F08	0.1-PSS	Yes	104	84	15	19-24	58	n.a.[(b)]
C01-F11b	C01-F11	Yes	28	21	13	17	18	11.5
Ma-32	0.1 medium-PH	Yes	29	24	7.7	Not determined	8.6	9
Ma-32b	Ma-32	Yes	29	24	10	Not determined	11.2	11.7
Ma-34b	0.1 coarse-PH	Yes	9	0.6	8	9.4	2[(c)]	9.5
Ma-42	0.1 medium-PH	Yes	46	30	5.6	Not determined	9.1	9.6
Ma-45	0.1 fine-PH	Yes	78	58	9	Not determined	26	8

[(a)] The values of α and β were measured at room temperature (293K) after oxidation for non-graded supports and after the deposition of the Al_2O_3-Pd layer in the case of graded supports.

[(b)] "n. a." stands for not applicable. The H_2 permeation of membranes C01-F03/4/5/7 and /8 decreased at temperatures higher than 275-300ºC due to inter-metallic diffusion. Intermetallic diffusion led to the increase in activation energy for H_2 permeation as it will be discussed in Chapter 8. Membranes C01-F11b, Ma-32/32b/34b did not show signs of intermetallic diffusion. The selectivity (H_2/He) was also higher than 400.

[(c)] The ξ_{250} value for membrane Ma-34/34b was very low. The reason for a low ξ was due to a relatively thick Pd layer deposited during the grading process. In fact, the grade layer led to the decrease of α and β, yet the layer was permeable to H_2. Therefore, ξ should be higher than 2.

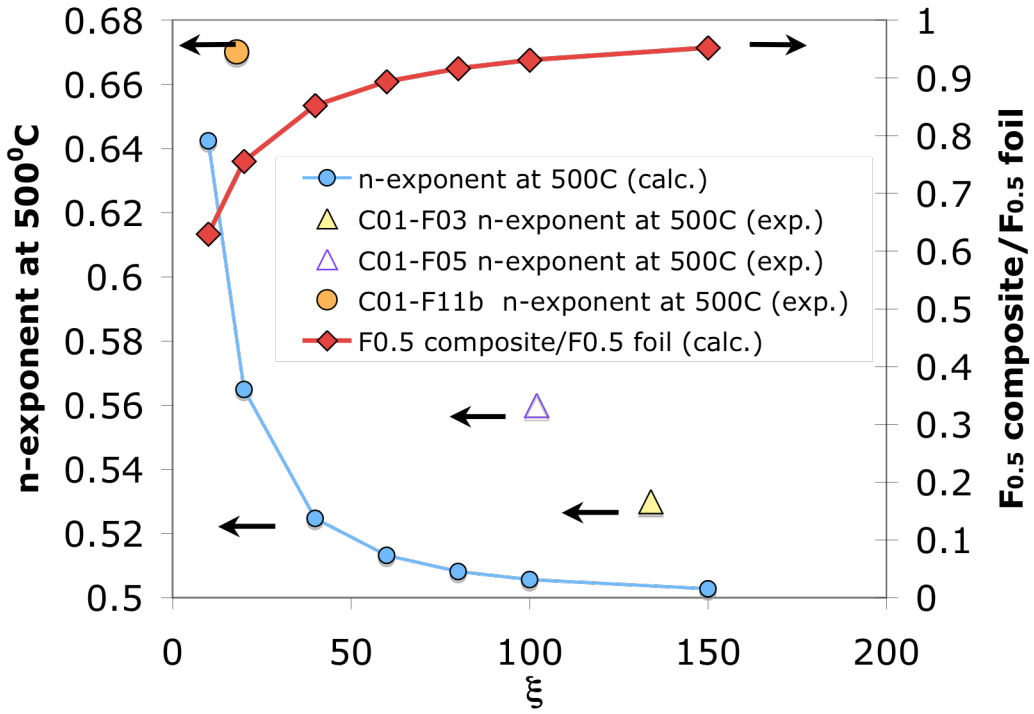

Figure 5-14 Calculated n-exponent and $F_{0.5\ composite}/F_{0.5\ foil}$ at 500°C as a function of ξ_{250}.. The experimental n-exponents determined at 500°C for membranes C01-F03/5/11b are also plotted

Therefore, mass transfer in composite Pd membranes with ξ_{250} values above 100 was negligible. The experimental n-exponents measured at 500ºC for membranes C01-F03, C01-F05 and C01-F11b also appear in Figure 5-14. As expected the experimental n-exponents measured at 500ºC increased as the ξ_{250} number decreased. Yet, the experimental n-exponents for C01-F03/5/11b were well above the n-exponents predicted by the mass transfer model indicating that experimental n-exponents were not just due to the mass transfer resistance within the support. With the ξ_{250} number being so high in the case of C01-F03/5, the mass transfer resistance within their porous support was considered as negligible. Indeed, membrane C01-F03 did not show signs of support resistance since the n-exponent at 500ºC (0.53) was close to 0.5. Moreover, the n-exponent of membrane C01-F03 decreased as the temperature was increased.

The contribution of mass transfer to the overall H_2 permeation resistance was easily detected in severe cases where the changes in the n-exponent and the changes in the activation energy for H_2 permeance as the temperature was increased were large enough to be measurable. The case of membrane C01-F11b was an ideal example since the membrane showed increasing n-exponents with temperatures and a decrease in E_p with temperature. For the cases where large variations in n-exponent and a large decrease in E_p were measured as temperature was increased, the composite Pd membrane only permeated 75% of the freestanding Pd film.

The n-exponents of membranes Ma-32, Ma-32b, Ma-34b and Ma-42 were not experimentally determined since their H_2 fluxes at high pressures were above the linearity range of the 0.3 m^3/h and/or the 1.2 m^3/h mass flow meters used. Hence, the mass transfer resistance within their support was investigated by calculating the ξ_{250} number and by considering the low activation energy for H_2 permeation measured within the 450-500ºC temperature interval. The activation energy within the 450-500ºC temperature range was determined by measuring the H_2 flux as the temperature was changed at a rate of 1ºC/min as described in Section 3.2.4. The experimental $E_{p(450-500)}$ were then compared to the $E_{p(450-500)}$ calculated by the mass transfer model of Section 5.2.1. Membranes Ma-32, Ma-32b, Ma-34b and Ma-42 were characterized by selectivities higher than 200 and did not show signs of intermetallic diffusion.

Figure 5-15 shows the calculated $E_{p(450-500)}$ as a function of ξ_{250}. The calculated $E_{p(450-500)}$ decreased as ξ_{250} decreased indicating that diffusion of H_2 through the porous media had a large contribution to the overall resistance as the He permeance of the graded support deceases and/or the thickness of the membrane becomes too thin (see Section 5.2.1). The experimental values of $E_{p(450-500)}$ measured for Ma-32, Ma-32b, Ma-34b and Ma-42 are plotted as a function of ξ_{250} in Figure 5-15.

The low activation energies for H_2 permeation measured in these membranes were in agreement with their low ξ_{250} values. Therefore, all composite Pd membranes prepared on graded PH supports were characterized by high mass transfer resistance and the H_2 permeance measured in these membranes was only equal to 60-80% of the H_2 permeance of the Pd thin film deposited on these supports.

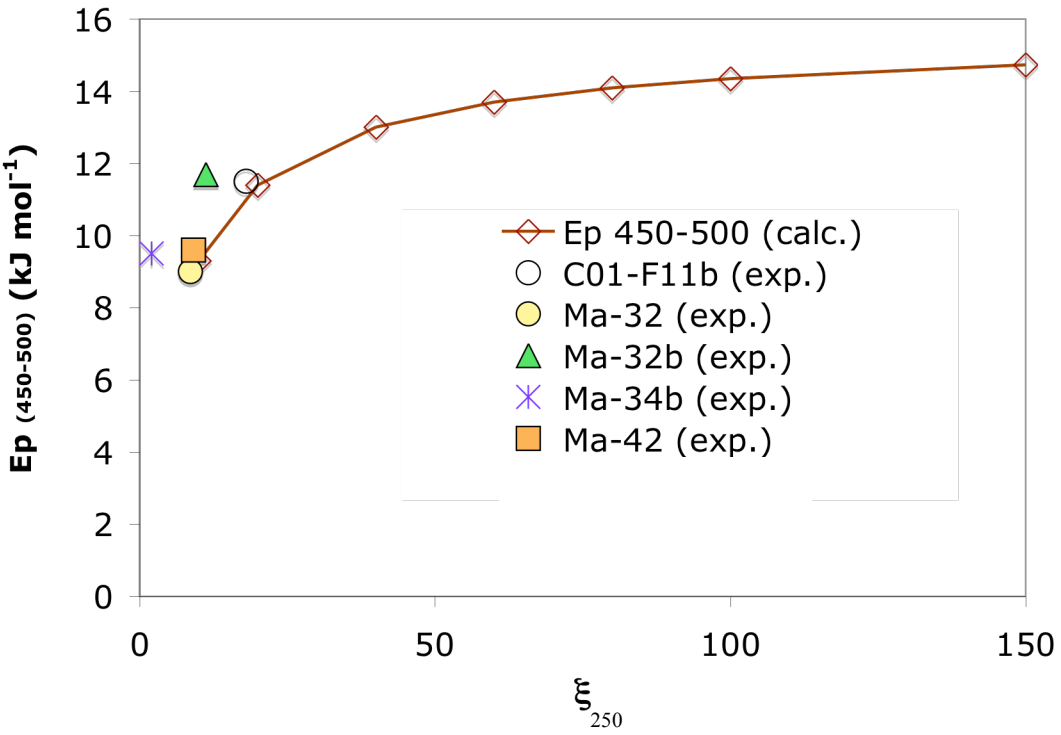

Figure 5-15 Calculated $Ep_{(450\text{-}500)}$ as a function of ξ_{250}. The experimental $Ep_{(450\text{-}500)}$ for membranes C01-F11b and Ma-32/32b/34b/42 are plotted.

5.4.4 Effect of Pd catalytic surface activity on H_2 flux

In order to accelerate the H_2 dissociation reaction on the surface of the Pd layer, C01-F05 was seeded with Pd crystallites before the H_2 characterization by Pd precipitation from a Pd plating bath containing an excess of hydrazine. The precipitated layer (light brown) was relatively thin since the shine from the underneath Pd surface was still visible. Also, the color of the membrane appeared brown due to the light scattering of small Pd crystallites on the surface. n-exponents lower than the ones shown by C01-F03 were expected. For comparison purpose, Figure 5-16 shows the n-exponent as a function of temperature for membrane C01-F03 and membrane C01-F05. Also, the n-exponents calculated from H_2 absorption isotherms (pressure effects in the 0-4.5 bar pressure range) are shown in Figure 5-16. The n-exponent from pressure effects is given by Figure 4-2 by taking the maximum pressure equal to 4.5 bar. In the temperature range 250-350ºC the n-exponents of membrane C01-F05 equaled 0.60 ±0.01 and were therefore, as expected, slightly lower than the n-exponents of membrane C01-F03 indicating a possible increase of the surface reactions rate. Surprisingly, the n-exponent of membrane C01-F05 was 0.05 units lower than the n-exponent predicted from H_2 absorption isotherms (see Figure 4-2). Above 350ºC, the n-exponents of C01-F05 membrane decreased very slowly (remained almost constant) as the temperature was increased with values similar to the n-exponents of C01-F03. Both membranes showed similar n-exponents at 500ºC (0.54 ±0.01). Therefore, Pd seeds were only effective for increasing the surface reactions rate at low temperatures. At high temperatures Pd grains in the thin Pd seeded layer increased in size leading to the loss of its catalytic activity.

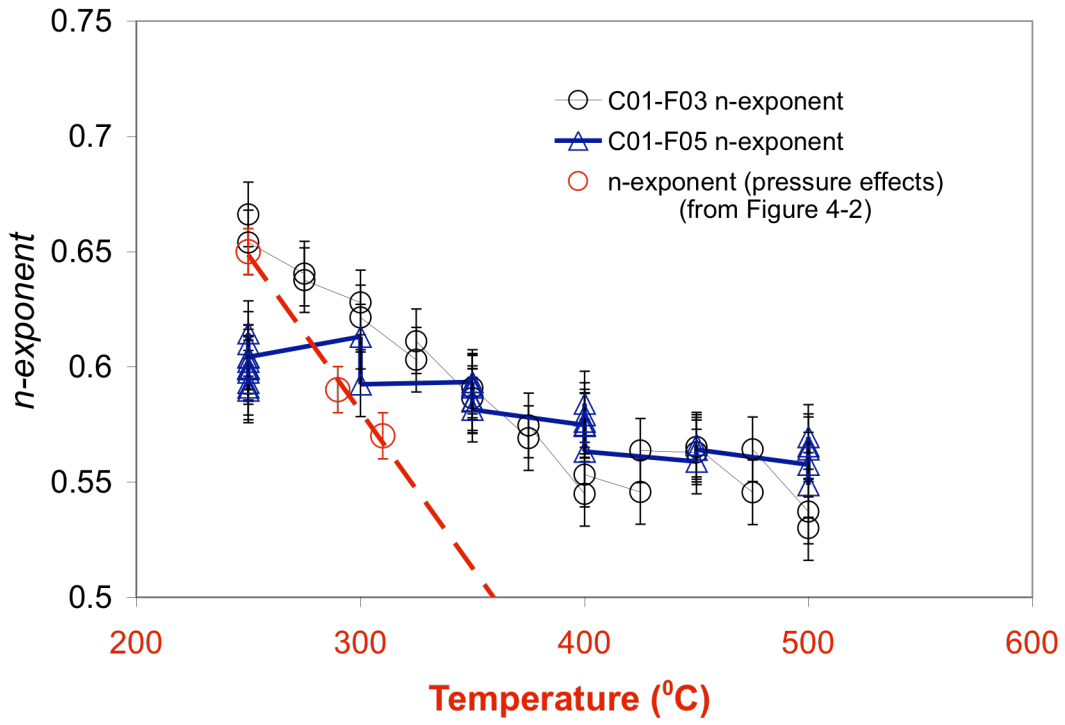

Figure 5-16 n-exponent as a function of temperature for membranes C01-F03 and C01-F05.

After the H_2 exposure at high temperatures the color of the Pd film appeared very bright indicating the growth or the sintering of Pd crystallites of the original seeded layer. Figure 5-17(a) and Figure 5-17(b) show the cross-section and the surface of membrane C01-F05, respectively. Both pictures were taken after the H_2 characterization i.e. after the exposure to H_2 at 700ºC. After H_2 exposure at 700ºC, the layer kept a very uniform thickness with a very smooth surface as shown in Figure 5-17(a). After Pd seeds sintered (T>350ºC) the surface lost its catalytic activity and membrane C01-F05 showed n-exponents similar to the n-exponents of an uncoated membrane at 500ºC, i.e. n-exponents similar to the ones shown by membrane C01-F03 in the 350-500ºC temperature range. At temperatures higher than 350ºC both membranes had similar n-exponents.

The second method used to increase the rate of H_2 dissociation on the catalytic surface of Pd was the oxidation in stagnant air at 350ºC for 48 hr, which was applied to membrane C01-F11b. The freshly prepared membrane C01-F11 was characterized at several temperatures from 250ºC to 500ºC following the same characterization procedure as C01-F03 and C01-F05. After the first characterization had been completed, the membrane was removed from the reactor, activated and Pd plated (1.5 μm) to repair the small leak that had developed during the first characterization. After the additional 1.5 μm of Pd, Pd seeds were deposited using the same procedure as on membrane C01-F05. The membrane was then oxidized in air at 350ºC for 48 hr. The surface of membrane C01-F11b after air cleaning/activation was slightly purple and not shining. Membrane C01-F11b was then characterized at temperatures ranging from 250ºC to 500ºC. The H_2 permeance based on Sieverts' driving force at 250ºC at the end of the first characterization was equal to 6.5 $m^3/(m^2\ h\ bar^{0.5})$.

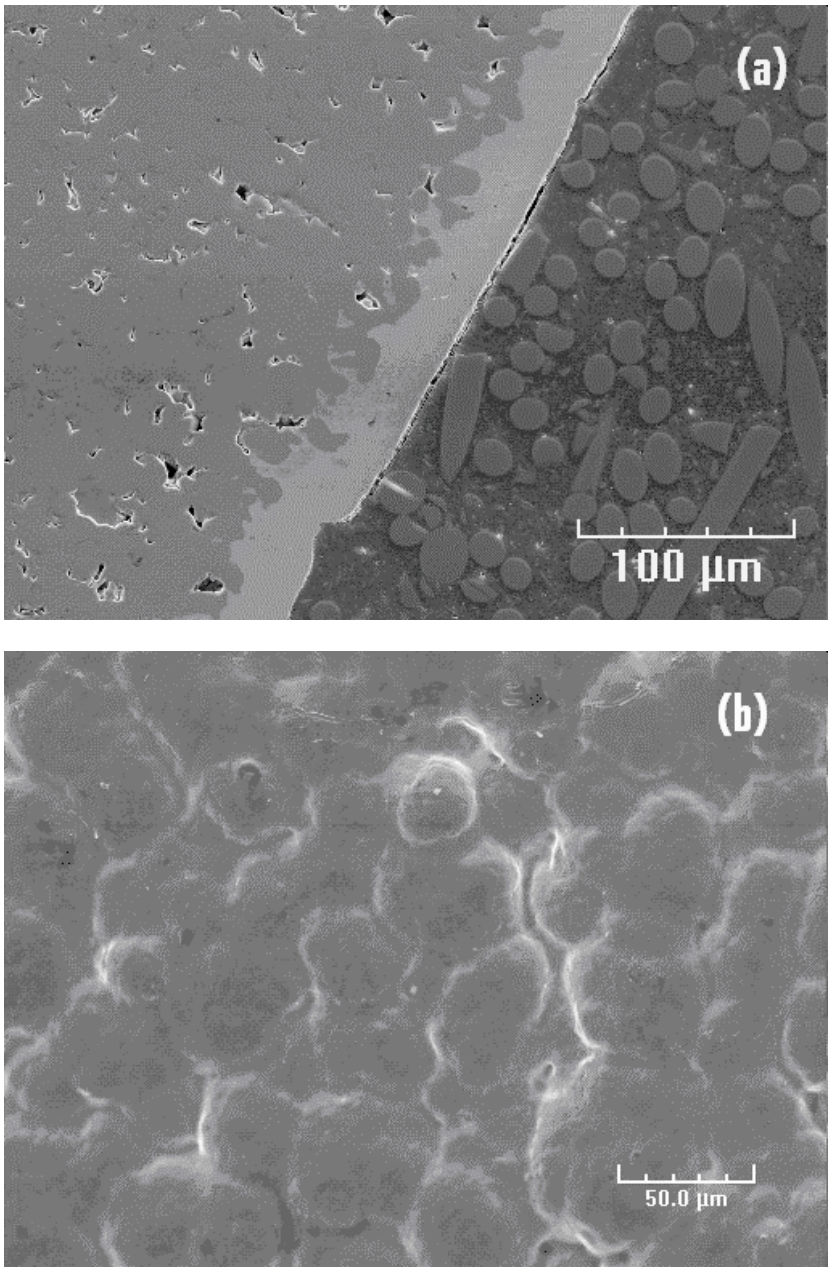

Figure 5-17 (a) Cross-section of membrane C01-F05. (b) Surface morphology of membrane C01-F05.

Even though more Pd was added on C01-F11, the H_2 permeance at 250ºC of C01-F11b equaled to 8.3 $m^3/(m^2\ h\ bar^{0.5})$ after 200 hr in H_2, which was higher than the H_2 permeance at 250ºC of C01-F11 by 1.8 $m^3/(m^2\ h\ bar^{0.5})$. Air oxidation enhanced the H_2 permeance of C01-F11. Figure 5-18(a) and Figure 5-18(b) show the cross-section and the surface morphology respectively for membrane C01-F11b after the H_2 characterization. The oxidation in air led to the formation of hills and valleys, encircled in Figure 5-18(a) and seen from the top in Figure 5-18(b), similar to the ones reported in the literature (Aggarwal et al., 2000; Roa et al., 2003). The formation of hills and valleys resulted in a composite Pd membrane with higher H_2 flux than the initial composite Pd membrane. It was also possible that air oxidation/H_2 reduction led to the formation of porous Pd layer, which increased the H solubility at the surface (Radzhabov et al., 1980; Roshan et al., 1983).

During the characterization of C01-F11 the n-exponents ranged between 0.64 and 0.68 over the entire studied temperature range (300ºC-500ºC) as shown in Figure 5-19. After Pd plating and surface reactivation, the n-exponent of C01-F11b was equal to 0.58 at 250ºC similar to the n-exponent shown by membrane C01-F05 at 250ºC. Hence, the n-exponent of membrane C01-F11b at 250ºC was also lower than the n-exponent predicted by the 250ºC H_2 absorption isotherm. As already shown, the n-exponents of membrane C01-F011b increased from 0.58 at 250ºC up to 0.66 at 500ºC with a similar trend as the one predicted by the mass transfer model. The n-exponents predicted by the mass transfer model were also plotted as a function of temperature in Figure 5-19 with 0.09 units added to all n-exponents calculated in order to fit the calculated and the experimental n-exponent at 250ºC.

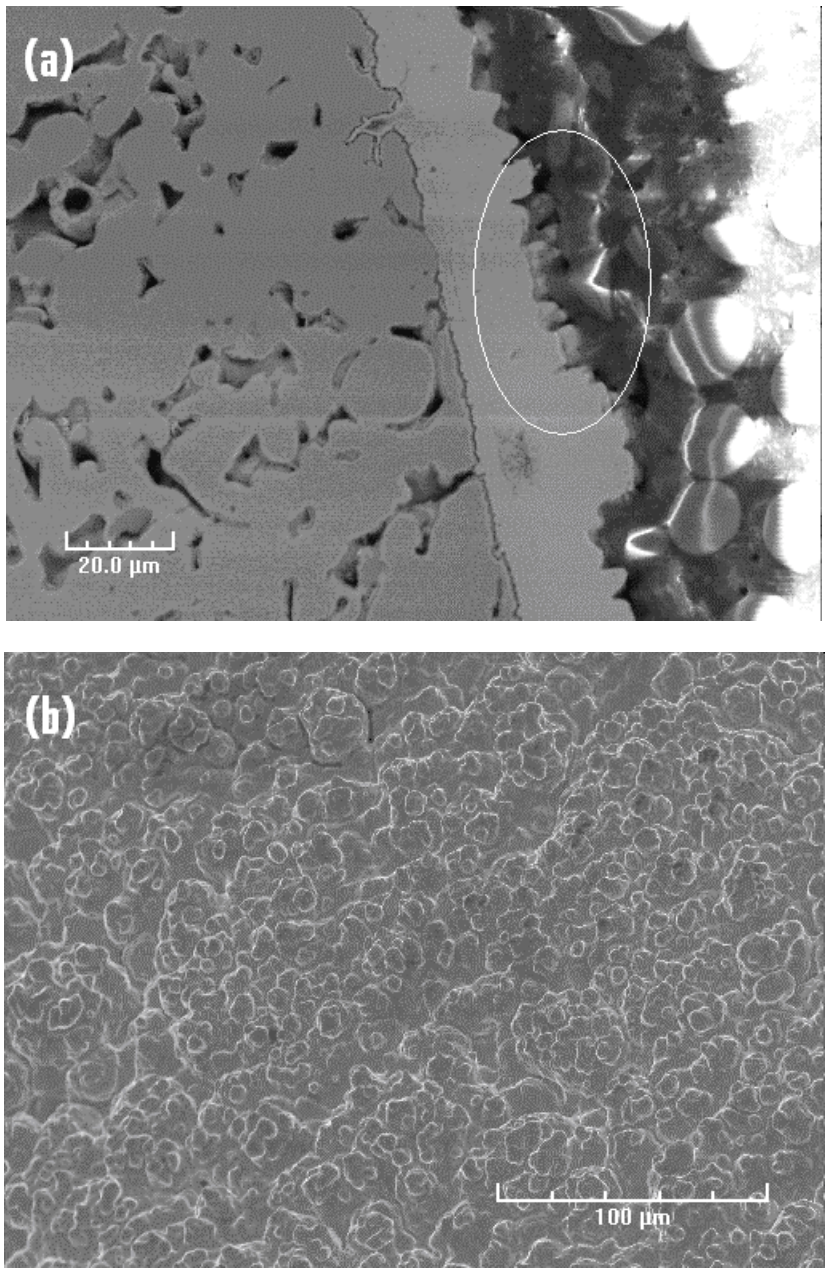

Figure 5-18 Cross-section (a) and surface analysis (b) of membrane C01-F11 after H_2 characterization.

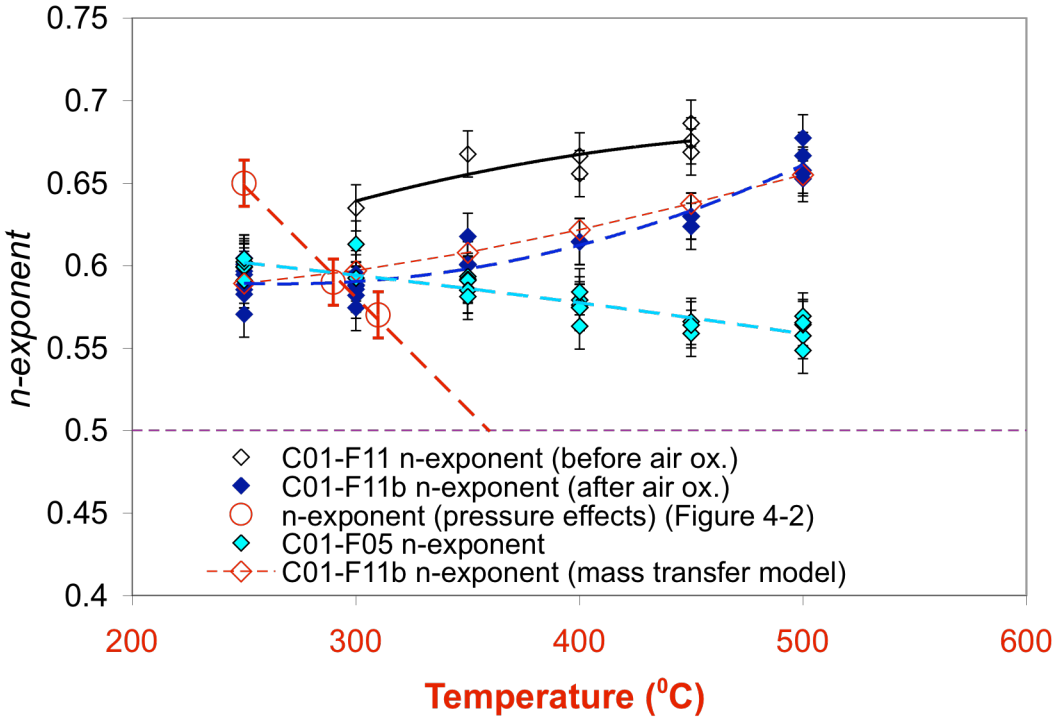

Figure 5-19 n-exponent as a function of temperature for membranes C01-F05, C01-F11a and C01-F11b. n-exponents due to pressure effects and the calculated n-exponents for C01-F11b due to mass transfer effect (Figure 5-12) were also added for comparison purposes.

A change in membrane color was also noticed for membrane C01-F11b after exposure to high temperatures in H_2 atmosphere. The surface of the membrane changed from purple after oxidation to silver color (Pd color) with little shine. A deactivation of the surface similar to C01-F05 membrane occurred. At 300-350ºC and higher temperatures Pd grains included in the spongy catalytic layer grew and lost their H_2 dissociative capabilities. Reactivation by surface oxidation at 350ºC also increased the reactions rate at the surface since the n-exponents shown by membrane C01-F11b were lower than n-exponents shown by C01-F11

Membranes C01-F05, C01-F11 and C01-F11b clearly showed that Pd seeding and air cleaning/oxidation increased the surface reaction rate. Therefore, even if the bulk diffusion was the main resistance for H_2 permeation, surface reaction resistances still contribute, though in a reduced extent, to the transport of H_2. Surface reactions even had a more pronounced resistance at lower temperatures mainly due to the presence of impurities adsorbed on the Pd surface. Impurities were removed by heating (n-exponent decreasing with temperature) and air oxidation at 300-350ºC.

5.4.5 The activation energy for H_2 permeation in fresh composite Pd membranes

5.4.5.1 The Ep in fresh composite Pd membranes

As already stated in Section 3.2.4, the activation energy for H_2 permeation was measured by using two different methods: (1) considering steady state permeance values, $F_{0.5}$, after the membranes spent a long time at a given temperature and (2) measuring the H_2 flux at a ΔP of 1 bar (2:1) while changing the temperature at a rate of 1ºC/min. The two

methods did not lead to the same numerical value of the activation energy in fresh composite Pd membranes. Indeed, all composite Pd membranes had a different H_2 permeance vs. time response. The H_2 permeance can increase as a function of time due to an increase of leaks, contaminants desorption from the surface and "rearrangements" (mostly seen in composite Pd membranes prepared on graded supports). In addition, the H_2 permeance can increase during alloying of Pd-Cu layers. The H_2 permeance can also decrease as a function of time, which is generally attributed to intermetallic diffusion. The objective of the following section was to demonstrate that using method (1) to determine E_p in a fresh membrane led to erroneous values of E_p. Also, that method (2) is more suitable for fresh composite Pd membranes.

Figure 5-20 shows the H_2 permeance, F_{H2}, of C01-F03 membrane as a function of time at different temperatures. The dashed lines represent the 50ºC temperature changes. At each temperature F_{H2} decreased due to intermetallic diffusion. Figure 5-21 shows the Arrhenius plot of $F_{0.5}$ permeance values determined twice at each temperature (see Section 3.2.3 to recall the difference between F_{H2} and $F_{0.5}$). The "saw" shape in Figure 5-21 is due to the fact that between each determination of $F_{0.5}$ the permeance decreased due to intermetallic diffusion. Hence, the determination of the activation energy for H_2 permeance based on $F_{0.5}$ values would be impossible in this case. Fitting a straight line to the experimental data of Figure 5-21 would lead to a negative value of E_p. In order to determine the activation energy for H_2 permeation the H_2 flux, J_{H2}, between each temperature change had to be considered.

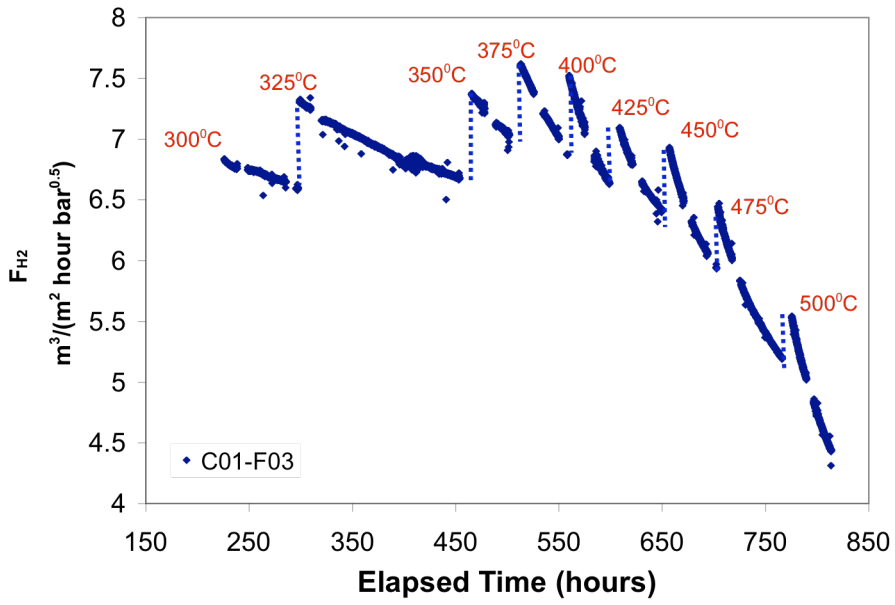

Figure 5-20 F_{H2} permeance as a function of time at different temperatures C01-F03

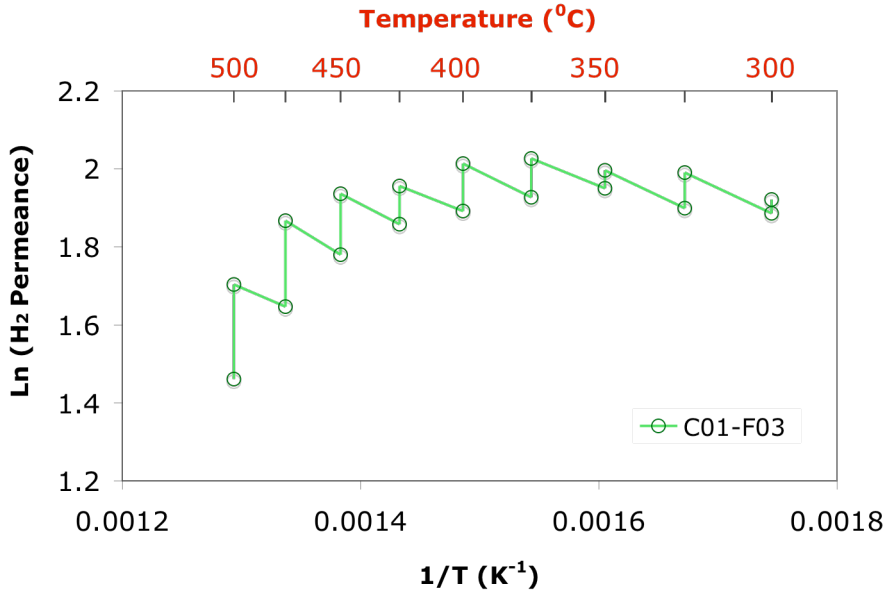

Figure 5-21 $Ln(F_{0.5})$ as a function of 1/T for membrane C01-F03

The determination of the activation energy from H_2 permeance from experimental data taken during temperature change at 1ºC/min leads to a better estimation yet, the following important condition needs to be fulfilled. Figure 5-22 shows the H_2 permeance and temperature as a function of time during the 300-350ºC temperature change for membrane Ma-41. Δ1 is the increase in permeance due to the 50ºC increase in temperature, Δ2 is the increase in permeance (due to any process leading to permeance increase in green membranes over time) during the next 50 minutes after the temperature change and Δ3 is the total increase in permeance after 50-100 hr. Considering H_2 data during the temperature change is only valid if the increase of permeance (due to processes affecting permeance over long periods of time) during the 50 minutes of the temperature change is negligible to the increase of H_2 permeance due to temperature. That is, the E_p from temperature change is accurate if $\Delta 2 << \Delta 1$.

Figure 5-23 shows the H_2 permeance, F_{H2}, as a function of time for the 250-300ºC temperature change for membrane Ma-41. This Figure shows that at this particular temperature change, Δ2 is not negligible compared to Δ1. The particular case of Figure 5-23 was due to the alloying of the Pd-Cu bi-layer. Composite pure Pd membranes showed a similar behavior at 250ºC, especially green membranes prepared on graded supports with pre-activated powder. However, for all membranes, the condition $\Delta 2 << \Delta 1$ was fulfilled for the 300-350, 350-400, 400-450, 450-500ºC temperature changes.

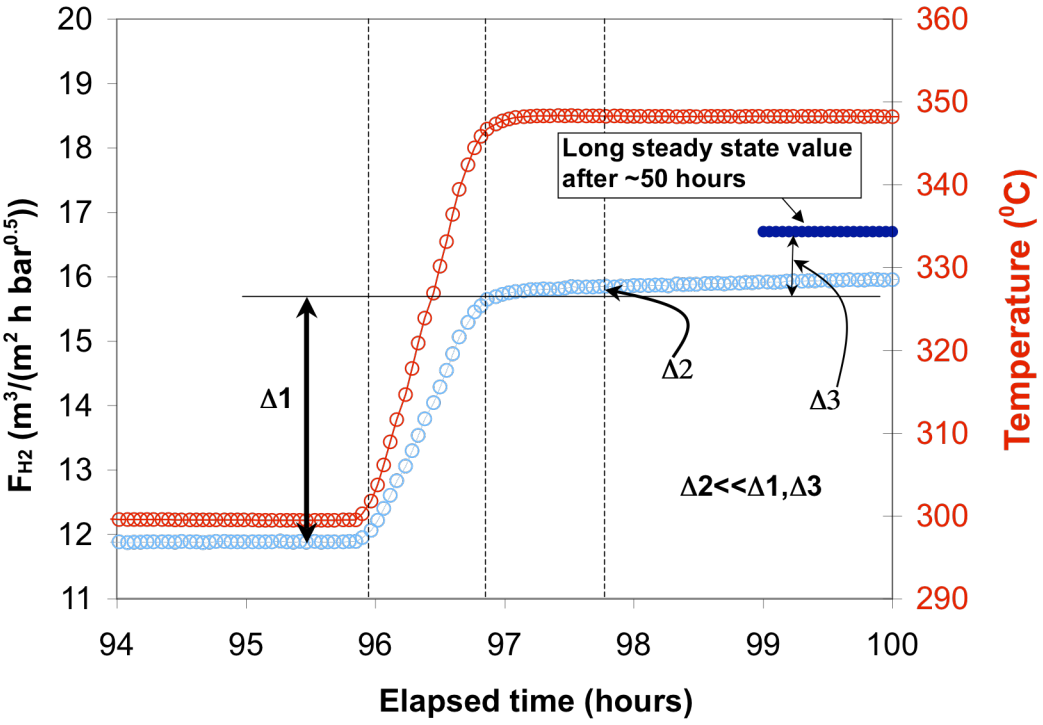

Figure 5-22 Temperature change between 300 and 350ºC of membrane Ma-41

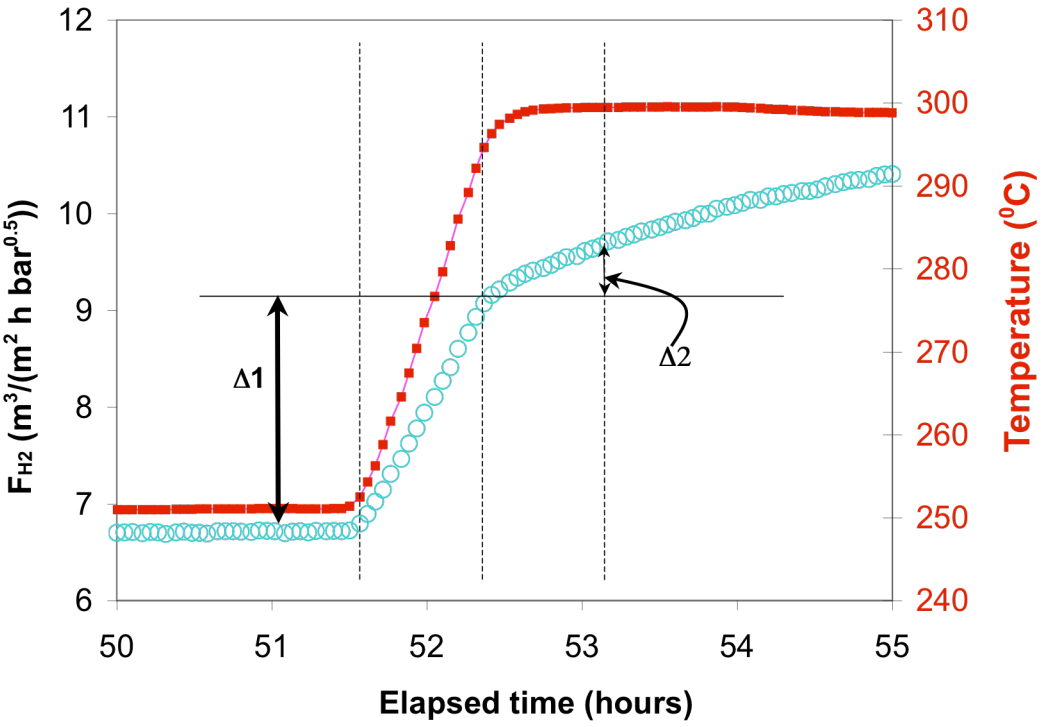

Figure 5-23 H_2 permeance, F_{H2}, as a function of time during the 250-300ºC temperature change in Ma-41

Figure 5-24 shows the activation energy determined in the 300°C-400°C temperature range of membrane C02-F01 by the two methods: based on long time steady states values and steady state values while changing the temperature. The discontinuity in the $Ln(F_{0.5})$ vs. 1/T function between points (b) and (c) and points (d) and (e) in Figure 5-24 are due to the growth of leaks (defects) during the time the membrane was held at 350°C and 400°C. The selectivity (H_2/He) of C02-F01 at 300, 350 and 400ºC was only around 30. The activation energy in the 300°C-350°C temperature range and in the 350°C-400°C temperature range determined while changing temperature were equal to 10.1 kJ mol^{-1} and 10.6 kJ mol^{-1} respectively and the overall activation energy estimated from $F_{0.5}$ values was equal to 14.2 $kJmol^{-1}$. Since defects formation results in an increase of the portion of the H_2 that flows by slip flow diffusion (Knudsen + viscous), the activation energy for H_2 permeance should decrease according to the activation energy of gas diffusion. Therefore, the H_2 permeance of a composite Pd membrane with low selectivity should have a lower activation energy than 14.9 kJ/mol (see Equation (4-11)). Activation energy values of 10.1-10.6 kJ mol-1 are then consistent with the low selectivity of C02-F01 membrane and the activation energy based on steady state values after long times (14.2 kJ/mol) has no real meaning.

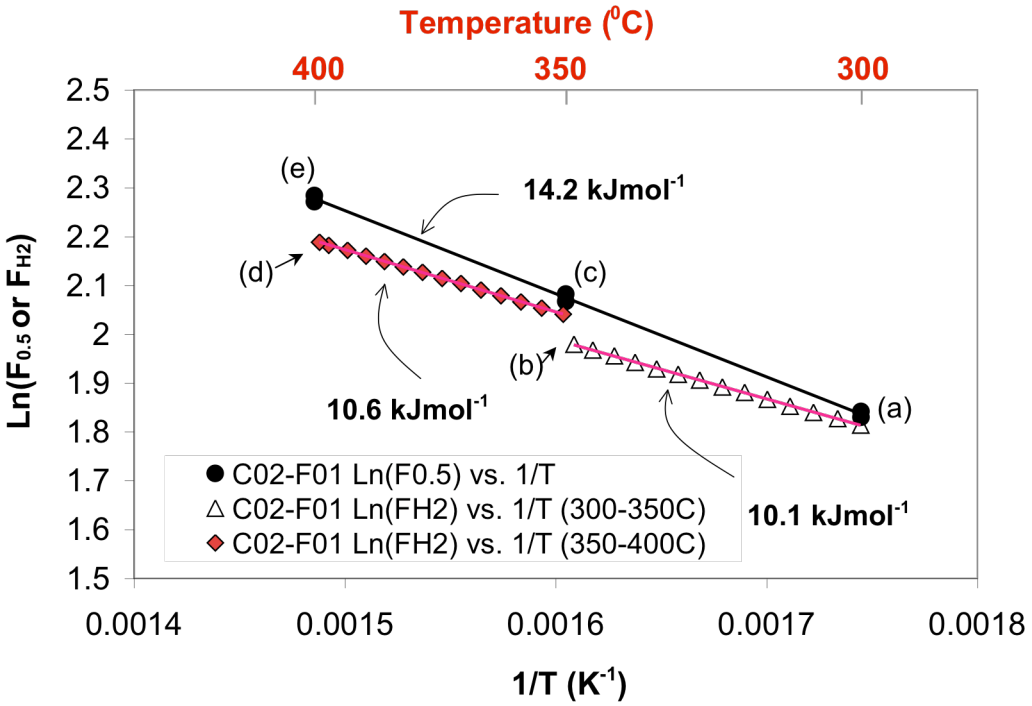

Figure 5-24 Ln($F_{0.5}$) and Ln(F_{H2}) vs. 1/T for membranes C02-F01.

Also, both methods (E_p based on $F_{0.5}$ H_2 permeance values and E_p based on F_{H2} H_2 permeance while changing the temperature) gave the same value for the activation energy of H_2 permeance in stable membranes, i.e. when no H_2 flux increase or decline is seen and when the membrane is perfectly dense. As example, the activation energy for H_2 permeation of membrane C01-F05 was determined by the two methods in the 250°C-350°C temperature range and the Arrhenius plot is shown in Figure 5-25. C01-F05 showed selectivities (H_2/He) over a 1000 at all temperatures.

The activation energy in the 250°C-300°C temperature range and in the 300°C-350°C temperature range determined while changing temperature were equal to 10.4 kJ mol^{-1} and 10.9 kJ mol^{-1} respectively. The overall activation energy estimated from $F_{0.5}$ H_2 permeance values was equal to 10.2 $kJmol^{-1}$.

Hence, considering F_{H2} when the temperature was changed at rates equal to or slower than 1°C/min led to a better determination of the activation energy for H_2 permeation. It has to be noted that the activation energy from method (1) and (2), if they did differ, they differed the first time the membrane was characterized at high temperatures. Indeed, once a membrane was exposed to the highest temperature (500ºC or higher), determining again the activation energy for all 250-300, 300-350, 350-400, 400-450 and 450-500ºC temperature intervals would give exactly the same value and, furthermore, a value equal to the E_p considering long term $F_{0.5}$ H_2 permeance. That was due to the fact that, during the second characterization, membranes did not undergo processes that would either lead to the decrease or the increase of the H_2 flux as a function of time.

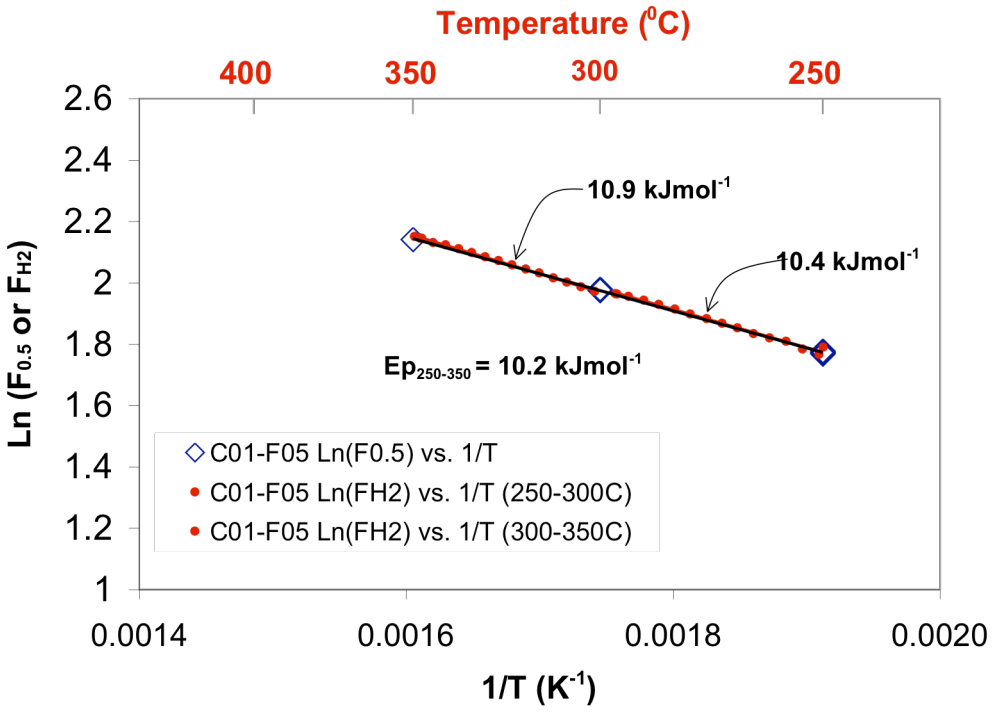

Figure 5-25 $Ln(F_{0.5})$ and $Ln(F_{H2})$ vs. 1/T for membranes C01-F05.

The determination of the E_p based on data taken during temperature change gave valuable information on the state and the H_2 permeation mechanism of the membrane at that particular moment. Therefore, it was possible to elucidate the processes taking place within the membrane as the temperature was increased. For instance, the E_p based on data taken during temperature changes decreased as higher temperature intervals were considered (300-350ºC -> 450-500º) if leaks appeared and grew. Also, a decrease in activation energy was explained by an increase of the support resistance contribution to the overall H_2 permeation resistance at high temperatures. On the contrary, an increase in activation energy was explained by intermetallic diffusion, which will be discussed in Section 8.3.2.

5.4.5.2 Activation energy measured at low temperatures in composite Pd membranes

From a fundamental point of view, it is very important to characterize the H_2 permeation properties of composite Pd membranes at low temperatures. At low temperatures, 250-300ºC, the microstructure of the electroless deposited Pd films was considered as "fresh" since no significant changes occurred (see Chapter 9, Figure 9-4). Table 5-2 lists the activation energy for the H_2 permeation determined by measuring H_2 flux as the temperature was increased for the 250-300ºC temperature range ($E_{p(250-300)}$) and the 300-350ºC temperature range ($E_{p(300-350)}$) for membranes C01-F03/5/7/8/11/11b. The activation energy for H_2 permeation of a fresh membrane, having a fine-grained structure, was found to be relatively low 9-12 kJ mol^{-1} in the 250-300ºC temperature range compared to the activation energy for H_2 permeance reported in the literature 13-19 kJ mol^{-1} (see Section 4.2.3). The low activation energy could not be explained by leaks since the He leak of all membranes was undetectable at such low temperatures. In addition, mass transfer

resistance at low temperature for membranes C01-F03/5/7/8/11/11b was negligible. It is believed that the reason for the low activation energy for H_2 permeance found in electroless deposited composite Pd membranes at low temperatures was due to the fine-grain structure that characterizes these membranes.

Table 5-2 $Ep_{(250-300)}$ and $Ep_{(300-350)}$ for C01-F03/5/7/8/11/11b membranes

Membrane	E_p (0.5) ±0.2 (250-300ºC)	E_p (0.5) ±0.2 (300-350ºC)
C01-F03	12.0	12.7
C01-F05	10.4	10.9
C01-F07	9.8	10.6
C01-F08	10.4	11.8
C01-F11	9.4	11.24
C01-F11b	10.3	12.3

Indeed, in a polycrystalline sample H_2 can diffuse along the boundaries between Pd crystallites i.e. grain boundaries. The diffusion through grain boundaries is characterized by an activation energy, which is believed to be lower than that of 'bulk diffusion' (Porter and Easterling, 1981). That is, at low temperatures, H_2 would essentially diffuse through grain boundaries in a polycrystalline Pd layer. At higher temperatures, both 'bulk diffusion' and grain boundary diffusion would occur and it is believed that the diffusion through the grain boundaries would still be faster than 'bulk diffusion'. However, grain boundaries represent a small fraction of the total diffusion sites, which are the sum of interstitial sites and grain boundaries sites. Therefore, more H_2 would diffuse through the bulk than through grain boundaries at high temperatures even though diffusion through 'narrow pathways' (the grain boundaries) is faster than 'bulk diffusion'.

5.5 Conclusions

The H_2 permeance of composite Pd membranes was determined using two methods: assuming Sieverts' law (n=0.5) and performing a non-linear regression on the experimental data to determine the n-exponent and the permeance. The n-exponent of a fresh composite Pd membrane (with no surface modification) decreased from 0.67 to 0.53 as temperature was raised from 300 to 500ºC mainly due to the fact that at higher temperatures the relation $P^{0.5}$ vs. n(H/Pd) could be considered as linear in the 0-4.5 bar pressure range (reduction of pressure effects). Also the n-value decreased due to the removal of contaminants. The activation of the surface by Pd seeding or air oxidation at T>300ºC slightly increased the rate of H_2 adsorption/desorption reactions. Air oxidation enhanced the H_2 permeance of membrane C01-F11b. The activity of the freshly formed Pd activated surface decreased due to Pd crystallites sintering at high temperatures. It was computed and validated that H_2 leaks through defects had no contribution to the n-exponent if the selectivities were over 200-300. Adjusting the n-exponent led to better fits of the H_2 flux than assuming Sieverts' law although it is important to understand that F_n and the n-exponent cannot be used to compare membranes. The n-exponent was used as a tool to assess the presence of large mass transfer resistance or large leaks although the right H_2 permeance value to report is $F_{0.5}$. The activation energy for H_2 permeation determined by the measurement of the H_2 flux, J_{H2}, while changing the temperature at a rate of 1ºC/min appeared to be accurate and a good method for the elucidation of the H_2 permeation mechanism or the internal modifications undergone by the composite Pd membranes as temperature was increased. It also appeared, that all fresh composite Pd membranes have a relatively low E_p, which was attributed to the fine grain structure.

6 Engineering substrate surface for the synthesis of ultra-thin composite Pd membranes

6.1 Introduction

It is well known that the deposition of Pd on Porous Metal (PM) supports requires a thicker layer of Pd to achieve a gas tight membrane than Pd deposition on Al_2O_3 and vycor glass supports. This difference in the thickness of the Pd layer is due to the average pore size, pore size distribution, roughness and the size of the largest pore at the porous metal support surface. PSS supports are characterized by a rather broad pore size distribution (0.1-8 μm) and the size of pores on the surface ranges between 0.1 to 20 μm in diameter. The size of the largest pore at the support surface is the crucial parameter to achieve a thin dense layer (Ma et al., 2001). Ma et al. (2001) deposited thin Pd layers on three PSS supports characterized by different grades: 0.1, 0.2 and 0.5 μm. Mercury intrusion analysis showed that the 0.1μm grade support included the smallest pores on the surface while the 0.5 μm grade included the largest pores on the surface. The Pd thickness needed to obtain a gas tight membrane was shown to be approximately three times the diameter of the largest pore on the surface for the three membranes. The typical Pd layer deposited by the electroless deposition method on PSS supports had a thickness of 15-50 μm with support grades in the 0.1 to 0.5 μm range. When special techniques are

coupled with the electroless deposition method, the thickness of the membrane can considerably be reduced. 8-10 μm Pd composite membranes were prepared on PSS (0.1μm grade) by the electroless plating method coupled with osmosis (Li et al., 1998; Souleimanova et al., 2000; Souleimanova et al., 2002; Souleimanova et al., 2001). Vacuum can also be applied across the porous support during Pd plating (Nam et al., 1999). The main disadvantage of osmosis and vacuum plating techniques is that Pd deposits very deep into the pore system of the porous support, thereby decreasing the permeance of the composite Pd membrane. Therefore, instead of "rushing" the deposition of Pd into the pores of the support, studies were undertaken to modify the pore size distribution at the surface of the porous support.

In order to smoothen the surface of the PSS supports, She (2000) performed a mechanical treatment by abrasion of the support (0.5 μm grade) with a metallic brush followed by treatment in 10 M HCl to reopen the pore structure. She (2000) prepared membranes as thin as 20 μm on polished supports by the electroless deposition method, which were quite thin taking into account the large grade of the support and the fact that no special technique (osmosis, vacuum plating) was used in addition to electroless deposition. Nam and Lee (2001) modified a PSS support (0.5 μm grade) by nickel powder deposition followed by the deposition of a silica layer by the sol-gel technique and obtained on such smoothed PSS support a 2 μm Pd-Cu membrane. Nam and Lee (2001) and Nam et al. (1999) obtained a 0.8 μm Pd-Ni membrane on a modified Ni powder-PSS support by using vacuum during electroless deposition. Poly-(dimethylsiloxane) sealing layer was also used to form a smooth surface on top of the α-Al_2O_3 (Athayde et al., 1994). They further prepared Pd/Ag membranes as thin as 0.25-1μm.

A new technique was described to smoothen the surface of any porous support characterized by a broad pore size distribution and large pores at the surface (Ma and Guazzone, 2004). This new technique consisted of depositing Pd seeded (pre-activated) Al_2O_3 powders of different sizes from a water-slurry, starting with coarse Al_2O_3 particles (3-5μm) and finishing with very fine Al_2O_3 particles (0.1-0.3μm). Each Al_2O_3 layer was consolidated by a short (10-15 min) deposition of Pd, which served as Al_2O_3 particle binder. The group of three Al_2O_3 layers was denoted as the grade layer.

The primary objective of the work described in this chapter was to understand the fundamental concepts behind the support surface modification leading to a regular and smooth surface. Hence, the surfaces of porous metal supports were modified by the deposition of Pd seeded Al_2O_3 powder (pre-activated powder), and the H_2 permeation properties of membranes formed on such supports were evaluated. Also, the ability of the grade layer to inhibit intermetallic diffusion was studied.

6.2 Experimental

6.2.1 Membranes considered in this chapter

Membranes C01-F03, C01-F04, C01-F05 and C01-F07 were prepared on oxidized PSS supports with no grade layer. Membranes C01-F08, C01-F09 and C01-F11b were prepared on graded oxidized PSS supports. Membranes Ma-32, Ma-32b, Ma-34, Ma-34b, Ma-41 and Ma-42 were prepared on graded oxidized PH supports. The grading of porous metal supports was performed according to the experimental protocol described in Section 3.1.2. However, different set of powders and different conditions were used for each

support. Table 6-1 summarizes all composite Pd membranes prepared on graded supports and the Al_2O_3 powder or the mixture of Al_2O_3 powders used for each layer.

C01-F08 was the first composite Pd membrane prepared on a graded support and only had one coarse Al_2O_3 layer as grade layer. The binding of Al_2O_3 was performed under vacuum. All other supports were graded using three groups of powders. Also, for all other membranes, the Al_2O_3 binding step was performed in the absence of vacuum. The binding step was performed by immersing the support with the deposited alumina layer into the Pd plating solution with the composition listed in Table 3-1.

Table 6-2 summarizes the characteristics of all membranes studied in this chapter. When no grade layer was applied to the supports (0.1 μm grade), 20-30 μm of Pd were needed to form a gas tight membrane. All membranes prepared on graded supports were significantly thinner (8-15 μm) than membranes obtained on the bare rough support. The He leak of all membranes before H_2 characterization was too low to be detected by the 0.01 sccm (0.1 sccm for large membranes) sensitivity digital mass flow meter except for membrane C01-F09 which had an initial He leak equal to 0.039 $m^3/(m^2$ h bar). The initial He leak of C01-F09 was due to a large and deep pore on the bare support that could not be completely closed with Pd. The He leak did not pose problems during the membrane characterization since the selectivity (H_2/He) of the membrane equaled 170 at 250ºC and a pressure difference of 1 bar (see Section 5.4.2).

Table 6-1 Al_2O_3 powders and binding conditions for the grading of C01-F08/9/11 and Ma-32/34/41/42

	1st Al_2O_3 layer	Binding step	2nd Al_2O_3 layer	Binding step	3rd Al_2O_3 layer	Binding step
C01-F08	-59 wt% of α Al_2O_3 5µm -29 wt% of α Al_2O_3 3µm -12 wt% of γ Al_2O_3 0.01-0.02µm ACTIVATED	20-30 min Under vacuum	-	-	-	-
C01-F09	-30 wt% of α Al_2O_3 5µm -5 wt% of α Al_2O_3 3µm -65 wt% of α Al_2O_3 1µm NOT ACTIVATED	-	-30 wt% of α Al_2O_3 3µm -10 wt% of α Al_2O_3 1µm -60 wt% of α Al_2O_3 0.3µm ACTIVATED	5 min. No vacuum	-30 wt% of α Al_2O_3 1µm -10 wt% of α Al_2O_3 0.3µm -60 wt% of γ Al_2O_3 0.01-0.02µm ACTIVATED	5 min. No vacuum
C01-F11	Same as C01-F09					
Ma-32	Same as C01-F09					
Ma-34	γ Al_2O_3 3µm ACTIVATED	15 min No vacuum	α Al_2O_3 0.3µm ACTIVATED	10 min No vacuum	γ Al_2O_3 0.01-0.02µm ACTIVATED	10 min No vacuum
Ma-41	γ Al_2O_3 3µm NOT ACTIVATED	-	α Al_2O_3 0.3µm ACTIVATED	20 min No vacuum	γ Al_2O_3 0.01-0.02µm ACTIVATED	20-25 min No vacuum
Ma-42	Same as Ma-41					

Table 6-2 Characteristics of all composite Pd membranes studied in this work.

membrane	Support	Surface (cm^2)	Thickness (From weight gain) (μm)	Permeance at 250ºC (m^3/m^2-h-$bar^{0.5}$)	Permeance at 500ºC (m^3/m^2-h-$bar^{0.5}$)	Permeance at 500ºC (m^3/m^2-h-$bar^{0.5}$) (Equation 4-11)	Selectivity at 500ºC (H_2/He)
C01-F03	0.1μm PSS	8.4	32	5.6	4.3	14.2	120
C01-F04	0.1μm PSS	8.4	28	7.8	4.7	18.7	1000
C01-F05	0.1μm PSS	8.4	33	5.9	10.3	15.9	587
C01-F07	0.1μm PSS	23	23	5.7	8	21.8	43
C01-F08	0.1μm PSS graded	23	15	8	22.5	23.8	300
C01-F09	0.1μm PSS graded	23	14	16	n.m.[(a)]	17 (at 250ºC)	170 (250ºC)
C01-F11	0.1μm PSS graded	23	15	8.9 (at 300ºC)	20.6	34.9	683
C01-F11b	0.1μm PSS graded	23	17	8.32	23.5	30.8	478
Ma-32	0.1 μm PH graded	120	7.7	21	50	68.1	42
Ma-32b	0.1 μm PH graded	120	10	15	42	52.5	27000→280[(b)]
Ma-34	0.1 μm PH graded	120	4	26 (at 300ºC)	49.6	131	300
Ma-34b*	0.1 μm PH graded	120	8	9.7	20	58	820→86
Ma-42	0.1 μm PH graded	120	5.6	20	39	93	980→818

[(a)] n.m = not measured

[(b)] The "→" indicates the change in selectivity at 500ºC from the selectivity value measured at time zero and the selectivity value measured at the end of the characterization procedure.

All membranes were characterized in H_2 atmosphere according to the characterization procedure described in Section 3.2.2 except for membrane C01-F09, which was only tested at 250°C to avoid the growth of the initial leak. Table 6-2 also lists the H_2 permeances all membranes should have had at 500ºC according to their thickness and equation (4-11). For ultra-thin membranes, Ma-32/34/34b/42, mass transfer limitations drastically decreased the performance of the membranes.

Figure 6-1 shows the surface of the thinnest (5.6 μm) composite Pd membrane, Ma-42, and the surface of membrane Ma-42, a Pd-Cu membrane. The surface of both membranes looked particularly shiny.

6.3 Results and discussion

6.3.1 The structure of composite Pd-graded support membranes

6.3.1.1 Thickness and structure of the grade layer

The thickness of the grade layer was difficult to measure since the weight gain after grading was close to the sensitivity of the scale, 0.01g, which corresponded to an average thickness of less than 1 μm. Table 6-3 lists the decrease in He permeance in percentage of the initial He permeance for C01-F08/9, Ma-32 and Ma-42 membranes. The grading of the supports led to a 20-60 % decrease of the initial He permeance. Such a broad variability in the He permeance loss was due to the support morphology, differences in Al_2O_3 powders used and differences in the short Pd deposition times used to bind Al_2O_3 particles.

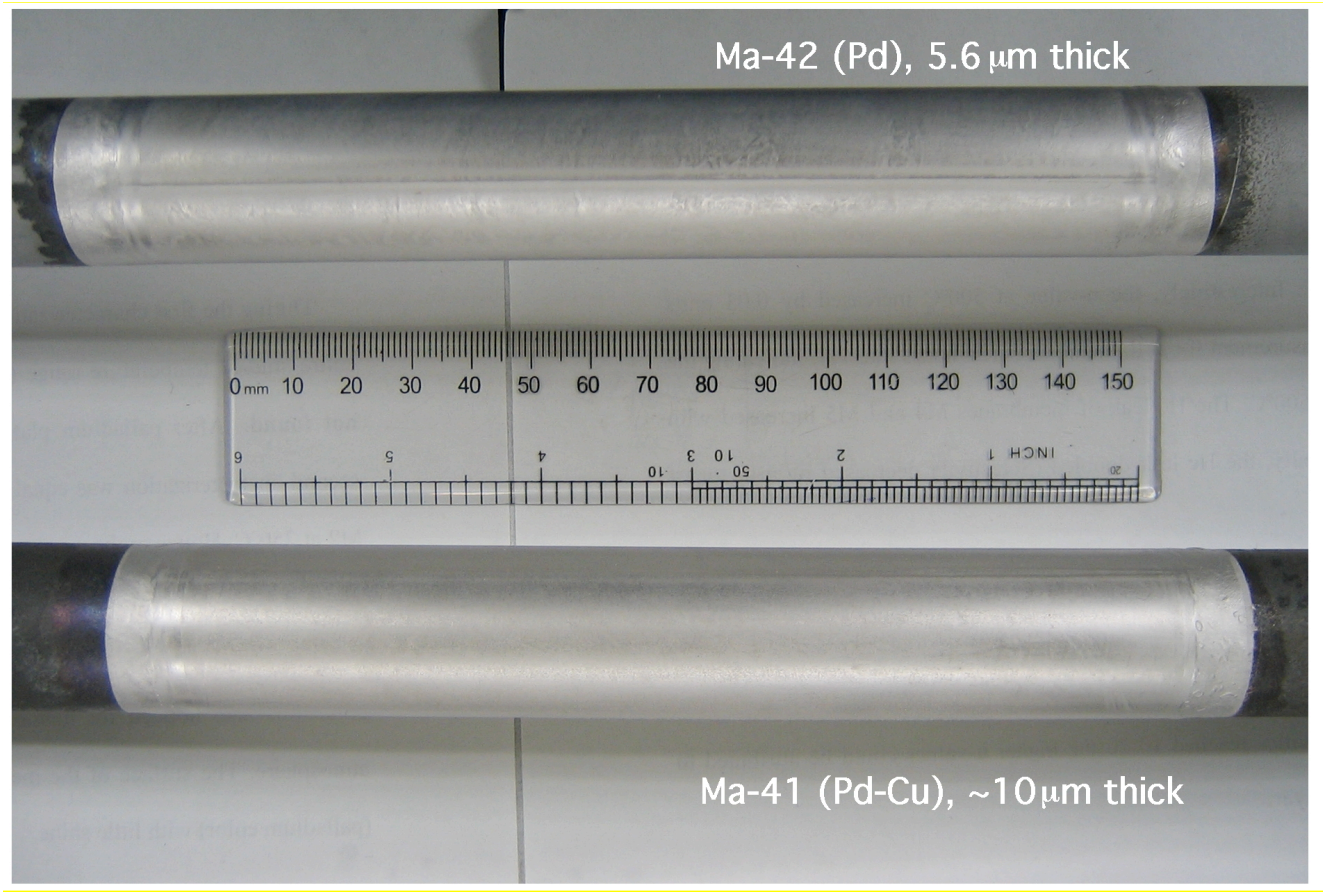

Figure 6-1 Surface of Ma-41 and Ma-42 composite Pd-based membranes.

Table 6-3 Percentage loss of the initial He permeance of the bare porous metal support after grading step.

membrane	He permeance after Ox. ($m^3/(m^2$ h bar))	He permeance loss. (% of initial flux)
C01-F08	274	16
C01-F09	286	25
Ma-32	155	60
Ma-42	114	20

Figure 6-2 is a high magnification SEM micrograph of a pore in membrane C01-F09. The figure clearly shows the structure of the grade Al_2O_3 layer within the mouth of the pore. The grade layer was exclusively located at the pores mouths of the support providing anchoring sites for the Pd layer to attach during the electroless plating deposition. The anchoring sites for the Pd layer are the tips[1] of PSS (or PH depending on the support) particles (see Section 3.1.2).

A 5 μm Al_2O_3 particle with no Pd on its surface (the first Al_2O_3 layer deposited on C01-F09's support was not activated) physically plugged the mouth of the pore allowing enough space for molecular H_2 to flow. The layer just on top of the 5 μm Al_2O_3 particle included fine Al_2O_3 particles (0.3-1 μm) coated with Pd. The third layer, including very small particles (0.01-0.3μm), was located on top of the second layer. Finally, the dense and uniform Pd layer was on top of the very fine Pd coated Al_2O_3 particles.

[1] The anchoring sites or tips of PSS (or PH) particles are shown in Figure 6-3, page 144

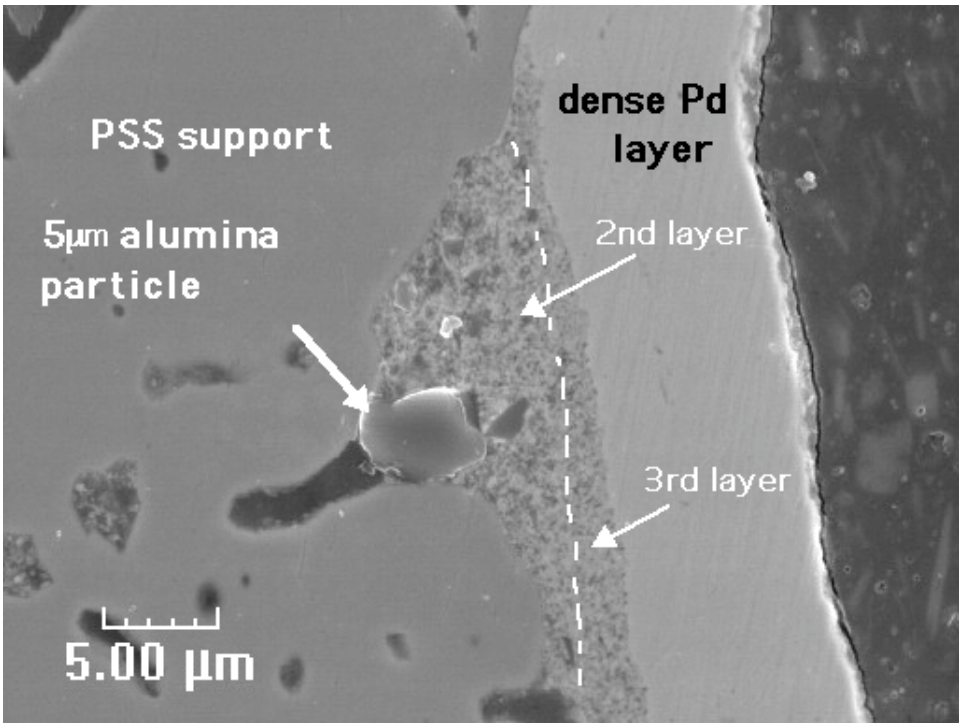

Figure 6-2 Structure within a pore achieved by sequential deposition of coarse, fine and very fine pre-activated powders.

6.3.1.2 Composite Pd membrane structure on "graded" supports

Figure 6-3(a) and (b) show the cross-section of membrane C01-F09 and Ma-34b respectively after exposure to H_2. Very uniform Pd layers were achieved on the rough surfaces of PM substrates after grading. Pd did not penetrate into the pore system due to the presence of the Pd coated Al_2O_3 grade layer. The grade layer is not visible in Figure 6-3(a) since Al_2O_3 particles initially present were removed during the polishing step[1] and left cavities between the PSS support and the Pd dense layer. Al_2O_3 particles remained on the support when the membrane was sintered at high temperatures increasing the cohesiveness of the grade layer. Since, membrane C01-F09 was only tested at 250ºC, the loosely packed powder was washed away except in small pores such as the one seen in Figure 6-2. The Al_2O_3 particles can be seen in Figure 6-3(b). Ma-34b was heated up to 600ºC in H_2 providing enough heat to the powder to bind and become more cohesive.

[1] The polishing step was part of the preparation technique for scanning electron microscope samples.

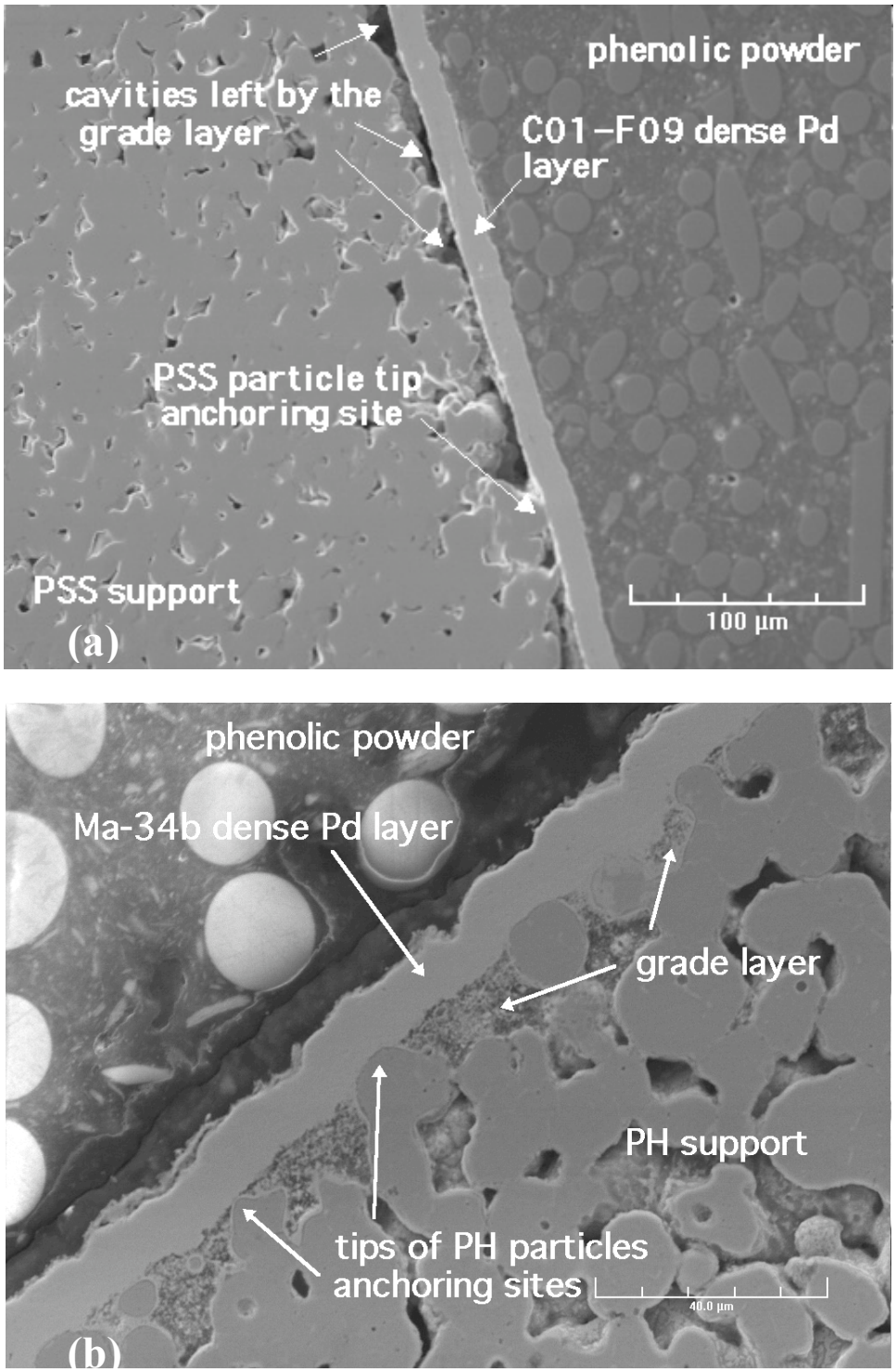

Figure 6-3 (a) Thin Pd layer (14µm) of C01-F09 membranes. (b) Thin Pd layer of (6-8µm) of Ma-34b membrane.

Figure 6-4(a) and (b) show the cross-section of membranes C01-F09 and C01-F03 respectively. C01-F03 was synthesized on a non-graded 0.1μm grade PSS support. When no pre-activated Al_2O_3 particles were deposited on the support, Pd penetrated quite deep into the pore system and the resulting Pd layer exhibited thicknesses that were at some points (inside the pores) twice as large as the ones determined by the gravimetric technique. Also, Figure 6-4(b) shows that the Pd layer followed the morphology of the support, therefore, grading the support provided a very smooth surface and the Pd layers of membranes C01-F09, Figure 6-4(a), and Ma-34b were very thin and uniform. C01-F04, C01-F05 and C01-F07 had a similar structure as C01-F03 since they were prepared following the same procedure as C01-F03

6.3.1.3 Effect of support quality on membrane thickness

Sequential deposition of coarse, fine and very fine pre-activated Al_2O_3 powders with intermediate short time of Pd deposition led to a smoother surface than the bare surface of the porous metal support. Theoretically, Pd layers having similar thickness would be obtained on graded supports independently of the original grade of the support. Indeed, it should be possible to form a thin Pd layer on a 0.5μm grade support after refining the pore size distribution at the surface with coarse, fine and very fine pre-activated powder.

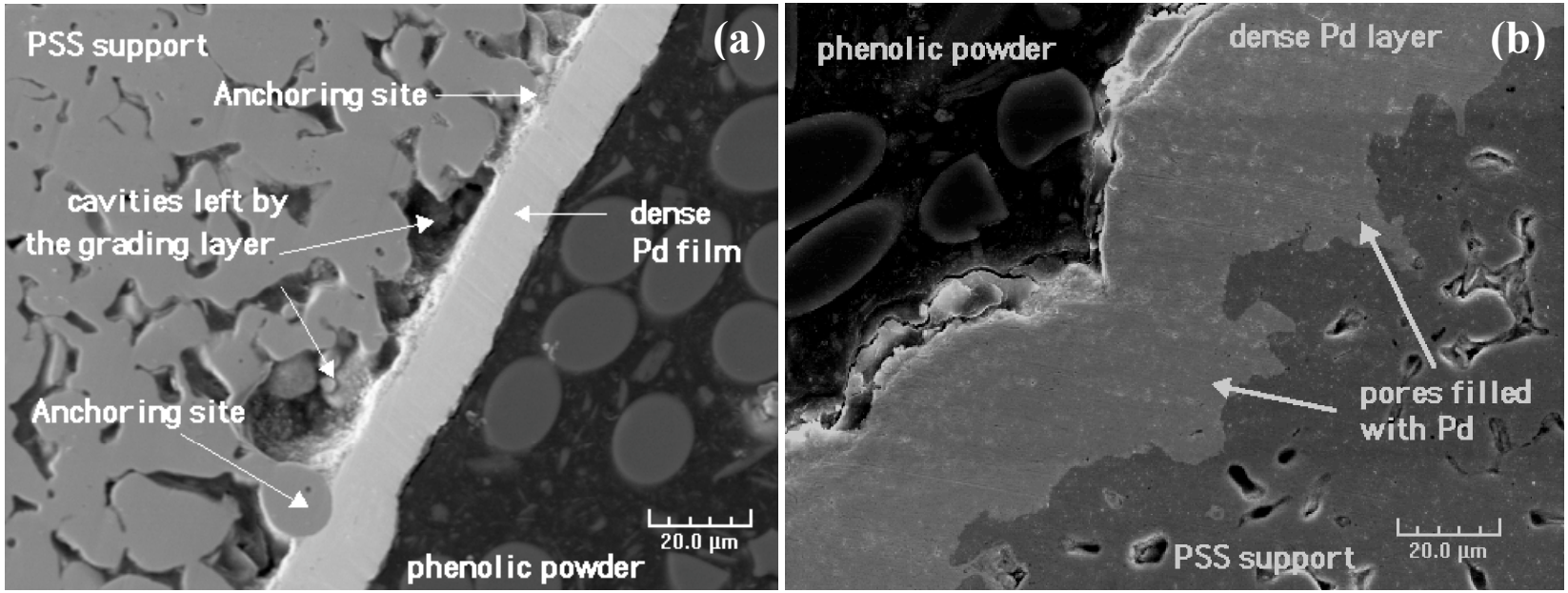

Figure 6-4 (a) SEM micrograph of membrane C01-F09. (b) SEM micrograph of membrane C01-F03. Mag: 1000X

However, the quality of the support had a strong influence on the membrane thickness, even after deposition of the grade layer, thereby affecting the H_2 flux of the membrane. Membranes C01-F08, C01-F09 and C01-F11b were prepared on 0.1 μm grade PSS supports. Ma-32, Ma-34 and Ma-42 membranes were prepared on 0.1 μm grade PH supports, which had a smoother surface than 0.1 μm grade PSS supports according to the metal support manufacturer. That is the reason why thinner membranes (Ma-32, Ma-34 and Ma-42) were achieved on PH supports than membranes prepared on PSS supports (C01-F08, C01-F09 and C01-F11) even if all supports were graded.

Figure 6-5 shows the He permeance as a function of the Pd thickness in the 0-12 μm range for C01-F03, C01-F05, C01-F07, C01-F09, Ma-32, Ma-34 and Ma-42 membranes. When no grade layer was applied (C01-F03, C01-F05 and C01-F07 membranes), the He permeance decreased by a maximum factor of ten after deposition of 12-15 μm of Pd. Grading the same supports that were used for the synthesis of C01-F03/5/7 membranes led to C01-F08, C01-F09 and C01-F11/11b in which 10 μm of Pd were sufficient to decrease the He permeance of their supports by a factor of 1000 attesting the importance of obtaining a smooth layer for the formation of thin membranes. Grading supports with an even smoother initial surface (PH supports) led to very thin gas tight membranes with Pd thicknesses in the order of 5-7μm.

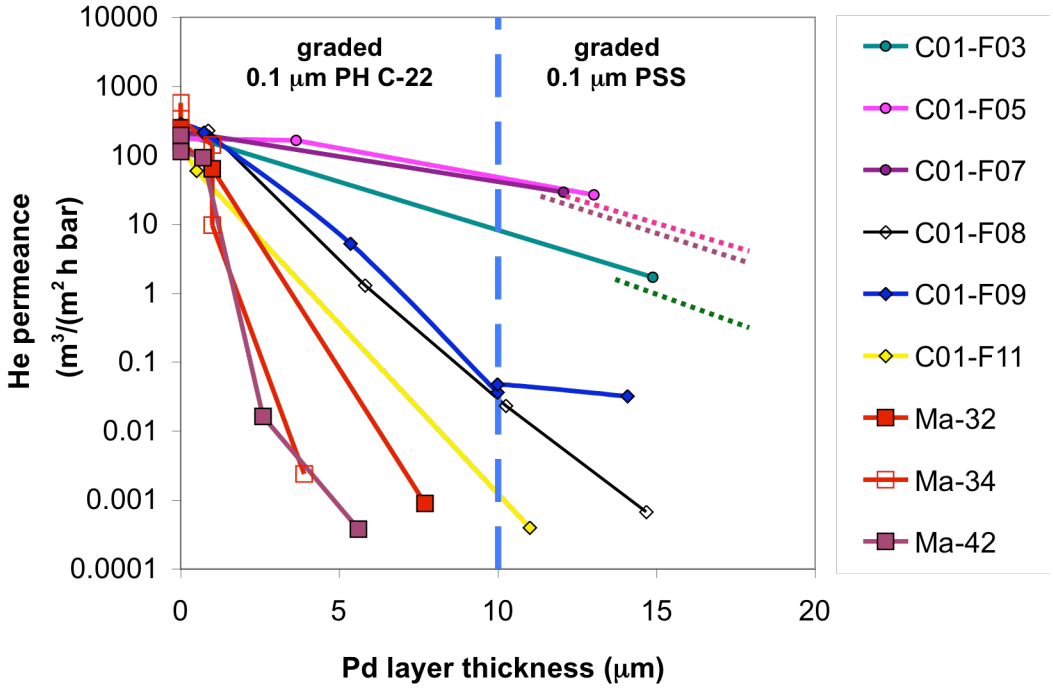

Figure 6-5 He permeance vs. Pd thickness for C01-F03/5/7 (PSS supports), C01-F08/9/11 (graded PSS supports) and Ma-32/34/42 (graded PH supports)

6.3.2 *H_2 permeance, selectivity and long-term stability of composite Pd graded-support membranes*

6.3.2.1 The H_2 permeance of composite Pd-graded supports membranes

Although membrane C01-F08 was only 15 μm thick, it showed a permeance of 15 $m^3/(m^2\ h\ bar^{0.5})$ at 500ºC, which was characteristic of a 21-25 μm membrane (see Table 6-2). This low permeance was attributed to a large quantity of Pd in the pores of the support. In deed, during synthesis, the pre-activated 3μm-5μm mixture Al_2O_3 powder was consolidated with Pd under vacuum (pulled from the tube side).

The driving force provided by the use of vacuum resulted in the Pd deposition very deep within the pores of the support. Pd plating after powder deposition resulted in a very thick membrane within the pores, i.e., around 5μm of pore path and 15μm of dense membrane led to a 20-25μm thick membrane. The first Al_2O_3 powder layer deposited on C01-F09 was not activated, thus preventing Pd deposition too deep into the pores, which allowed for a higher permeance than C01-F08.

Figure 6-6 shows the H_2 permeance, F_{H2}, at 250ºC of membrane C01-F09 as a function of time. The permeance was calculated from the H_2 flux at 1 bar pressure difference (2:1) assuming the pressure exponent equal to 0.5 (Sieverts' law). The H_2 permeance sharply increased up to 8.5 $m^3/(m^2\ h\ bar^{0.5})$, then showed a slower increase up to 16 $m^3/(m^2\ h\ bar^{0.5})$ in 40 hr. The mechanism leading to the H_2 flux increase with time in fresh composite Pd membranes was the opening of channels within the grade layer after either moisture desorption or slight rearrangements of Al_2O_3 particles. All composite Pd membranes prepared on graded supports showed a transition period where the permeance increased as a function of time for about 40 to 100 hr.

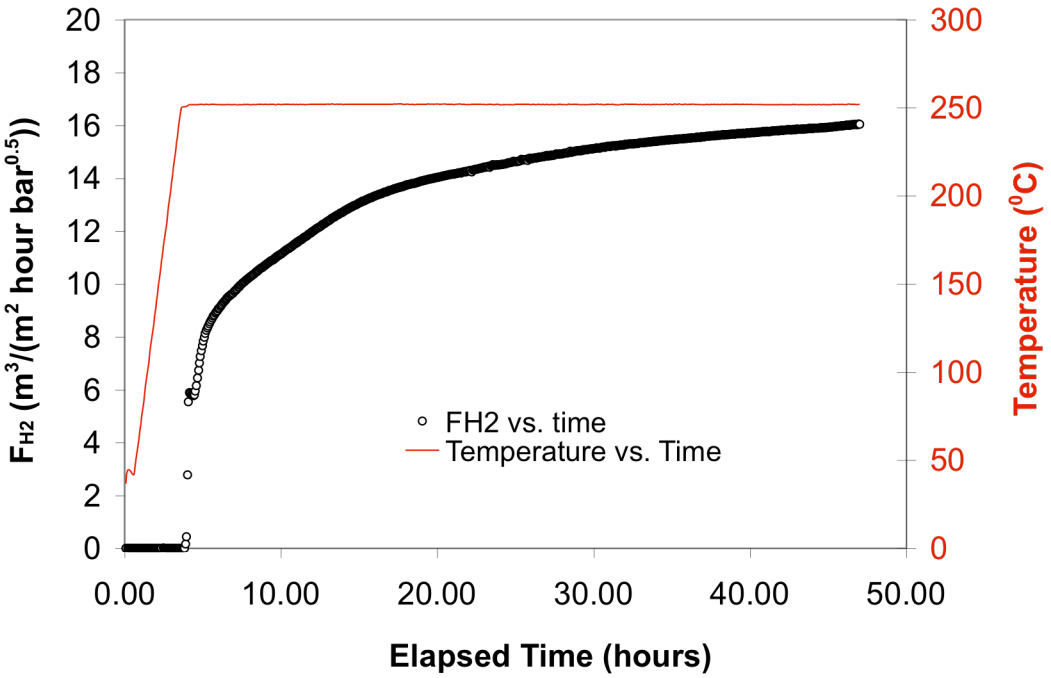

Figure 6-6 H_2 permeance vs. time at 250ºC for membrane C01-F09.

It is important to note that the permeance of C01-F09 at 250ºC was two times higher than the permeance of C01-F08 membrane (8 $m^3/(m^2\ h\ bar^{0.5})$) even though both membranes were prepared on graded supports. This result clearly demonstrated the fact that grading with pre-activated Al_2O_3 powders without the use of vacuum during powder binding avoided Pd deposition deep in the neck of the pores resulting in a very thin membrane. Hence, for all membranes prepared after C01-F08 (C01-F09, Ma-32 and Ma-42) powder consolidation with short time Pd deposition was performed in the absence of vacuum. The use of vacuum during powder binding and during Pd deposition was the cause for C01-F08 to have such a low permeance compared to C01-F09.

Figure 6-7 shows the Arrhenius plot of H_2 permeance for all membranes considered in this chapter. The H_2 permeance of membranes C01-F03 and C01-F04 decreased as the temperature was increased due to intermetallic diffusion. The causes and the mechanism of intermetallic diffusion are elucidated in Chapter 8 Sections 8.3.2 and 8.3.3. The H_2 permeance of membranes C01-F05 and C01-F07 were only slightly affected by intermetallic diffusion since the support of these membranes were oxidized at 500ºC as it will be explained in Chapter 8. Membranes C01-F08/9/11/11b did not show signs of intermetallic diffusion most probably due to the presence of the grade layer. Membranes C01-F08/9/11/11b also showed higher H_2 permeances than C01-F03/4/5/7 since they were prepared on graded PSS supports and had a thinner Pd layer. Membranes Ma-32 and Ma-42 showed very high H_2 permeance values due to the uniformity and the thinness of the Pd layers achieved on graded PH supports. The H_2 permeance of membranes Ma-32 and Ma-42 did not decline at high temperatures due to the good capability of the grade layer and oxidized PH supports to inhibit intermetallic diffusion (see Section 0). Figure 6-7 also shows the calculated H_2 permeance vs. 1/T (dashed line) of an hypothetical Pd foil with the same thickness as Ma-32. The H_2 permeance of this hypothetical Pd foil was calculated with equation (4-11) of Section 4.2.3. It appears then evident that Ma-32 had a low activation energy for H_2 permeance of 9 kJ mol^{-1} indicative of mass transfer resistance within the support.

Figure 6-8 shows the H_2 permeability of all membranes as a function of 1/T. The average H_2 permeability computed in Section 4.2.3 was also plotted in Figure 6-8 for comparison purposes.

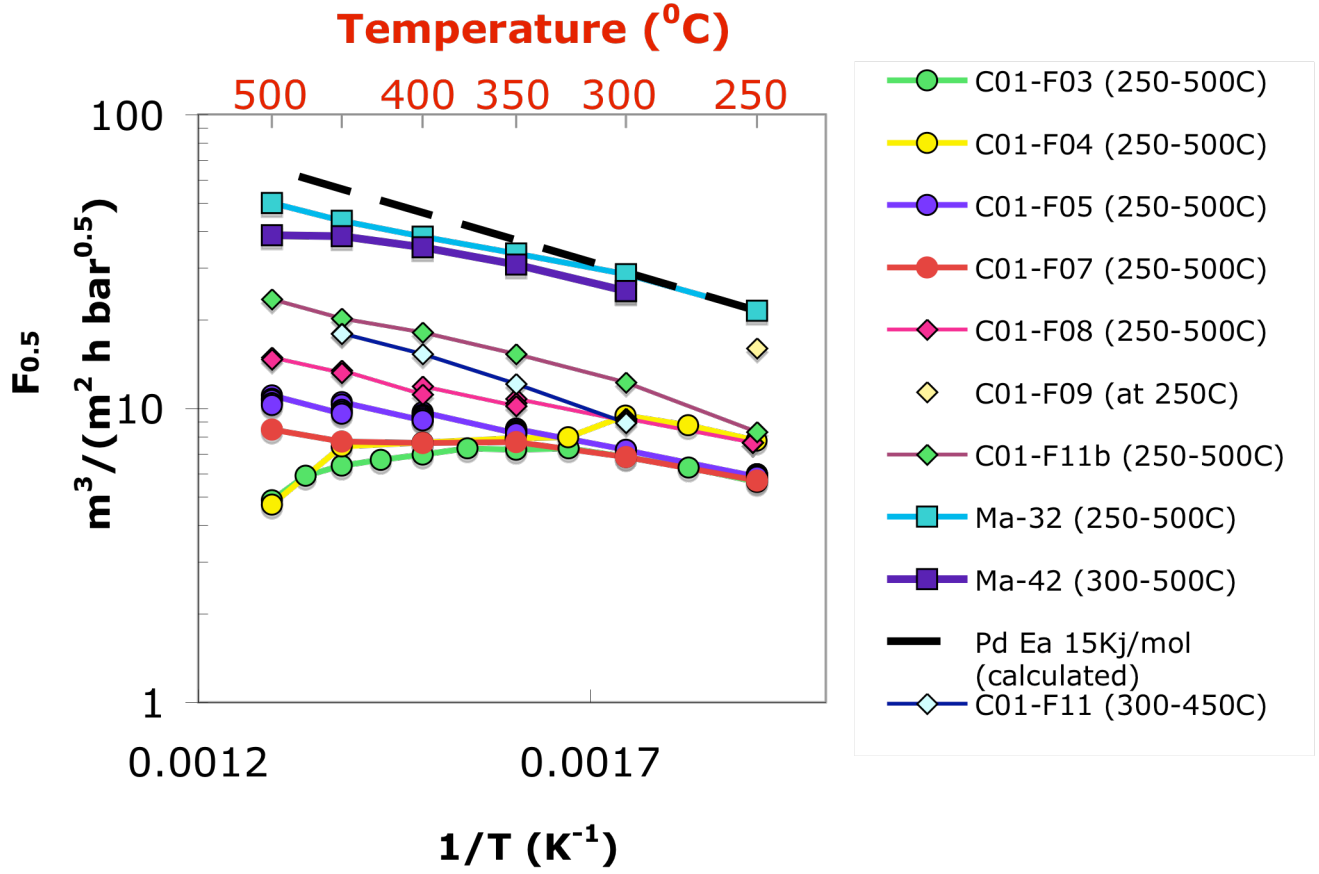

Figure 6-7 Arrhenius plot of H_2 permeance, $F_{0.5}$, for composite Pd membranes prepared on non graded supports (circles) and graded supports (squares)

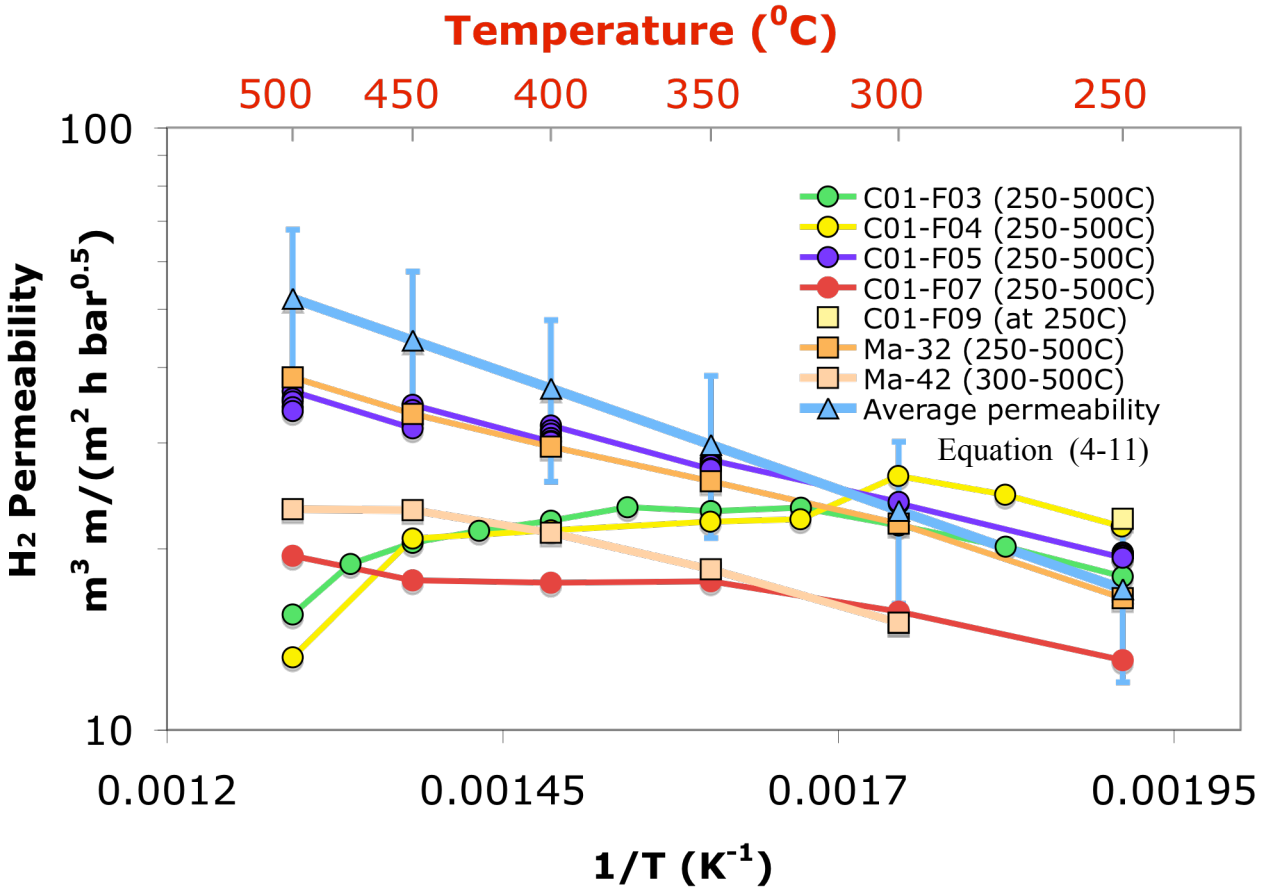

Figure 6-8 Arrhenius plot of H_2 permeability for composite Pd membranes prepared on non graded supports (circles) and graded supports (squares)

Figure 6-8 shows that composite Pd membranes prepared in this entire study have the same H_2 permeability at low temperatures (250-350ºC) as the average H_2 permeability in Pd foils. At higher temperatures (350-500ºC) the H_2 permeance declined due to intermetallic diffusion (C01-F03/4/5) or deviated from the ideal H_2 permeability due to mass transfer resistance in the porous support (Ma-32 and Ma-42). Figure 6-7 and Figure 6-8 clearly show that the overall effect of mass transfer resistance was the lowering of the activation energy for H_2 permeance from 14.9 $kJmol^{-1}$ to 9-10 kJ mol^{-1}. This effect is modeled in Section 5.2.1 and experimentally confirmed in Section 5.4.3.

The higher permeance of composite Pd membranes prepared on graded supports was essentially due to the thinness and uniformity of the Pd layer that one can achieve on "graded" supports. Indeed, as listed in Table 6-2, membranes prepared on non-graded supports had a relatively thick Pd layer ranging from 20 to 30μm while composite Pd membranes prepared on graded supports had a thinner Pd layer ranging from 6 to 14 μm. Such thin Pd layers were only possible due to the support uniformity achieved after grading.

Figure 6-9 shows the H_2 permeance, $F_{0.5}$, of C01-F09, Ma-32/34/42 membranes as a function of 1/T as well as the H_2 permeance of recent composite Pd membranes reported in the literature and listed in Table 6-4. It is quite interesting to note that Tong et al. (2005c), who graded their PSS support with $Al(OH)_3$ colloids, achieved similar H_2 permeance as the H_2 permeance shown by Ma-32/34. Su et al. (2005) also reported quite high H_2 permeance values for composite Pd membranes prepared on PSS supports graded with a SiO_2 layer deposited by the sol-gel technique.

Table 6-4 Characteristics recent composite Pd membranes reported in the literature.

Reference	Support	Deposition method	Thickness (μm)	Temperature (ºC)	Permeance at Temp. (m^3/m^2-h-$bar^{0.5}$)	Selectivity
(Li et al., 1998)	PSS	Electroless+Osmosis	10	480	19[1]	1400 (H_2/N_2)
(Yan et al., 1994)	Al_2O_3		8	500	41	1000 (*which gas?)
(Uemiya et al., 1991d)	Al_2O_3	electroless	4.5	400	36.9	∝
(Collins and Way, 1993)	Al_2O_3	electroless	11.4	550	31.8[2]	650 (H_2/N_2)
(Mardilovich et al., 1998)	PSS	electroless	21	500 (350)	16.4 (7.8)	5000 (H_2/N_2)
(Jun and Lee, 2000)	Al_2O_3	MOCVD	1-2	450	38[3]	780 (H_2/N_2)
(Jun and Lee, 2000)	Ni-PSS	MOCVD	0.5-3	450	324[4]	1600 (H_2/N_2)
(Wang et al., 2004)	ZrO_2-PSS	electroless	10	500	16.5	156 (H_2/Ar)
(Tong et al., 2005c)	Al(OH)-PSS	electroless	6.4	500	50[5]	Not reported
(Tong et al., 2005c)	Al(OH)-PSS	electroless	6.4	500	58.8[5]	Not reported
(Cheng et al., 2002)	γ-Al_2O_3/α-Al_2O_3	electroless	3	450	12.1	250 (H_2/N_2)
(Su et al., 2005)	SiO_2-PSS	electroless	5-6	500	49.5[6]	300 (H_2/N_2)

[1] Determined from Figure 4 in the original publication

[2] Calculated assuming n=0.5 with the original data: J_{H2} = 0.71 mol/(m^2 s); feed pressure: 790610 Pa; permeate pressure: 101325 Pa.

[3] Calculated assuming n=0.5 with the original data: J_{H2} = 18.8 (cm^3/ cm^2 min); ΔP: 51.7 cm Hg; permeate pressure: 101325 Pa.

[4] Calculated assuming n=0.5 with the original data: J_{H2} = 160 (cm^3/ cm^2 min); ΔP: 51.7 cm Hg; permeate pressure: 101325 Pa. The H_2 flux value is obviously mistaken.

[5] Calculated assuming n=0.5 with the original data: J_{H2} = 0.260 mol/(m^2 s); feed pressure: 100 kPa; permeate pressure: 101325 Pa. (J_{H2} = 0.302 mol/(m^2 s) for the membrane having a permeance of 58.8 $m^3/(m^2$ h $bar^{0.5}$)).

[6] Reported H_2 permeance: 2.5-2.7 10^6 mol/m^2 s Pa. The permeance of 49.5 $m^3/(m^2$ h $bar^{0.5}$)) was determined by calculating the H_2 flux at ΔP=0.5 bar, n = 0.5 and the permeate pressure = 1 bar.

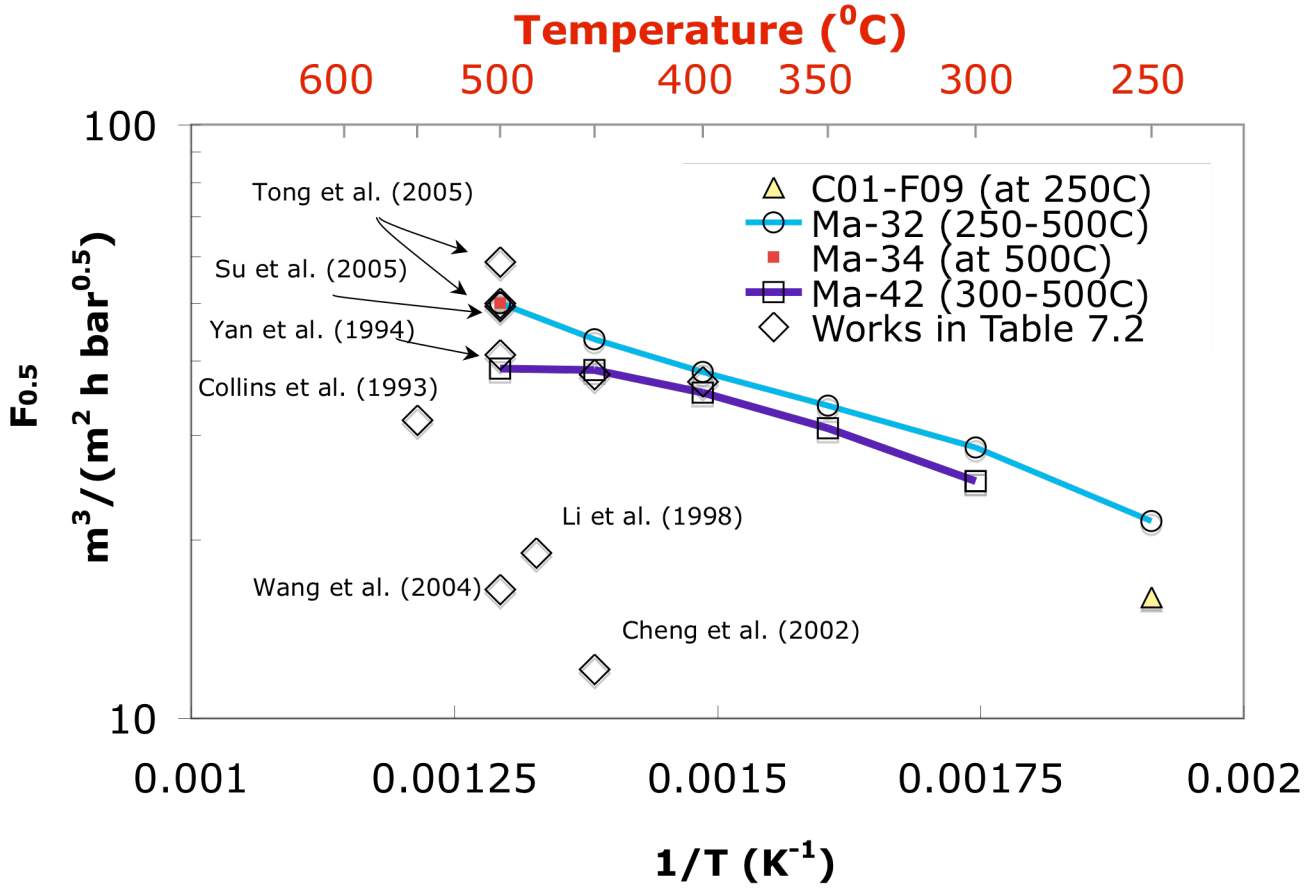

Figure 6-9 Comparison of H_2 permeance for membranes C01-F09 Ma-32/34 and Ma-42 with recent works listed in Table 6-2

Composite Pd membranes prepared on either α-Al_2O_3 or γ-Al_2O_3-α-Al_2O_3 supports were thinner (Cheng et al., 2002; Jun and Lee, 2000; Uemiya et al., 1991a) although their H_2 permeance was lower than the H_2 permeance of Ma-32/32b/34 and membranes prepared by Tong et al. (2005c) and Su et al. (2005), which were prepared on porous metal supports. Alumina supports have a lower porosity than porous metal supports, therefore, a possible reason for the low H_2 permeances reported by Jun and Lee (2000) and Uemyia et al. (1991a) was the presence of mass transfer resistance within the alumina support. Tong et al. (2005c) and Su et al. (2005) did not report the long-term H_2 permeance and selectivity stability for their membranes.

6.3.2.2 The selectivity of composite Pd graded-support membranes

Figure 6-10 shows the selectivity (H_2/He), or ideal separation factor, of membranes C01-F11/11b and Ma-34b/41/42 as a function of temperature. For some membranes, e.g. Ma-34b, several data points were plotted at a given temperature when the selectivity was determined several times at a given temperature. All membranes showed very high selectivities at temperatures equal to or lower than 400ºC. The selectivity at T<400ºC for all membranes was higher than 1000. C01-F11 and Ma-34b/42 membranes showed selectivities values higher than 3000 at temperatures lower than 400ºC. The selectivity of all membranes started to decrease at 450ºC and became low at 500ºC. The red line at 475ºC in Figure 6-10 represents the temperature above which the selectivity of all membranes was lower than 1000, which is still a very good selectivity. Membrane Ma-42 showed a high selectivity of 818 even after 185 hr at 500ºC in pure H_2.

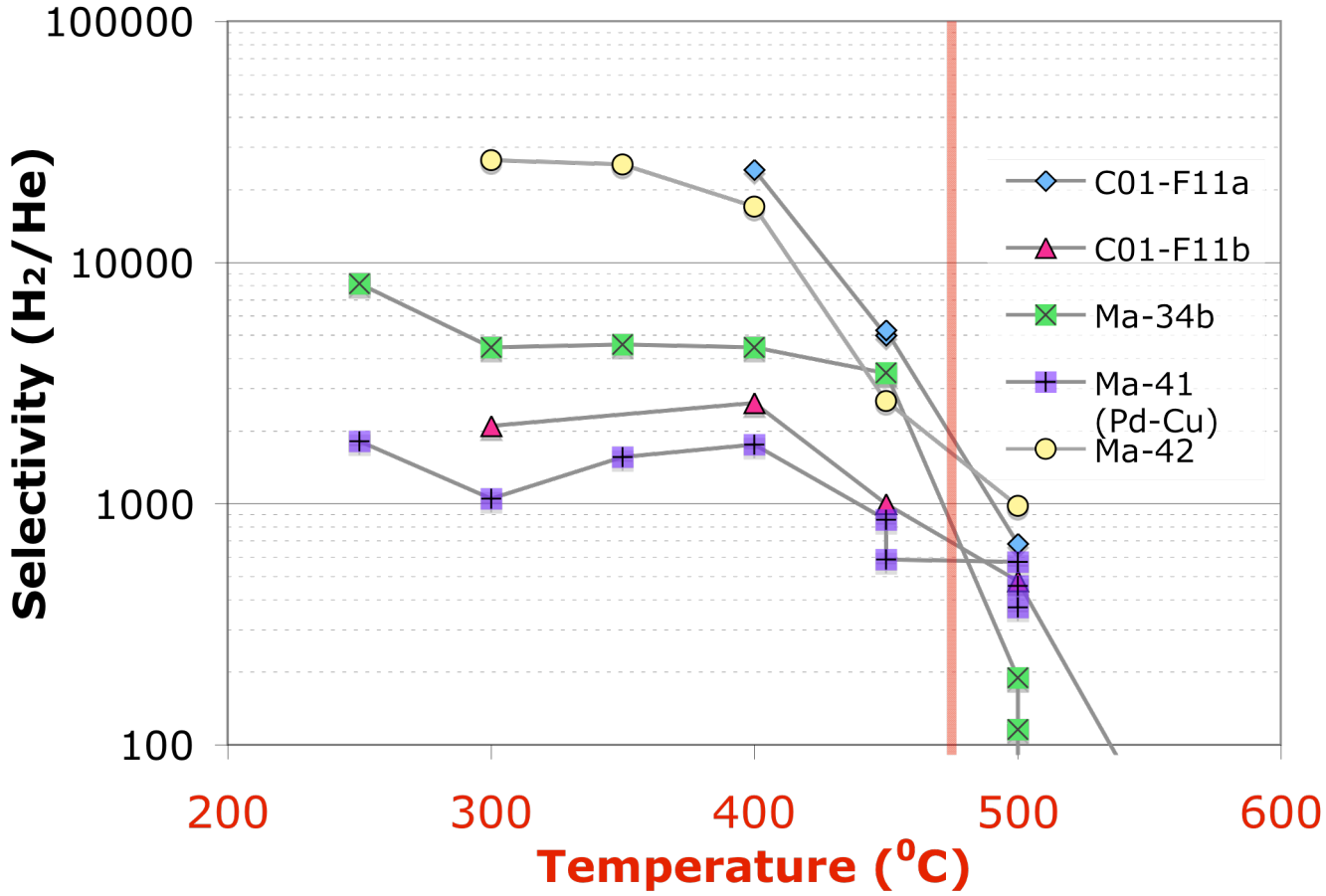

Figure 6-10 Ideal selectivity of some membranes prepared on graded supports as a function of temperature

Ma-41 also showed a good selectivity of 370 even after 215 hr at 500ºC in pure H_2.

The selectivity of C01-F03 membrane was not plotted since its He leak rate was only measured at room temperature after cooling the membrane from 500ºC. The He leak rate at room temperature was equal to 0.0148 $m^3/(m^2$ h bar), hence, its selectivity at 500ºC was above 120. The selectivity of C01-F04 was only determined at 500ºC and was close to 1000. The selectivity of C01-F05 was equal to 587 after 100 hr at 500ºC in H_2 and higher than 380 after excursions up to 700ºC for a few hours in H_2. The membrane suffered from severe intermetallic diffusion at 700ºC. The Pd layer and the PSS support fused and blocked all the porosity at the Pd-PSS interface.

6.3.2.3 Long term stability of composite Pd graded PH membranes

All composite Pd membranes prepared on graded oxidized PH supports showed a very good H_2 permeance long-term stability. Figure 6-11 shows the H_2 flux, J_{H2}, and the H_2 permeance, F_{H2}, as a function of time at 500ºC for membrane Ma-32b. The H_2 permeance was equal to 39 $m^3/(m^2$ h $bar^{0.5})$ and slowly increased up to 42.5 $m^3/(m^2$ h $bar^{0.5})$ after 1100 hr at 500ºC in H_2 atmosphere. As of today, no research group reported stable H_2 permeance over 1000 at the high temperatures of 500ºC for composite Pd membranes prepared on PM supports. Figure 6-12 shows the selectivity, the H_2 permeance and the He leak rate of Ma-32b as a function of time at 500ºC in H_2 atmosphere. The selectivity (H_2/He) of Ma-32b decreased from 27000 at the beginning of the experiment to 300 at the end of the experiment. Hence, even though the H_2 flux through defects slightly increased, it did not affect the H_2 permeance value (see Section 5.4.2) and the membrane was still considered as a composite Pd membranes with high separation properties.

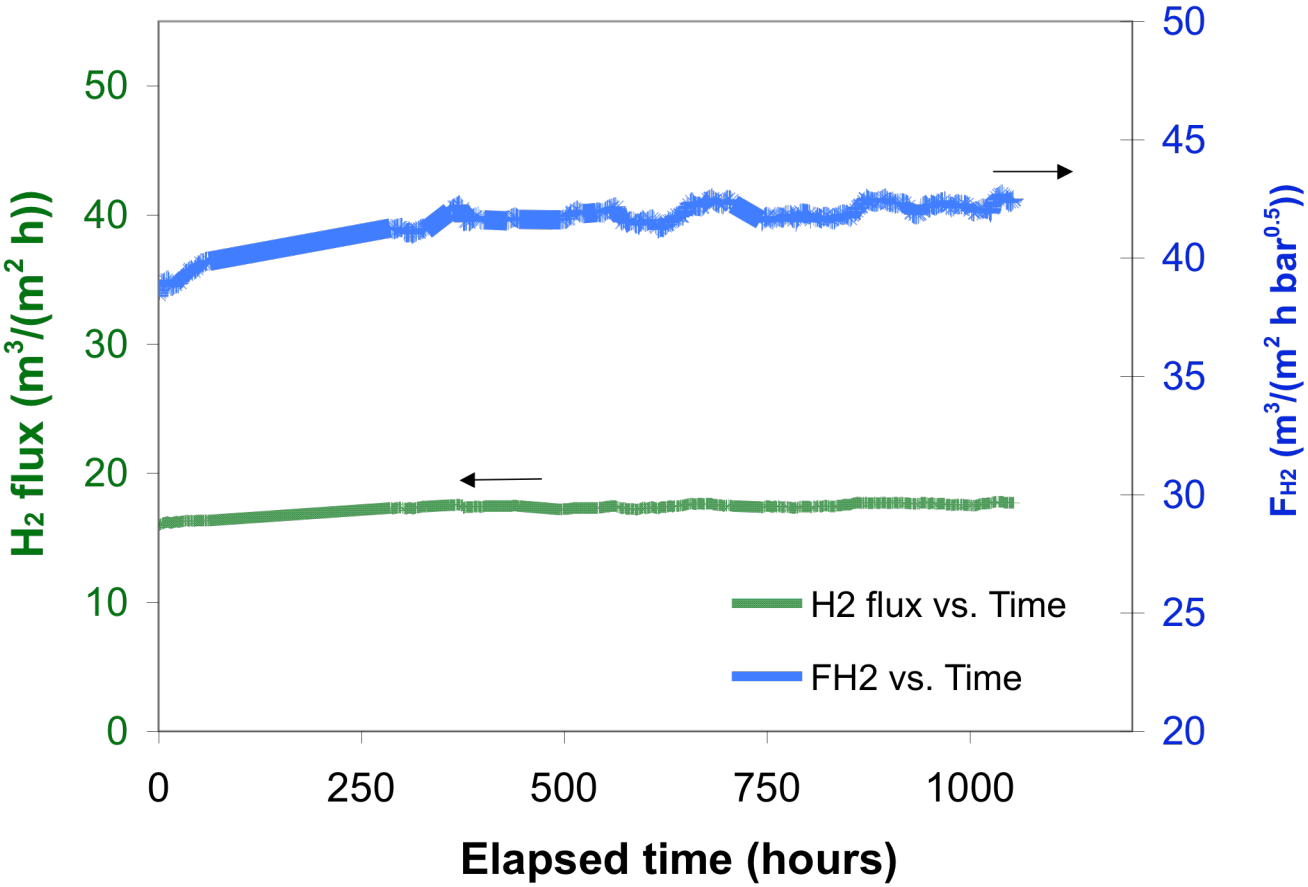

Figure 6-11 Long-term H_2 permeance stability at 500°C for membrane Ma-32b

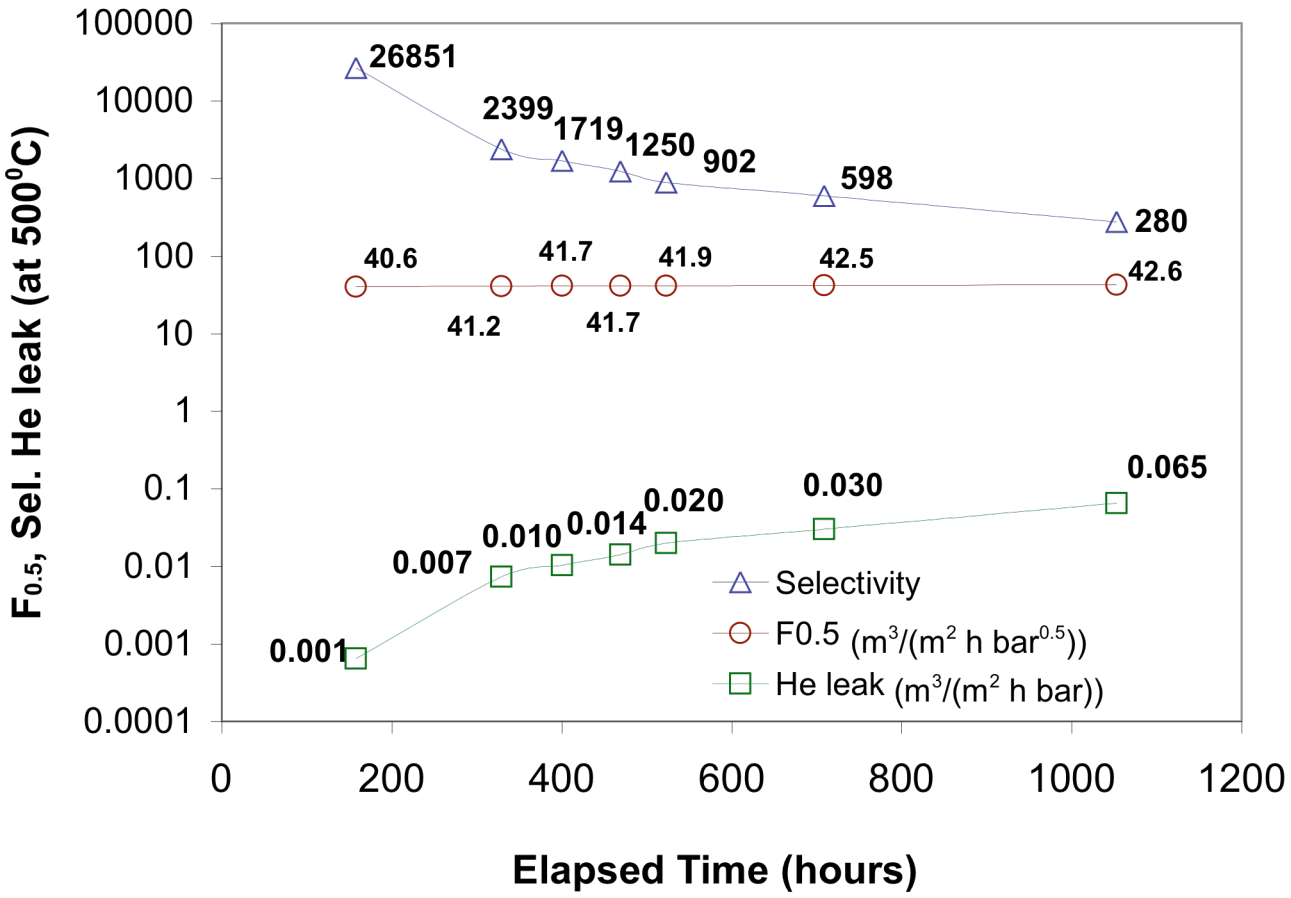

Figure 6-12 Selectivity, H_2 permeance and He leak rate as a function of time at 500ºC for Ma-32b

The increase from 39 to 42.5 $m^3/(m^2\ h\ bar^{0.5})$ was due to structural changes in the grade layer as explained in Section 6.3.2.1. The good long-term H_2 permeance stability of composite Pd membranes prepared on graded PH supports was due to: (1) the fact that only Cr_2O_3 oxide appeared on the surface of PH after oxidation, (2) the low driving force for Fe diffusion due to the low Fe concentration in PH and (3) the presence of the Pd-Al_2O_3 grade layer as it is explained in the following section. Points (1) and (2) are discussed in Chapter 8.

6.3.3 The grade layer as a barrier against intermetallic diffusion

6.3.3.1 The H_2 flux stability at high temperatures (>500ºC) of membrane C01-F08

The H_2 flux stability at high temperatures was tested on membrane C01-F08. The H_2 permeance and He leak of membrane C01-F08 were measured at 500, 550 and 600ºC. The membrane was held at a given temperature for 72 hr. Figure 6-13 shows H_2 permeation of membrane C01-F08 and the temperature as a function of time. At 500ºC the H_2 permeance of membrane C01-F08 equaled 22.5 $m^3/(m^2\ h\ bar^{0.5})$) and stayed relatively stable for 72 hr. When the temperature was increased to 550ºC a linear decrease in H_2 permeance was observed. Such a decrease in H_2 permeance was attributed to the diffusion of mostly Fe (see Section 8.3.1.2) from the support into the dense Pd layer, which became important at temperatures above the Tamman temperature of stainless steel (550ºC). At 600ºC a large H_2 flux loss was recorded during the first 17 hr followed by a large H_2 flux increase from 25.8 to 29.7 $m^3/(m^2\ h\ bar^{0.5})$) due mainly to defects formation in the dense film. Figure 6-14 shows the H_2 permeance, He leak and selectivity (H_2/He) for membrane C01-F08.

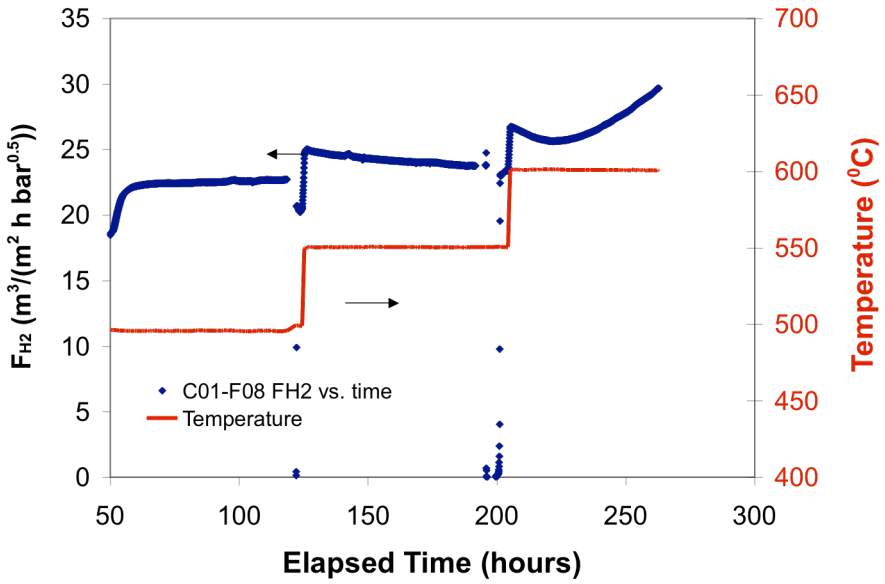

Figure 6-13 H_2 permeance as a function of time for membrane C01-F08 at 500, 550 and 600ºC

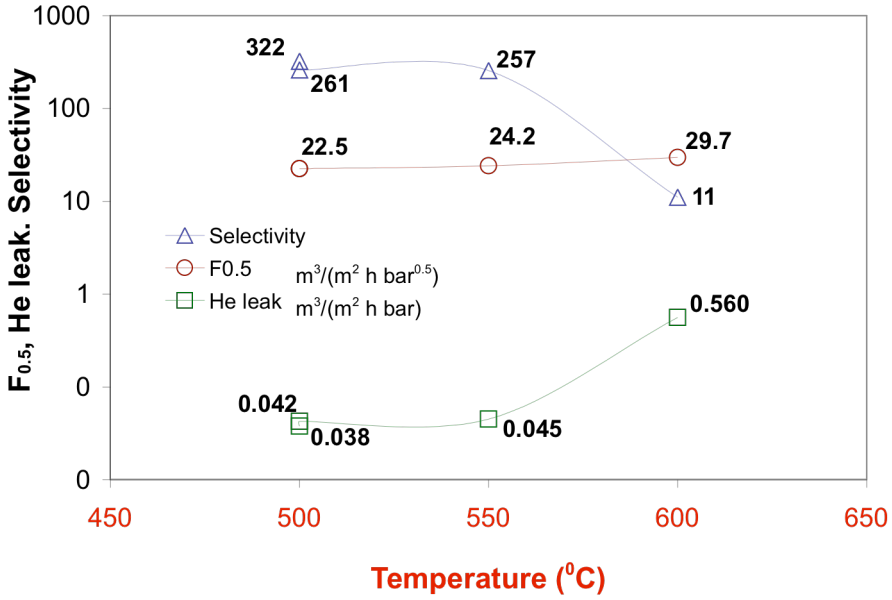

Figure 6-14 Selectivity (H_2/He), H_2 permeance and He leak for membrane C01-F08 at 500, 550 and 600ºC

At the end of the H_2 characterization the selectivity of the membrane was only 11. Pinholes were estimated to be as large as 1.6 μm in diameter from the He permeance vs. P_{ave} data (see Section 10.3.1.1).

Membranes prepared on graded PH supports showed very good H_2 permeance stability. That is, no decline in H_2 permeance was observed at 500ºC for over 1000 hr (Ma-32b). The reasons for such an outstanding stability of Pd composite membranes on PH were due to the type of oxide that is formed on PH supports. The oxide structure formed on PSS and PH supports and their effect on long term H_2 permeance stability is studied with great detail in Chapter 8. In addition, the presence of the Al_2O_3 grade layer significantly reduced intermetallic diffusion in C01-F08 membrane. Therefore, the long term H_2 permeance stability of Ma-32b/34b/42 was also due to the presence of the Al_2O_3 grade layer.

6.3.3.2 The grade layer as intermetallic diffusion barrier

The following section aimed at the understanding of the ability of the Al_2O_3 grade layer to mitigate intermetallic diffusion. After the H_2 characterization at 250ºC, the porous section of membrane C01-F09 was cut in three pieces and each piece was heat-treated at a different temperature in order to investigate the temperature stability of the grade layer. It was especially desired to establish if the grade layer could reduce or inhibit the diffusion of Fe, Cr and Ni from the PSS support into the Pd dense film at 500ºC. The temperature treatment of samples cut out of C01-F09 membranes was performed in H_2 atmosphere at 400, 500 and 600°C for 48 hr.

Figure 6-15(a), (b) and (c) represent the cross-section of three different samples from C01-F09 heated at 400, 500 and 600ºC respectively. The structure and morphology of the grade layer in Figure 6-15(a) and (b) are the same as the grade layer seen in Figure 6-2. Therefore, no visible structural changes occurred at temperatures equal to or higher than 500ºC. However, at 600ºC, intermetallic diffusion led to the white patches seen in the grade layer as well as white patches seen on the stainless steel particles (diffusion of Pd into the stainless steel particles and vice versa).

Figure 6-16 and Figure 6-17 show the elemental composition across the grade layer for the sample heated at 500ºC and 600ºC respectively. Both elemental composition lines were performed at a position where the grade layer was around 5μm thick. The traces of Fe, Cr and Ni fell below the detection limit within the first micron of the grade layer in the sample heated at 500ºC (Figure 6-16). Therefore, the grade layer successfully protected the selective Pd layer from intermetallic diffusion at 500ºC. The Fe, Cr and Ni traces were visible all across the grade layer for the sample heated at 600ºC indicating that intermetallic diffusion occurred through the fine grain structure of the grade layer at 600ºC. However, no traces of Fe, Cr and Ni were detected in the dense Pd layer.

The Al_2O_3 grade layer was very porous since only 15-25% of the porous support's initial He permeance was lost after its deposition in the case of C01-F09 and Ma-42 membranes. Therefore, even if intermetallic diffusion occurred in the Al_2O_3 grade layer no H_2 permeance decline should be observed since H_2 mostly diffused as molecular H_2 through the porosity of the Al_2O_3 grade layer. In summary, the grade layer effectively protected the dense Pd film from intermetallic diffusion at temperatures equal to or lower than 500ºC.

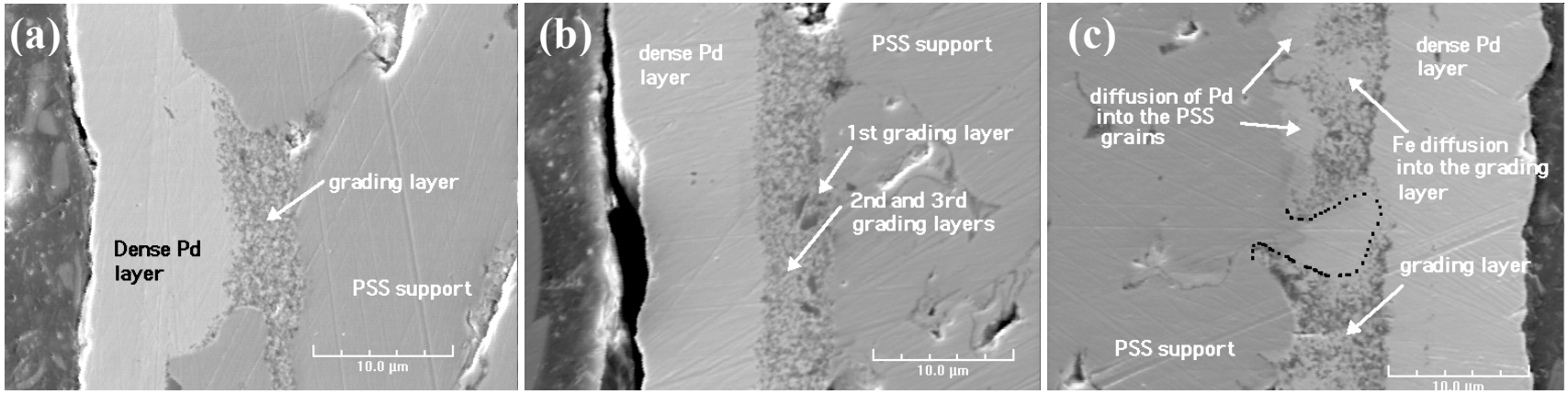

Figure 6-15 Sections of C01-F09 heated at (a) 400ºC, (b) 500ºC and (c) 600ºC. Mag:2000X

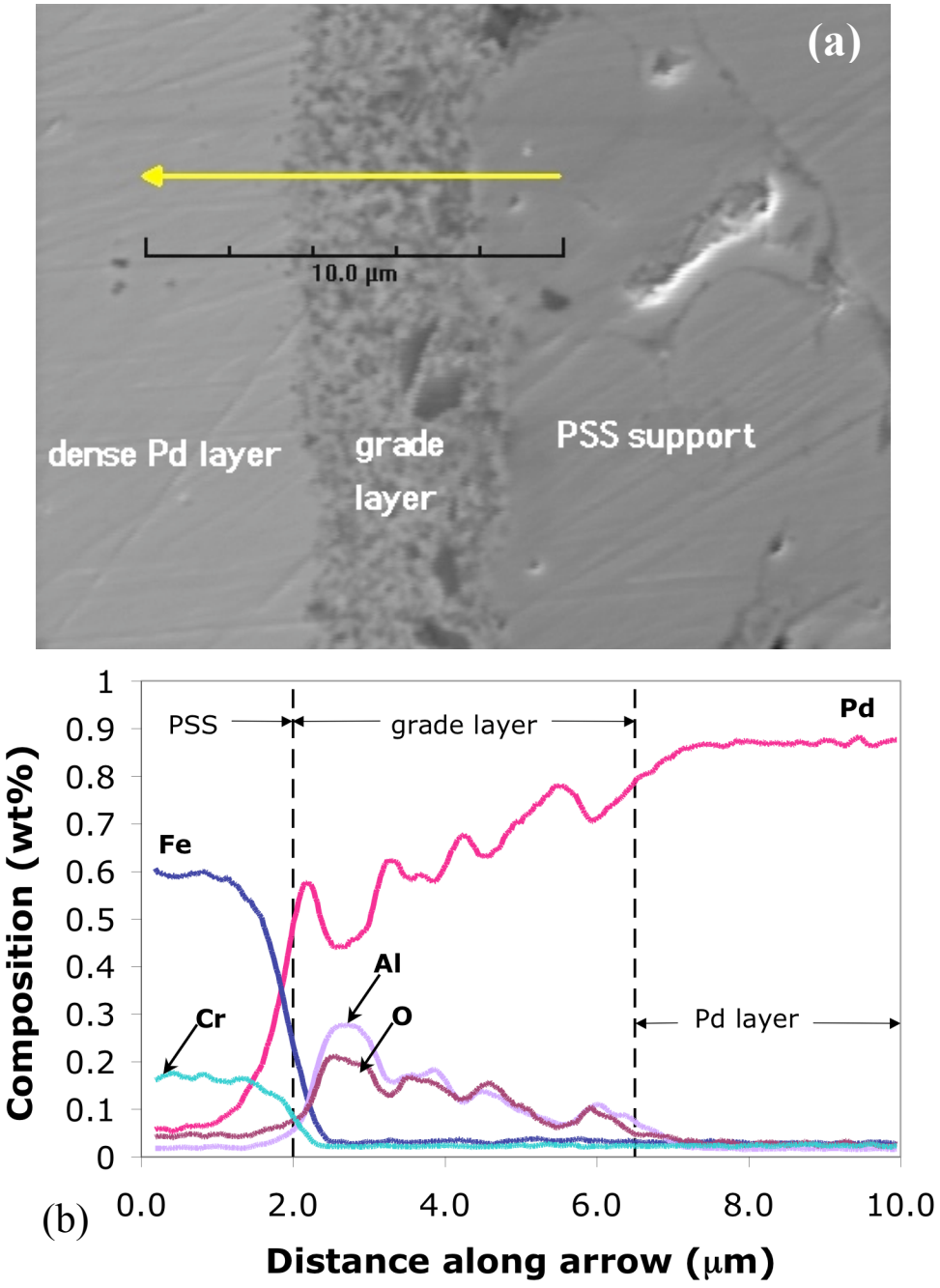

Figure 6-16 Composition analysis across the grade layer for the sample heated at 500°C in H_2.

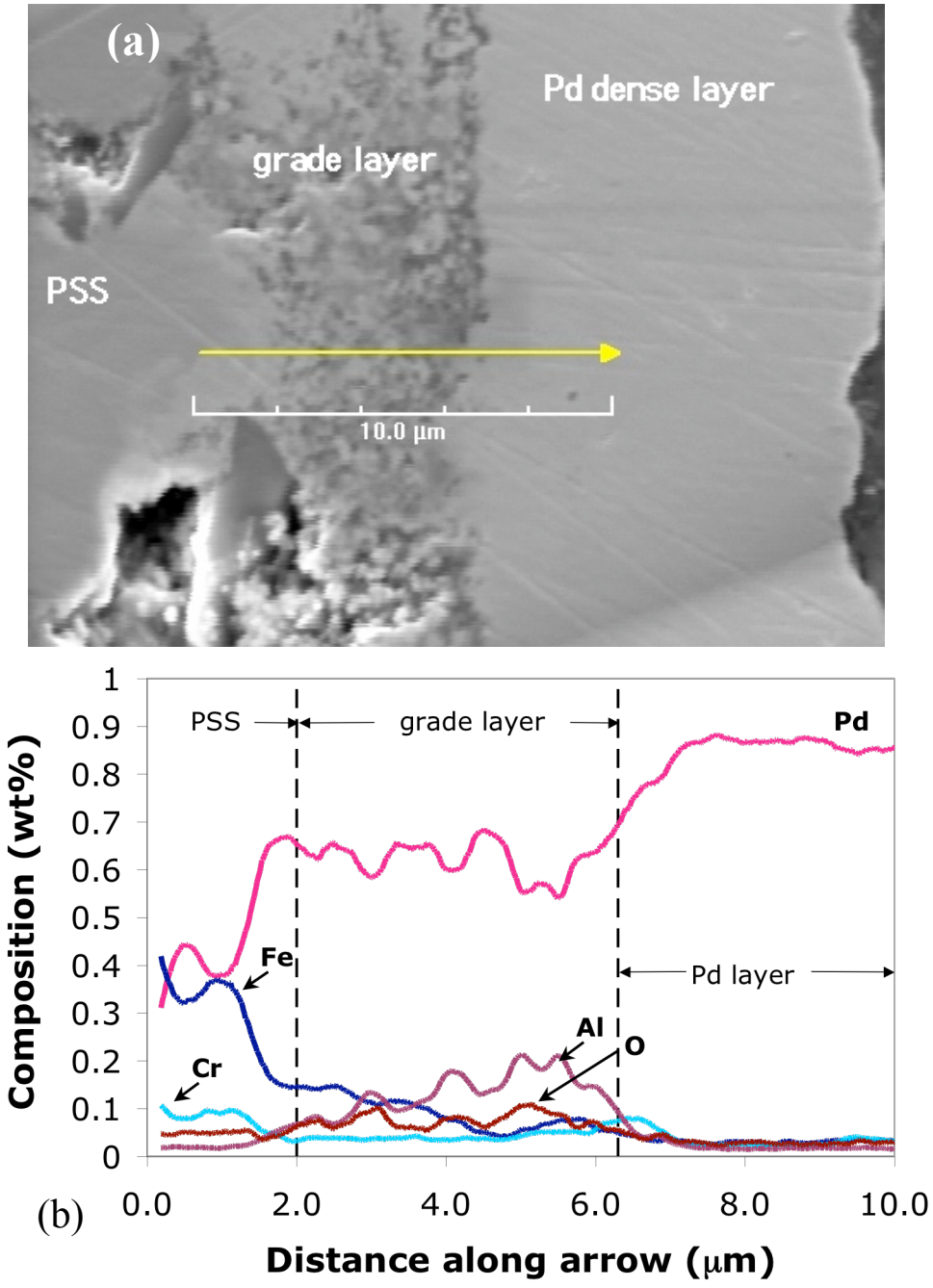

Figure 6-17 Composition analysis across the grade layer for the sample heated at 600ºC in H_2 (a) SEM micrograph (b) Elemental analysis along arrow.

6.4 Conclusions

This chapter detailed a new and unique procedure to achieve ultra-thin composite Pd membranes on porous metal supports, which were characterized by rough surfaces and broad pore size distribution at the surface. The deposition of pre-activated Al_2O_3 particles followed by short time of Pd deposition led to a structure where big particles blocked pore mouths, fine particles filled the pores and very fine particles smoothed and narrowed the pore size distribution at the surface of the porous metal support. Pd layers deposited on such modified surfaces were very uniform and very thin. Thin membranes prepared on "graded" supports exhibit H_2 permeances as high as 21 $m^3/(m^2\ h\ bar^{0.5})$ at 250ºC and as high as 50 $m^3/(m^2\ h\ bar^{0.5})$ at 500ºC. However, the H_2 permeance of a freestanding Pd layer with the same thickness of 5.6 μm as that of Ma-42 was estimated to be 96 $m^3/(m^2\ h\ bar^{0.5})$ at 500ºC. Mass transfer resistance within the pores of the support was responsible for the lower H_2 permeance measured on the composite Ma-42 membrane. Composite Pd membranes were also characterized by good mechanical stability and very high selectivies (H_2/He), which were higher than 1000 at temperatures equal to or lower than 400ºC. The selectivity of all composite Pd membranes decreased at temperatures higher than 450ºC. Finally, and most important, the H_2 permeance and the selectivity (H_2/He) of this composite Pd membranes prepared on graded supports were stable over 1100 hr at 500ºC, which represented a major breakthrough of the formation of thin composite Pd membranes.

7 Synthesis of composite Pd-Cu membranes on engineered substrate surface

7.1 Introduction

Pd-Cu membranes are believed to be more robust than pure Pd membranes since Pd-Cu alloys absorb less H_2, thereby, being less prone to the problems related to the expansion upon H_2 absorption. In a previous preliminary work (Guazzone, 2003, PhD proposal), the synthesis of composite Pd-alloy membranes on 316L 0.5 μm grade PSS supports represented a challenge. Since Pd and Cu could not be co-deposited from electroless plating baths, the two metals had to be sequentially deposited and heat-treated to form the Pd-Cu alloy ("coating and diffusion" technique). While applying the "coating and diffusion" technique for the preparation of Pd-Cu alloys on 316L 0.5 μm grade PSS supports, several difficulties were encountered. The alloying of the Pd and Cu layers was limited by temperature since high temperatures (T>550-600ºC) led to intermetallic diffusion and the formation of large leaks. If low temperatures were used (500ºC), thin Pd and Cu layers were preferred in order to decrease the annealing time, hence, a Pd-Cu-Pd-Cu – etc… structure was needed. However, plating Pd on top of Cu was not possible since the ammonia in the Pd plating bath dissolved part of the Cu layer. An attempt to plate Pd and Cu followed by heat-treatment and repetition of the Pd/Cu deposition and annealing steps several times was made to achieve a gas tight composite Pd-Cu membrane. Such tech-

nique was tedious and success was not guaranteed since some of the membranes came out black after any of the annealing steps. For the rare cases when the Pd-Cu had an acceptable appearance, large chemical gradients across the membrane layer were found.

The main difficulty in the synthesis of composite Pd-Cu membranes is the fact that no chemical gradients across the thickness of the alloy layer are allowed since Pd-Cu alloys only exhibit a sharp maximum in H_2 permeance at exactly Pd-Cu 40. Deviations from the optimal composition led to a drastic decrease in H_2 permeance (McKinley, 1967), which was due to the changes in relative amount of α and β phase. For instance at 500ºC[1], the relative amount of β phase is 92% with 42 wt% Cu and only 54% with 40 wt% Cu. It became clear that to achieve a composite Pd-Cu 40wt% membrane, prepared with only one annealing step, the total thickness of the two metal layers, Pd and Cu, needed to be thin and not exceeding 5-10 μm. The preparation of such a thin composite Pd membrane on a 0.5 μm grade PSS supports was discarded due to the thick Pd layers (30-50μm) needed to achieve a dense layer on 0.5 μm grade PSS supports. A composite Pd-Cu 40wt% membrane could be achieved on a graded PH support yet the preparation of such a composite membrane was not undertaken. Morreale et al. (2004) recently proved that the low H_2 permeable Pd-Cu α phase was more resistant to sulfur poisoning than the highly permeable β phase. Therefore, a low (10-20wt%) Cu content Pd-Cu alloy membrane would preferably be used at high temperatures (>500ºC) in a H_2S contaminated atmosphere.

The objective of the work described in this chapter was twofold. First, a fundamental study by means of High Temperature X-Ray Diffraction (HTXRD) on the nucleation of

[1] Relative amounts of α and β phase can be calculated at any temperature using the lever rule on the portion of the Pd-Cu phase diagram shown in Figure 7-14, page 196.

the β phase in Pd-Cu alloys was carried out along with a study on the alloying mechanism of Pd-Cu bi-metallic layers. Secondly, from a more practical point of view, the work described in this chapter aimed at the possibility of preparing a thin (<10μm) and stable low Cu content (10wt%Cu) Pd-Cu membrane on a graded PH support.

7.2 Theory

7.2.1 The study of metal transformations with XRD

The ordering α(fcc)→β(bcc) + α(fcc) transformation is shown in Figure 7-1 for an hypothetical Pd-Cu 39wt% cooled from 620ºC to 500ºC. If the alloy is kept at 500ºC for a sufficiently long amount of time the equilibrium amount of β phase is given by the lever rule shown in Equation (7-1)

$$X_{\beta,equilibrium}(500^0C) = \frac{\overline{bc}}{\overline{ac}} \qquad (7\text{-}1)$$

However, ordering transformations are nucleation and growth type of transformations. The growth of the β phase is shown with the dashed arrow starting at point c and ending at point b. Nucleation can also occur simultaneously with growth. At any time between point c and b the amount of β phase is given by the lever rule and denoted as X_β.

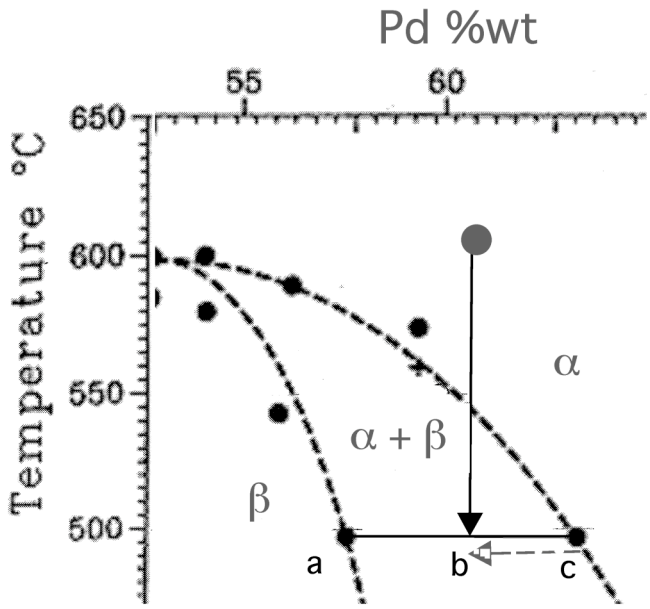

Figure 7-1 fcc → bcc ordering transformation in PdCu alloys

The rate at which the α(fcc)→β(bcc) + α(fcc) transformation occurs depends on the thermodynamic driving force i.e. $X_{\beta,\,equilibrium}$ and the diffusion rate of species, Pd and Cu atoms in this case. If the system temperature is dropped from 620ºC to 550ºC the thermodynamic driving force for the transformation is small yet the diffusion is high. If the system temperature is dropped from 620ºC to 300ºC the thermodynamic driving force is very high yet the diffusion is slow. These kinetic phenomena are characteristic of phase transformations in many metallic systems (Porter and Easterling, 1981). When cooling the hypothetical Pd-Cu 39wt% from 620ºC to temperatures between 300 and 550ºC a

maximum transformation rate should be found. The rate at which the transformation occurs, X_β vs. time, can be followed by XRD techniques in a HTXRD diffractometer by simultaneously collecting the (111) reflection of the α phase and the (110) reflection of the β phase as a function time. The simultaneous collection of both reflections was possible with an LPD detector taking a 2θ range of 10º. The (111) reflection of the α phase and the (110) reflection of the β phase were collected every 15 seconds. X_β was determined from XRD data using integrated intensities according to Equation (7-2)

$$X_\beta = \frac{I_\beta}{I_\beta + I_\alpha} \qquad (7\text{-}2)$$

The rate of the transformation at a given temperature has to be normalized with the amount of β phase at equilibrium at the temperature T since $X_{\beta,\,\text{equilibrium}}$ depends on the temperature the system is cooled to (see Figure 7-1). Hence, the rate of the ordering reaction is given by $X_\beta / X_{\beta,\,\text{equilibrium}}$ as a function of time. The transformation at a given temperature, X_β vs. time, can then be plotted on the Pd-Cu phase diagram by placing $X_\beta(t)$ between the β/(α+β) and (α+β)/α boundaries according to the lever rule, Equation (7-1).

7.3 Experimental

7.3.1 XRD sample preparation

The bimetallic Cu-Pd-Al_2O_3 samples consisted of a thin Pd layer covered by a thin Cu layer on a sintered α-Al_2O_3 substrate (1×1.5 cm, thickness 2 mm). Prior to Pd and Cu deposition, the α-Al_2O_3 substrates were treated at 800°C in air for 12 hr for cleaning purposes and seeded with Pd nuclei by alternatively immersing the substrates in $SnCl_2$ (1 g/l,

pH=2) and $PdCl_2$ (0.1 g/l, pH=2) solutions. Pd and Cu were deposited by the electroless plating method using the plating bath composition listed in Table 7-1. The thickness and Cu content of each layer was determined by the gravimetric method. Since the α-Al_2O_3 substrates were totally immersed in the plating bath, each sample had two faces. The studied face was numbered as "face 1" and the opposite face laying on top of the Pt-Rh heating strip was numbered as "face 2". Three different Cu-Pd-α Al_2O_3 samples were considered: Pd/Cu-40wt% (sample Pd-Cu-1), Pd/Cu-46wt% (sample Pd-Cu-2) and Pd/Cu-50wt% (sample Pd-Cu-3). Table 7-2 lists all samples analyzed in this study. Cu-Pd-α Al_2O_3 samples were initially heat-treated by raising the temperature from room temperature to 650ºC in less than 2 minutes. A dwell time ranging from 4 to 6 hr was set so that the chemical composition across the thicknesses of the layer was homogeneous. After homogenization, the samples were cooled in three different ways: a fast quench to room temperature (sample Pd-Cu-1), a slow ramp (3ºC/min) to room temperature (sample Pd-Cu-2) and, for sample Pd-Cu-3, a quench to 400ºC (dwell time 2 min) followed by a dwell at 525ºC (2 hr) and a slow cool down to room temperature. All temperature changes and annealing steps were carried out in He atmosphere.

Table 7-1 Chemical composition of Pd and Cu plating bath

Chemical	Pd Bath	Cu Bath	Function
$Pd(NH_3)_4Cl_2 \cdot H_2O$ (g/l)	4	-	Pd^{2+} ions source
$CuSO_4 \cdot 5H_2O$ (g/l)	-	20	Cu^{2+} ions source
$Na_2EDTA\ 2H_2O$ (g/l)	40.1	30	Complexant-stabilizer
NH_4OH (28%) (ml/l)	198	-	Buffer
H_2NNH_2 (1 M) (ml/l)	5.6	-	Reducing agent
HCHO (37%) (ml/l)	-	14	Reducing agent
EDA (ppm)	-	100	Grain refiner
$K_4Fe(CN)_6 \cdot 3H_2O$ (ppm)	-	35	Accelerator
$(C_2H_5)_2NCS_2Na \cdot 3H_2O$ (ppm)	-	5	Stabilizer
pH	10-11	12-13	
Temperature (°C)	60	20-25	

The alloying process of the Cu-Pd-substrate composite structures, as well as the ordering fcc →bcc transformation taking place in Pd-Cu alloys, were studied using the time resolved HTXRD described in Section 3.4.2.1.

Table 7-2 List of Pd-Cu samples used in this Chapter

Sample	support	Cu content (wt% from gravimetric)	Experiment
Pd-Cu-1	α-Al_2O_3	40	Annealed, quenched (650ºC to 20ºC
Pd-Cu-2	α-Al_2O_3	46	Annealed, slowly cooled (650 to 20ºC at 3ºC/min)
Pd-Cu-3	α-Al_2O_3	50	Annealed, quenched to 400ºC (dwell, 2min), heated at 525ºC for 2 hr, slowly cooled 20ºC
Pd-Cu-4a	PH	41	β phase nucleation rate (1st experiment)
Pd-Cu-4b	PH	41	β phase nucleation rate (2nd experiment)

7.3.2 The preparation of a composite Pd-Cu membrane, Ma-41

The composite Pd-Cu membrane, Ma-41, was prepared by the coating and diffusion technique. The coarse PH support was characterized, cleaned, graded and activated according to Sections 3.1.1-3.1.3. A 5μm thick Pd layer and a 2μm thick Cu layer were sequentially deposited by the electroless plating method using the metal plating baths

listed in Table 7-1. The composite Cu-Pd-PH structure was annealed in H_2 atmosphere by holding the membrane for 12-24 hr at each of the following temperatures: 250, 300, 350, 400, 450, 500 and 550ºC. After the annealing process, the surface of the membrane had a silver color with a slight orange tint. Finally, the annealed Pd-Cu membrane was coated with an additional 3μm of Pd to achieve a leak free membrane. Figure 7-2 and Figure 7-3 show the silver color of Ma-41's surface and the entire support respectively.

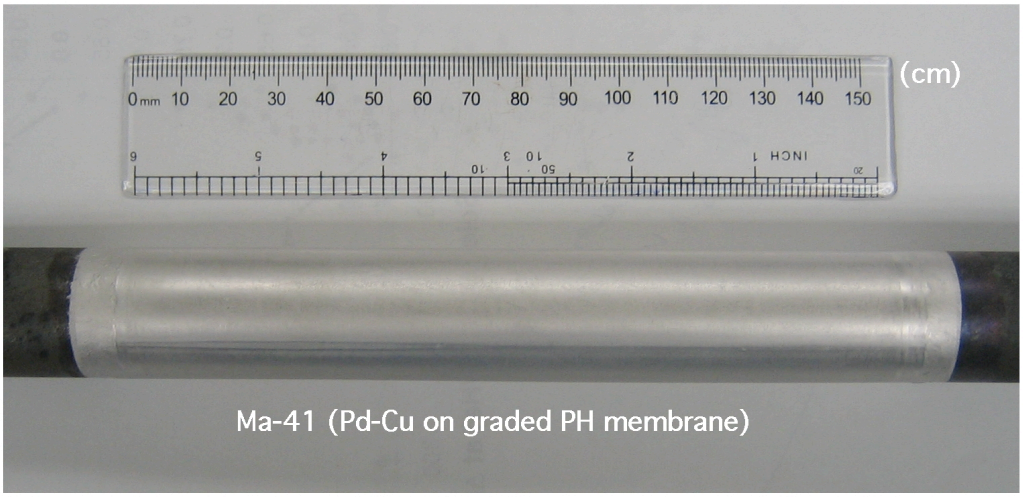

Figure 7-2 Ma-41 composite Pd-Cu membrane

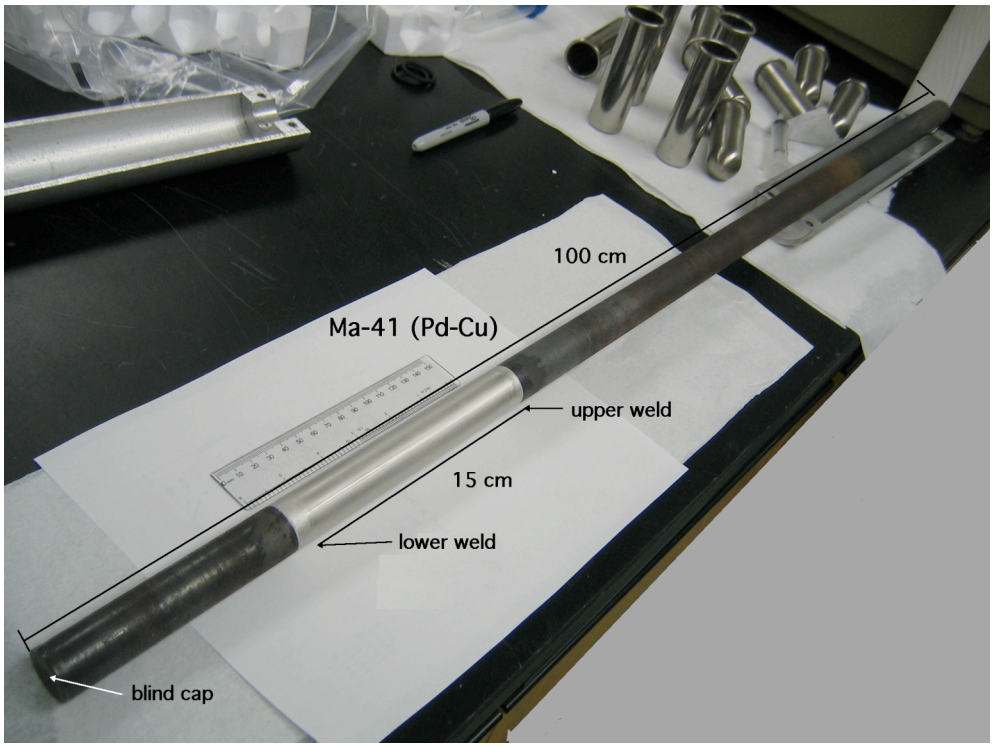

Figure 7-3 Ma-41 composite Pd-Cu membrane

The total surface of the H_2 permeable membrane was 120 cm^2 and its thickness was estimated to be 10 μm. The membrane was characterized in H_2 atmosphere as described in Section 3.2. The He leak of the membrane was measured either in pure He atmosphere or in H_2 atmosphere by feeding the shell side with a 99%H_2-1%He mixture gas and analyzing the tube flow with Gas Chromatography (GC). UHP H_2 was used as the carrier gas and the TCD detector gain was set to high.

7.4 Results and discussion

7.4.1 The inter-diffusion of Pd-Cu bi-layers

Figure 7-4 shows the phase transformation in sample Pd-Cu-1 taking place at 650ºC as a function of time. The first two patterns only showed the two distinctive fcc phases of Pd and Cu. The intensity of the Pd (111) and Cu (111) reflections rapidly decreased and within 6 min (3rd pattern) the peaks of pure Pd and Cu phases were no longer visible. Instead, a Cu rich fcc phase with very broad peaks, due to large concentration gradients, were seen in the 3rd pattern. As Cu atoms diffused into the Pd layer, the Cu rich fcc phase faded out and the peaks of a Pd rich fcc phase appeared in the 4th pattern. In addition, since concentration gradients disappeared, peaks became sharper (pattern 4 to 20). After 40 minutes at 650ºC no further changes took place in the XRD patterns, which theoretically corresponded to a homogeneous Pd-Cu alloy. The sample was held at 650ºC for a total time of 5 hr.

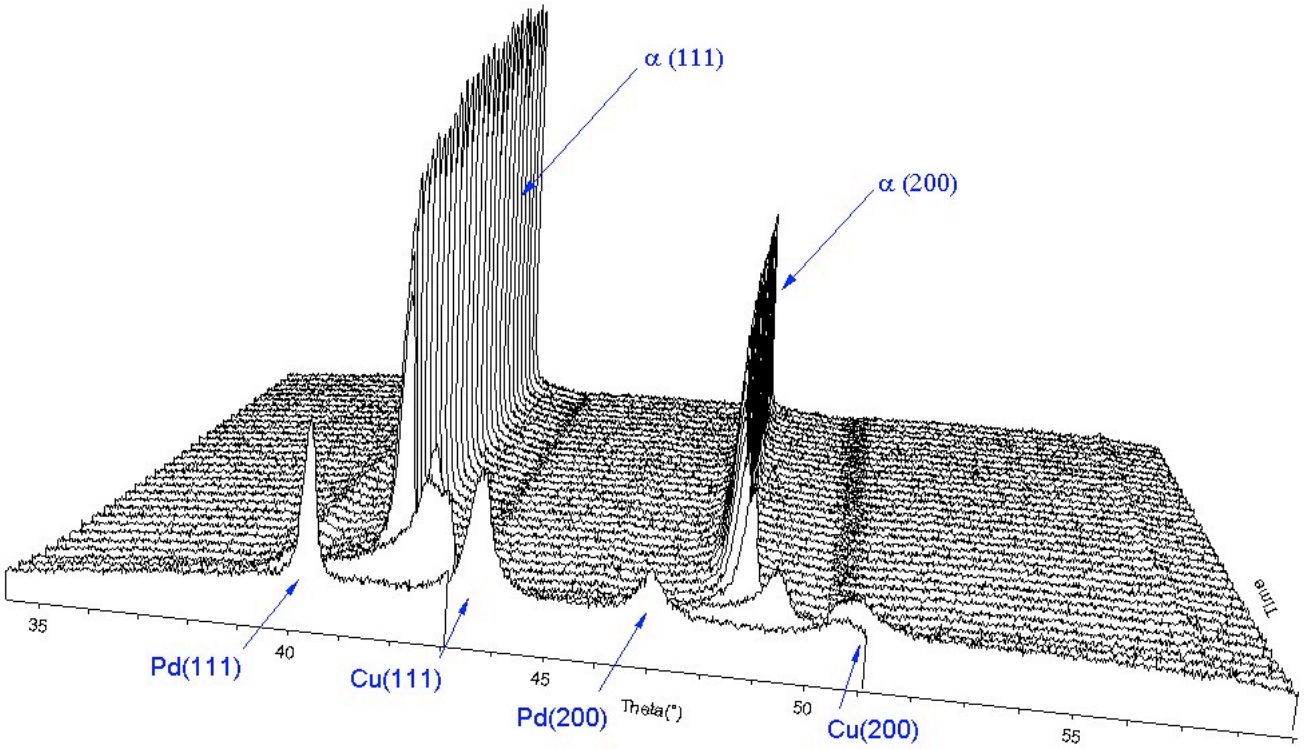

Figure 7-4 Phase changes as a function of time in sample n1 (650ºC in He)

However, the existence of very small concentration gradients were not excluded. Therefore, in order to ensure homogeneity the temperature was increased up to 800ºC for 30 minutes. Sample Pd-Cu-1 was then quenched to room temperature. No ordered bcc β phase nucleated indicating that either the α phase stable at 800°C was retained after the fast drop in temperature, or the Cu concentration of sample Pd-Cu-1 fell outside the coexistence domain of the β and α phase (i.e. the Cu concentration was lower than ca. 30wt%). In the case the α phase was retained, sample Pd-Cu-1 was heat-treated at 400°C in He in order to trigger the nucleation of the β phase. No nucleation took place indicating that the Cu concentration was lower than 30wt%. EDX analysis of sample Pd-Cu-1 surface indicated the presence of a Pd-Cu alloy with a Cu concentration of 27 wt% in agreement with the final fcc phase.

Figure 7-5(a) shows the phase transformation that occurred as a function of time at 650ºC for sample Pd-Cu-2. The first two XRD patterns showed pure Pd and pure Cu peaks with decreasing intensities as diffusion took place (1st and 2nd pattern). However, in this case, two α phases appeared in the 3rd pattern. The first α phase, Pd rich, with (111) reflection exiting at 2θ ca. 41.1º was initially characterized by broad peaks due to concentration gradients. As diffusion occurred, the peaks of the Pd rich phase shifted from values of 2θ ca 41.1º to values of 2θ ca 40.5º, an indication of the progressive enrichment in Pd. Moreover, the peaks of the (111) reflection sharpened and increased in intensity indicating the growing of the Pd rich phase. The second α phase, which was very rich in Cu, had a very sharp (111) reflection peak located at 2θ ca. 42º.

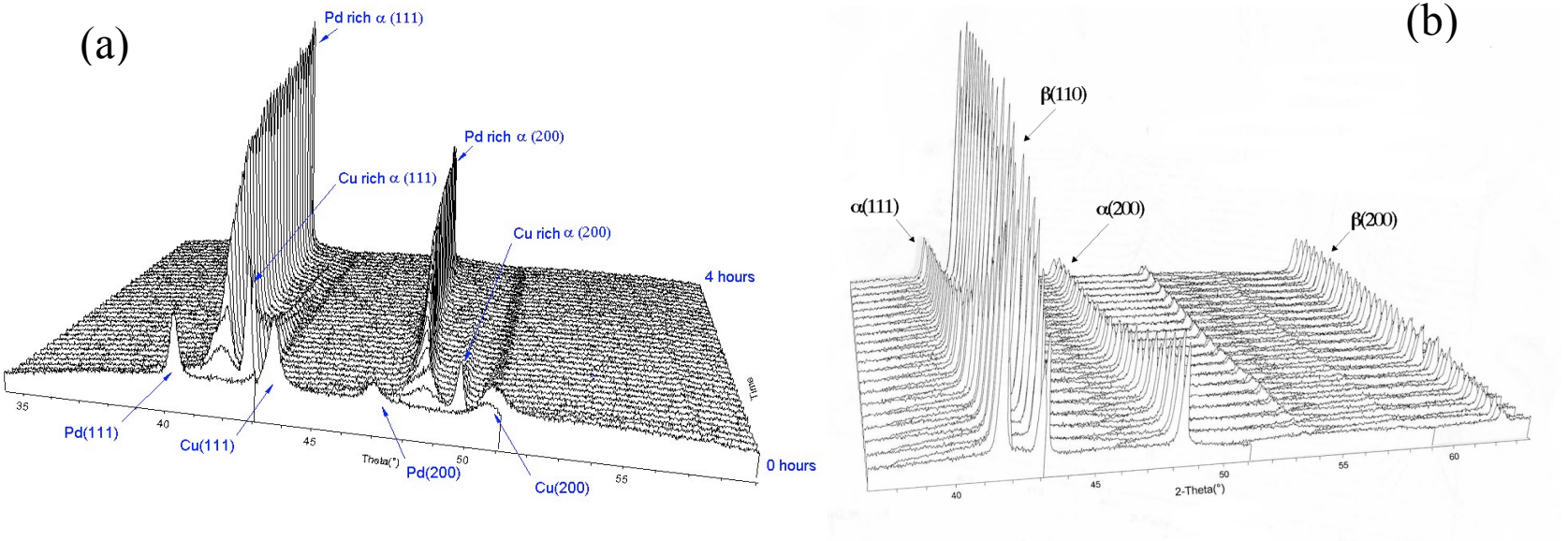

Figure 7-5 (a) left. XRD pattern collection of sample Pd-Cu-2 as a function of time. (650ºC in He). (b) right. XRD pattern collection while cooling from 650ºC to 300ºC. Nucleation of the β phase occurred at a temperature above 525ºC.

The sharpness of the (111) reflection was due to the absence of chemical gradients within the phase. As diffusion occurred, the (111) reflection of the second α phase only decreased in intensity as a function of time with no shifting to lower 2θ values. The sharpness of the (111) reflection of the Cu rich α phase was also invariant. In the case of sample Pd-Cu-2, the XRD reflections of the Cu rich α phase were observed for two hours. Only a Pd rich α phase was observed after a total annealing time of 5 hr at 650ºC. Figure 7-5(b) shows the XRD patterns collected while decreasing the temperature from 650 to 300ºC at a cooling rate of 3ºC/min. The ordered β phase nucleated at a temperature higher than 525ºC and grew at the expense of the initially present α phase.

The XRD pattern of sample Pd-Cu-2 face 1 at room temperature showed essentially β phase and a small amount of α phase as seen in Figure 7-6. However, the XRD pattern of face 2 of sample Pd-Cu-2 at room temperature, also in Figure 7-6, showed essentially α phase and a small amount of β phase. EDX analysis across the Pd-Cu alloy in face 1 and face 2 indicated a Cu concentration, within the volume irradiated by electrons (0.5-1 μm in thickness), higher in face 1 than in face 2 by 4 wt% as seen in Figure 7-7. Figure 7-7 also shows that even after an annealing time of five hours at 650ºC a uniform Pd-Cu alloy was not reached. In fact the Pd content below the volume irradiated by X-rays (from 0 to 3 μm in Figure 7-7) is higher than 70 wt% in both faces indicating the presence of the α phase. Therefore, sample Pd-Cu-2 face 1 had a structure consisting of 3 μm thick Pd-rich α phase and 3μm thick β phase. Sample Pd-Cu-2 face 2 was essentially consisting of a Pd-rich α phase.

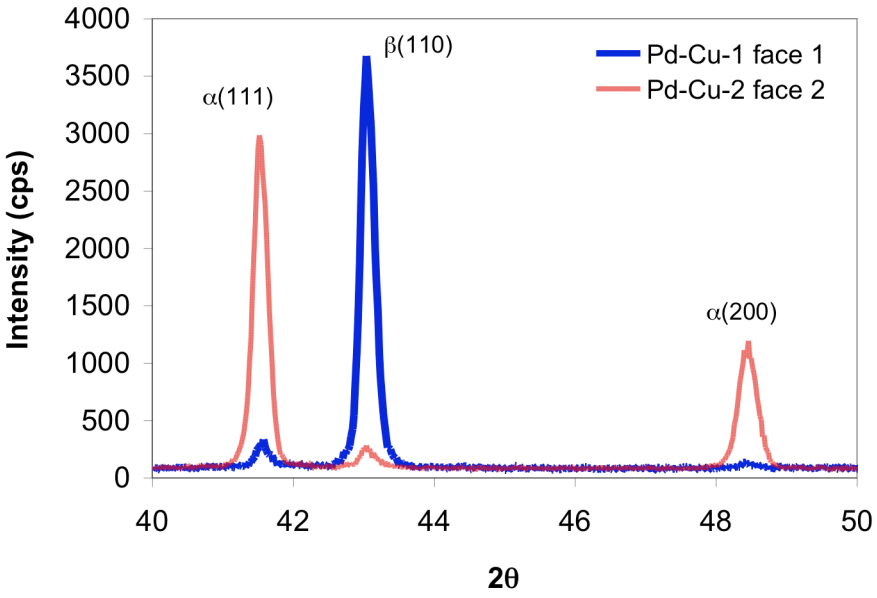

Figure 7-6 XRD patterns of sample Pd-Cu-2 face 1, mainly β phase, and face 2 mainly α phase

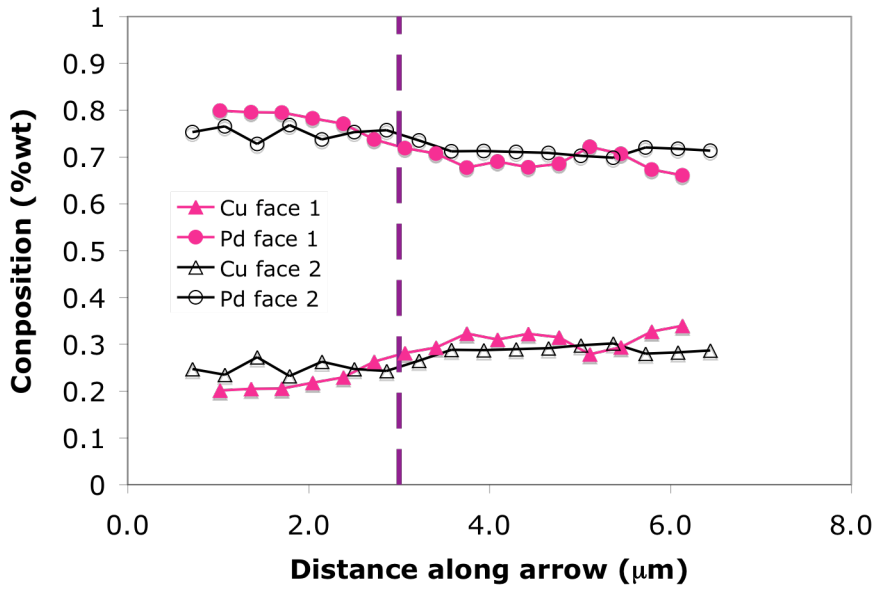

Figure 7-7 Elemental composition across the thickness of sample Pd-Cu-2 after heat-treatment for face 1 and face 2. The dashed line represents the penetration of X-rays at an angle of 2θ=40°

This example showed that a difference in Cu concentration of only 4 wt% led to a completely different structure in Pd-Cu alloys. Also, according to the Pd-Cu phase diagram[1], it is crucial to target a Cu concentration of exactly 42 wt% if the β phase is desired in the 450-500ºC temperature range.

Figure 7-8 shows the phase changes as a function of time at 650ºC, as well as XRD patterns during quench and dwell at 525ºC of sample Pd-Cu-3. The very first pattern was mainly pure Pd and pure Cu phases. However the second pattern already included, after a short time, two α phases similar to the two α phases seen during the annealing of sample Pd-Cu-2. The first α phase, initially Cu rich with the (111) reflection exiting at 2θ ca. 42°, was characterized by very broad peaks due to concentration gradients. As diffusion occurred the peaks of the Cu rich phase shifted from values of 2θ ca. 42° to values of 2θ ca. 41° indicating the progressive Pd enrichment.

[1] The Pd-Cu phase diagram is shown in Figure 7-14, page 196

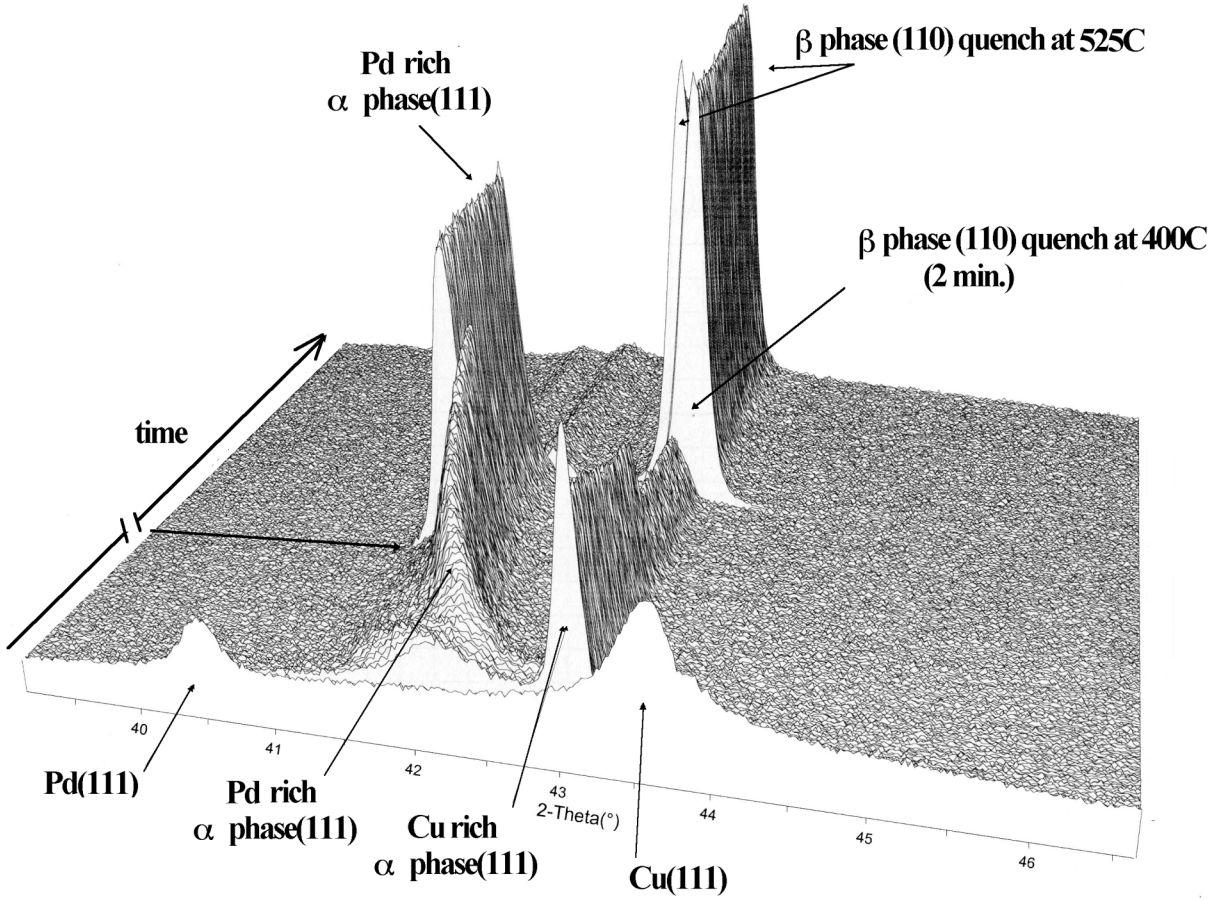

Figure 7-8 XRD pattern collection of sample Pd-Cu-3 during heat-treatment. Part of the pattern for the homogenization process was eliminated in the 3D spectra collection.

Moreover, peaks sharpened and increased in intensity as a function of time indicating the growth of a Pd rich phase. The second α phase, very rich in Cu and characterized by a very sharp (111) reflection, behaved the same way as in sample Pd-Cu-2. That is, the (111) reflection peaks only decreased in intensity with neither shifting towards Pd rich side nor changes in sharpness. The decrease in intensity indicated the dissolution of the Cu rich α phase with time.

After 5 hr at 650ºC, the sample was quenched to 400ºC (the sample was brought from 650°C to 400°C in less than 1 min.) and stayed at 400°C for 2 minutes. The β phase, with its characteristic (100) reflection at 2θ ca. 43°, nucleated within 30 seconds. It can be seen that some of the parent phase still remained. After 2 min at 400ºC, the sample was heated up to 525ºC to trigger the β to α transformation. No decrease in intensity of the β peak was seen for two hours indicating that at that particular Cu concentration, the β phase was stable at temperatures equal to or below 525ºC. Also, no increase in the intensity of the remaining α phase was seen. Therefore it appeared that the Cu concentration of the volume irradiated by X-rays was higher than or equal to 42 wt%.

The peaks seen on sample Pd-Cu-3 corresponding to the α phase might have been due to the Cu concentration gradient across the thickness. The XRD pattern of sample Pd-Cu-3 face 1 at room temperature showed essentially β phase and a slight amount of α phase (Figure 7-9). The XRD pattern of sample Pd-Cu-3 face 2 at room temperature only showed β phase. EDX analysis across the Pd-Cu alloy in face 1 and face 2 indicated a Cu concentration, within the volume irradiated by X-rays, were very similar as seen in Figure 7-10.

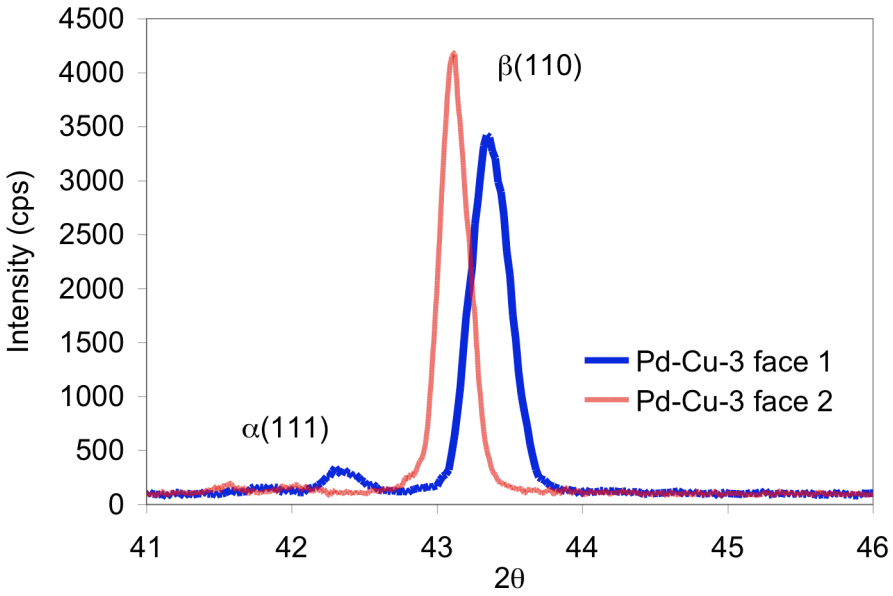

Figure 7-9 XRD patterns of sample Pd-Cu-3 face 1 and 2

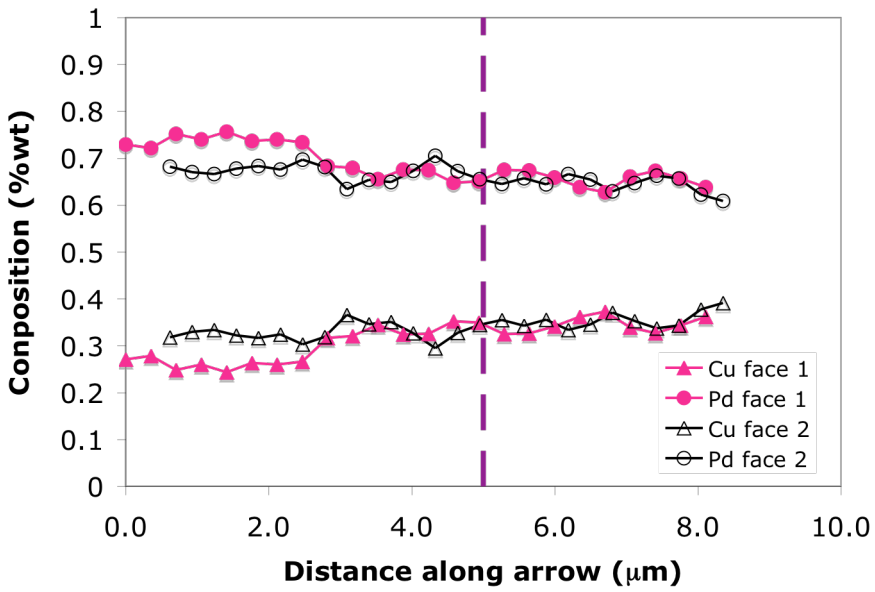

Figure 7-10 Elemental composition across the thickness of sample Pd-Cu-2 after heat-treatment for face 1 and face 2. The dashed lined represents the penetration of X-rays at an angle of 2θ=40°

Figure 7-10 also shows that even after an annealing time of five hours at 650ºC a uniform Pd-Cu alloy was not reached. In fact the Pd content below the volume irradiated by X-rays (from 0 to 3 μm in Figure 7-10) was higher than 70 wt% in both faces indicating the presence of the α phase.

Figure 7-11(a) shows the surface of sample Pd-Cu-1 after heat-treatment and accidental slight oxidation. It is important to note that even after quenching (from 800°C to room temperature in less than a minute) neither cracking of the membrane nor peeling from the support occurred, which is in agreement with the reported mechanical robustness of the Pd-Cu alloy (McKinley, 1967). Particularly, Mc Kinley, (1967) observed no wrinkles or distortions in Pd-40wt% Cu cycled ten times between 350°C and room temperature. Pure Pd underwent severe distortions after similar treatment.

Figure 7-11 (b) shows the morphology of sample Pd-Cu-2 after heat-treatment. Several pinholes were presented on the surface, which were formed by metal particles aggregation (sintering) due to the high temperatures used. The SEM micrograph of sample Pd-Cu-1, Figure 7-11(a), did not show any pinholes. The thin oxide layer, accidentally formed, could have covered the pinholes. A very uniform alloy was also seen after heat-treatment. Figure 7-11 (c) is an SEM photograph of sample Pd-Cu-3 after the described heat-treatment. The surface of the alloy showed light and dark regions. Numerous pinholes were seen. The absence of cracks in the Pd-Cu layers even after rapid cooling and heating demonstrate the robustness of the alloys, however, the surface of all samples was characterized by numerous pinholes after heat-treatment.

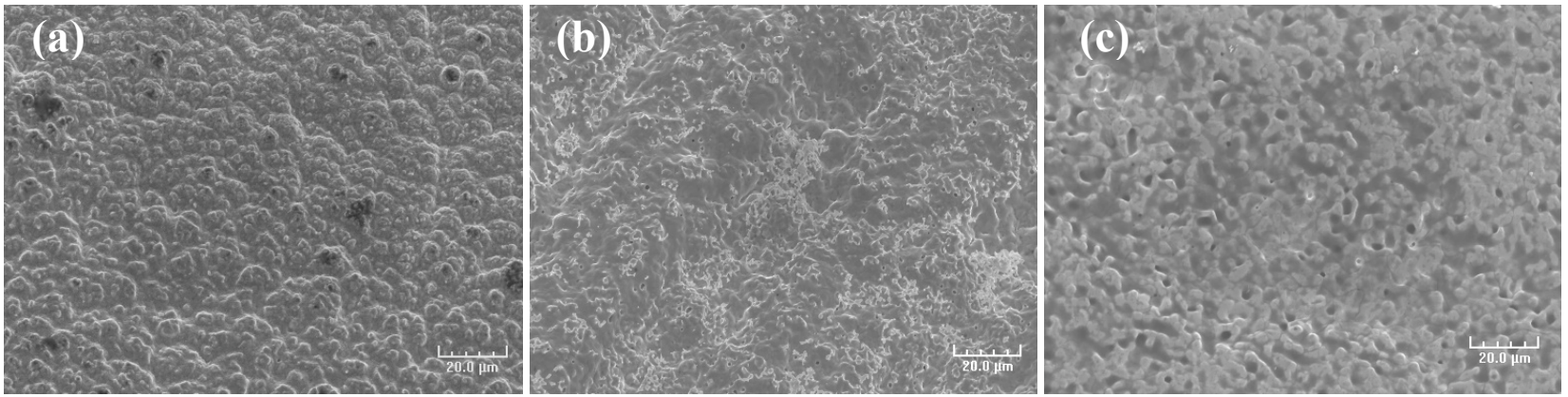

Figure 7-11 SEM picture of sample Pd-Cu-1 (a), sample Pd-Cu-2 (b) and sample Pd-Cu-3 (c) after heat-treatment

.

The formation of pinholes is detrimental to membrane selectivity therefore, it appeared, as expected, that a temperature of 650ºC was too high for alloying these bimetallic layers.

According to the Pd-Cu phase diagram, page 196, only a disordered fcc phase is stable at temperatures higher than 600°C regardless of the Cu concentration. Therefore, during annealing of bimetallic layers only one fcc phase with very broad peaks should be seen assuming that, at the initial stage of the treatment, some Cu diffused into the Pd and some Pd diffused into the Cu. However, two phases were seen in the case of sample Pd-Cu-2 and sample Pd-Cu-3. Particularly, the sharpness of the Cu rich fcc phase (111) reflection indicated that its composition hardly changed as a function of time, only the relative quantity (or thickness) decreased. Therefore, the alloying process of a Pd-Cu bimetallic layer took place across the interface that separated the Pd rich phase from the very rich Cu phase. As diffusion occurred, Cu atoms diffused into the Pd rich phase through the interface faster than Pd atoms diffused into the Cu rich phase. The diffusion of Cu within the Pd rich phase was relatively fast since the Pd rich phase originally showed broad peaks (Cu gradients across the thickness of the Pd rich phase) but sharpened at the end of the annealing process. Schematically, the alloying process of Pd-Cu bi-layers took place as if a Cu layer, analog to a Cu atoms reservoir, disappeared at the expense of a Pd rich phase. The diffusion of Cu through the Cu/Pd-Cu interface led to the shifting of the Cu/Pd-Cu interface in the outer direction. The above-described alloying process is in agreement with results reported by Ma et al. (2004). Figure 7-12(a), shows the cross-section of a 12μm Pd-12μm Cu bimetallic layer annealed at 500°C for 120 hr from Ma et al. (2004).

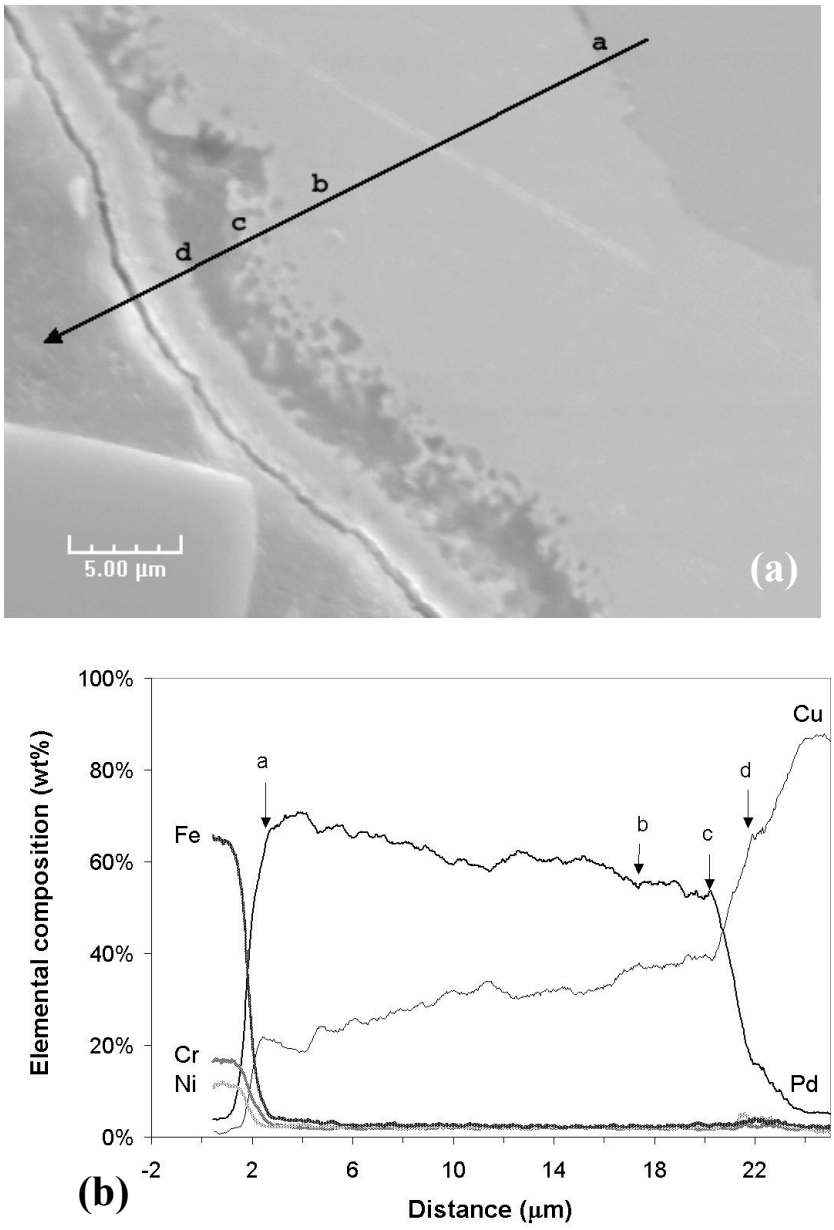

Figure 7-12 (a) SEM micrograph (b) Composition profile of different elements along the arrow in by EDX line scan.

The annealing conditions were not the same, however, the analysis of the composition across the membrane revealed a very rich Cu layer, >80wt% in Cu, starting at point d. Underneath the rich Cu layer a dark layer appeared between points c and d, which was the Cu/Pd-Cu interface layer. The Pd rich phase, a-c region in Figure 7-12(b), would certainly appear as the Pd rich phase with broad peaks at the beginning of the annealing procedure, though sharper at the last stages due to the fast diffusion of Cu within that phase. The Cu rich layer starting at point d, was the Cu atoms reservoir leading to the sharp peaks and the barrier c-d shifted from the initial interface at 12μm outwards due to the incorporation of Cu atoms from the reservoir by Pd-rich phase.

7.4.2 The nucleation and growth of the β phase

The nucleation of the ordered β phase took place instantaneously at 400°C when sample Pd-Cu-3 was quenched from 650°C. The α to β transformation is theoretically accompanied by a shrinkage in the lattice parameter form ca. 0.3758 nm to ca. 0.2977 nm, which represents a contraction of 21% of the initial lattice. The fast change in lattice parameter leads to the cracking of thin supported Pd-Cu layer. The nucleation of the ordered β phase can be better controlled by slowly decreasing the temperature to the operating temperature such as in sample Pd-Cu-2.

The nucleation and growth of the β phase was studied in great detail with sample Pd-Cu-4. Sample Pd-Cu-4 had a theoretical Cu concentration of 40 wt%. The sample was held at 650ºC in He atmosphere until the peaks of the disordered fcc α phase were visible. The sample was quenched to 550ºC and the nucleation and growth of the β phase were followed as a function of time at 550ºC. After a given dwell time (10-90 min.) at 550ºC the temperature was brought up to 650ºC to re-dissolve the formed β phase. After

30 min at 650ºC the sample was quenched again to 500ºC and the nucleation and growth of the β phase was followed as a function of time. The dissolution at 650ºC-quenching procedure was performed at 550, 500, 450, 400, 350 and 300ºC. The β phase dissolution was always performed at 650ºC for 30 min. The dwell time at a given temperature was 10-15 minutes during the first experiment (Pd-Cu-4a) and 1-1.5 hr during the second experiment (Pd-Cu-4b). Both experiments were performed with the same sample Pd-Cu-4. Figure 7-13 shows $X_\beta / X_{\beta,\,equilibrium}$ as a function of time at 550, 500, 450, 400, 350 and 300ºC after quenching from 650ºC. The transformation path was also plotted in the Pd-Cu phase diagram as seen in Figure 7-14.

Figure 7-13 shows $X_\beta / X_{\beta,\,equilibrium}$ as a function of time at 300, 350, 400, 450, 500 and 550ºC after rapid cooling from 650ºC. The ordering transformation fcc → bcc that took place when quenching the sample from 650ºC to any given temperature was limited by diffusion at 300, 350 and 400ºC. At 300, 350 and 400ºC the initial percentage of β phase was equal to 0.3 due to the nucleation and growth that took place during the 2 minutes needed to cool the sample from 650ºC to 300, 350 and 400ºC. The diffusion was so sluggish at 300ºC that the β phase did not grow. At 350 and 400ºC the transformation rate increased even though the transformation appeared to be limited by diffusion. At 450ºC the rate of transformation was the fastest and decreased as the quenching temperature was increased due to thermodynamic limitations. Figure 7-14 shows the ordering transformation path after 15 seconds and 10 minutes within the Pd-Cu phase diagram. The 10 minutes lines starts to curve to the right at 450ºC indicating that for temperatures lower than 450ºC the diffusion of metal atoms was the limiting process.

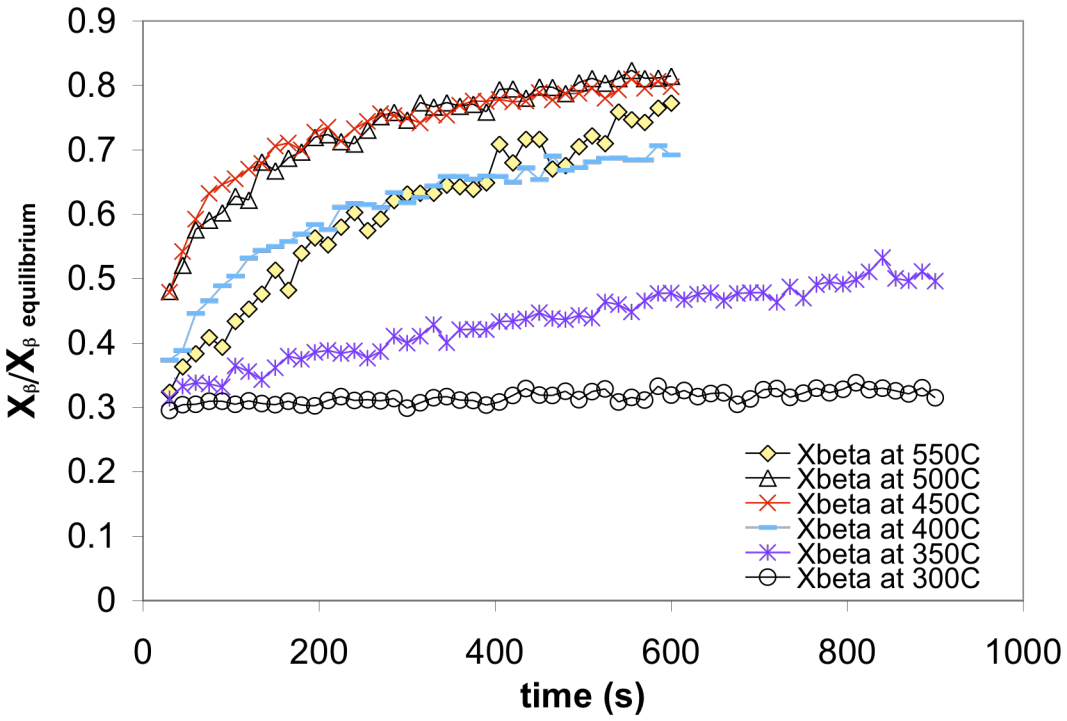

Figure 7-13 X_β as a function of time at different temperatures after quenching from 650°C

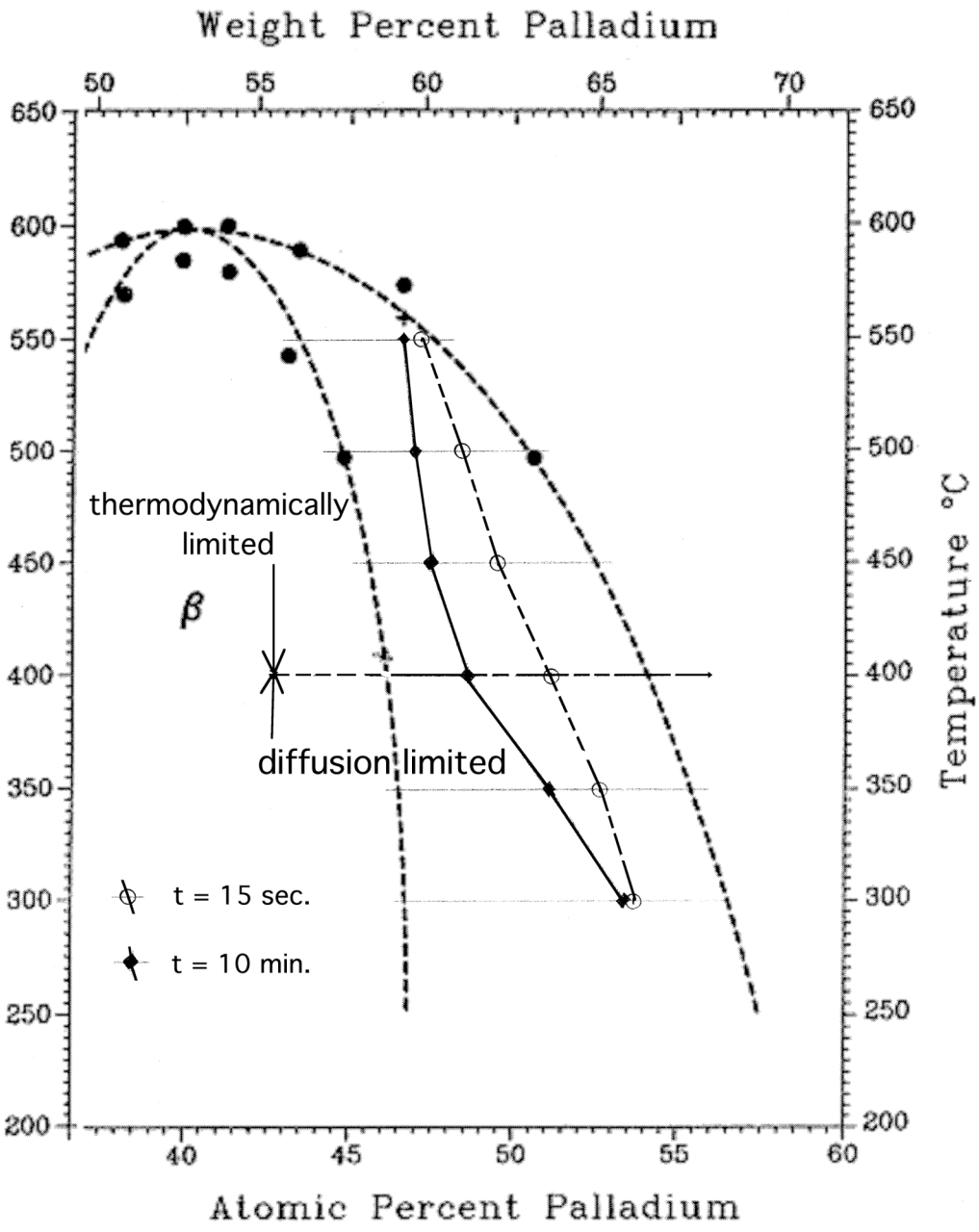

Figure 7-14 phase transformation path at different times t=0 sec and t=10 min

In order to better elucidate the ordering transformation the sample was held for longer times, 1 – 1.5 hr, at 400, 450, 500 and 550ºC. The ordering transformation is plotted during the first 200 seconds in Figure 7-15(a) for all temperatures. The cooling rate from 650 to 450 and 400ºC was very fast although some β phase nucleated and grew during the time, 1-2 min., it took to "quench" the sample. Hence, the β phase percentage at t=0 did not equal 0 but 0.28 as pointed by the black arrow. Also the curves at 400 and 450ºC are characterized by an inflection point indicating that the initial β phase concentration due to the cooling was taken over by the β phase growth that really happened at those temperatures. Hence, the first data point at 450ºC was neglected as well as the two first data points at 400ºC.

Figure 7-15(b) shows the ordering transformation in the 0-3600 sec. time interval. The ordering transformation was characterized by a sharp nucleation and growth during the first 200 sec. an intermediate regime between 200 and 1000 sec. and a linear increase with time after 1000 sec. As seen in Figure 7-16(a) and (b) the ordering transformation, even though it was a "nucleation and growth" transformation, could not be fitted with either an Avrami model or a quadratic model. When the experimental data were fitted with the Avrami model, time exponents close to 0.2-0.5 were found (see Figure 7-16(a)), which were not proper of usual time exponent values found in metals i.e. 3-4. When the experimental data were fitted with a quadratic model, no linear relation could be found for the $X_\beta / X_{\beta,\,equilibrium}$ vs. $t^{0.5}$ data points. However at times higher than 1000 sec. the growth of the β phase was considered as linearly dependent on √t.

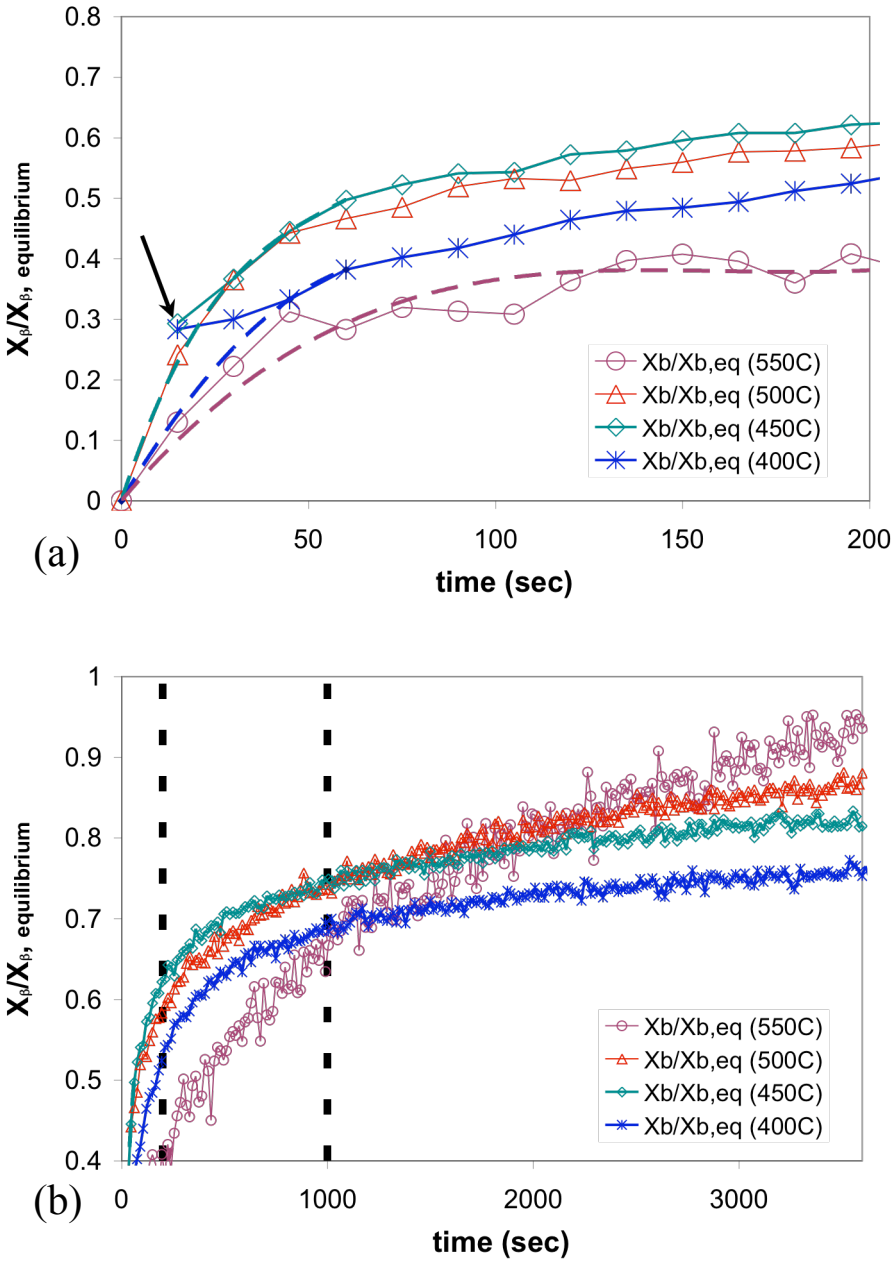

Figure 7-15 (a) fcc → bcc ordering transformation in the 0-200 sec. time range. (b) ordering transformation in the 0-3600 sec time range

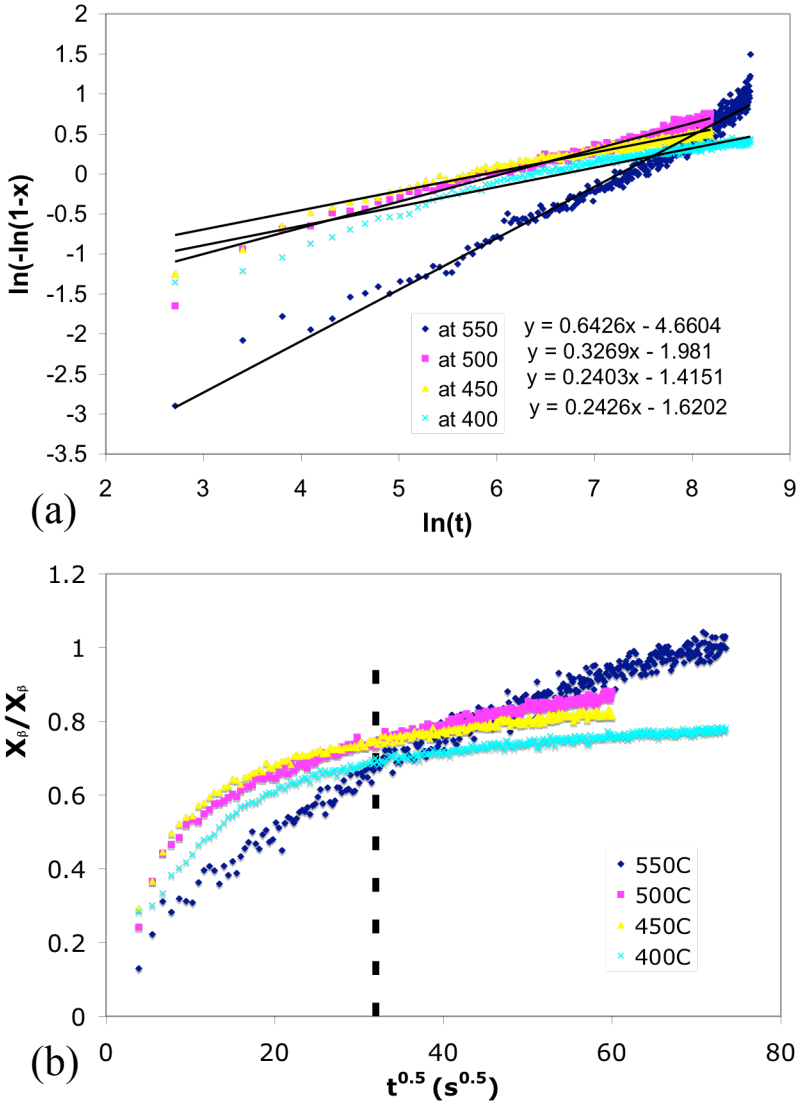

Figure 7-16 (a) Avrami model (b) quadratic model

The kinetics of this ordering transformation was therefore studied by determining the initial transformation rates at t=0 sec and the growth rates between 1000 and 3000 sec.

In order to calculate the initial rates, the experimental $X_{\beta}/ X_{\beta, \text{equilibrium}}$ vs. time functions were interpolated between 0 and the first 10 data points neglecting the first datum point at 450ºC and omitting the two first data points at 400ºC (see Figure 7-15(a)). Interpolation curves are shown with dashed lines in Figure 7-15(a). The initial rate was given by the tangent at *t*=0 sec. The growth rate between 1000 and 3000 sec was assumed to be linear with time. Figure 7-17 shows the Arrhenius plot of the initial rates and $r_{1000\text{-}3000}$ rates.

As already found for the first experiment, a maximum initial rate was found at 400-450ºC. At times higher than 1000 sec. the activation energy for the ordering transformation was 40kJ mol^{-1}. The activation energy for Pd-Cu inter-diffusion is in the order of 200kJ mol^{-1}, therefore, it appeared that the rate-limiting step for the ordering transformation was not diffusion.

In fact, as seen in Figure 7-15(b), it appeared that the rate at which the β phase fraction reached its equilibrium value ($X_{\beta, \text{equilibrium}}$) was independent of the temperature. Several studies pointed out the ordering fcc → bcc transformation had a bainitic or a martensic character. The transformation path was also plotted in the Pd-Cu phase diagram as seen in Figure 7-18

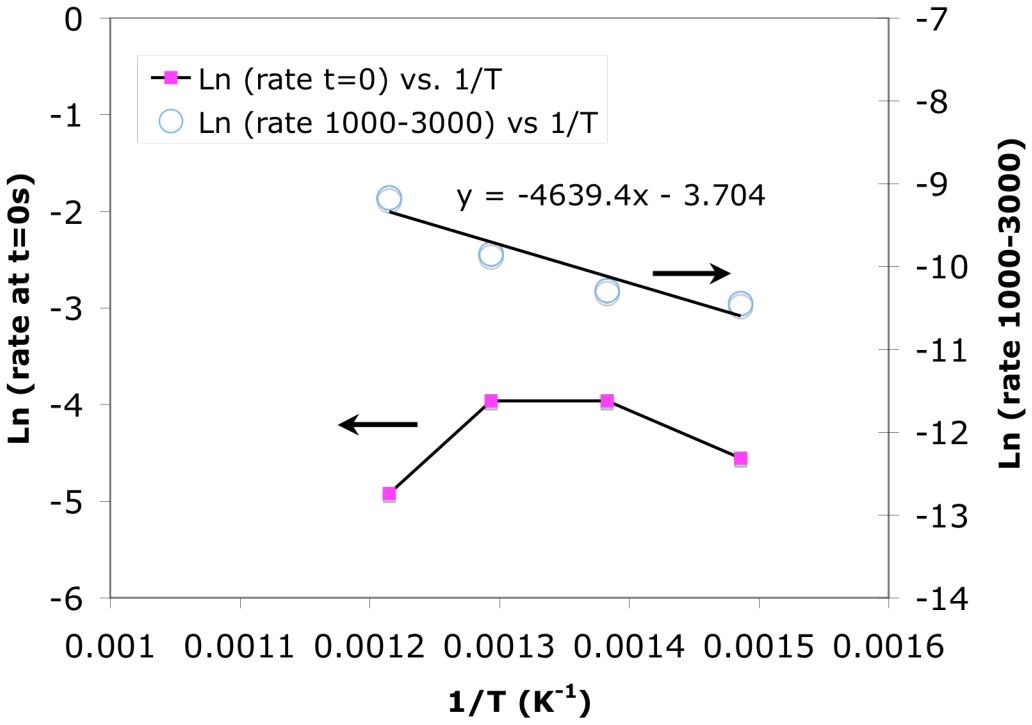

Figure 7-17 Ln (rate t=0 sec) and Ln (rate 1000-3000 sec) as a function of 1/T

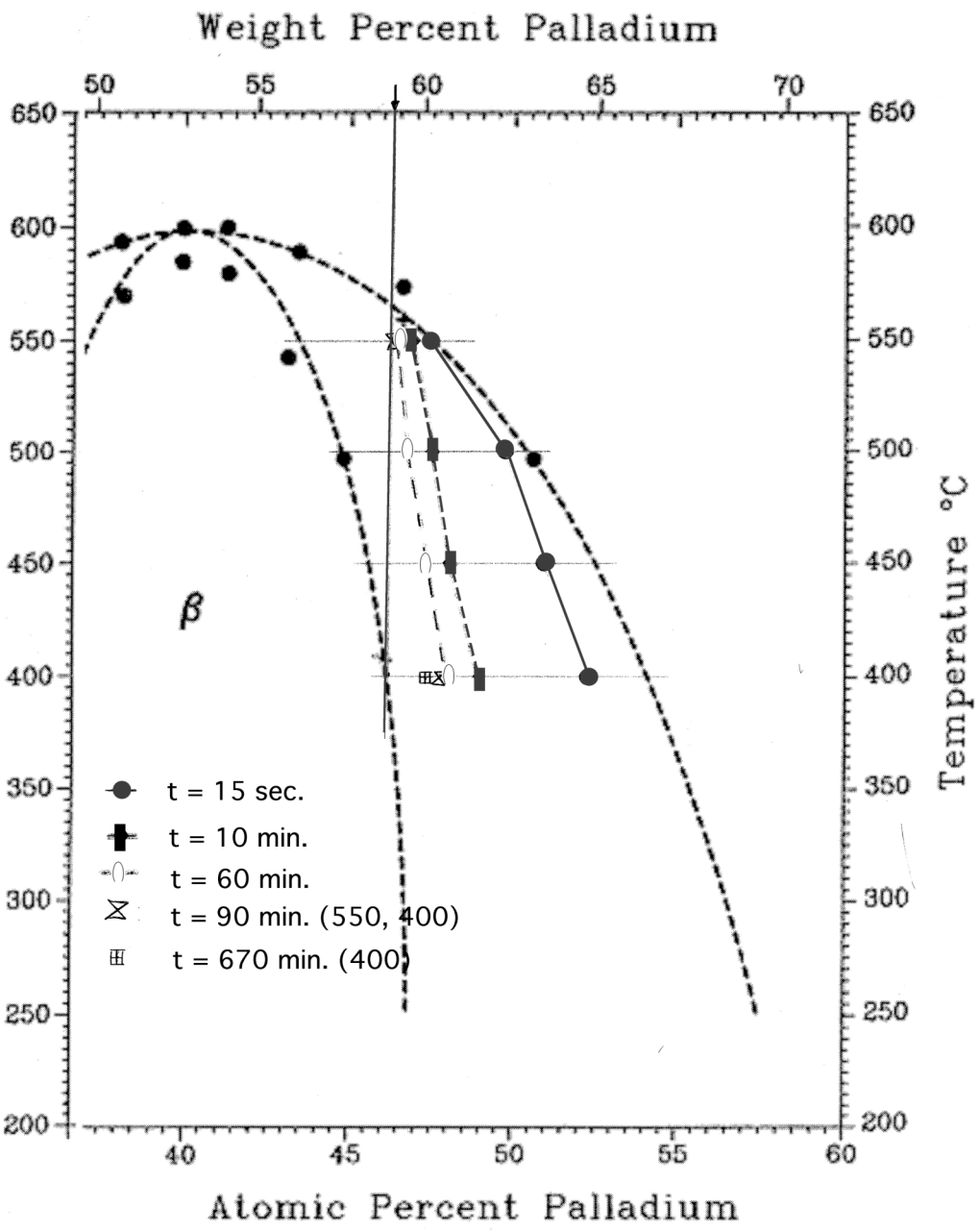

Figure 7-18 Phase transformation path at different times t=0 sec, t=10 min

7.4.3 H_2 permeation through a composite Pd-Cu membrane

The H_2 permeance of Ma-41 was measured at 250, 300, 350, 400 and 450ºC. As seen in Figure 7-19, no decline in H_2 permeance was observed at 450ºC for over 500 hr indicating that no intermetallic diffusion occurred for temperatures below or equal to 450ºC

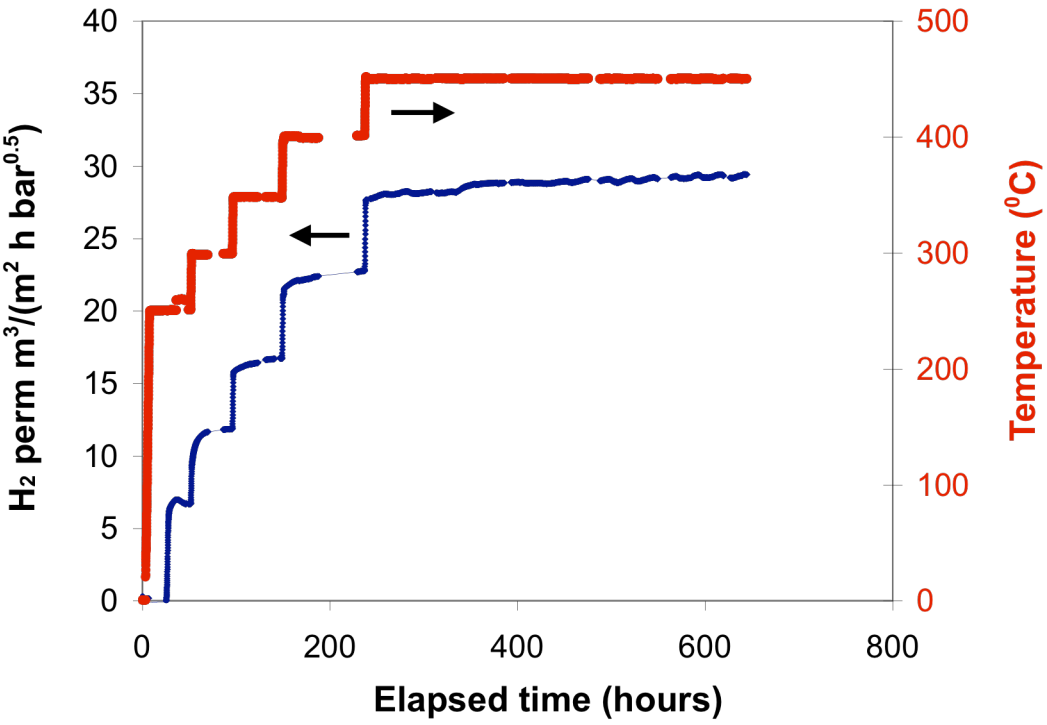

Figure 7-19 Long term H_2 stability for Ma-41 membrane.

Figure 7-20 shows the H_2 flux of Ma-41 membrane as a function of $\Delta(P^{0.5})$ at 250, 300, 350, 400 and 450ºC. When the H_2 flux data in Figure 7-20 were fitted by adjusting the n-exponent with Equation (3-3), the n-exponent was equal to 0.57-0.58 ±0.1 indicating that assuming Sieverts' law was valid. Moreover, the value of the ξ_{250} parameter for the graded support of Ma-41 was estimated to be higher than 40, therefore, deviations from Sieverts' law at high temperatures due to mass transfer resistance were negligible. Hence, the H_2 flux was consider as a linear function of $\Delta(P^{0.5})$ and bulk diffusion was the rate-limiting step. The flux data in Figure 7-20 were then fitted with Equation (3-2) to determine the H_2 permeance, $F_{0.5}$. Figure 7-21 shows the values of the H_2 permeance, $F_{0.5,}$ of membrane Ma-41 in an Arrhenius type of plot. The activation energy for H_2 permeation based on $F_{0.5}$ values determined after long annealing times equaled 20.6 kJ/mol. The activation energy for H_2 permeation was also determined by measuring H_2 flux as the temperature was changed at a rate of 1ºC/min. During each temperature change, an average of 15 (H_2 flux, Temperature) data points were recorded. The H_2 permeance, F_{H2}, was then determined using Equation (3-1). $Ln(F_{H2})$ vs. 1/T for each of the 250-300, 300-350, 350-400 and 400-450ºC temperature changes was plotted in Figure 7-21. For each temperature change the activation energy was determined and plotted in Figure 7-22. The activation energy for H_2 permeation, F_{H2}, was equal to 17.1 $kJmol^{-1}$ in the 300-350 temperature window and 15.6 $kJmol^{-1}$ in the 400-450ºC temperature range. The activation energy for H_2 permeation was higher when considering $F_{0.5}$ after long annealing periods than when considering F_{H2} during the different temperature changes. The difference was due to the fact that at all temperatures the H_2 permeance slightly increased over time as the alloying process took place as explained in Section 3.2.4. The increase in H_2 per-

meance was not due to leaks since the selectivity (H_2/He) of this membrane was well above 300 at all temperatures.

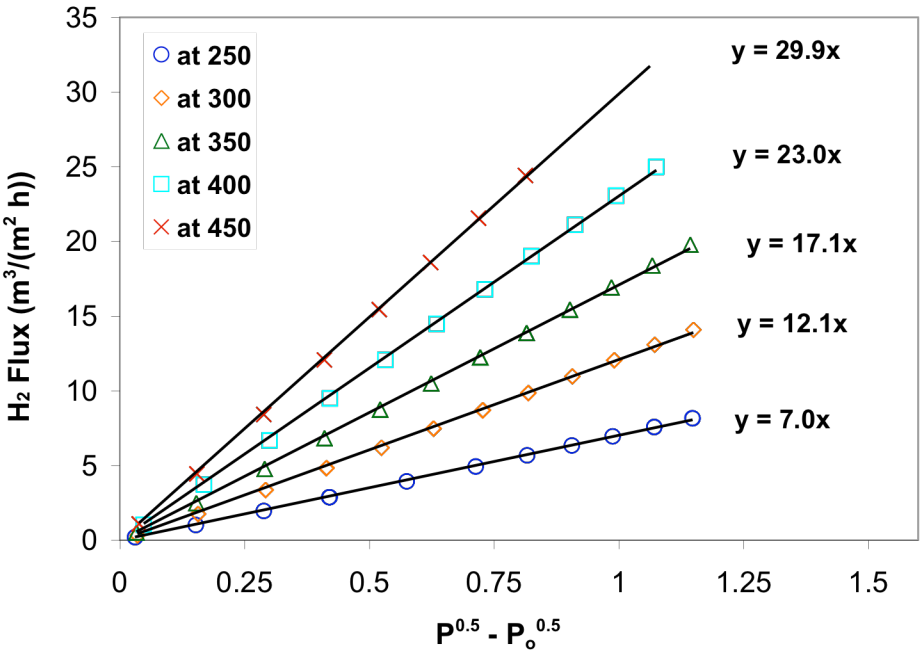

Figure 7-20 H_2 flux at 250-450°C for Ma-41 membrane as function of Sieverts' driving force. Numbers beside experimental lines are the H_2 permeance $F_{0.5}$.

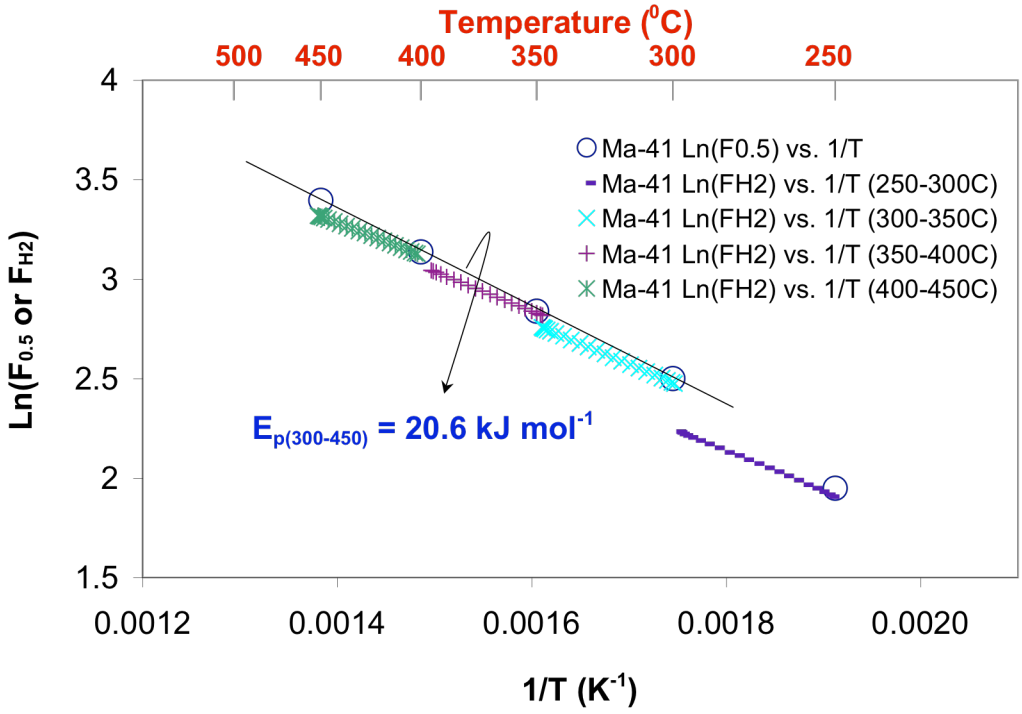

Figure 7-21 Arrhenius plot for membrane Ma-41. (open circles) permeance values $F_{0.5}$ from flux data in Figure 7-20.

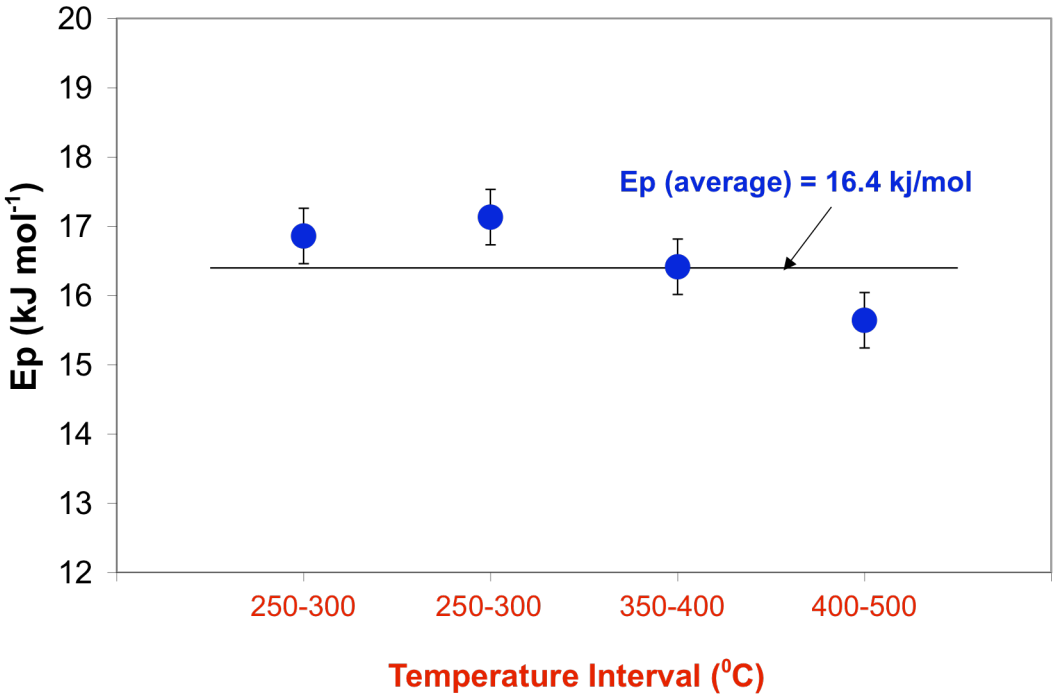

Figure 7-22 Activation energy for H_2 permeation for each temperature change.

The Cu content of membrane Ma-41 was estimated from the activation energy for H_2 permeation value. The average value of the E_p determined during each temperature change was equal to 16.4 kJ mol^{-1}. Figure 7-23 shows the activation energy for H_2 permeation for several PdCu alloys measured by Howard et al. (2004) in foils. The experimental data reported by Howard et al. (2004) was fitted with a 3rd degree polynomial function, which was equaled to 16.4 kJ mol^{-1} to solve for the Cu content in membrane Ma-41. A Cu content of around 7wt% was estimated as seen in Figure 7-23.

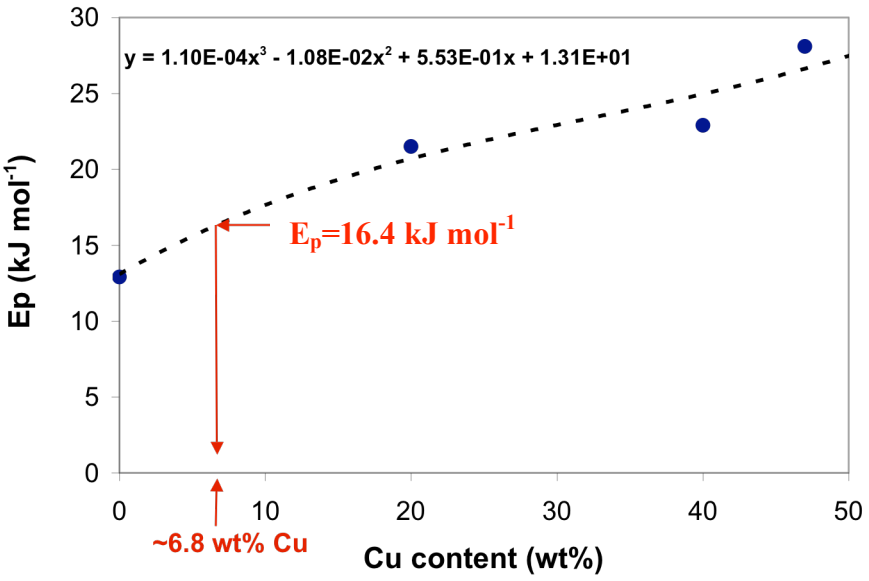

Figure 7-23 Activation energy for H_2 permeation in PdCu alloys as a function of Cu content.

7.5 Conclusions

Depending on the amount of Cu deposited on top of the Pd layer different phases appeared during the homogenization of the alloy. At low Cu loads only a Pd rich α phase was formed, at medium and high loads two phases were formed consisted of a Pd rich growing and a Cu rich dissolving phase. The transformation of α phase to β phase at a temperature of 400ºC was very fast. Indeed, the growth of the ordered β phase from the α phase only took 30 seconds. The formed phase was stable at temperatures lower than 525ºC. The preparation of a low Cu content Pd-Cu alloy membrane was possible on a graded PH support by the coating and diffusion method. The thin, 10μm, Pd-Cu membrane had a H_2 permeance as high as 30 $m^3/(m^2\ h\ bar^{0.5})$ at 450ºC and was stable for over 500 hr. The activation energy for H_2 permeation of Ma-41 was higher than the E_p of all other composite Pd membranes prepared on graded PH supports, in agreement with higher E_p for Pd-Cu alloys reported in the literature.

8 The intermetallic diffusion mechanism in composite Pd membranes

8.1 Introduction

Intermetallic diffusion is the migration of the elements in the porous metal support (mostly Fe, Cr and Ni) into the Pd layer, thereby affecting the H_2 permeance of the membrane. Intermetallic diffusion can be mitigated by forming or depositing an oxide or a high melting point metal layer on the porous metal support. Intermetallic diffusion barriers (also named thermal barrier coatings) can be formed by oxidation in air (Akis et al., 2003; Ma et al., 2004; Ma et al., 1998; Ma et al., 2000), deposition of nickel particles coated by a sol gel γ -Al_2O_3 layer (Nam and Lee, 2001), sandwiching of an Al_2O_3 foil (Edlund and McCarthy, 1995; Edlund and Pledger, 1993, 1994), deposition of tungsten or tantalum oxide (Gryaznov et al., 1993) and titanium nitride (Nam and Lee, 2005; Shu et al., 1996).

Metallic atoms start to acquire sufficient mobility at temperatures close to half of the material's melting point in Kelvin. 316L PSS supports melt at 1375-1400ºC, hence at 500-550ºC metallic atoms in the PSS support start to acquire enough mobility to diffuse into the Pd layer. Therefore, the H_2 permeance in composite Pd-PSS membranes should start to decrease at temperatures close to 500ºC. However, H_2 flux decline was observed in composite Pd-oxidized PSS membranes at temperatures as low as 275-350ºC

(Rothenberger et al., 2004). The diffusion of Fe, Cr and Ni into the Pd lattice, and vice versa, takes place at a very slow rate if not at all at 300ºC. Therefore, other processes such as: grain boundary diffusion of Fe, Cr or Ni in between the Pd grains, Pd clusters and grain growth, reduction of surface oxides with subsequent grain boundary diffusion of reduced elements into the Pd layer might lead to the decrease in H_2 permeance observed by many researchers at low temperatures (275-350º).

The activation energy for H_2 permeation through Pd-Fe or Pd-Cr alloys is higher than the activation energy for H_2 permeation through pure Pd (Flanagan et al., 1977; Swansiger et al., 1976). Therefore, intermetallic diffusion in composite Pd-PM support membranes should lead to an increase of the activation energy for H_2 permeation.

The main objective of this chapter was to understand the underlying mechanisms leading to the H_2 permeation loss in composite Pd-PM supports membranes at low and high temperatures. The capability of oxides formed on PM supports by air oxidation to mitigate or inhibit intermetallic diffusion in Pd-oxidized PM membranes was also investigated. Finally, a kinetic approach was undertaken to study the diffusion mechanism of the elements from the PM support into the Pd layer.

8.2 Experimental

Composite Pd membranes studied in this chapter are listed in Table 8-1. Membranes designated as C01-F0i were prepared according to the procedure described in Chapter 3 on oxidized PSS supports. Membranes designated as Ma-ii were prepared on "graded" PH supports. PH supports were graded with Pd seeds pre-activated Al_2O_3 powder following the experimental protocol described in Chapter 3 Section 3.1.2. The synthesis of C01-F06 was terminated since the deposition of as much as 19 μm of Pd only led to a very

small decrease of the original He permeance of the support, which was an indication of defects in the support. Therefore, the membrane was cut in several rings for the study of the oxide layer formed at 600ºC in air. Samples from C01-F06 were annealed in H_2 atmosphere at 300, 400, 500 and 600ºC for 48 hr.

Table 8-1 Characteristics of membranes studied in this chapter.

Membrane	Support Grade (μm)	O.D. (cm)	Length (cm)	Mem. Surf. [(a)] (cm^2)	Ox. Temp. (ºC)	Ox. Time (hr)	L (μm)
C01-F03	0.1 PSS	1.27	2.54	8.4	400	10	32
C01-F04	0.1 PSS	1.27	2.54	8.4	-	-	27
C01-F05	0.1 PSS	1.27	2.54	8.4	500	10	33
C01-F06[(b)]	0.1 PSS	1.27	6.35	23	600	10	19
C01-F07	0.1 PSS	1.27	6.35	23	500	10	23
Ma-32b	0.1 PH	2.54	15.24	120	700	12	10
Ma-34b	0.1 PH	2.54	15.24	120	700	12	8
Ma-42	0.1 PH	2.54	15.24	120	700	12	5.6

[(a)] The membrane surface area does not match the calculated surface using support OD and length due to the fact that the weld area for all membranes was taken as around $2cm^2$ of the porous area.
[(b)] C01-F06 was not a dense membrane. The synthesis was stopped due to large defects in the support. The membrane was cut in several pieces to study the structure of the oxide formed at 600ºC and its stability at different temperatures.

8.3 Results and discussion

8.3.1 The oxidation of porous metal supports

8.3.1.1 Oxide structure upon heating

After heating in air, the color of PSS supports changed from silver to gold when oxidized at 400ºC, to green when oxidized at 500ºC, to red-purple when oxidized 600ºC and to grey when oxidized at 800ºC. Each color responded to a different oxide structure. Oxidizing 316L PSS supports at 600ºC for 12 hr led to a thin, 0.8μm in thickness, oxide layer, which appeared as a dark layer in the SEM micrographs.

Figure 8-1(a) shows the cross-section of C01-F06 sample after heat-treatment at 300ºC under H_2 atmosphere for 48 hr. The elemental composition of the oxide layer was determined with EDX. Figure 8-1(b) shows four distinctive zones: (I) the stainless steel, (II) a chromium rich layer on the stainless steel, (III) an iron rich layer on top of the chromium oxide ("iron shoulder") and (IV) the Pd layer. The chromium and iron rich layers were obviously oxide layers since oxygen was also present. Oxidizing at 600ºC in stagnant air led to a thin (0.5-0.8μm) oxide layer, which consisted of a chromium oxide layer (0.1-0.2μm) and an iron oxide layer on top (0.4-0.6μm). The oxide layer was not uniform throughout the sample. The oxide structure found upon heating at 600ºC in air was in agreement with the oxide structure found by Ma et al. (2004).

The oxidation of 316L PSS at 400ºC and 500ºC led to oxide layers, which were too thin to be visible by SEM techniques and/or analyzed by EDX techniques. Therefore, the nature and the structure of oxides formed on PSS support upon heating at low temperatures could not be investigated. Yet, the green color of the 500ºC oxidized 316L PSS supports (for instance C01-F07's support after oxidation) suggested the presence of Cr_2O_3. Hence the structure of a composite Pd membrane prepared on a PSS support oxidized at temperatures higher than or equal to 600ºC was Pd-Fe_2O_3-Cr_2O_3-PSS. The structure of a composite Pd membrane prepared on a PSS support oxidized at temperatures lower than or equal to 500ºC was most probably Pd-Cr_2O_3-PSS. The Cr_2O_3 layer formed at low temperatures (<500ºC) was most probably thinner than 0.1-0.2 μm.

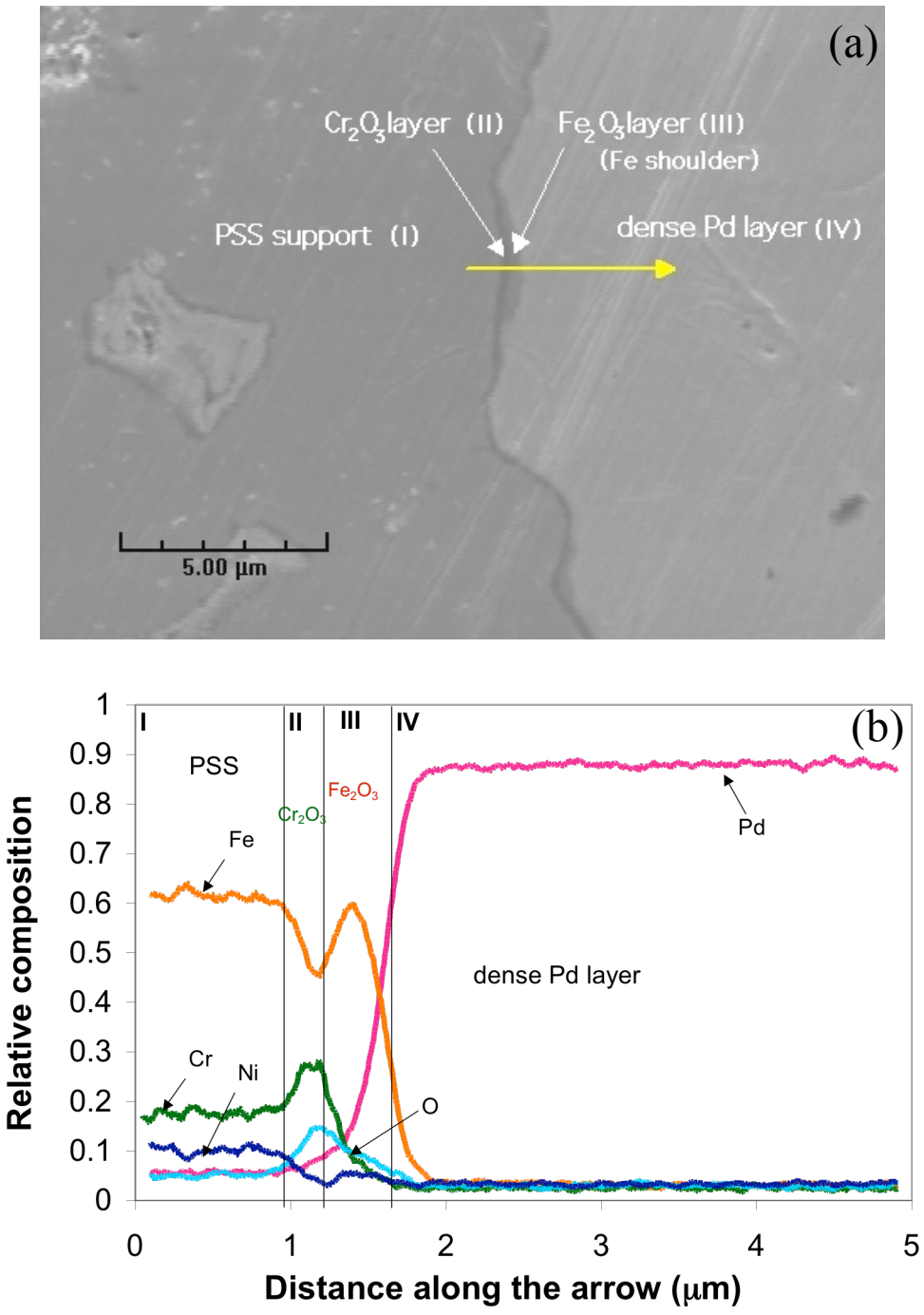

Figure 8-1 (a) SEM micrograph of the Pd-600ºC oxidized PSS interface. (b) Elemental composition across the Pd-oxidized PSS interface.

The oxidation of PH supports for membrane preparation was only conducted at 700ºC and led to a decrease in He permeance of 40-50 % of the initial He permeance. The oxidation at higher temperatures of PH supports for membrane application would have resulted in the complete clogging of the support's porosity. The oxide layer formed at 700ºC was thin and only Cr_2O_3 was detected with EDX. PH plates were oxidized at 900ºC for 12 hr to understand whether PH also has a tendency to form Fe_2O_3 on top of Cr_2O_3 as 316 L stainless steel does.

The crystallographic structure of Fe_2O_3, Cr_2O_3 and all Fe-Cr mixed oxides is very similar and their XRD patterns are therefore also very similar. The XRD pattern of Fe_2O_3 oxide has distinctive reflections ($I/I_0 > 30$) at $2\theta \approx 24.138$, 33.152, 35.611, 49.479, 54.089, 62.449 and 63.994º. The XRD pattern of Cr_2O_3 oxide has the same distinctive reflections with a slight shift to right: 24.496, 33.597, 36.196, 50.219, 54.853, 63.448 and 65.108º. The XRD reflections of all Fe-Cr mixed oxides lie between the XRD reflections of Fe_2O_3 and Cr_2O_3 with peak positions depending on the Fe/(Fe+Cr) ratio. Figure 8-2 shows the XRD pattern of the oxide layer formed after oxidation at 900ºC for 12 hr in stagnant air (316L PSS (blue peaks) and PH (green peaks)). Figure 8-2 (a), (b) and (c) show the XRD spectra in the low 2θ region, medium 2θ region and high 2θ region respectively. Figure 8-2 also shows the characteristic reflections of Fe_2O_3, Cr_2O_3 and $NiCrO_3$ references. The XRD pattern of the PSS support oxidized at 900ºC for 12 hr revealed the presence of Fe_2O_3 at the surface of the sample in agreement with the Fe_2O_3-Cr_2O_3-PSS structure found using EDX technique.

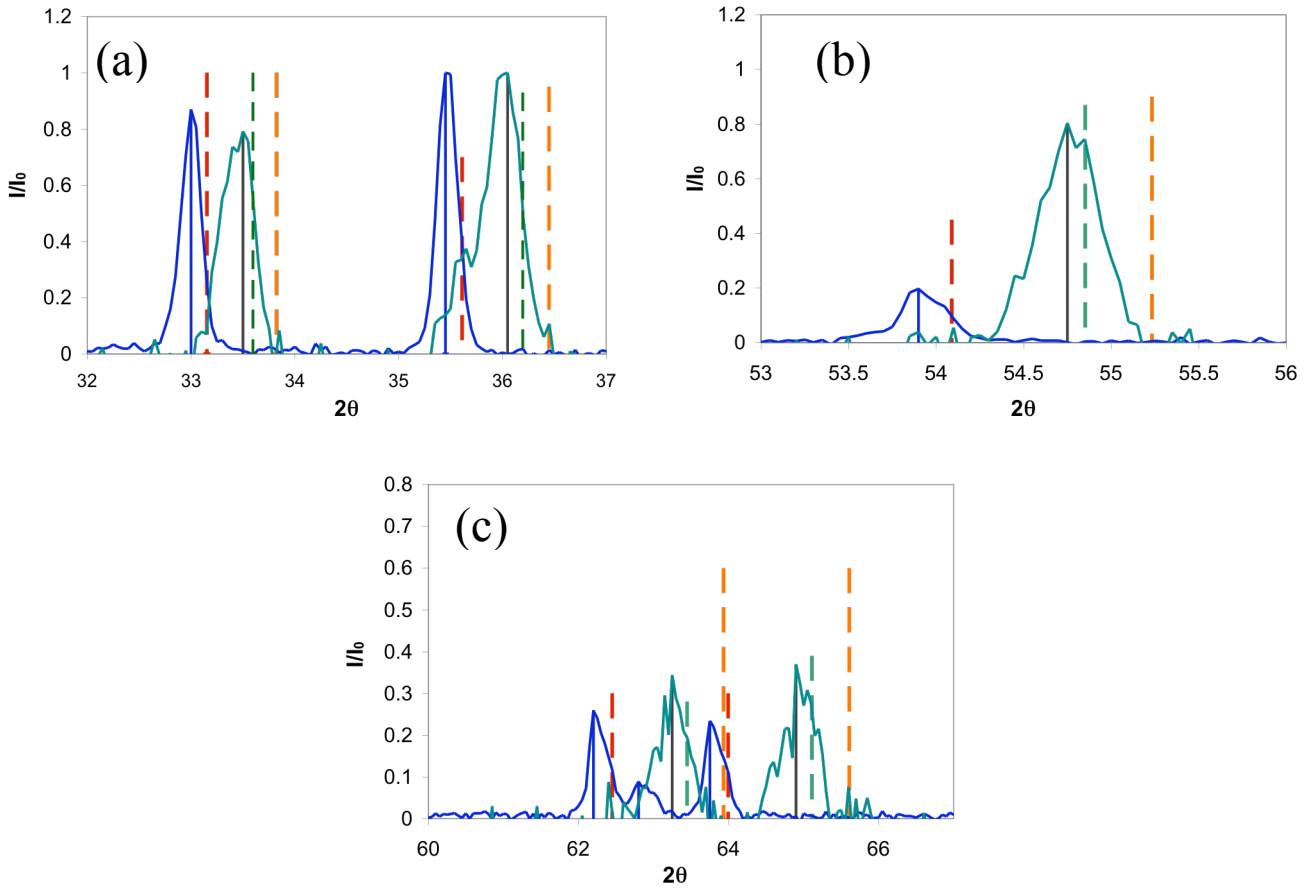

Figure 8-2 XRD spectra of PSS (blue) and PH (green) oxidized at 900ºC for 12 hr. (a) low 2θ range, (b) medium 2θ range and (c) high 2θ range. The reference XRD peaks of Fe_2O_3 (red dashed lines), Cr_2O_3 (green dashed lines) and $NiCrO_3$ (orange dashed lines) are also plotted for peak matching.

Moreover, the XRD peaks from the support were not detectable after oxidation indicating the formation of a very thick Fe_2O_3 layer (>5μm). The XRD pattern of the oxidized PH sample had the characteristic reflection of the support indicating that the oxide layer formed on PH samples upon oxidation at 900ºC for 12 hr was in the order of a micron (1-2μm). The XRD peaks of the oxide formed on PH were located to the right of the XRD peaks of the oxide formed on PSS at the same conditions. Therefore, oxides formed on PH were richer in Cr_2O_3. In fact, the XRD pattern of oxidized PH corresponded to the XRD pattern of the Cr_2O_3 reference.

The small shifts in both experimental Fe_2O_3 and Cr_2O_3 patterns were due to errors in sample height position. Since PH had up to 65wt% of Ni, Ni-rich oxide layers can be formed after oxidation. The presence of Ni-rich oxide layers was disregarded since the reference XRD peaks of $NiCrO_3$ laid far from the experimental oxide peaks.

PH has a tendency to develop thicker Cr_2O_3 oxide layers than 316L PSS. Moreover, no Fe_2O_3 layer was found on the outer surface of oxidized PH at high temperatures (900ºC) opposite to the oxidation of PSS samples.

8.3.1.2 Oxide stability in reducing atmosphere

The stability of the oxide layer formed on 316L PSS after heat-treatment at 600ºC was investigated by studying the cross-section of C01-F06 samples annealed at 400 and 500ºC in H_2 for 48 hr. The oxide layer formed at 600ºC was still visible after annealing at 400ºC in H_2 atmosphere as seen in Figure 8-3(a). Figure 8-3(b) shows the iron concentration profile of six different line-composition scans (lines 1 to 6) across the stainless steel-Pd interface of the 400ºC-annealed sample.

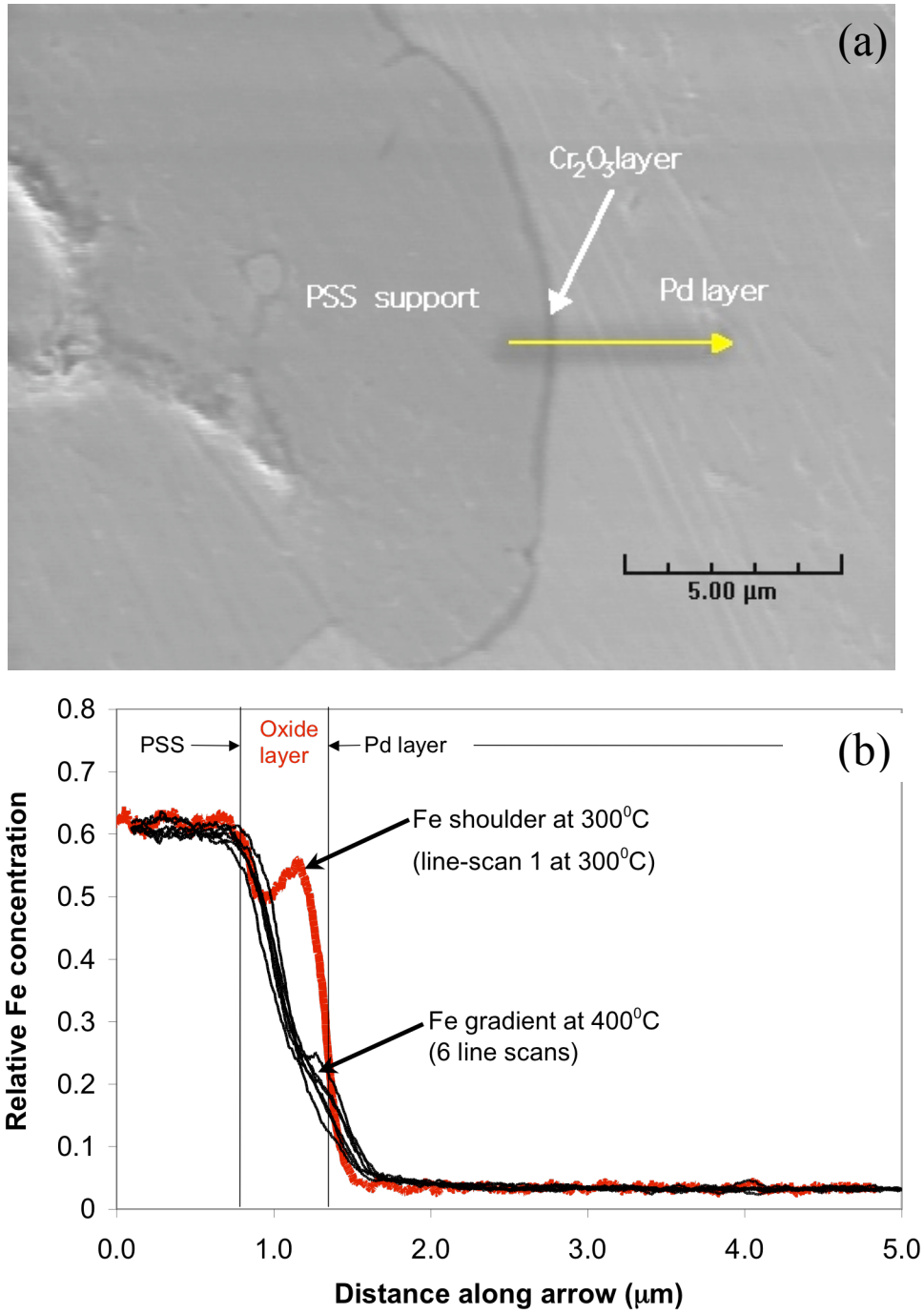

Figure 8-3 (a) SEM photograph of the Pd-oxidized PSS interface after heat-treatment at 400ºC in H_2 (b) Fe concentration across the steel-Pd interface for the sample annealed at 400ºC in H_2 for 48 hr at 6 different locations in the sample (line-scans 1-6). One of the scans (line-scan 1) of the sample at 300ºC was added for comparison.

The line-composition scan 1 from the 300ºC-annealed sample was superimposed for comparison purposes. In all scans performed on the 400ºC-annealed sample no iron oxide shoulders were detected but a gradient between the Fe content in the support (63wt%) and the Fe content of the Pd layer adjacent to the PSS support (0wt%). All scans, 1 through 6, can be considered as a single line scan as seen in Figure 8-3(b). It appeared that the reduction of the Fe_2O_3 layer took place at 400ºC when H_2 was dissolved in the Pd layer. The reduced Fe slightly diffused into the Pd layer leading to the Fe gradient seen in Figure 8-3(b).

Figure 8-4 (a) and (b) show a SEM micrograph of the oxide after heat-treatment at 500ºC in H_2 and the iron concentration profile across the interface respectively. At 500ºC, the thickness of the initial oxide layer dramatically decreased and a non-uniform gray layer was seen instead. The gray layer resulted from the inter-diffusion between the Pd layer and the support. No iron shoulders were detected but iron traces were measured up to 2μm in the Pd. Hence, at 500ºC the reduced iron readily diffused into the Pd layer.

A fourth sample of C01-F06 membrane was heat-treated at 600ºC for 48 hr in H_2. Figure 8-5(a) shows the SEM micrograph of the Pd-oxidized PSS interface after heat-treatment at 600ºC. Due to the intermetallic diffusion of Fe, the non-uniform grey layer visible at 500ºC grew thicker and corresponded to the diffusion of Pd into the stainless steel. Also, a thin oxide layer was still visible and appeared as a dark gray line in Figure 8-5(a). The Pd layer at the vicinity of the support was characterized by a darker color, due to the diffusion of Fe into the Pd layer. Figure 8-5(b) shows the Pd, Fe, Cr and Ni profile across the interface.

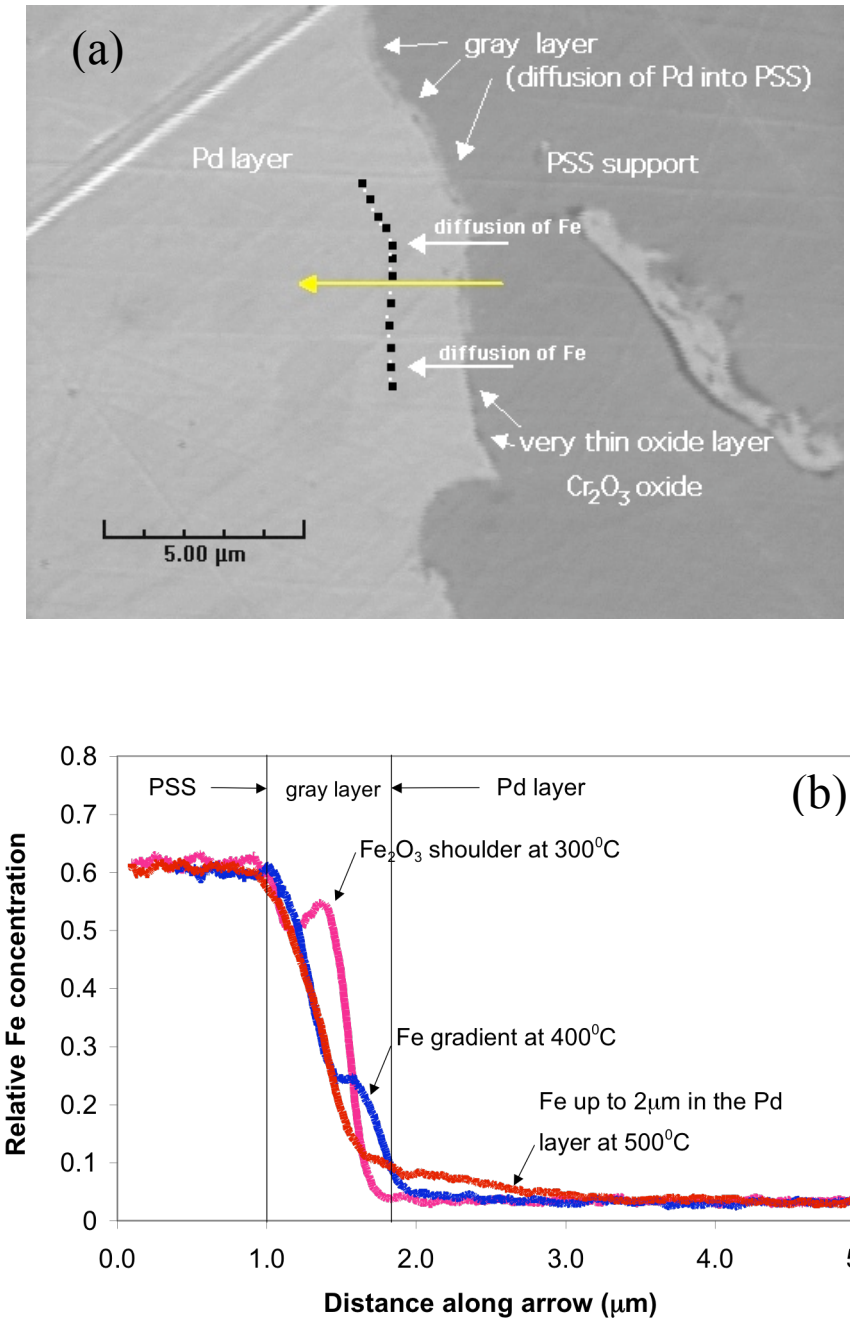

Figure 8-4 (a) SEM photograph of the Pd-oxidized PSS interface after heat-treatment at 500ºC in H_2 (b) Fe concentration profile of samples from C01-F06 annealed at 300ºC, 400ºC and 500ºC under H_2 atmosphere.

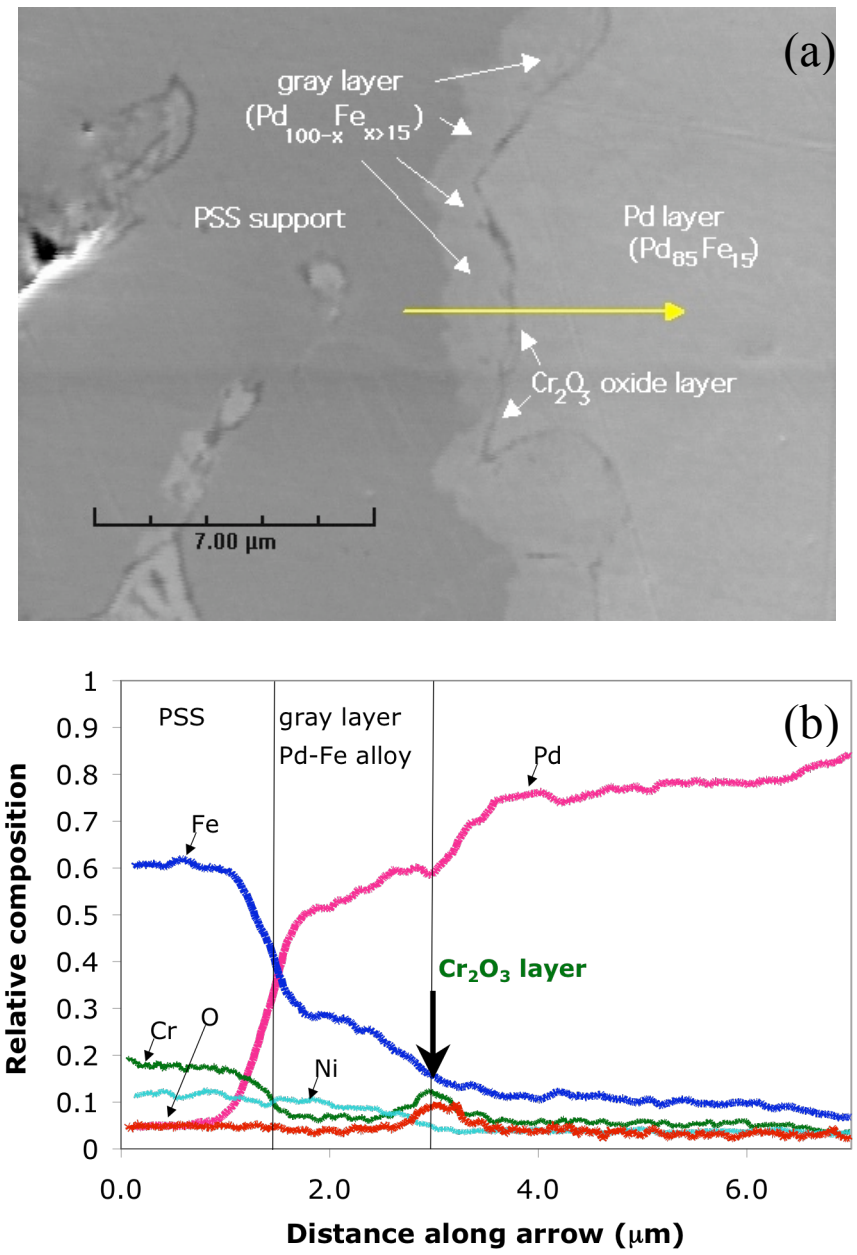

Figure 8-5 (a) SEM photograph of the Pd-oxidized PSS interface after heat-treatment at 600°C in H_2 (b) Fe, Pd, Cr and Ni concentration profile across the interface.

Large amounts of Pd diffused into the stainless steel and traces of Fe were detected up to 4 μm inside the Pd layer. Interestingly, the Cr concentration profile was characterized by a small peak, which corresponded to the thin dark grey layer still visible between the thick region where Pd diffused into the stainless steel and the Pd layer. Therefore, the thin 0.1-0.2 μm Cr_2O_3 layer resulting from the oxidation at 600ºC in air was not reduced when the composite Pd-oxidized PSS structure was in H_2 atmosphere at 600ºC. Figure 8-5(b) also shows that intermetallic diffusion was mostly the diffusion of Fe and some Cr into the Pd layer. Ni diffusion into the Pd layer was not observed.

The stability and ability of oxides formed on porous PH to suppress intermetallic diffusion was studied with a cross section sample of membrane Ma-34b. Figure 8-6 (a) shows the cross-section of Ma-34b after H_2 characterization at 600ºC. The distinctive gray layer of Cr_2O_3 was still present. Also, Pd diffused across the Cr_2O_3 porous layer into the PH forming a thin light grey region behind the Cr_2O_3 layer. The elemental composition across the Pd-oxidized PH interface is shown in Figure 8-6 (b). A Cr peak corresponding to the Cr_2O_3 layer was present at the Pd-PH interface. Pd diffused deep (up to 2μm) into the hastelloy grain, however, hardly any Ni or Cr was detected in the Pd layer. No large Fe concentrations were detected since PH had only 2-3wt% Fe.

The amount of intermetallic diffusion at 600ºC in H_2 atmosphere was significantly less in the Pd-PH system than in the Pd-PSS system. The reasons for such a strong ability of oxidized PH supports to prevent intermetallic diffusion was due to the fact that PH had a tendency to form a thicker Cr_2O_3 layer without any Fe_2O_3 formed on top the Cr_2O_3 layer.

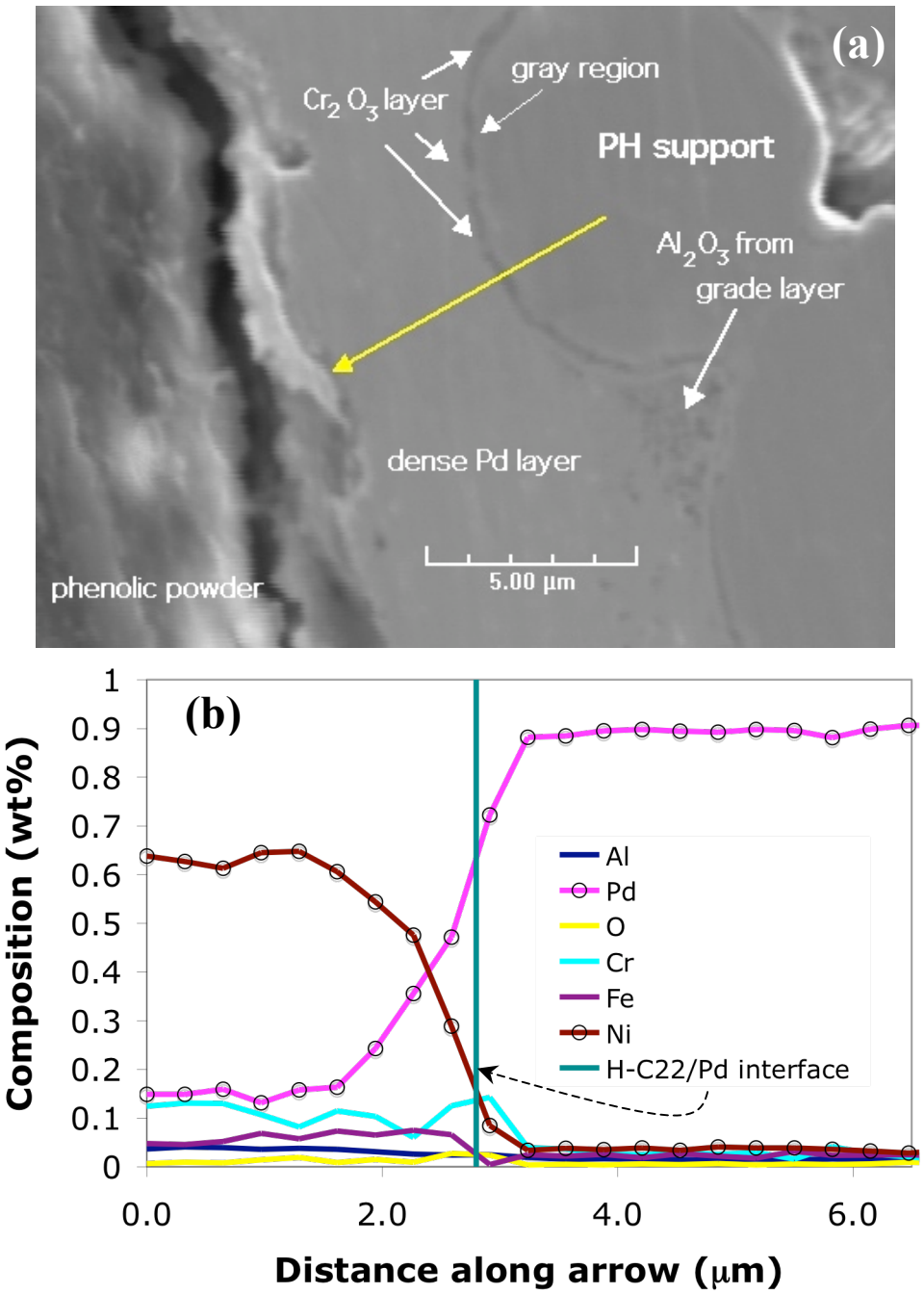

Figure 8-6 (a) Cross-section of Ma-34b after heat-treatment at 600°C in H_2 atmosphere. (b) Elemental composition across the Pd-Oxidized PH interface.

Fe_2O_3 was indeed found to undergo reduction to Fe in H_2 atmosphere in the Pd-Fe_2O_3-Cr_2O_3-PSS composite structure. Also, since the Fe content of PH was only 2-3wt% the driving force for Fe diffusion into the Pd layer was negligible.

8.3.2 Effect of intermetallic diffusion on H_2 permeance

8.3.2.1 Effect on H_2 permeance

Figure 8-7 shows for every temperature the H_2 flux/H_2 $flux_0$ as a function of time for membrane C01-F03. H_2 $flux_0$ was the initial H_2 flux at any given temperature. The initial rate at which the H_2 flux declined was given by the slope of the curve (H_2 flux/H_2 $flux_0$, time) at time t=0. It is clearly seen in Figure 8-7 that the slope of the (H_2 flux/H_2 $flux_0$, time) curved increased as the temperature was increased from 300 to 500ºC in membrane C01-F03. Figure 8-8 shows the H_2 flux/ H_2 $flux_0$ decline as a function of time at 450 and 500ºC for Membrane C01-F04. The initial rate at which the H_2 flux declined, slope of the curve (H_2 flux/H_2 $flux_0$, time) at time t=0, also increased with temperature.

Figure 8-9 shows the H_2 flux/ H_2 $flux_0$ decline for membrane C01-F07. It is interesting to note that the rate at which H_2 flux declined, increased from 300 to 400ºC and then decreased from 400 to 500ºC. The SEM investigation of the surface of membrane C01-F07 revealed the presence of blisters and the detachment of the second Pd layer from the first Pd layer. The selectivity (H_2/He) of the membrane at the end of the characterization process was measured at room temperature and equaled 43. Therefore, the H_2 flux decline at 450, 450 and 500ºC was mostly masked by a large leak development. Since leaks hardly developed at low temperatures, experimental data in the 300-400ºC were taken to be valid.

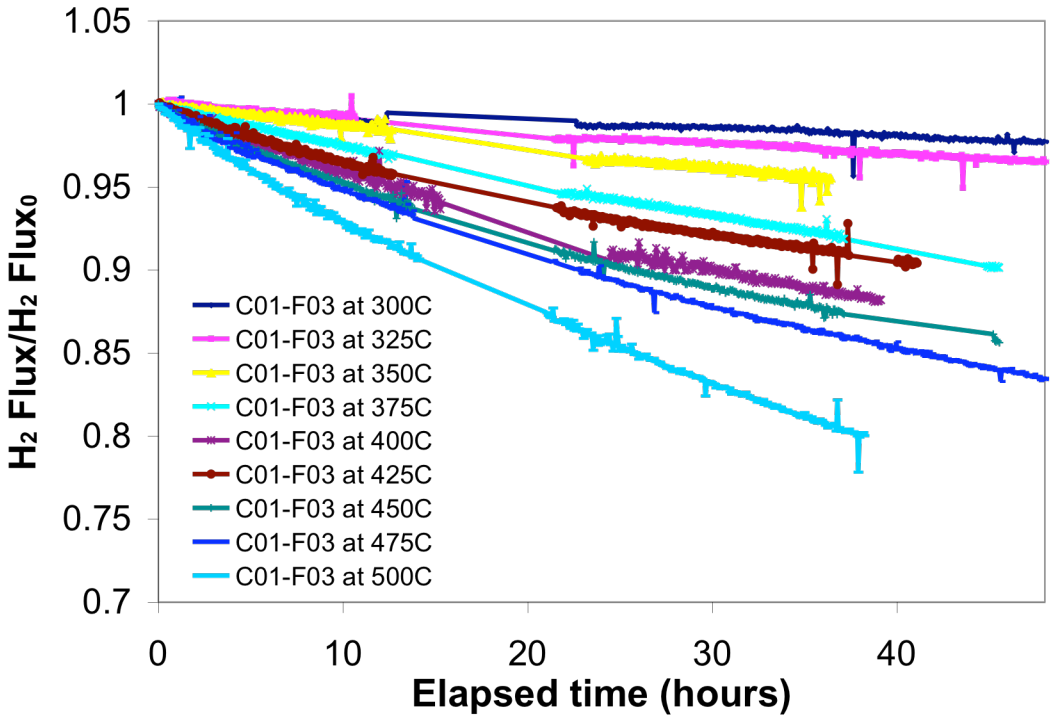

Figure 8-7 H_2 flux/H_2 flux$_0$ as a function of time for all temperatures membrane C01-F03, was tested

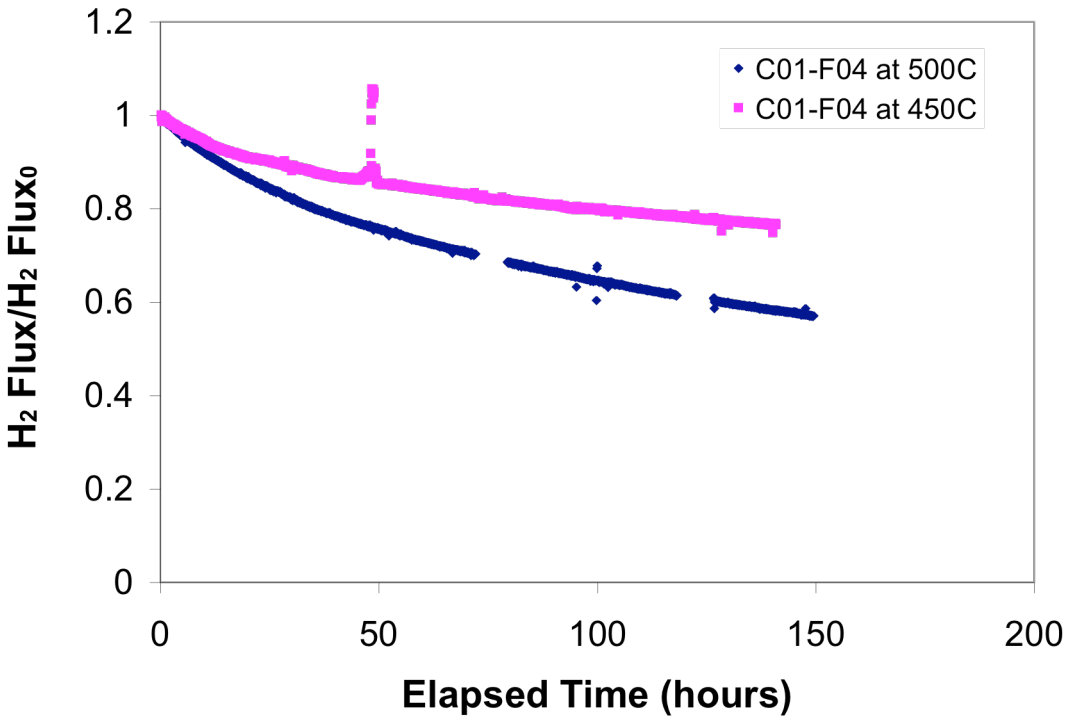

Figure 8-8 H_2 flux/H_2 flux$_0$ vs. time for membrane C01-F04

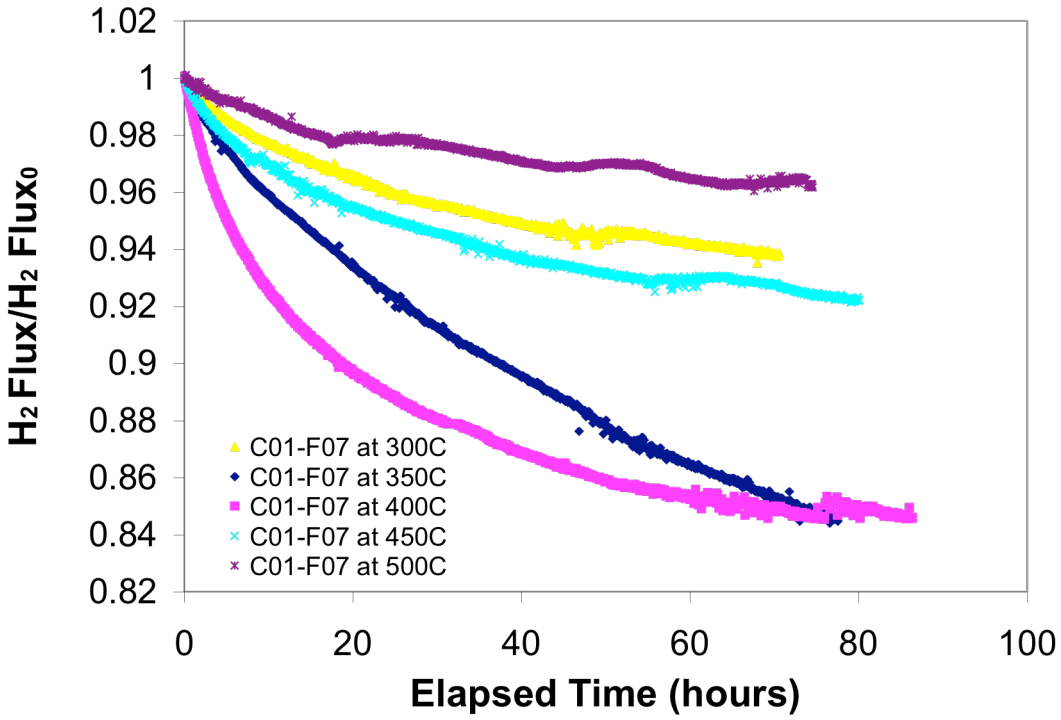

Figure 8-9 H_2 flux/H_2 flux$_0$ vs. time for membrane C01-F07

The H_2 flux of all membranes prepared on oxidized PSS supports (C01-F03, C01-F04, C01-F05, C01-F07 and C01-F08), except for C01-F11 and C01-F11b, started to decrease at a temperature close to 275-300ºC.

The diffusion coefficient of Fe in Pd, $D_{Fe->Pd}$, is equal to $0.18 \cdot \exp(-260000/RT)$ cm^2 s^{-1} (Brandes and Brook, 1998) and the Fe penetration depth into Pd is approximated by $(D_{Fe->Pd}\, t)^{0.5}$ with t in seconds[1] . After 50 hr[2] at 300ºC the penetration depth of Fe into Pd was only $2.54 \cdot 10^{-10}$ m. Hence, Fe diffusion through the lattice of Pd was not responsible for H_2 flux decline at 300ºC seen for membrane C01-F03. After 50 hr at 500ºC the penetration depth of Fe into Pd was $0.3 \cdot 10^{-6}$ m. That is, after 50 hr at 500ºC, the Fe concentration in the Pd layer was higher than around 30wt% up to 0.3 μm, and lower than 30wt% after the 0.3μm (see Figure 8-4(b)). Therefore, at temperatures equal to or higher than 500ºC, the diffusion of Fe through the Pd lattice appeared to be the predominant mechanism leading to the H_2 flux decline seen in all composite Pd-PSS membranes.

Figure 8-10 shows the H_2 flux loss as a function of time for membrane Ma-42 prepared on graded PH supports. Compared to the composite Pd membranes prepared on the PSS support, H_2 flux in Ma-42 membrane decreased at a slower rate. For instance, Ma-42 only lost 10% of its initial H_2 flux after 100 hr at 500ºC. After 100 hr at 500ºC the H_2 flux of Ma-42 became stable.

[1] The penetration depth $(Dt)^{0.5}$ is defined as the distance in the Pd layer from the Pd-PSS interface where the Fe concentration is equal to half of the Fe concentration of the support, which is equal to around 60wt%.

[2] 50 hours was the average time C01-F03 was held at each temperature, see Figure 8-7.

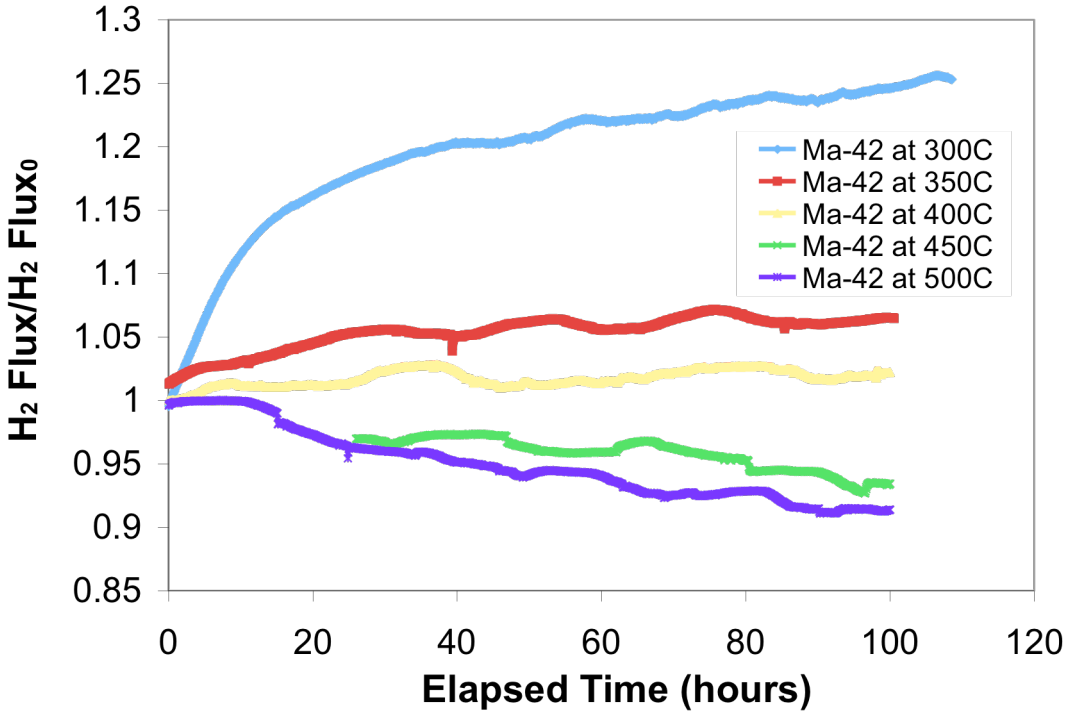

Figure 8-10 H_2 flux loss at different temperatures as a function of time for membrane Ma-42

The H_2 flux of Ma-32/34/42 membranes increased during the first 50-100 hr at 250, 300 and only slightly at 350ºC as seen in Figure 8-10(a). The increase in H_2 flux was not due to leak development since the selectivity of Ma-42 equaled 25000 at 350ºC. This phenomenon, mostly seen in "fresh" composite Pd membrane prepared on graded supports, was described in Section 0.

Table 8-2 lists the temperature at which the H_2 permeance started to decline in each membrane. Membranes prepared on oxidized PSS supports were less stable than membranes prepared on oxidized PH supports. The grade layer (Pd-Al_2O_3) can also act as an intermetallic diffusion barrier since the H_2 permeance of membranes C01-F08/11/11b prepared on graded PSS supports showed greater stability.

Table 8-2 Temperature at which H_2 permeance loss was first recorded for several membranes.

Membrane	Support	Ox.	Graded	Thickness	Temp. of first decrease
C01-F03	0.1 PSS	400	No	32	300
C01-F04	0.1 PSS	none	No	28	300
C01-F05	0.1 PSS	500	No	33	350
C01-F07	0.1 PSS	500	No	23	300
C01-F11	0.1 PSS	500	Yes	15	500
C01-F11b	C01-F11	500	Yes	17	T>500*
Ma-32	0.1 M PH	700	Yes	7.7	T>500
Ma-32b	Ma-32	700	Yes	10	T>500
Ma-34	0.1 MC PH	700	Yes	4	T>500
Ma-34b	Ma-34	700	Yes	8	600
Ma-42	0.1 M PH	700	Yes	5.6	450

*T>500ºC stands for: no H_2 permeance loss was recorded up to 500ºC, which was the maximum temperature the membrane was exposed to

8.3.2.2 Intermetallic diffusion effect on activation energy for H_2 permeation

The H_2 flux decline due to the intermetallic diffusion that occurred during the 50 minutes necessary to perform a 50ºC temperature change at temperatures lower than 550ºC

was negligible compared to the increase of H_2 flux due to the 50ºC temperature change, (see Section 5.4.5). Therefore, it was possible to determine the changes in the activation energy for H_2 permeation as the temperature was increased to 250, 300, 350, 400, 450, 500 and 550ºC. However, at temperatures higher than 550°C, the intermetallic diffusion rate was fast enough leading to a significant H_2 flux decrease during the 50 minutes of the temperature change and no valid activation energy could be determined by the temperature ramp method. The activation energy for H_2 permeation was determined for membrane C01-F05 by measuring H_2 flux (ΔP=1bar) at every temperature change (1:250ºC-300ºC; 2:300ºC-350ºC; 3:350ºC-400ºC; 4:400ºC-450ºC; 5:450ºC-500ºC; 6:500ºC-550ºC; 7:550ºC-600ºC and 8:600ºC-650ºC). Figure 8-11 shows the activation energy values for each temperature interval for membrane C01-F05. The activation energy for H_2 permeation, F_{H2}, increased from 10.5 kJ mol^{-1} in the 250°C-300°C temperature window to 18 $kJmol^{-1}$ at 500°C-550°C. Above 550°C, the activation energy for H_2 permeation, F_{H2}, decreased due to the fact that the H_2 flux loss during temperature change was no longer negligible compared to H_2 flux increase due to temperature increase. In order to measure the activation energy for H_2 permeation, F_{H2}, at temperatures higher than 550-600ºC, membrane C01-F05 was annealed at a maximum temperature of 700°C for one hour and the activation energy for H_2 permeation through a Fe-Cr rich Pd layer was determined while decreasing temperature in one step from 600ºC to 250ºC. The activation energy for H_2 permeation was measured to be 31 $kJmol^{-1}$ in the 250°C-600ºC temperature range, which was consistent with the fact that the E_p for Pd-Fe and Pd-Cr alloys is higher than the E_p for pure Pd (Flanagan et al., 1977; Swansiger et al., 1976).

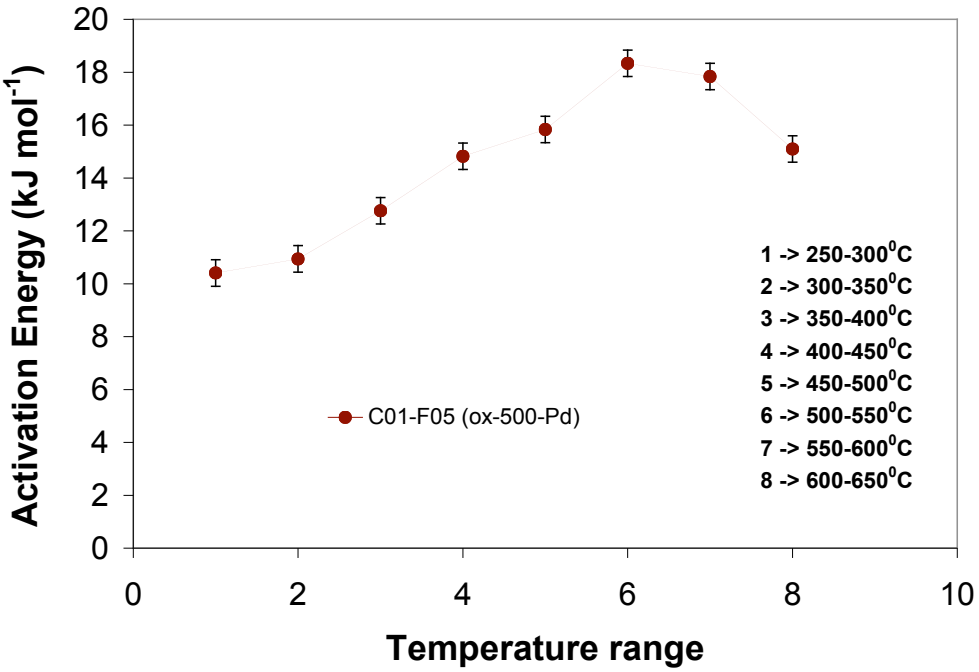

Figure 8-11 Activation energy for H_2 permeation vs. temperature change for membrane C01-F05.

Figure 8-12(a) and (b) show the cross-section micrograph and the elemental composition across the Pd-oxidized PSS interface for membrane C01-F05 after heat-treatment at 700ºC for one hour. The original Pd layer, which had a thickness close to 33μm, showed a Pd-Fe-Cr-Ni alloy layer with a thickness of around 15μm and a rich Pd layer of 20 μm. The 15μm thick Pd-Fe-Cr-Ni alloy layer represented the main resistance for H_2 permeation, thereby explaining the high activation energy found for the H_2 permeation in C01-F05 membrane. Hence, intermetallic diffusion led to the increase of activation energy for H_2 permeation due to the presence of Fe rich Pd alloys at the vicinity of the PSS support.

The activation energies for H_2 permeation of membranes C01-F03, C01-F07, Ma-32, Ma-32b and Ma-34b were also calculated at all temperatures changes and plotted with the values of C01-F05 in Figure 8-13. Membranes C01-F03 and C01-F07 showed a similar trend than C01-F05: an increase in the H_2 permeation activation energy from values of 9-12 kJ mol^{-1} in the 250°C-300°C temperature window to 16-18 kJ mol^{-1} in the 450°C-500°C temperature window. A slight increase in activation energy was consistently noticed after some H_2 flux decline at a given temperature similar to the H_2 flux declines recorded for membranes C01-F03, C01-F04 and C01-F07 seen in Figure 8-7, Figure 8-8 and Figure 8-9.

In Section 5.4.3.2, all composite Pd membranes prepared on graded PH supports (Ma-32/32b/34/34b/41/42) were proven to have mass transfer resistance within their porous support. Therefore, the activation energy for H_2 permeation, F_{H2}, of membranes Ma-32/32b and Ma-34b was lower than the activation energy for H_2 permeation of C01-F03/5/7 membranes as seen in Figure 8-13. All membranes have similar activation energies for H_2 permeation in the 250-300ºC temperature interval.

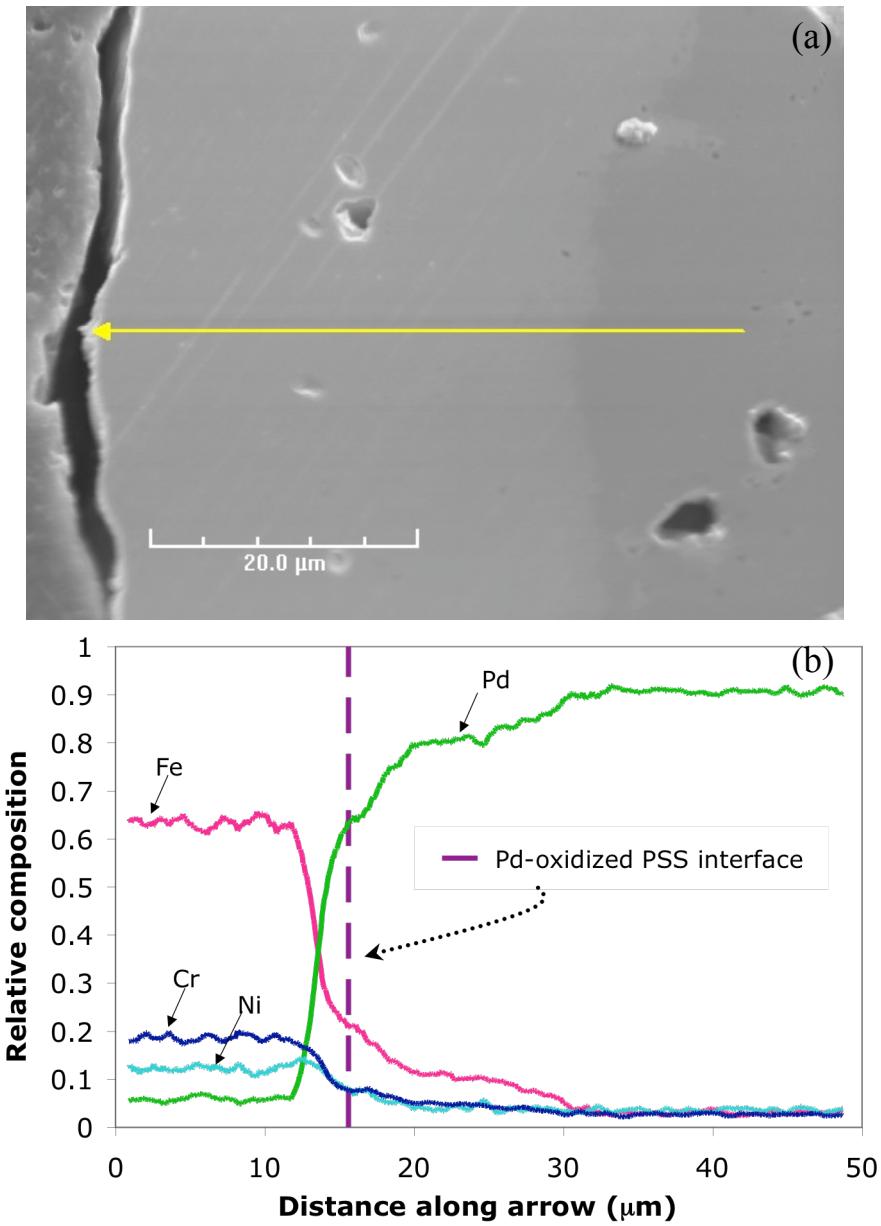

Figure 8-12 (a) Cross-section of C01-F05 after heat-treatment at 700ºC in H_2 atmosphere for 1 hr. (b) Elemental composition across the Pd-Oxidized PSS interface

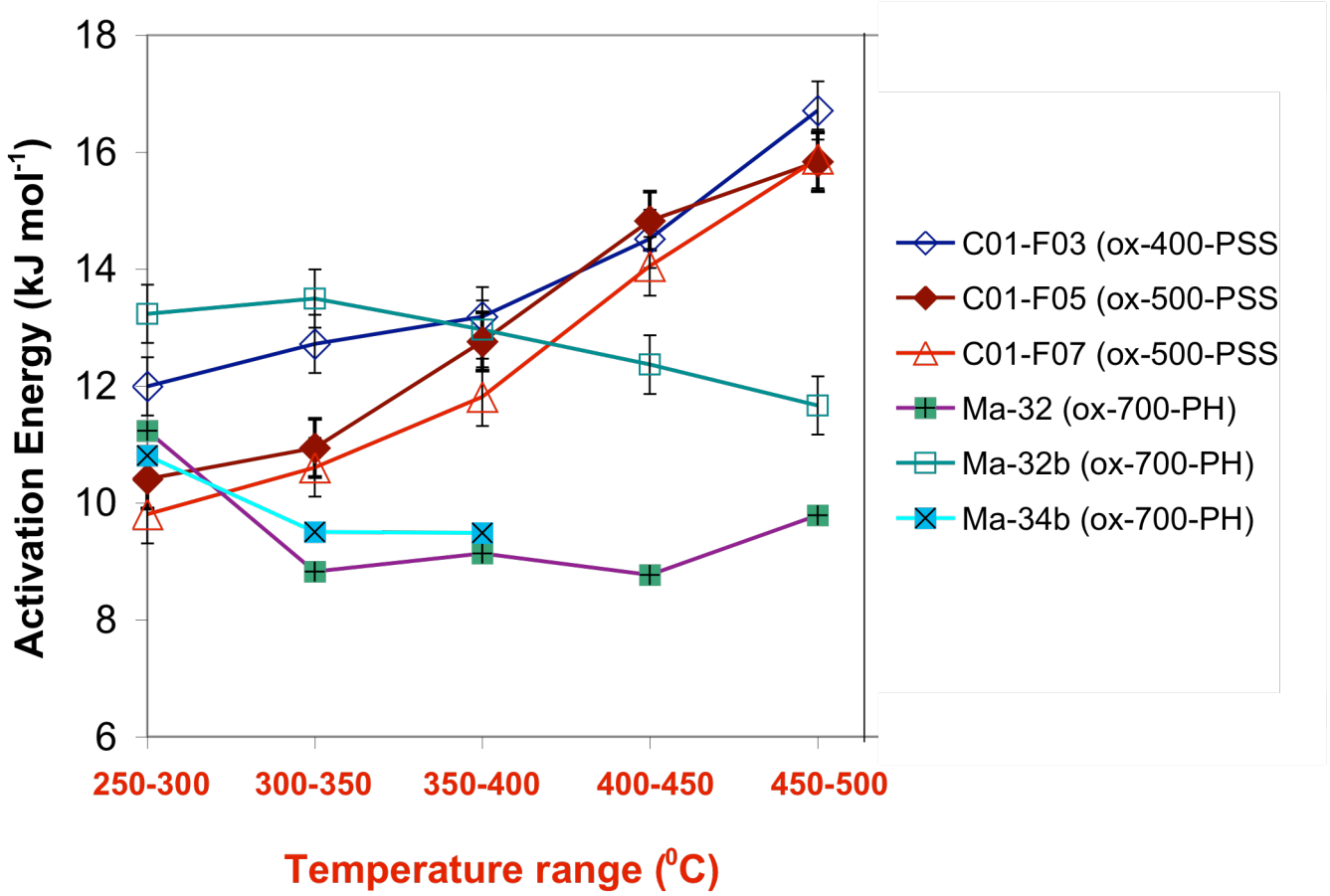

Figure 8-13 Activation energy of H_2 permeation, F_{H2}, determined in several temperature ranges for membranes C01-F03, C01-F05, C01-F07, Ma-32, Ma-32b and Ma-34b

The E_p of C01-F03/5/7 membranes increased with temperature due to the intermetallic diffusion, while the E_p of Ma-32/32b/34b membranes decreased with temperature due to the mass transfer resistance.

It is interesting to note that the activation energies for all membranes determined in the 250°C-350°C temperature range were slightly lower than the average activation energies calculated for Pd foils in Section 4.2.3 and equal to 14.9 $kJmol^{-1}$. As already stated in Section 5.4.5.2 the low activation energies for the H_2 permeation were found at low temperatures in all the composite Pd membranes in this study. The low activation energies for H_2 permeation were due to the H_2 diffusing through Pd grain boundaries (in the nanometers range), leaks (Knudsen and viscous of H_2) and/or in the case where the support represented an important resistance for H_2 permeation as explained in Section 5.4.3.1.

The activation energy of grain boundary diffusion is about 1/2 to 2/3 of the activation energy of lattice diffusion. Therefore, composite Pd membranes having Pd crystallites in the nanometer size were expected to show a lower activation energy for H_2 permeation than the activation energy measured in Pd foils, which had very large Pd crystallites.

All membranes showed high selectivities, especially in the 250-350°C temperature range where defects formation was unlikely. Therefore, the low activation energies for H_2 permeation observed at low temperatures in all composite membranes were not due to leaks. In the case of thick membranes the main resistance to H_2 permeation was "bulk" diffusion, therefore, the mass transfer resistance within the porous support of C01-F03, C01-F05 and C01-F07 did not have any effect on the H_2 permeance. Moreover, their ξ_{250}, defined in Section 5.4.3.2, values were higher than 100. Hence, the small grain sizes

found in all composite Pd membranes affected the activation energy for H_2 permeation at low temperatures.

In summary, intermetallic diffusion led to the increase of the activation energy for H_2 permeation.

8.3.3 Intermetallic diffusion mechanism

In order to clearly understand the diffusion mechanism of elements from the support into the Pd layer, a kinetic approach was undertaken. The rate of the H_2 flux loss of membrane C01-F05 was measured at ΔP=1 bar at different temperatures for long periods of time. The H_2 flux of membrane C01-F05 was stable at 250ºC and 300ºC. However, at 350ºC the H_2 flux of C01-F05 started to decrease. The rate at which the H_2 flux declined increased up to 650ºC. Figure 8-14(a) shows the normalized H_2 flux (H_2 flux divided by the initial H_2 flux) as a function of time for temperatures equal to and lower than 500ºC. Figure 8-14(b) shows the normalized H_2 permeance as a function of time for temperatures higher than 500ºC. The rate at which the H_2 flux declined was calculated by assuming the loss to be linear during the first 50 hr in the low temperature range (T<500ºC). In the high temperature range (T>500ºC) the H_2 flux decline was rapid and measurements were taken within 3 to 10 hr.

Figure 8-15 is the Arrhenius plot of the initial (measured over 3-50 hr) H_2 permeance loss rate for membrane C01-F05. An average activation energy of 25 kJ mol^{-1} can be derived in the 350°C-500ºC temperature range. The activation energy at higher temperatures, 500°C-650ºC was determined to be 168 $kJmol^{-1}$. Due to the high activation energy shown at temperatures higher than 500ºC, the nature of the process with the high activation energy (above 500ºC) was most probably due to the intermetallic diffusion, i.e.

mostly diffusion of Fe from the supports through the lattice of the dense Pd layer and vice versa (Pd diffusing into the lattice of the support).

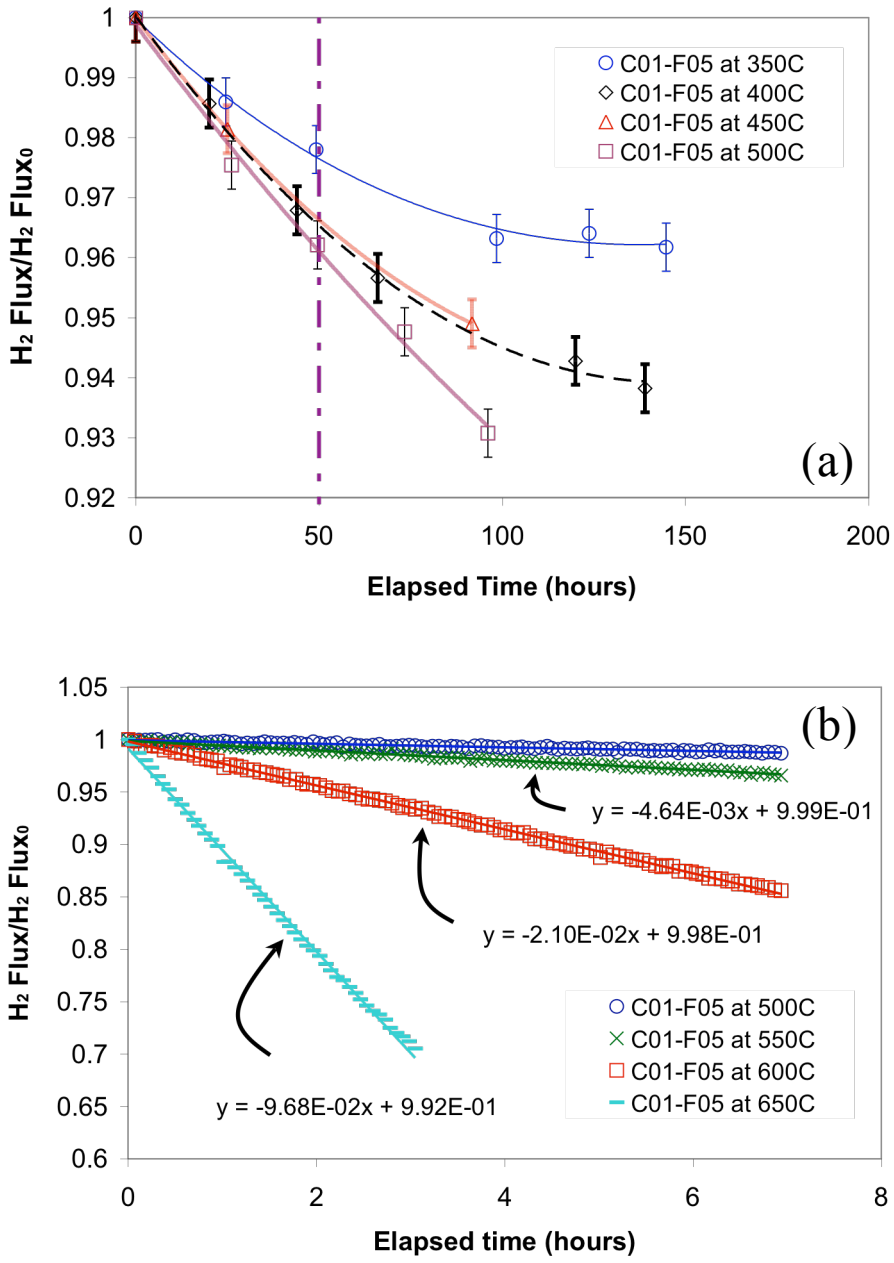

Figure 8-14 H_2 flux loss as a function of time at (a) 350, 400, 450 and 500ºC and (b) 500, 550, 600 and 650ºC for C01-F05 membrane.

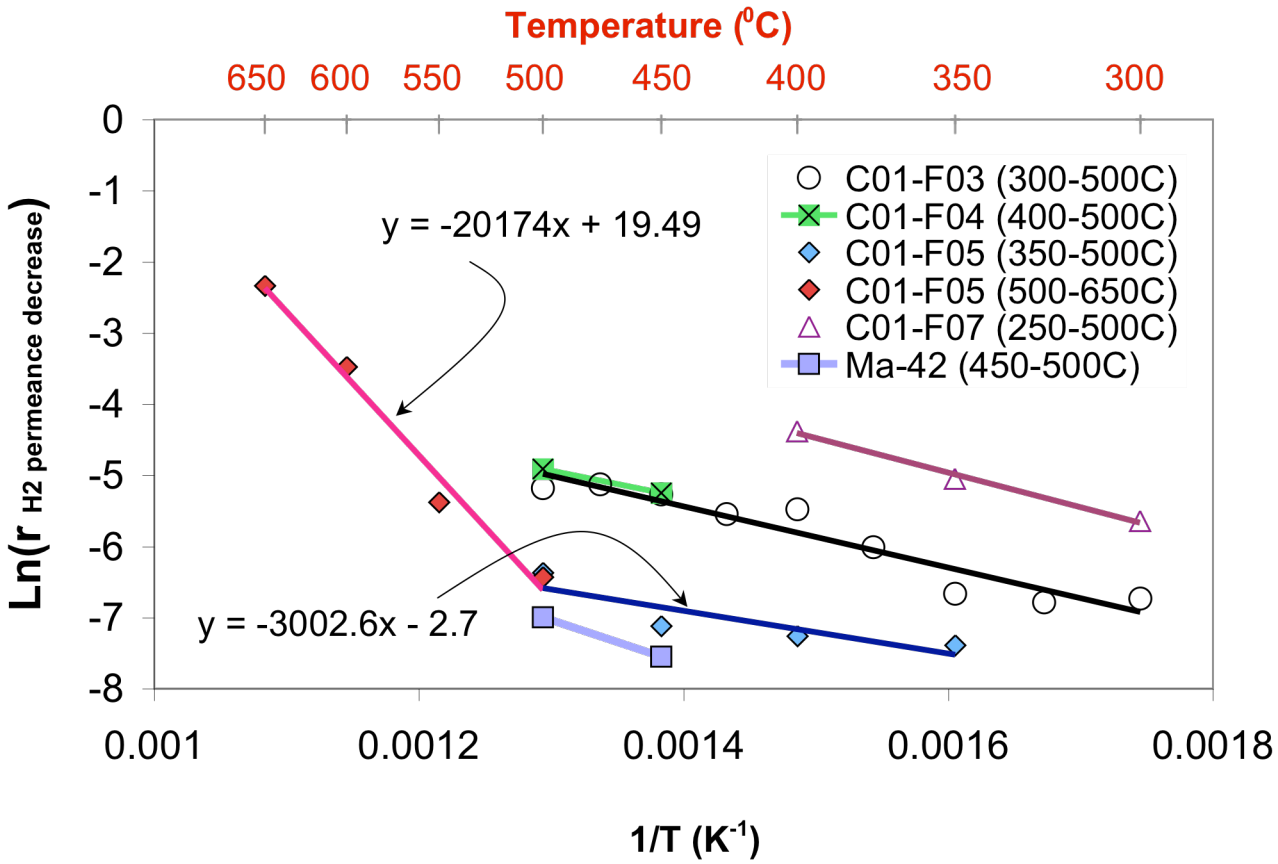

Figure 8-15 Ln(H_2 flux loss rate) as a function of 1/T for C01-F03/4/5/7 and Ma-42 membranes

Indeed, the activation energy for most of the metal-metal lattice diffusion couples is 100-300 kJ mol^{-1}. The initial H_2 permeance loss rate was also measured for C01-F03 (see Figure 8-7(a)), C01-F04 (see Figure 8-7(b)), C01-F07 in the 300-400ºC temperature range (see Figure 8-7(c)) and Ma-42 (see Figure 8-10(b)). The Arrhenius relations of the H_2 permeance loss for membranes C01-F03/4/7 and Ma-42 were also plotted in Figure 8-15. The activation energy for the H_2 permeance decline is listed for all membranes in Table 8-3.

Table 8-3 Activation energy for H_2 flux loss rate for all membranes in Figure 8-15 in the low (T<500ºC) and high (T>500ºC) temperature range

Membrane	Ea below 500ºC (kJ mol^{-1})	Ea above 500ºC (kJ mol^{-1})
C01-F03	35.8	
C01-F04	31.4	
C01-F05	**25**	**167.7**
C01-F07	40.4	
Ma-42	51.3	

The mechanism that took place at lower temperatures (T<500ºC) was significantly different from lattice intermetallic diffusion. The H_2 permeation loss was characterized by a low activation energy in the 300°C-500ºC temperature window for all membranes.

Possible mechanisms with low activation energies are: grain boundary diffusion of Fe, Cr or Ni in between the Pd grains (the activation energy for grain boundary diffusion is usually equal to 10-50 kJ mol^{-1}), Pd grain growth leading to a decrease in H_2 permeation (20-60 kJ mol^{-1}) or reduction of the Fe_2O_3 oxide, formed by the oxidation in air, and subsequent lattice or grain diffusion of Fe into Pd as seen in Section 8.3.1.2.

Figure 8-16 (a) and (b) show a composite (secondary electrons image + backscatter image) micrograph of membrane C01-F03 cross-section at low and high magnification respectively. The sample was slightly etched with diluted aqua regia for 10 seconds in order to generate more contrast and see the microstructure. Pd is slowly etched by diluted aqua regia, however, Fe is readily etched by aqua regia. Hence, the etchant preferentially dissolved the regions in the Pd layer having a high Fe content.

The structure of the outermost part of the Pd layer seen in Figure 8-16 (a) appeared quite uniform while the structure of the innermost part (close to the PSS support) appeared to be grainy. A dashed grey line separates the highly etched part of the Pd layer from the non-etched part of the layer. The fact that the outermost part of the Pd layer was not etched and the innermost part of the Pd layer was etched indicated that the Pd layer was richer in Fe at the vicinity of the support. Therefore, the etchant preferentially dissolved the innermost part of the Pd layer. White arrows in Figure 8-16(a) point at grey regions. The grey color is due to the presence of Fe and it appears that in those regions Fe diffused through the lattice of Pd.

Figure 8-16 (b) is a high magnification micrograph of the region of the Pd layer adjacent to the PSS support. The etchant clearly reveals Pd grains and Pd grain boundaries. The Pd grains had sizes in the order of one micron. Also, since the etchant preferentially removed Fe rich regions it can be concluded that the dark grain boundaries seen in Figure 8-16(b) were rich in Fe. Also, in the backscatter mode, dark regions corresponded to low Z elements, therefore, the Fe concentration along the grain boundaries was very high.

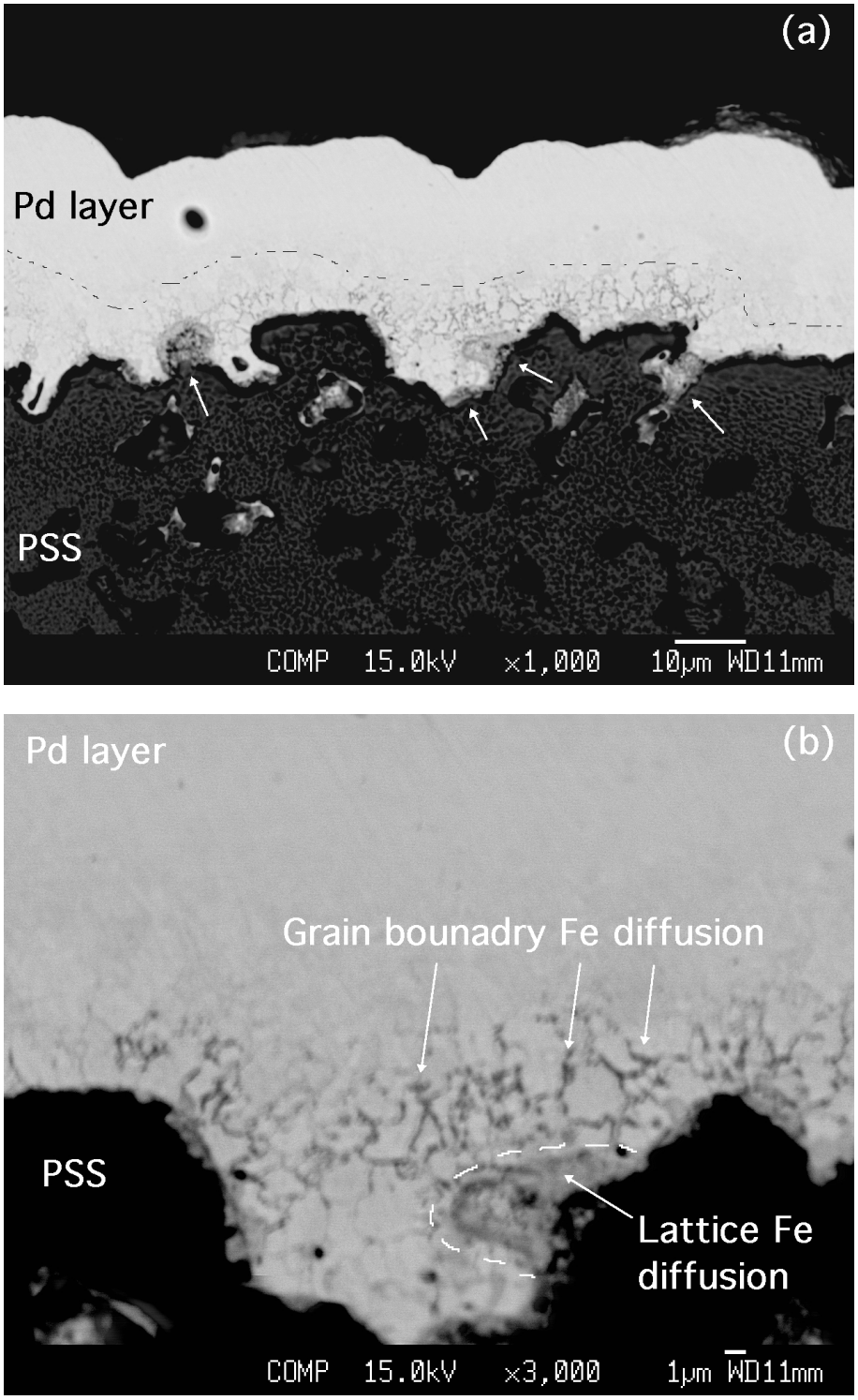

Figure 8-16 Composite image (secondary electron and backscatter of C01-F03 membrane cross-section at (a) low magnification and (b) high magnification of the same area. (Pictures taken by Larry Walker at the html, ORNL, TN)

In fact, the dark grain boundaries indicate that Fe diffused along the grains boundaries rather than through the Pd lattice. Membrane C01-F03 was characterized up to 500ºC, which was the temperature limit for the low activation energy mechanism leading to H_2 flux decline in composite Pd membranes.

In the 250-500ºC interval, the average activation energy for H_2 flux declined equaled 36.8 kJ mol^{-1}, which was consistent with the activation energy for grain boundary diffusion (50kJ mol^{-1}). Hence, most probably, the H_2 flux decline in the low temperature (230-400ºC) range seen in many membranes was due to Fe diffusion through the Pd grain boundaries.

If the presence of Fe within the Pd grain boundaries affected the H_2 permeance, part of the H_2 permeating through the Pd layer must have diffused through the grain boundaries. The activation energy for H_2 permeation in composite Pd membranes was relatively low in the 250-300ºC (see Section 5.4.5.2), which was found to be consistent with H_2 flowing through grain boundaries. Although H_2 diffuses faster in the grain boundaries (Janßen et al., 1997), it is still not known if and how the size of Pd grains affects the H_2 permeance of a composite Pd membrane. The fact that the presence of Fe within the Pd grain boundaries led to H_2 flux decrease attests to the fact that some H_2 diffused through the grain boundaries.

8.4 Conclusions

The oxidation of 316L PSS supports at a temperature lower than 500ºC resulted in a thin Cr_2O_3 layer. When the oxidation temperature was higher than 600ºC, a PSS-thin Cr_2O_3-thick Fe_2O_3 composite structure was formed. Oxidation of PH supports at 900ºC resulted in a thin (several microns) Cr_2O_3 layer. Fe_2O_3 oxide was reduced to metallic Fe,

even when covered with Pd, when the composite Pd-Fe_2O_3-Cr_2O_3-PSS structure was put in H_2 atmosphere at low temperatures. Experimental evidence showed that Cr_2O_3 was not reduced in H_2 atmosphere. PH supports had a stronger tendency to develop thicker Cr_2O_3 layer with no Fe_2O_3 layer at the surface. PH supports showed better properties in preventing intermetallic diffusion. In composite Pd-PSS membranes the intermetallic diffusion led to a decrease of H_2 permeance and an increase of activation energy for H_2 permeation from 10-12 $kJmol^{-1}$ to 16-18 $kjmol^{-1}$ in agreement with the higher activation energies for H_2 permeation shown by Pd-Fe and Pd-Cr alloys. The intermetallic diffusion occurred according to a process with low activation energy (25-50$kJmol^{-1}$) at low temperatures (300°C-500ºC) and a process with a high activation energy (170$kJmol^{-1}$) at high temperatures (500°C-650ºC). The process at high temperatures was demonstrated to be lattice intermetallic diffusion i.e. diffusion of Fe through the lattice of Pd and vice versa. The mechanism involved in the low temperature range was the diffusion of Fe within the Pd grain boundaries.

9 Effects of stress relaxation on the microstructure of fresh Pd thin films

9.1 Introduction

The deposition (by CVD, sputtering, electro and electroless methods) of Pd onto a substrate leads to a composite structure including large amounts of extra energy. Part of the excess energy in these fine grain films is stored as microstrains and surface energy, which is released by the growth of Pd grains at high temperatures. Tschöpe at al. (1992) showed, by calorimetric measurements, that thermal relaxation in freestanding Pt and Pd nanocrystalline samples prepared by inert gas condensation occurred in two stages. The first reduction in the total Gibbs free energy corresponded to the relaxation of internal strains and/or non equilibrium grain boundaries. The second reduction in the total Gibbs free energy corresponded to grain growth. The remnant excess energy in composite structures is due to film/substrate interactions and is stored as "intrinsic" stresses within the film. Intrinsic stresses are also released at high temperatures.

Yet, at high temperatures, new stresses (thermal stresses) appear due to the difference in the thermal expansion coefficient of the metal and the substrate. In addition to thermal stresses, H_2 stresses will appear upon H_2 dissolution within the Pd lattice when the membrane is exposed to H_2 atmosphere. The resulting Pd lattice expansion is constrained by the support, which does not expand, and stresses build up within the film. Thermal

stresses and H_2 stresses are "extrinsic" stresses since they involve parameters outside the boundaries limiting the Pd thin film.

When the appropriate amount of energy is given to the composite system (Pd/substrate + H_2), microstrains, "intrinsic" and "extrinsic" stresses are released inducing changes in the microstructure within the Pd thin film. The changes in microstructure resulting from stress release can cause a composite Pd membrane to fail.

The main objective of the experiments described in this chapter was to investigate the stresses and their release occurring in composite Pd-PH structures. Specifically, the parameters affecting H_2 stresses were studied. In addition, the Pd microstructure and its changes with temperature were correlated with Pd grain growth, microstrains and stress release using diffraction techniques. Finally, the total stress in a composite Pd membrane was calculated for temperature and pressure conditions similar to conditions during membrane characterization.

9.2 Stress theory

9.2.1 Thermal stresses

The coefficients of thermal expansion of Pd and the substrate can be considered as linear functions of temperature within the temperature range (20-600ºC) considered in this study. Hence, the thermal stress (σ_{th}) along the Pd/substrate interface direction to which the thin film is subjected can be approximated by Equation (9-1) (Koch, 1994).

$$\sigma_{th} = \frac{(L_{sub} - L_{film}) \cdot \Delta T \cdot E_{film}}{1 - \nu} \qquad (9\text{-}1)$$

where L_{sub} and L_{film} are the thermal expansion coefficients of the substrate and the thin film respectively, ΔT the increment in temperature from a reference T_0 (T_0 = 20ºC), E_{film}

is Young's modulus and ν the Poisson's ratio of the metal film. According to Equation (9-1), thermal stresses are a linear function of temperature. However, the linear character of thermal stresses with temperature is only observed in the elastic region of the metal. When the thermal stresses exceed the elastic limit of the film they are released by plastic deformations.

9.2.2 H_2 stresses

H_2 stresses are equal to the H_2 strain times Pd Young's modulus (E_{film}) and are given by Equation (9-2)

$$\sigma_H = \varepsilon_H \cdot E_{film} \tag{9-2}$$

where ε_H, is the H_2 strain, which was derived from experimental data reported by (Baranowski et al., 1971). Baranowski et al. (1971) found the volume increase due to interstitial H_2 to be a unique and linear function of n(H/Pd) for many fcc metals and alloys (Pd, Pd-Ir, Pd-Au, Pd-Ag, Pd-Pt and Pd-Cu) regardless of the initial lattice volume and the hydride phase (α or β). The linear volume increase as a function of n(H/Pd) holds for 0<n<0.7 and is shown in Equation (9-3).

$$\Delta V = (a^3 - a_0^3) = 11.56 \cdot n(H/Pd)^{1} \tag{9-3}$$

where ΔV is the volume increase of the lattice cell in $Å^3$, a is the lattice parameter in Å and n(H/Pd) the H_2 content. a_0 is the metal lattice parameter in inert atmosphere. Hence, the increase in the lattice parameter is given by Equation (9-4)

$$a = (11.56 \cdot n(H/Pd) + a_0^3)^{1/3} \tag{9-4}$$

[1] Equation (9-3) was derived by measuring ΔV and n(H/Pd) on the graphic reported by Baranowski et al. (1971)

Performing a Taylor expansion around n(H/Pd)=0 to the first order leads to Equation (9-5)

$$a \approx a_0 + \frac{1}{3} \cdot \frac{11.56}{(a_0^3)^{\frac{2}{3}}} \cdot n(H/Pd) + o(n(H/Pd)) \tag{9-5}$$

Substituting a_0 with the value for Pd (a_0=3.889Å) leads to Equation (9-6)

$$\frac{a - a_0}{a_0} = \frac{1}{3} \cdot 0.19 \cdot n(H/Pd) \tag{9-6}$$

Equation (9-6) was also derived by Eastman et al. (1993), which found the same expression for ε_H vs. n(H/Pd). Hence, the H_2 stress is a linear function of the H_2 content, n(H/Pd) within an elastic region. Stresses will also be released if the elastic limit of the metal is exceeded.

9.2.3 Stresses in a composite Pd/substrate structure

The total stress in a composite Pd/substrate structure is the sum of all stresses. A composite Pd membrane under reaction conditions will be subjected to the total stress (σ_{total}) given by Equation (9-7)

$$\sigma_{total} = \sigma_{th} + \sigma_H = [\frac{(L_{sub} - L_{film}) \cdot \Delta T}{1 - \nu} + \frac{k_H}{3} \cdot n(H/Pd)] \cdot E_{film}$$
$$with \tag{9-7}$$
$$k_h = 0.19 \pm 0.01$$

9.3 Experimental

9.3.1 The preparation of samples

The composite Pd membranes listed in Table 3-2 have a very small thickness compared to the outside diameter (OD) of the cylindrical substrate. Hence, any composite Pd membrane can be considered as a flat thin film and the study of stresses can be undertaken using small flat porous plates covered with a Pd film with the same thickness.

0.2μm grade PSS plates (1.5cm^2, 1mm thick), 0.5μm grade PH plates (1.5cm^2, 1mm thick) and α Al_2O_3 supports (1.5cm^2, 2mm thick) were cleaned according to the procedure described in Section 3.1.1. PSS plates were oxidized at 600ºC for 12 hr. PH plates were oxidized at 900ºC for 12 hr to ensure the formation of a thick Cr_2O_3 layer. Activation and Pd deposition were performed as described in Section 3.1.1. For the bimetallic Cu-Pd-PH samples, Cu was deposited by the electroless plating method using plating baths listed in Table 7-1. The thickness and Cu content of each layer was determined by the gravimetric method. After the metal deposition the Pd-Cu samples were annealed in UHP H_2 atmosphere at 650ºC for 24 hr. Two different Cu-Pd-PH samples were considered for stress calculation: Pd/Cu-40wt% (sample Pd-Cu-4), Pd/Cu-41wt% (sample Pd-Cu-5) and Pd/Cu-13wt% (sample Pd-Cu-6). Samples studied in this chapter are listed in Table 9-1.

Table 9-1 List of samples studied in this chapter.

Sample	Pd thickness, L (μm)	Pressure (bar), atmosphere	Temp. range (ºC)	Experiment description
PH-1a ("fresh")	12	1, He	25-600	Measurement of microstrains, Pd grain size, Pd lattice parameter (a) and stresses as temperature was increased
PH-1b	12	1, He	60-400	Measurement of microstrains and stresses of a heat-treated sample as temperature was increased
PH-1c	12	1.5, H_2	60-500	Measurement of stresses as a function of H_2 concentration in the Pd layer (n=H/Pd)
PH-2a (Pre-treated in He at 400ºC for 1 hr)	12	1, He	60-400	Measurement of stresses in a pre annealed sample. Comparison with PH-1b
PH-3a (Pre-treated in He at 400ºC for 1 hr)	12	1, He	300-500	Measurement of stresses in a pre annealed sample at T>400.
PH-4a (Pre-treated in He at 400ºC for 1 hr)	12	1, He⇆1.5 H_2 5 times switching	50	Effect of atmosphere switching on microstrains and Pd morphology
Al_2O_3-1a ("fresh")	10	1, He	20-500	Microstrains release as a function of temperature in He
Al_2O_3-2a ("fresh")	10	1, H_2	20-500	Microstrains release as a function of temperature in H_2
Al_2O_3-3a/4a/5a/6a ("fresh")	6	1, H_2	300/400/500/600	Pd microstructure after annealing in H_2 for 48 hr at 300 (Al_2O_3-3), 400 (Al_2O_3-4), 500 (Al_2O_3-5) and 600ºC (Al_2O_3-6)
PSS-1a ("fresh")	10	-	-	Pd microstructure of a fresh Pd thin film
PSS-1a ("fresh")	10	1, H_2	500	Pd microstructure after heat-treatment at 500ºC for 48 hr in H_2
Pd-Cu-5	PH	1, He	20-400	Stress measurements in PdCu –PH composite structures (β phase)
Pd-Cu-6	PH	1, He	20-400	Stress measurements in PdCu –PH composite structures (α phase)

The letter following the sample number designates the experiment. For instance, PH-1b stands for "sample PH-1, second experiment". "Fresh" samples are the ones which were only dried at 120ºC overnight before any experiment. Only samples PH-2a, PH-3a and PH-4a were pre-treated in He atmosphere at 400ºC for one hour to release initial microstrains and "intrinsic" stresses present in every "fresh" Pd film.

9.3.2 X-ray diffraction procedures

9.3.2.1 X-ray diffractometers

Diffraction data were collected using Cu-Kα radiation on a PANalytical X'Pert Pro MPD located at the High Temperature Materials Laboratory (HTML) in Oak Ridge National Laboratory (ORNL), Oak Ridge, Tennessee. Parallel-beam optics, consisting of an incident-side graded multilayer parabolic X-ray mirror and a diffracted-side 0.09° parallel-plate flat collimator, were used to alleviate errors associated with sample displacement. Samples were loaded into an Anton Paar XRK900 reaction chamber which allowed the temperature to be varied between 25 and 900 °C and the gas environment to be varied between 1 and 1.5 atm of He or He-4%H_2 (static or flowing).

All experiments listed in Table 9-1 were performed on the PANalytical diffractometer except for Al_2O_3-1a and Al_2O_3-2a. Diffraction data of experiments Al_2O_3-1a and Al_2O_3-2a were collected with the time resolved HTXRD diffractometer already described in section 3.4.2.1.

9.3.2.2 Microstrains-size separation: the Williamson-Hall method

In metals, two types of strains (% of elongation, $(d-d_0)/d_0$) can be encountered: non-uniform strains (microstrains) and uniform strains (macrostrains). Non-uniform strains

are pictured as a distribution of d-spacings and lead to XRD peak broadening while uniform strains, which arise from "intrinsic" and "extrinsic" stresses, lead to XRD peak shifting. This section deals with the determination of microstrains and grain size by XRD peak broadening measurements.

Not only microstrains lead to the broadening of XRD peaks (β_{total}) but also small grain sizes (<100nm), stacking faults and twins, and machine limitations contribute to the broadening of XRD peaks according to Equation (9-8)

$$\beta_{total} = \beta_{size} + \beta_{microstrains} + \beta_{faulting} + \beta_{machine} \quad (9\text{-}8)$$

The density of stacking faults and twins in fcc metals can be determined by measuring the shift of two pairs of reflections such as the (111)-(200) pair and the (222)-(400) pair (Warren and Averbach, 1950). However, several reports showed (by Transmission Electron Microscope (TEM) techniques) that thin films formed with a gentle deposition method such as electrodeposition, cold condensation and sputtering did not include severe defects in the atomic layers. Since electroless deposition involves a gentle chemical process the density of stacking faults and twins was considered to be negligible. Therefore, XRD peak broadening was considered to be only a function of crystallite size, microstrains and machine broadening according to Equation (9-9)

$$\beta_{total} = \beta_{size} + \beta_{microstrains} + \beta_{machine} \quad (9\text{-}9)$$

The contribution of machine broadening ($\beta_{machine}$) to the total peak broadening is readily measured using a standard Si or LaB_6 powder supplied by NIST. Equation (9-9) can then be easily reduced to Equation (9-10)

$$\beta_{total} = \beta_{size} + \beta_{microstrains} \quad (9\text{-}10)$$

Two approaches can then be undertaken to determine crystallite size and microstrains: the use of Williamson-Hall's method (Williamson and Hall, 1953) to separate grain size contribution from microstrains contribution or the use of the Warren-Averbach's method (Warren and Averbach, 1950) to measure simultaneously grain size, grain size distribution and microstrains. Warren-Averbach's method leads to consistent data when several orders of diffraction can be collected for a given set of planes, for instance when reflections (111), (222), (333) etc. are available. In conventional X-ray diffractometers with a Cu radiation source only 2 orders of diffraction are available for Pd making the use of Warren-Averbach's method unworthy. Therefore, microstrains-size separation in Pd deposits was performed using Williamson-Hall's method described in detail by Williamson and Hall (1953).

In Williamson-Hall's method the peak broadening (β), expressed in radians, was assumed to be the sum of a tan(θ) term for the microstrains, and a 1/cos(θ) term for the grain size as given in Equation (9-11)

$$\beta = 4e \cdot \tan(\theta) + \lambda_{Cu} / (t \cdot \cos(\theta)) \qquad (9\text{-}11)$$

where $e \approx (\Delta d/d)_{hkl}$ is an approximate upper limit of the maximum distortion, λ_{Cu} the Cu X-ray wavelength, t the grain size and θ the half peak position. Equation (9-11) can also be written as Equation (9-12)

$$\beta \cdot \cos(\theta) = \frac{\lambda}{t} + 4e \cdot \sin(\theta)$$
$$with \qquad (9\text{-}12)$$
$$e = 1.25 \cdot \sqrt{<\varepsilon^2>}$$

where $\sqrt{<\varepsilon>^2}$ is the root mean square strain (rms), which is a measurement of the Pd lattice distortion. Peak width (β) was determined by fitting every reflection with a Lor-

entz peak function after subtracting the $K\alpha_2$ component and the background. $\beta \cdot \cos(\theta)$ was then plotted as a function of $\sin(\theta)$ for all available reflections: (111), (200), (220), (311), (222), (400), (331) and (420). The plotted data were then fitted with a straight line, where the slope equaled $4e$ and the intercept with the "y" axis equaled λ_{Cu}/t.

9.3.2.3 Stress measurement: lattice strain Vs. $Sin^2\psi$ method

Diffraction data were collected from the (422) peak of Pd between 146 and 157°2θ at ψ tilts of 0, ±28.2, ±42, ±55°psi. The peak position, and ultimately the total stress in the sample, was determined using PANalytical X'Pert Stress by performing a routine which included absorption intensity correction, subtraction of linear background, Lorentz-Polarization correction, stripping of the Cu-$K\alpha_2$ peak, and then determining the peak position using a Lorentz fitting method. The variation of peak positions as a function of ψ tilt were then analyzed using a uniaxial $\sin^2\psi$ plot to determine the macrostrain within the plane of the coating. This macrostrain was converted to a stress using a Young's modulus of 133.52 GPa and a Poisson's ratio of 0.3847. The $\sin^2 \psi$ plot uses the change in peak position at different tilts of ψ to determine the macrostrain to which the sample is subjected within the surface plane of the sample.

9.4 Results and discussion

9.4.1 Microstructure of a fresh electroless plated thin Pd film

9.4.1.1 The morphology of fresh electroless Pd deposits

Figure 9-1 shows top view SEM micrographs of sample PSS-1a. The fresh, i.e. dried at 120ºC overnight, Pd coating had a "cauliflower" type of structure with different features. In the low magnification picture, Figure 9-1(a), shows large (70μm×50μm) agglomerates delimited by pronounced dark boundaries. One of these features, called "super structure" was framed in Figure 9-1(a). Figure 9-1(a) also shows that the "super structure" is characterized by features delimited with dark boundaries (black arrows) or light boundaries (circle). Figure 9-1(b) shows a high magnification SEM micrograph within the "super structure" framed in Figure 9-1(a). The "super structure" included Pd clusters, pointed by arrows in Figure 9-1(b), with sizes in the order of one micron. Pd clusters merged to form larger globules (encircled in Figure 9-1(b)) having sizes within 3-5μm. Most important was the very fine grain structure within a Pd cluster shown by Figure 9-1(c). The surface of a large Pd cluster (framed with a black square in Figure 9-1(c)) was in fact constituted of many small grains, which were considered to be Pd crystallites due to their small size (50-100 nm). The black arrow in Figure 9-1(c) points to a group of Pd crystallites.

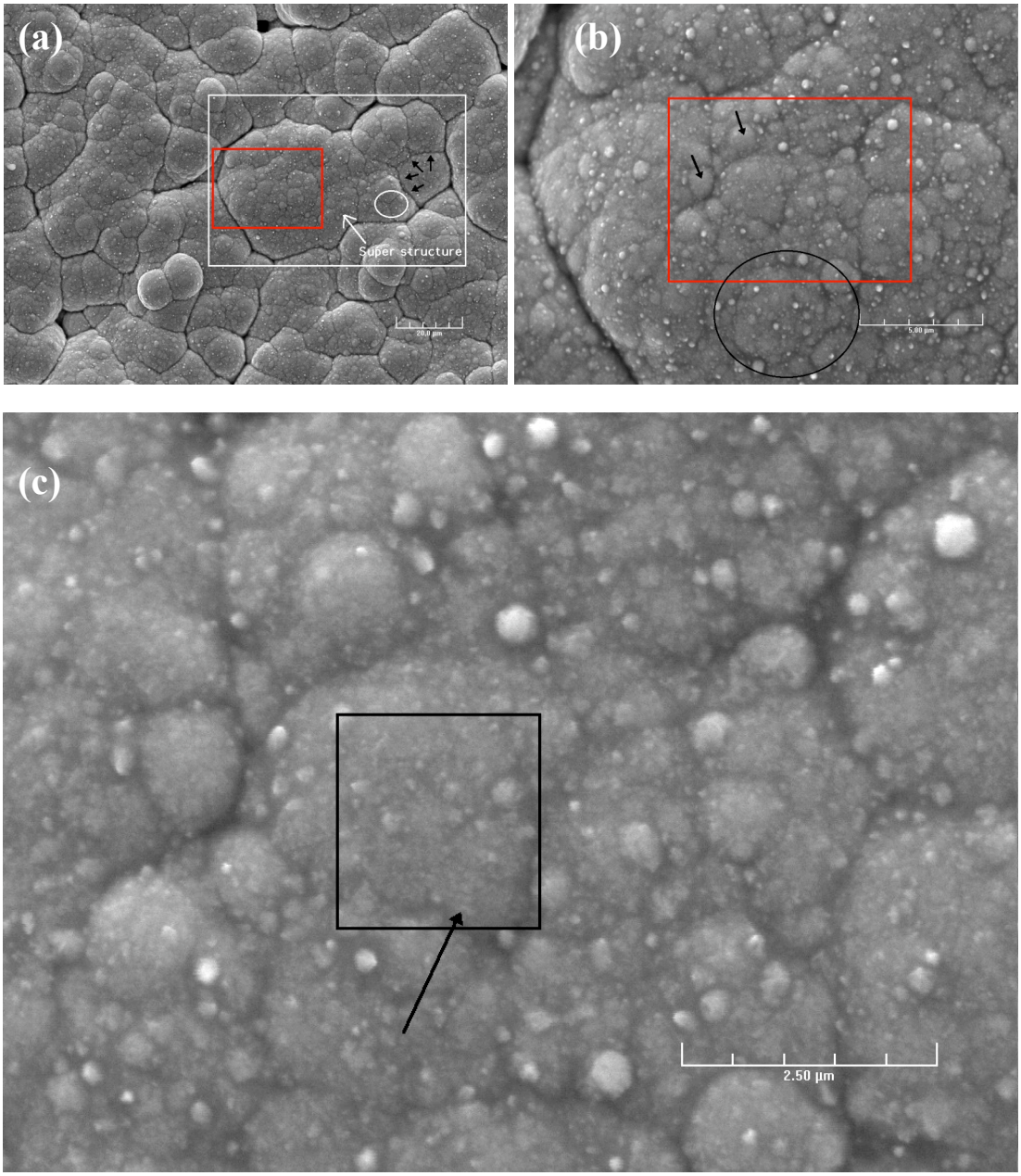

Figure 9-1 Surface structure of sample PSS-1a. (a) mag: 1kX, Pd "super structure" (b) mag: 5kX, Pd clusters and (c) mag: 10kX domains of crystallites in a Pd clusters. Red squares represent the area of the next picture.

Hence, fresh Pd deposits were characterized by a "cauliflower" structure with large structures delimited by pronounced boundaries, characterized by agglomerates of Pd clusters, which consisted of thousands of Pd crystallites having 50-100nm in diameter.

9.4.1.2 Initial Pd grain size, microstrains and "intrinsic" stresses

Using only Scherrer equation ($t_{hkl}=0.9\lambda/\beta\cos\theta$) on the (111) and (222) reflections led to t_{222} higher than t_{111} by a factor of two, which was also reported on Pd black when microstrains were not accounted for (Bogdanov et al., 1984). Hence, microstrains were also present in electroless Pd deposits. Therefore, the initial microstrains present in the fresh Pd film and initial Pd grain size were estimated by performing a strain-size separation on sample PH-1a using Williamson-Hall plot, shown in Figure 9-2(a). Initial rms equaled $2.9\cdot10^{-3}$ and initial Pd grain size equaled 97nm, which was in agreement with Pd grain size measured on SEM micrographs. It has been shown in the case of nanocrystalline Pd that microstrains decreased from 0.5% to 0.05% as crystallite size increased from 10nm to 100 nm (Sanders et al., 1995; Weissmuller et al., 1995). Based on Sander's and Weissmuller's findings it was hypothesized that since microstrains decreased with increasing grain size, microstrains were confined to small crystallites and/or shells adjacent to the interfaces within the crystallites (Reimann and Wurschum, 1997). The initial microstrains measured in PH-1a (0.29%) appeared to be higher than the values reported in the literature (0.05%) when the Pd grain size measured with SEM and XRD was around 100nm.

Figure 9-2(a) also shows that the (111) and the (222) reflections were considerably sharper than the (200) and (400) reflections, which was also noted by other researchers (Bogdanov et al., 1984; Reimann and Wurschum, 1997). Indeed, Reimann and Wur-

schum, (1997) and Bogdanov et al. (1984) also reported this unexpected anisotropic variation of β cos(θ) with respect to the reflection.

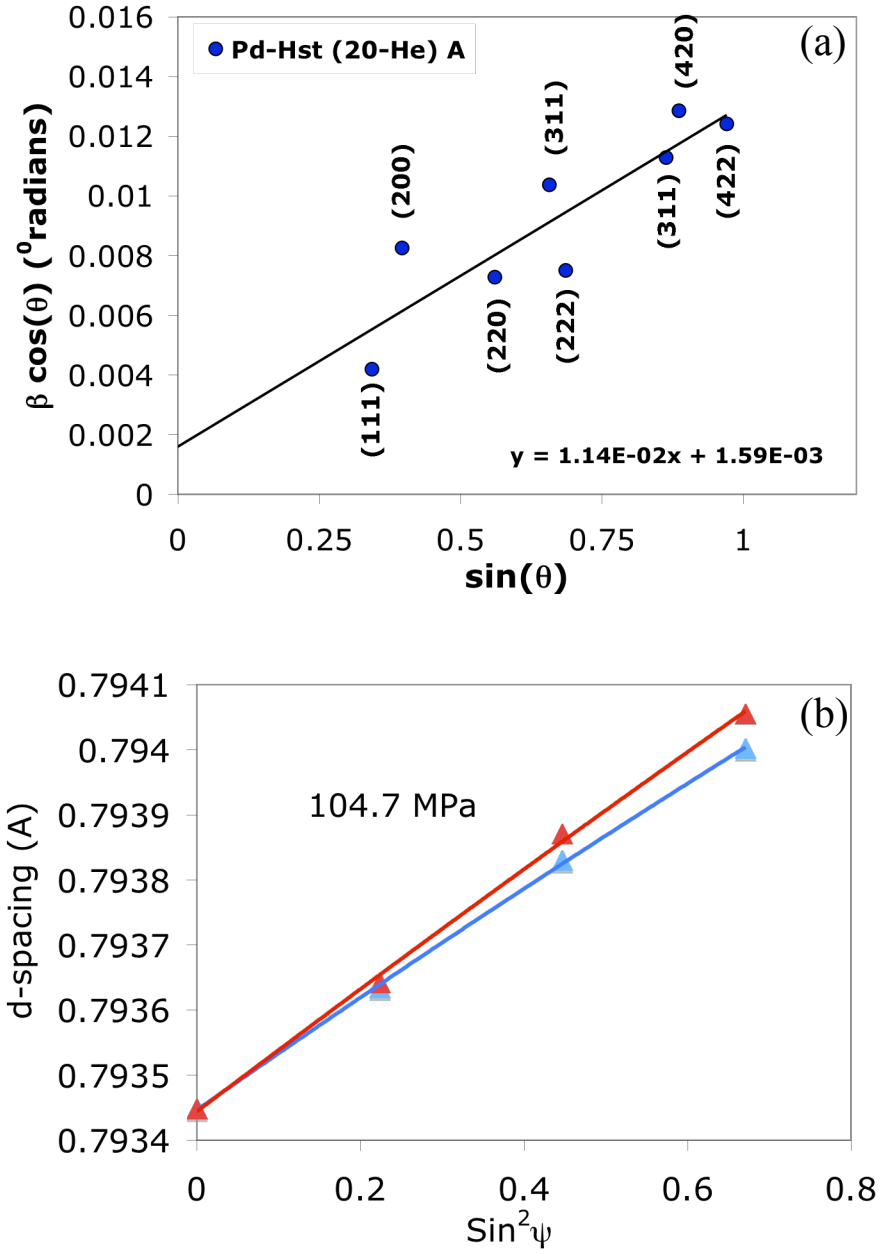

Figure 9-2 (a) Williamson-Hall plot of PH-1a sample. (b) Strain-sin$^2\psi$ plot for the same Pd coating. Data taken at 20°C.

The anisotropic variation of $\beta \cos(\theta)$ indicated that either grains were longer along the [111] direction than along the [200] direction or that a high density of stacking faults and twins was present along the [200] direction. According to Reimann and Wurschum, (1997) neither the high density faults nor the anisotropic grain shape hypothesis were compatible with Pd crystallite shape from high resolution TEM investigations. Hence, they postulated that the large variations of $\beta \cdot \cos(\theta)$ with respect to the peak reflection were due to the anisotropic elasticity factor of Pd. They plotted $\beta \cdot \cos(\theta)$ as a function of $\sin(\theta)/E_{hkl}$ (E_{hkl} is the Pd Young's modulus for the hkl reflection) and found a straight line. Therefore, the anisotropy seen in Figure 9-2(a) was due to the anisotropy in Pd elasticity.

The initial "intrinsic" stresses of the fresh PH-1a sample were determined using d-$\sin^2\psi$ experimental data plotted in Figure 9-2(b). An initial tensile stress of 104.7±9 MPa was measured along the y direction. The tensile nature of the initial stress can be explained by the high melting point of Pd and the low temperature (60ºC) at which the deposition was carried out.

Indeed, during Volmer-Weber growth, the nature of the initial "intrinsic" stresses depends on the mobility of the metal being deposited. The mobility of the metal depends on its melting point (the concept of Tamman temperature) and the temperature of the substrate at which the deposition is performed. Therefore, the initial "intrinsic" stress of a fresh coating depends on the $T_{substrate}/T_{melt}$ ratio and, given a substrate temperature, metals are categorized in low-mobility ($T/T_m<0.2$) and high mobility ($T/T_m>0.2$) metals (Koch, 1994). Low mobility metals show tensile stresses during deposition. Moreover, the tensile stress increased linearly with film thickness. These stresses are mostly located at the grain

boundaries. In the particular case of Pd deposited at a temperature of 60ºC, the T/T_m ratio (333K/1823K) equaled 0.18, so that Pd can be considered as a low mobility metal, which was in agreement with the tensile nature of the initial stress of the coating.

Grain boundaries are known to be sources of intrinsic stresses and according to Hoffman "*the inter-atomic forces at the grain boundaries tend to close any existing gap, with the result that the neighboring crystallites are strained in tension*"[1]. Weissmuller and Lemier, (1994) also reported that grain boundary stress in Pd-H tended to expand the crystal lattice.

[1] Citation from Koch (1994).

9.4.2 Pd microstructure changes with temperature

9.4.2.1 Morphology changes with temperature

Figure 9-3(a), (c) and (e) show the Pd morphology of PSS-1a at 1000X, 5000X and 10000X respectively. Figure 9-3(b), (d) and (f) show the Pd morphology, at the same magnifications, of a thin Pd film after heat-treatment at 500ºC for 48 hr in H_2 (PSS-2a). Figure 9-3(b) shows that after treatment at 500ºC the boundaries between "super structures" were less pronounced than the same boundaries in the fresh sample. The change in appearance of pronounced boundaries between large structures can be better seen in Figure 9-3(d). The black arrows in Figure 9-3(d) point to boundaries between large structures, where some sintering can be clearly seen. Figure 9-3(d) also shows that Pd clusters, and Pd grains inside "super structures" sintered after heat-treatment leading to a relatively uniform microstructure within each "super structure" having Pd grains as large as 0.5-1μm. The large Pd grains formed upon heating can be clearly seen in Figure 9-3(f) pointed out by the arrows.

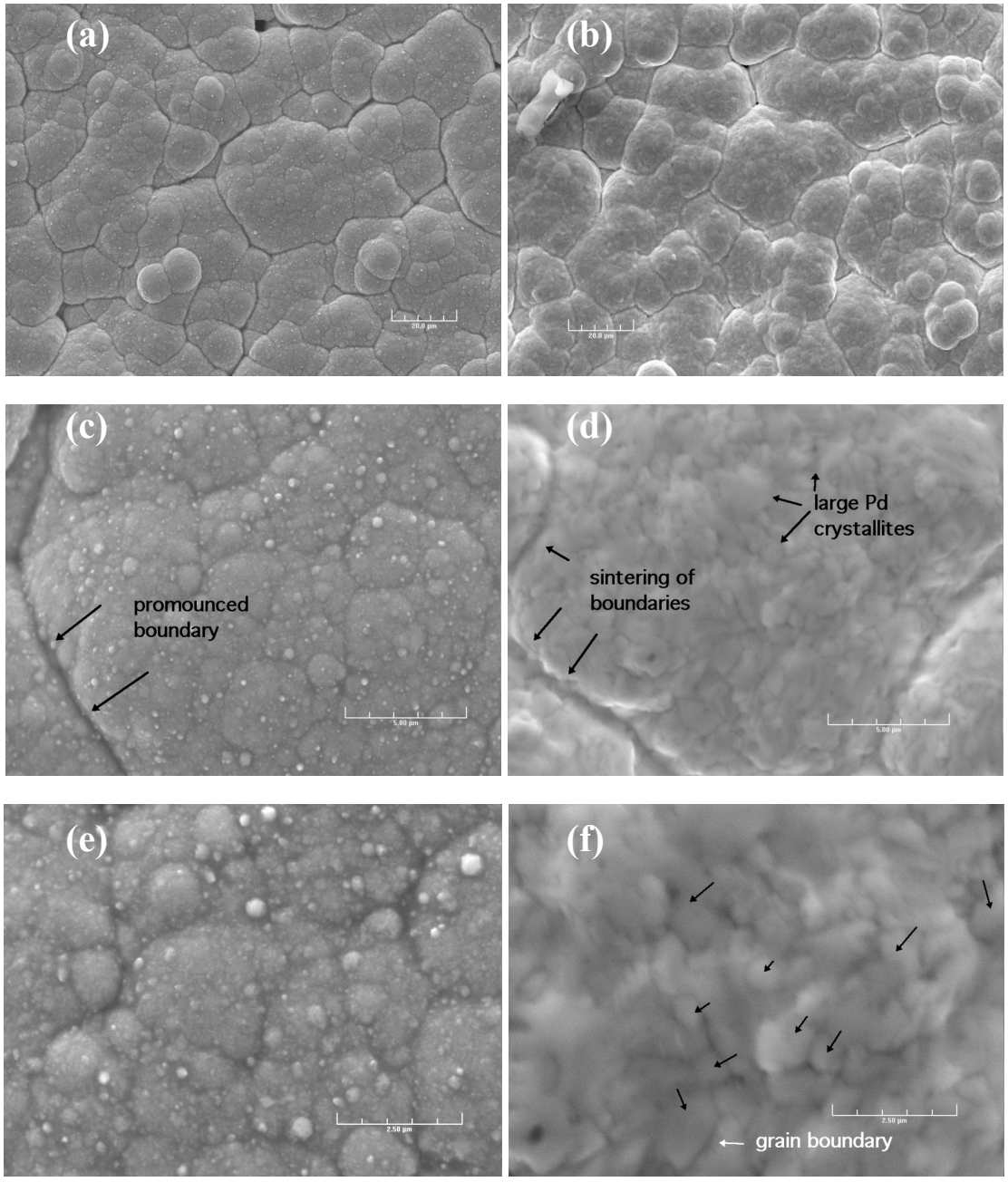

Figure 9-3 surface pictures of PSS-1a (a) mag.: 1kX, (c) mag.: 5kX and (e) mag.: 10kX. Surface microstructure of PSS-2a (upon heating at 500ºC for 48 hr) is shown at (b) mag.: 1kX, (d) mag.: 5kX and (f) mag.: 5kX. mag1KX, scale bar: 20 μm, mag 5KX scale bar: 5 μm and mag 10KX scale bar:2.5 μm.

Pd layers (6μm thick) were deposited on α-Al_2O_3 supports and annealed at different temperatures (300, 400, 500 and 600ºC) for 48 hr in H_2. The morphology of the annealed Pd layers (samples Al_2O_3-3a/4a/5a/6a), studied by SEM, is shown in Figure 9-4(a)(b)(c) and (d) respectively. No significant changes were noticed in the shape of clusters for the samples annealed at 300 and 400ºC. Indeed, the clusters in both samples had similar size and sharp edges. Pd clusters in the 500ºC annealed sample did not show sharp edges indicating that Pd grain and Pd cluster sintering process started at a temperature between 400 and 500ºC. At 600ºC Pd clusters were hardly discerned, instead, a distinguished uniform Pd layer with Pd grains as large as 5μm were present.

9.4.2.2 Grain growth and microstrains release with temperature

Figure 9-5 shows the Williamson-Hall plot of sample PH-1a annealed in He atmosphere at different temperatures (400, 500 and 600ºC). Experimental data obtained at 20ºC, "(20-He) A", was also added for comparison purposes. At high temperatures (>400ºC), plotting $\beta \cdot \cos(\theta)$ as a function of $\sin(\theta)$ led to a straight line having a very low slope value (rms=$3.2 \cdot 10^{-4}$) and passing through the origin indicating that microstrains, initially present in the Pd deposit, were released (0.03% at high temp.) and that grains grew very large. Performing the microstrains-size separation at room temperature after heat-treatment, "(20-He) B" filled circles, led to the same results found at high temperatures. Therefore, initial microstrains were irreversibly released after treatment in He atmosphere at 400ºC for one hour.

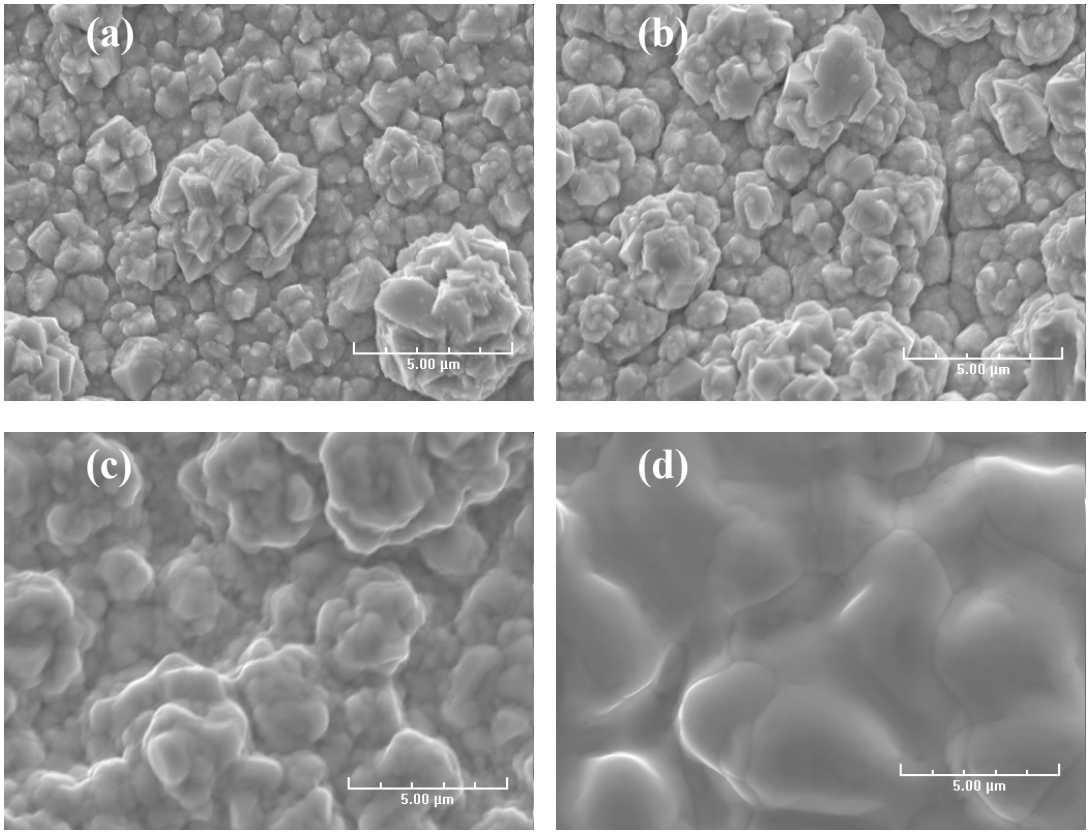

Figure 9-4 Pd-α -Al_2O_3 deposits annealed in H_2 at (a) 300 (Al_2O_3-3a), (b) 400 (Al_2O_3-4a), (c) 500 (Al_2O_3-5a) and (d) 600ºC (Al_2O_3-6a) for 48 hr (Mag 5000)

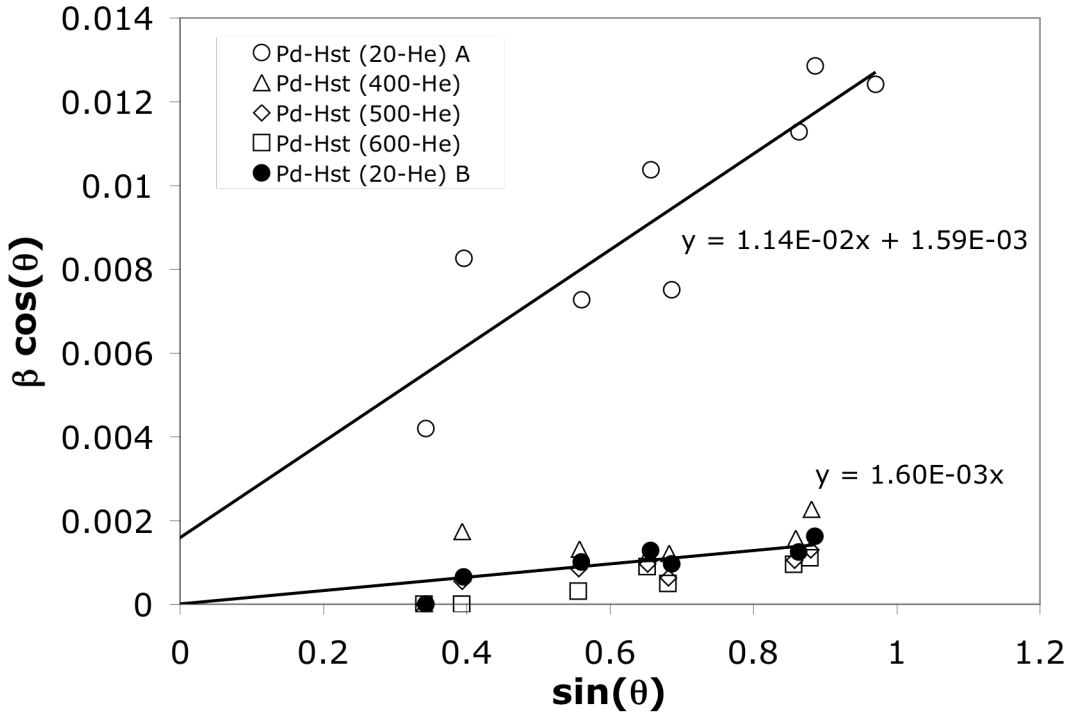

Figure 9-5 Strain-size separation for PH-1a at different temperatures. Letters A and B correspond to the scan at room temperature before high temperatures (A) and after high temperatures exposure treatment (B).

Since Pd grains were initially large (100nm) peak broadening was primarily due to microstrains in the Pd lattice. The peak broadening (FWHM or β) of the (111), (200), (220), (311) and the (222) reflections was followed as a function of temperature in He atmosphere for sample Al_2O_3-1a (pure Pd thin film). The experiment consisted of collecting x-ray data for all reflections while the temperature was increased at a rate of 3ºC/min. Figure 9-6 shows that the FWHM of all reflection, except the (111) reflection, reached the machine-broadening limit (0.1°) at temperatures higher than 350ºC, that is, above 350ºC in He atmosphere, all microstrains initially present in the thin film were released, which was in agreement with experiment PH-1a.

Microstrains release in H_2 atmosphere is shown in Figure 9-7 as a function of time at 200, 300, 400 and 500ºC for sample Al_2O_3-2a (pure Pd thin film). The experiment consisted of collecting x-ray data for all reflections as a function of time at a given temperature. The temperature was increased by 100ºC increments. In H_2 atmosphere, Pd reflection peaks (except the (111) reflection) were still broad at 400ºC, however, at 500ºC peaks sharpened readily and the FWHM of all peaks reached the machine broadening limit. Moreover, at each temperature equal to or below 400ºC, some microstrains release occurred in the first 60 minutes after which strains reached a constant value. Therefore, it appeared that microstrains release mechanism took place at a faster rate in He atmosphere than in H_2 atmosphere, which was due to the adsorbed H atoms along the grain boundaries.

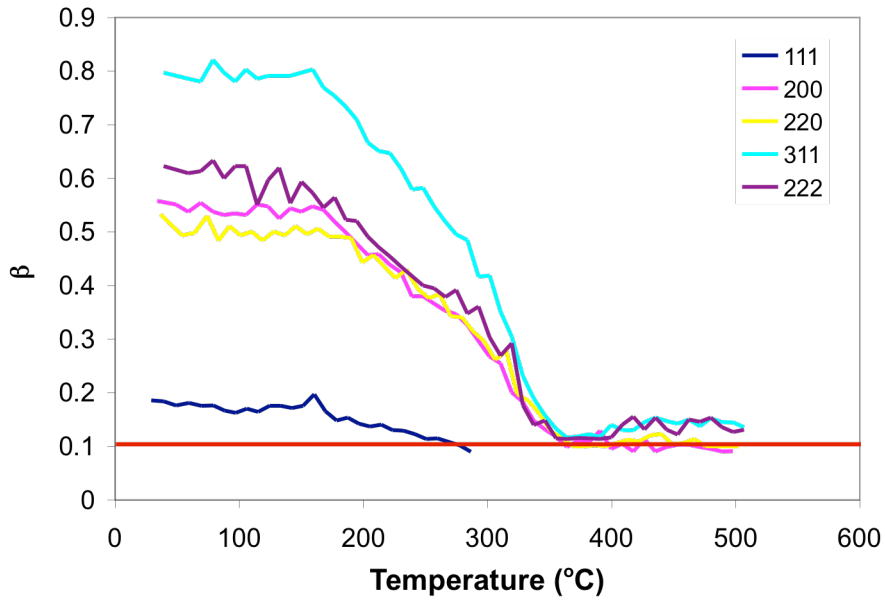

Figure 9-6 Microstrains release in He atmosphere in sample Al_2O_3-1a as a function of temperature. Heating rate 3°C/min.

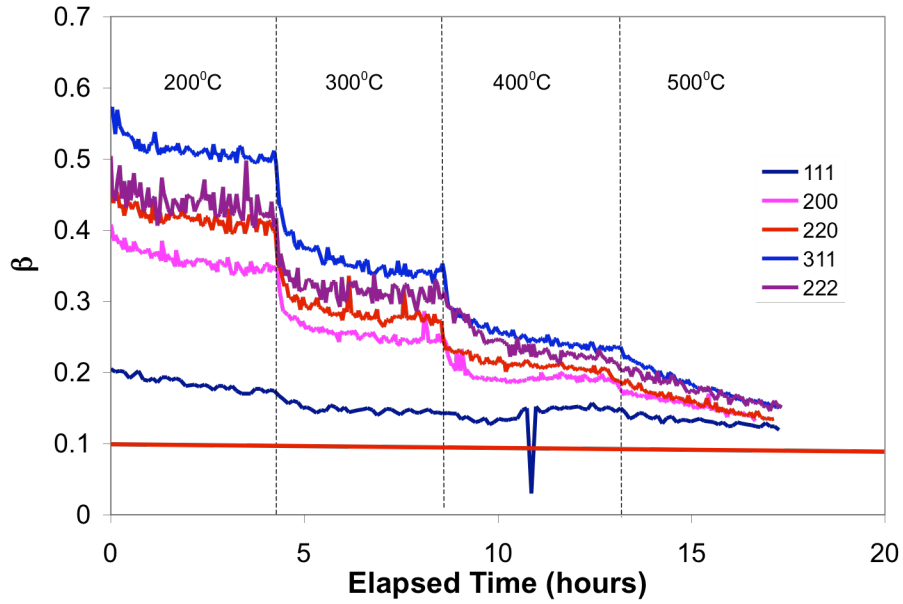

Figure 9-7 Microstrains release as a function time for sample Al_2O_3-2a in H_2 atmosphere at 200, 300, 400 and 500°C.

The study of Pd grain growth was not possible since their size was already large (100nm) at the "fresh" stage. However, according to Tschöpe et al. (1992), grain growth occurs after microstrains are released, therefore, Pd grain growth in electroless plated films started to occur at temperatures ranging between 350-400ºC depending on the atmosphere. The hypothesis that Pd grains started to grow at T>350-400ºC can be substantiated by the fact that, as seen in Figure 9-4(b), no significant structure modification occurred at 400ºC in H_2 atmosphere.

9.4.2.3 "Intrinsic" and "extrinsic" stresses release with temperature

Upon heating sample PH-1a, "extrinsic" thermal stresses were added to the already existing "intrinsic" stress. The total stress in sample PH-1a was measured at several temperatures (250, 400, 500 and 600ºC) in He atmosphere. Figure 9-8 shows the total stress to which the thin Pd film was subjected as a function of temperature. Initially, before any treatment at high temperatures, the film was under a tensile stress of 104.7 MPa. At temperatures higher than 250ºC, the thin film was subjected to compressive stresses. The magnitude of the compressive stresses was equal to 25 MPa at 250ºC and 400ºC and 13MPa at 500ºC and 600ºC as seen in Figure 9-8. When cooled to room temperature (25°C), after the high temperature treatment, the thin film was back under a tensile stress although the magnitude of the tensile stress was lower (41 MPa) than the value at the "fresh" state (104.7 MPa).

The difference in the tensile stress before and after exposure to high temperatures indicated that the initial "intrinsic" stress was released. In fact, stress release started at a temperature between 250 and 400ºC since the film was under the same compressive stress at those two temperatures.

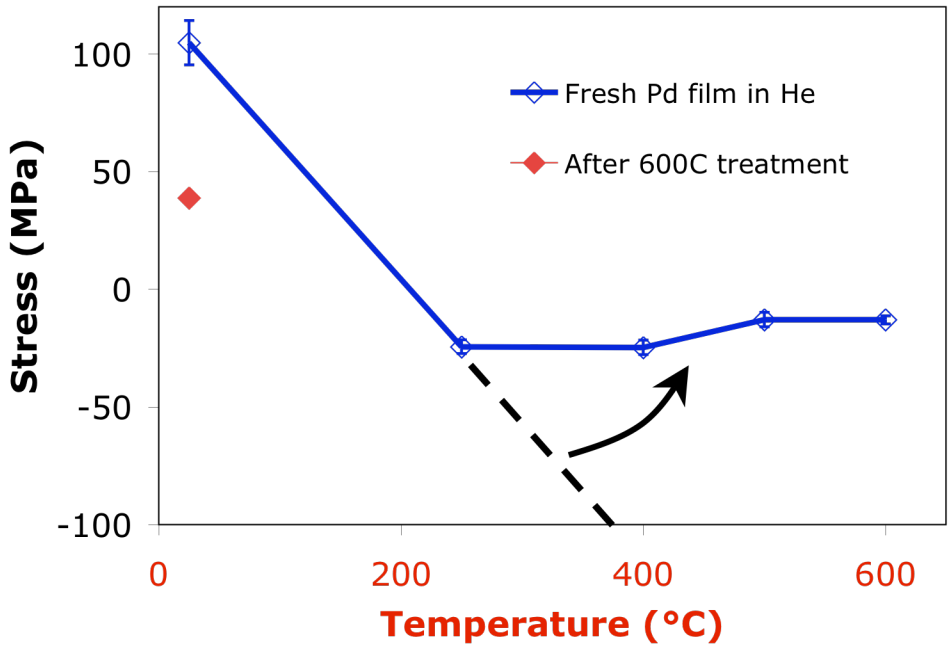

Figure 9-8 Stress release in sample PH-1a as a function of temperature

Further stress release occurred at 500ºC since the film was under a less compressive stress than at 400ºC. The stress-temperature plot seen in Figure 9-8 was characteristic of the first high temperature treatment of the "fresh" PH-1a sample where the initial stresses were released by dislocations in the metal.

The stress-temperature plot during the temperature treatment of sample PH-1b is shown in Figure 9-9 (diamonds). During the heat-treatment of sample PH-1b, the stress was found to be, within the temperature-range studied (60-400ºC), a linear function of the temperature as predicted by Equation (9-1). The negative slope indicated that the thin Pd film expanded more than the PH substrate by $1.25 \cdot 10^{-6}$ m/(m K). Since, the thermal stress was a linear function of temperature, the elastic region for a Pd sample annealed at 600ºC was found to be 60-400ºC.

In order to better understand the release of stresses that occurred during the heat-treatment of sample PH-1a, sample PH-2a was pre-treated in He atmosphere at 400ºC for one hour to release the initial microstrains and the initial stress present in the film. The total stress of sample PH-2a was then measured at 60, 200 and 400ºC and is also plotted in Figure 9-9 (squares). As seen in Figure 9-9, the total stress-temperature function of PH-2a corresponded to the same stress-temperature function of sample PH-1b, which indicated that the heat-treatment at 400ºC was sufficient to release the initial tensile stress. Furthermore, the elastic region of a thin Pd film annealed at 400ºC was also found to be 60-400ºC. Sample PH-3a, also pre-treated at 400ºC for one hour in He, was studied in order to elucidate the thermal stress at temperatures higher than 400ºC.

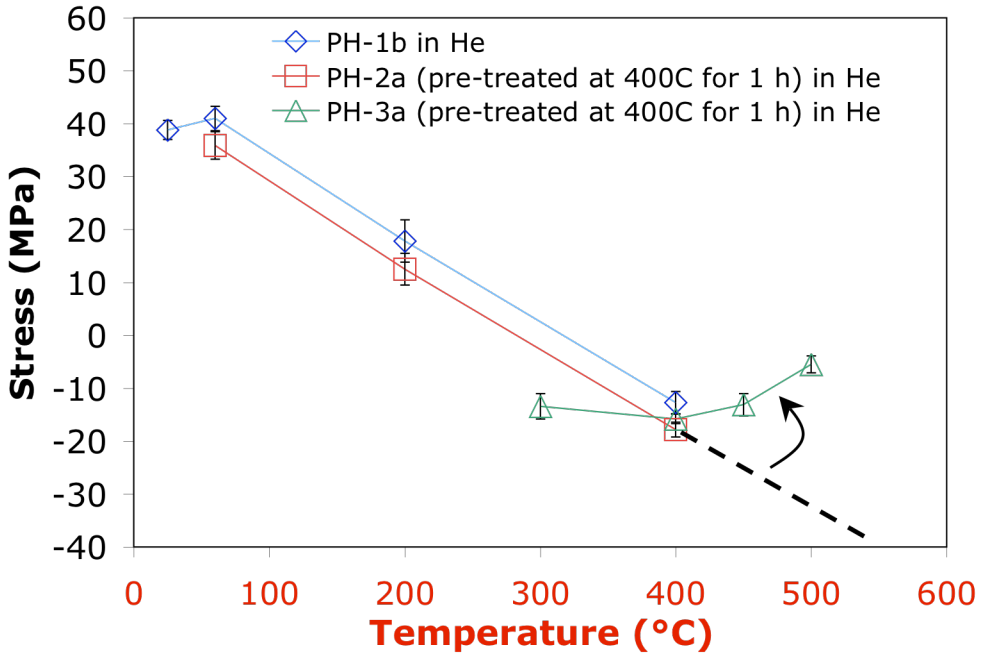

Figure 9-9 Stress in thin Pd films as a function of temperature. (◇) PH-1b, (□) PH-2a and (△) PH-3a.

Figure 9-9 shows the thermal stress vs. temperature behavior shown by sample PH-3a (triangles) in the 350-500ºC temperature range. The stress at 350 and 400ºC was similar to the stress shown by samples PH-1b and PH-2a at the same temperatures.

However, at 450ºC thermal stress started to relax and at 500ºC compressive stresses were totally released (-2.7MPa) as a result of plastic deformations. Hence, the elastic region of thin Pd films annealed at 400ºC was found to be 20-400ºC and thermal stress within the determined elastic region were given by Equation (9-13) with T in ºC.

$$\sigma_{th} = -0.157 \cdot T + 44.8 \qquad (9\text{-}13)$$

It is interesting to note that if a "fresh" composite Pd-PH structure was taken and pre-treated at 400ºC for one hour in He, its initial microstrains and initial stress were relaxed although its general microstructure was hardly affected (see Figure 9-4 (b)). Moreover, plastic deformations occurred at temperatures higher than 400ºC that also corresponded to temperatures at which significant changes in microstructure were observed as seen in Figure 9-4 (c). The decrease of microstrains at elevated temperatures with minor crystallite growth was also reported in earlier works (Reimann and Wurschum, 1997).

9.4.3 "Extrinsic" stresses upon H_2 loading

9.4.3.1 The determination of n (H/Pd) at T and P

The amount of H_2 absorbed, n (H/Pd), can be determined from Pd lattice parameter using Equation (9-6). However, the use of Equation (9-6) gives n(H/Pd) only up to ± 0.05. All membranes throughout this study were characterized at a maximum H_2 pressure of 5 bar and a minimum temperature of 250ºC. Figure 9-10 shows in blue the pressure/n(H/Pd) region where all membranes were characterized.

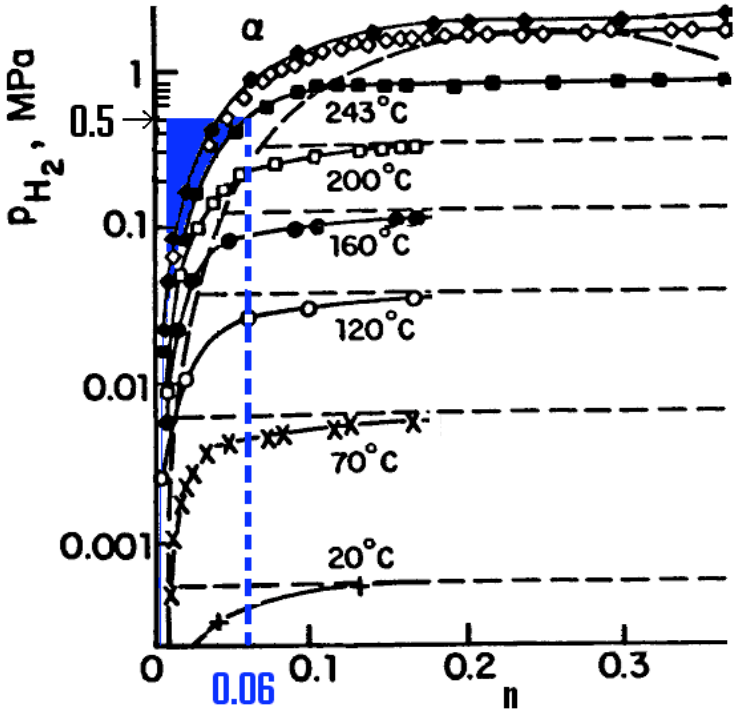

Figure 9-10 Pd-H system in the high pressure and moderate temperature region. The blue dashed line represents the H_2 content (mol H/mol Pd) at 243ºC and an absolute pressure of 5 bar.

The maximum H_2 content, n(H/Pd), was reached at the highest pressure (5 bar) and the lowest temperature (250ºC) and estimated to be 0.06. Hence, any experiment performed with the goal of understanding the influence of H_2 concentration on H_2 stress was carried out at temperature and pressure conditions so that n(H/Pd) would lie within the region of interest (0-0.06). Therefore, due to low accuracy of Equation (9-6) (±0.05) and the narrow window of n(H/Pd) at which the experiments in this section were carried out, the use of Equation (9-6) to determine n(H/Pd) appeared inappropriate.

The H_2 content, n(H/Pd), had to be determined from temperature and pressure values using Sieverts' constant, which relates $P^{0.5}$ to n(H/Pd) by the following linear equation

$$P_{H_2}^{1/2} = K(T) \cdot n(H/Pd) \qquad (9\text{-}14)$$

where K is the Sieverts' constant in $Pa^{0.5}$ or $Torr^{0.5}$ determined from the H_2 absorption isotherm at the temperature T. K was determined for temperatures ranging from 0 to 300ºC from experimental data (H_2 pressure, n(H/Pd)) reported by Gillespie and Hall (1926), Gillespie and Galstaun (1936) and Wicke and Nersnt (1964). The experimental data reported by Gillespie and Hall (1926) and Gillespie and Galstaun (1936) were available in a tabular form so that H_2 absorption isotherms were plotted at 0, 30, 80, 160, 180, 200, 250, 290 and 300ºC and K was determined by considering only the linear portion of $P^{0.5}$ vs. n(H/Pd) as shown in Figure 9-11 for the 30 and 160ºC isotherms. Data of Wicke and Nersnt (1964) were only available in a high quality graph, and K was determined with graphical methods for the 0, 30, 50, 60 and 75ºC isotherms. The natural logarithm of K was then plotted as a function of the inverse temperature for all K values. The resulting Arrhenius type of plot is shown in Figure 9-12. Hence, the H_2 content, n(H/Pd), was determined from the following equation

$$n(H/Pd) = \frac{P^{0.5}}{Exp(\frac{-1114.2}{T} + 9.3)} \qquad (9\text{-}15)$$

with P in torr and T in K. Equation (9-15) in only valid in the stability domain of the α phase and, for a given temperature, in a pressure range where $P^{0.5}$ is a linear function of n(H/Pd).

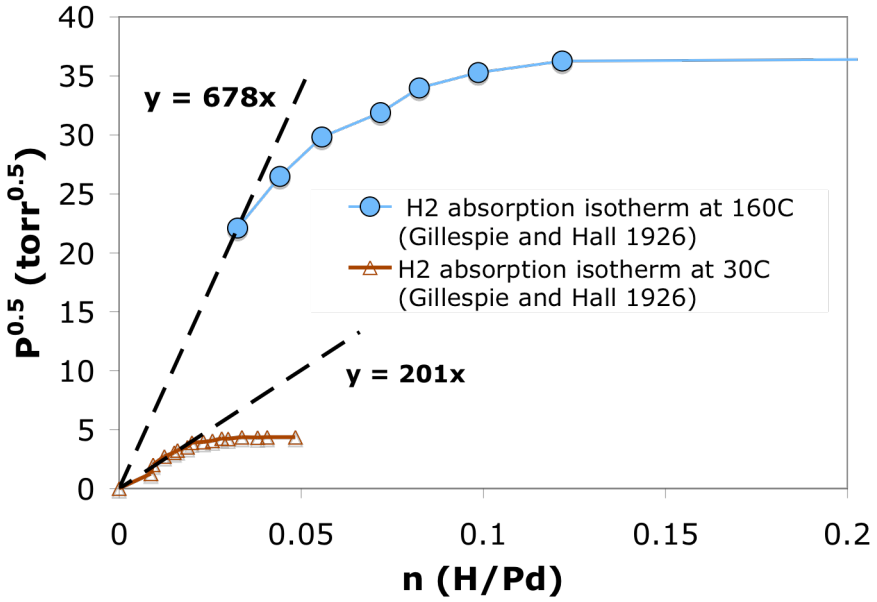

Figure 9-11 $P^{0.5}$ vs. n(H/Pd) at 30 and 160°C. Experimental data from (Gillespie and Hall, 1926).

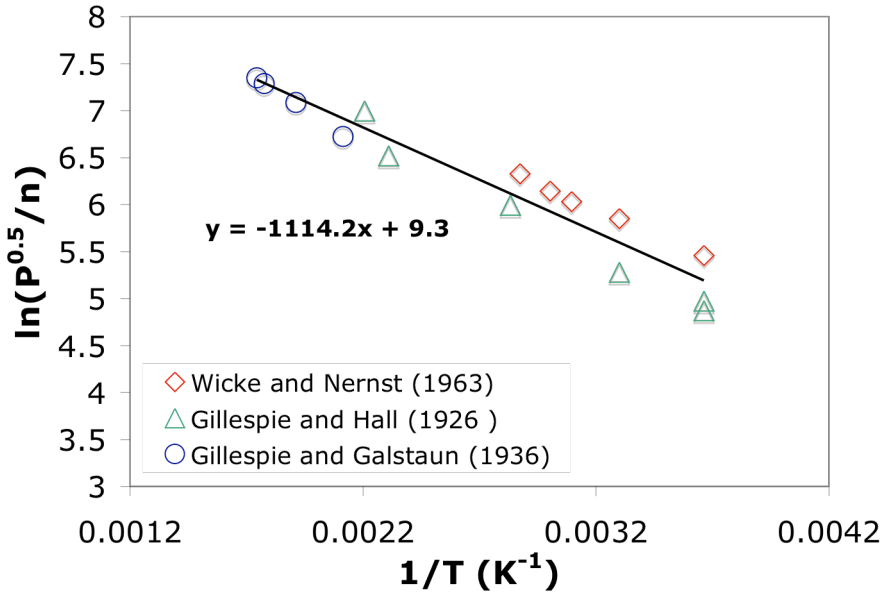

Figure 9-12 Arrhenius plot for $K(=P^{0.5}/n(H/Pd))$ derived from experimental data reported by (Gillespie and Hall, 1926), (Gillespie and Galstaun, 1936) and (Wicke and Nernst, 1964). Temperature range: 0-300°C

Figure 9-13 shows a comparison between H_2 concentration n(H/Pd) determined from 250 and 300ºC isotherms equations reported by Gillespie and Galstaun, (1936) and H_2 concentration, n(H/Pd), determined from Equation (9-15) for the same temperatures and pressures.

The model lines (dashed lines) overestimated by 0.001-0.002 n(H/Pd) the true H_2 concentration at low values of n(H/Pd). At higher pressures, which corresponded to higher values of n(H/Pd), the $P^{0.5}$ vs. n(H/Pd) relation is no longer linear (specially for the 250ºC) and Equation (9-15) underestimates the true value of n(H/Pd).

At each temperature there is a pressure range where the relation P0.5 vs. n(H/Pd) is linear. The higher the temperature the wider the pressure-range within which the relation P0.5 vs. n(H/Pd) is linear. Therefore at temperatures higher than 300ºC the model fits adequately the isotherms as seen in Figure 9-13. The accuracy on the H_2 concentration n(H/Pd) given by Equation (9-15) was estimated to be 0.002, which is significant higher than the accuracy on n(H/Pd) given by Equation (9-6).

9.4.3.2 The presence of compressive stresses upon H_2 loading

The expansion of the Pd lattice as a result of H_2 absorption led to large compressive stresses that can cause a composite Pd membrane to fail. Therefore, it was of great interest to estimate the maximum compressive stresses a composite Pd membrane would be subjected to during membrane characterization and/or membrane operation. This section aims at the fundamental relation between H_2 stress and n(H/Pd).

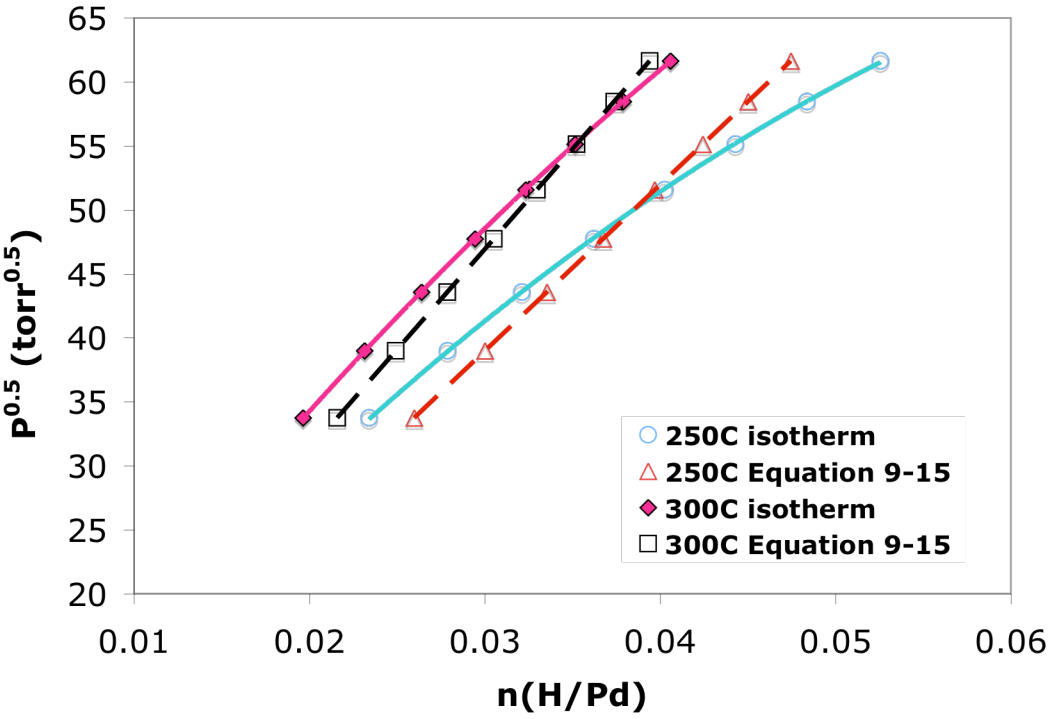

Figure 9-13 Comparison in H_2 concentration n from isotherms and using Equation (9-15)

The total stress of sample PH-1c was measured in a flowing 4% H_2-balance N_2 mixture atmosphere at a temperature of 60ºC and a pressure of 1.5 bar (H_2 partial pressure of 6 kPa). Therefore, the initial H_2 content corresponded to a H_2 solubility c.a. 0.017 (H/Pd) represented by the blue line in Figure 9-14. The use of Equation (9-15) taking P equal to 45.6 torr and T equal to 333K led to n= 0.0177, which supports the validity of Equation (9-15). The total stress of sample PH-1c was then measured at 60, 100, 150, 200, 300 and 500ºC along with the lattice parameter of Pd. Increasing the temperature led to the desorption of H_2 and consequently to the decrease of compressive stresses.

Figure 9-15 shows Pd lattice expansion ($\Delta a/a_0$ in %) as a function of temperature in He atmosphere (open circles) and in the 4%H_2-N_2 balance atmosphere (solid circles). As expected, at 60ºC, the absorption of H_2 led to an expansion of the lattice in addition to the one caused by dilation. As the temperature was increased and the pressure kept constant, H_2 desorbed from the Pd film leading to the asymptotical approach of the lattice parameter to the lattice parameter values measured in He atmosphere. The Pd lattice expansion solely due to the contribution of H_2 content ($(a_H-a_0)/a_0$) was determined by subtracting the contribution of lattice dilation due to temperature from the measured lattice parameter. The H_2 content n(H/Pd) was then determined making use of Equation (9-15) with P equal to 45.6 torr and T ranging from 60 to 500ºC. The values of $(a_H-a_0)/a_0$ were then plotted as a function of n(H/Pd) as shown in Figure 9-16 and fitted with a straight line.

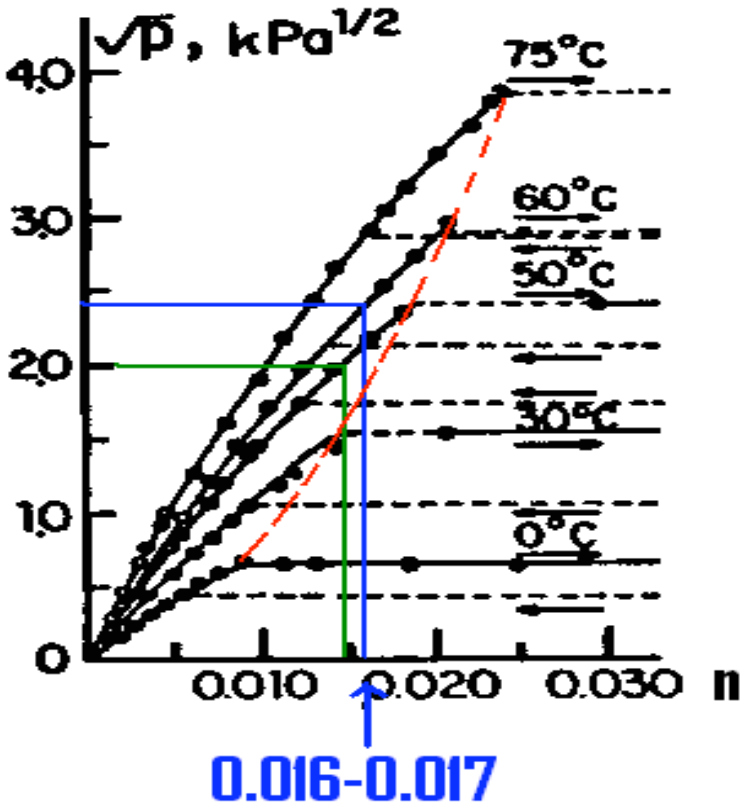

Figure 9-14 Pd-H system in the low pressure and low temperature region. The red line represents the $\alpha/(\alpha+\beta)$ boundary. The blue line represents the H_2 loading (mol H/mol Pd) at 60ºC and an absolute H_2 pressure of 0.06 bars. The green line represents the H_2 loading (mol H/mol Pd) at 50ºC and an absolute H_2 pressure of 0.04 bar.

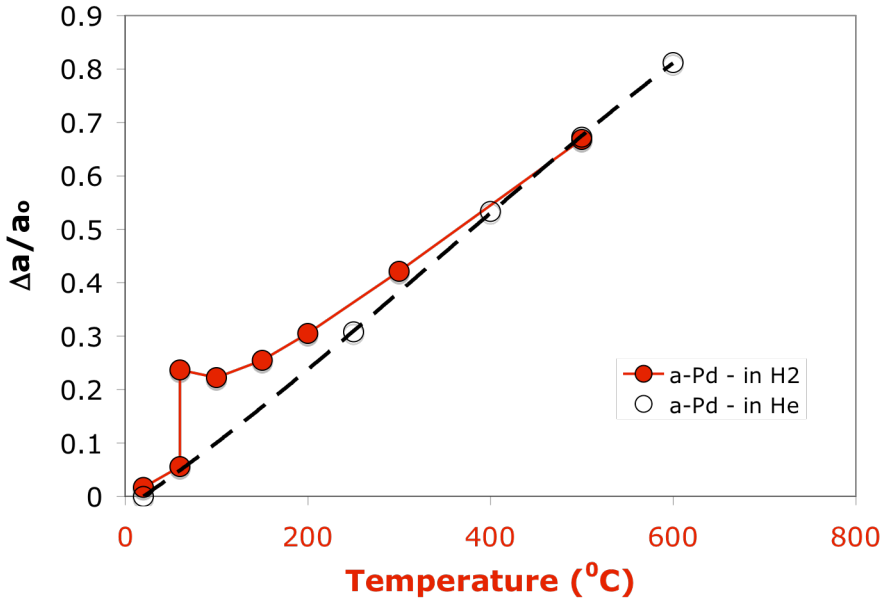

Figure 9-15 Pd lattice expansion due to H_2 uptake and temperature in sample PH-1c

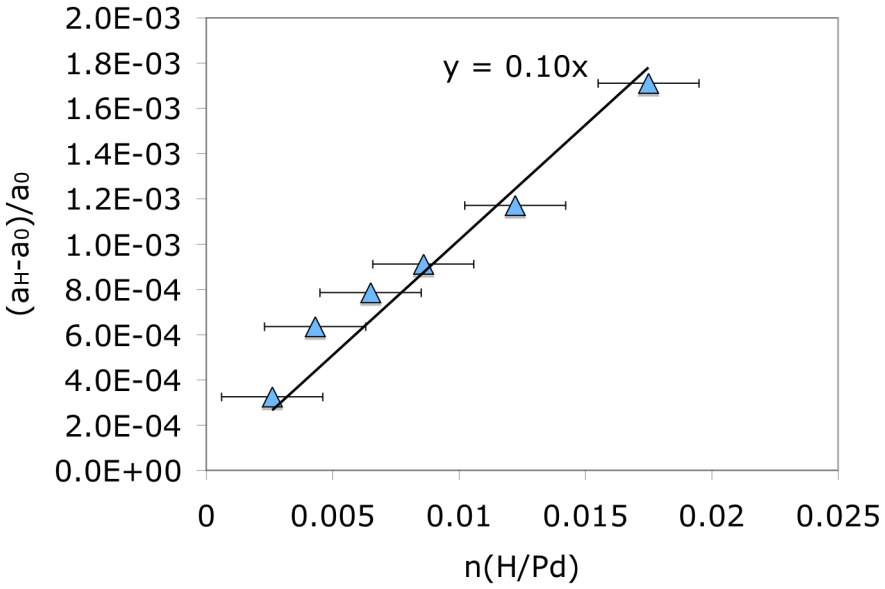

Figure 9-16 Lattice increase due to interstitial H_2 for sample PH-1c.

Pd lattice parameter increased linearly with n(H/Pd) according to Equation (9-16) with a slightly different n(H/Pd) coefficient than Equation (9-6).

$$3 \cdot \frac{a - a_0}{a_0} = 0.30 \cdot n(H/Pd) \qquad (9\text{-}16)$$

Indeed, in this case k_H equals to 0.3 and not 0.19, which is due to the fact that the film is adhered to the substrate and can only expand perpendicularly (Zabel and Hjorvarsson, 2001).

The total stress induced by the Pd lattice expansion due to H_2 loading and thermal stresses is shown in Figure 9-17 for sample PH-1c. H_2 absorption at 60ºC (n=0.017 H/Pd) led to a 0.17% expansion in addition to temperature. The large Pd lattice parameter expansion, constrained by the support, caused the switch from a 40MPa tensile stress in He to a 60MPa compressive stress in H_2 as seen in Figure 9-17. As the temperature was increased the compressive stress slowly decreased from 60MPa at 60ºC to 0MPa at temperatures higher than 200ºC, which corresponded to stress values recorded in He atmosphere. The H_2 stress component was derived by subtracting the elastic thermal stress given by Equation (9-13) from the total measured stress Equation (9-7). The H_2 content, n(H/Pd), was calculated using Equation (9-15) with P equal to 45.6 torr and T ranging from 60 to 500ºC. Figure 9-18 shows the H_2 stress component (σ_H) as a function of n(H/Pd). As expected σ_H was a linear function of n(H/Pd) in the 60-400ºC temperature range. At 500ºC Equation (9-13) was no longer valid due to the stress relaxation by plastic deformations, and the 500ºC experimental data point fell outside the predicted stress line.

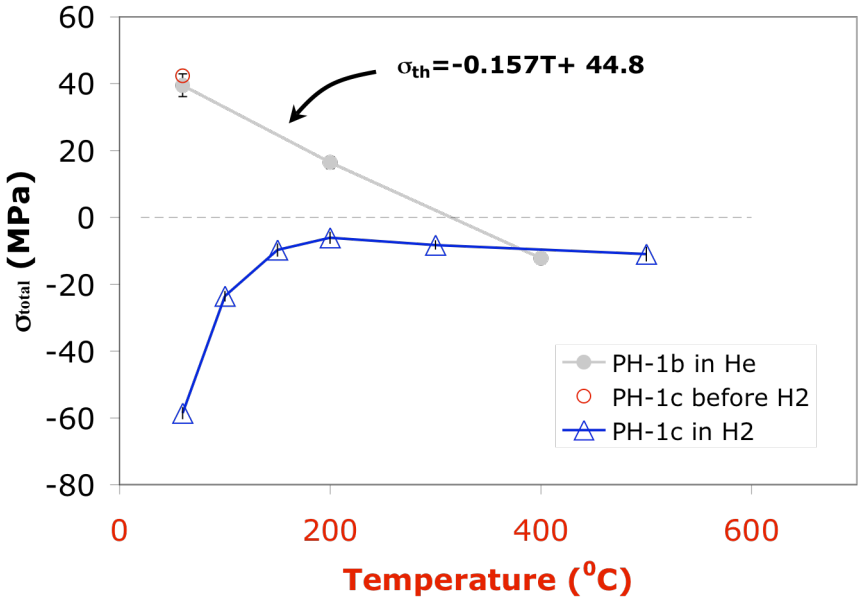

Figure 9-17 Stresses arisen in the Pd thin film due to H_2 uptake

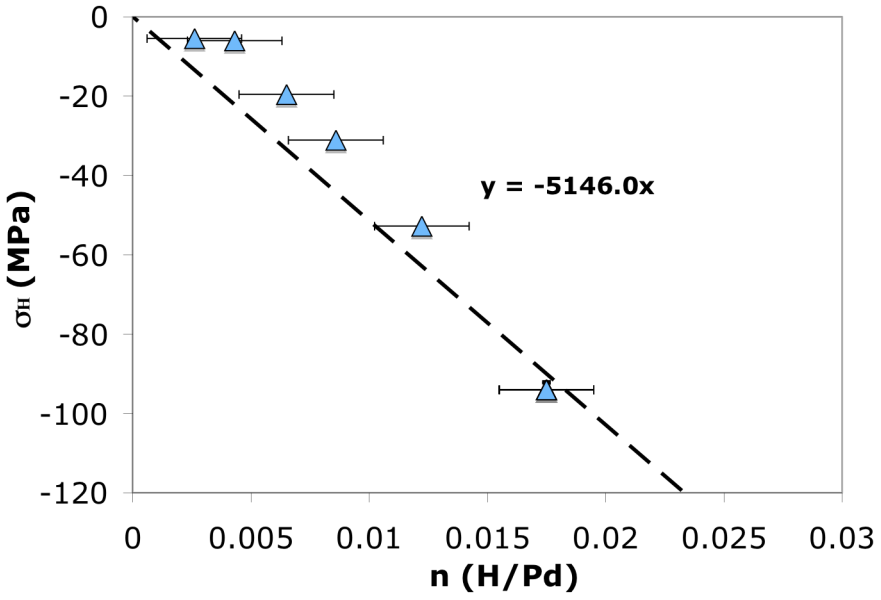

Figure 9-18 H_2 stress as a function H_2 content n(H/Pd)

Therefore, for any composite Pd-PH structure pre-treated at 400ºC, the H_2 stress is given by Equation (9-17)

$$\sigma_H = -5146.0 \cdot n(H/Pd) \quad (9\text{-}17)$$

The total stress in the composite Pd structure is given by the sum of Equation (9-13) and Equation (9-17)

$$\sigma_{total} = -0.157 \cdot T - 5146.0 \cdot n(H/Pd) + 44.8 \quad (9\text{-}18)$$

where σ_{total} is in MPa, T is in ºC and n in mol H/mol Pd. Equation (9-18) is only valid within the elastic region of Pd, which was shown to be 20-400ºC. At temperatures above 400ºC, the elastic energy accumulated in stresses was released by dislocation or grain boundary diffusional creep.

9.4.4 Estimation of stresses during membrane characterization

Knowing the fundamental principles and equations of thermal and H_2 stresses it was possible to estimate the total stress a composite Pd-PH membrane is subjected to by using Equation (9-18). The use of Equation (9-18) implied that the composite Pd membrane was already preanneled in He at 400ºC for one hour. To determine the total stress at 250 and 300ºC, n (H/Pd) was determined by using the experimental isotherms at 250 and 300ºC reported by Gillespie and Galstaun (1936) but also using Equation (9-15) in order to see the differences between the stress values calculated from the model (Equation (9-18)) and those calculated using the Pd-H isotherms.

Figure 9-19 shows the total stress calculated at 250, 300, 400 and 500ºC using Equation (9-15) (dashed lines) and the experimental isotherms from Gillespie and Galstaun (1936) (solid lines).

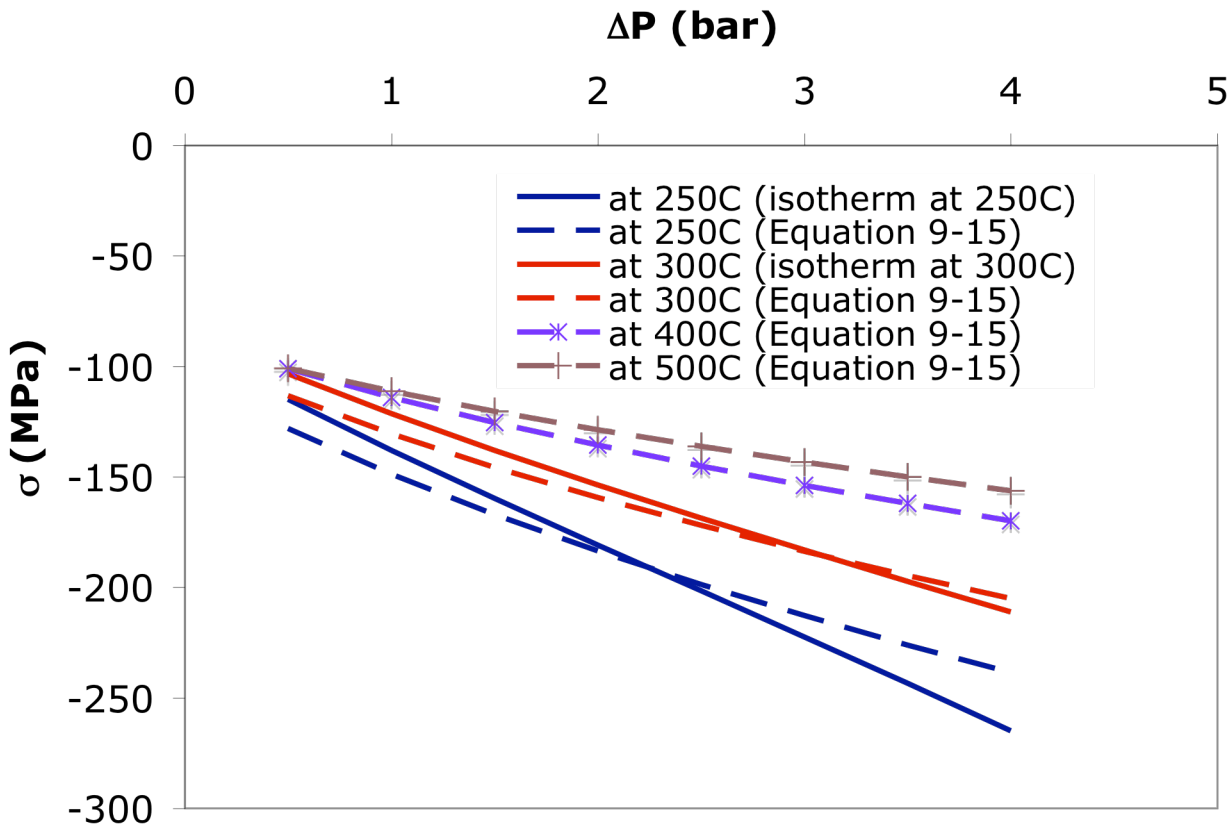

Figure 9-19 Total stress calculations for a Pd composite membrane as a function of pressure difference at 250, 300, 400 and 500ºC. Solid lines at 250 and 300C represent stress calculation using the actual isotherms at 250 and 300C (Gillespie and Galstaun (1936) for the determination of n (H/Pd). Dashed lines represent stress calculations using Equation 5.19 for the determination of n (H/Pd)

In the low pressure range the model overestimates the stress value since Equation (9-15) overstimates n(H/Pd) at low H_2 content values. However, in the high pressure range the model sligtly underestimates the stress value. Moreover, at high pressures and low temperatures, for instance 5 bar at 250ºC, the difference in total stress between the model and the true stress value is quite high (26MPa) since at 250ºC the relation $P^{0.5}$ vs. n is not linear in the 0-5bar pressure range and the model undersestimates the H_2 content. As the temperature is increased to 300ºC, the difference between the model and the true stress value is smaller (6MPa) since at 300ºC the experimental $P^{0.5}$ vs. n(H/Pd) relation could be fitted quite well with a straight line in the 0-5 bar pressure range.

Therefore, the model will always slightly overestimate the stress at low pressure. However, at high temperatures (T>300ºC) Equation (9-15) can estimate the stress very well due to the linearity of $P^{0.5}$ vs. n(H/Pd) in the 0-5 bar pressure range.

Figure 9-19 also shows that a composite Pd-PH membrane pre-annealed at 400ºC will always be under compressive stresses. The calculated stress values at 500ºC are obviously an indication of what would be the stress without relaxation. Indeed, at temperatures higher than 400ºC the elasticity region of Pd is exceeded and stresses relax leading to lower values than the predicted ones. However, experiments on samples PH-1a, PH-2a, PH-3a and especially PH-1c suggested that at 500ºC composite Pd-PH structures were still under small compression stresses. Finally, the maximum stress to which these composite Pd membranes were subjected at 250ºC and 5 bar was estimated to be compressive with a magnitude of 265 MPa (see Figure 9-19).

The experimental data collected for all membranes at 250ºC in He and H_2 atmosphere suggested that holding a composite Pd membrane at 250ºC in H_2 atmosphere did not lead

to leakages. That is, even after excursion up to H_2 pressures equal to 4.5 bar at 250ºC, where compressive stresses are the highest and equaled 260MPa, no leaks were measured in the composite Pd membrane. At 500ºC and at 2 bar H_2 pressure in the shell side the total stress was calculated to be compressive 100MPa if no stress release occurs. Therefore, it appears that stresses do not have a crucial role in leak development.

9.4.5 The effect of atmosphere cycling

During membrane operation, H_2 was introduced at 250ºC at a ΔP of 1 bar, which corresponded to a change in total stress from 6MPa tensile to 150 MPa compressive. It was of interest to understand how critical this change in nature and magnitude of the total stress was to the composite Pd membranes. Figure 9-20 shows the Williamson-Hall plot of sample PH-4a pre-annealed at 400ºC in He for 1 hr. The atmosphere was changed five times at 50ºC using UHP He and 4% H_2-balance N_2 at a 1bar pressure. Therefore, ten sets of data were plotted in Figure 9-20, five in He atmosphere and five in H_2 atmosphere. The experimental temperature and H_2 pressure parameters allowed us to study the introduction of microstrains by changing H_2 concentration in Pd between 0 and 0.015 n (H/Pd) (see green line in Figure 9-14). The changes in the H_2 concentration corresponded to changes in total stress between 40 MPa tensile in He and 40 MPa compressive in H_2.

For the atmospheres, He and H_2, no trend has been seen as a result of cycle number, that is, microstrains or the slope of the lines $\beta \cdot \cos(\theta)$ vs. $\sin(\theta)$ did not increase systematically with cycle number.

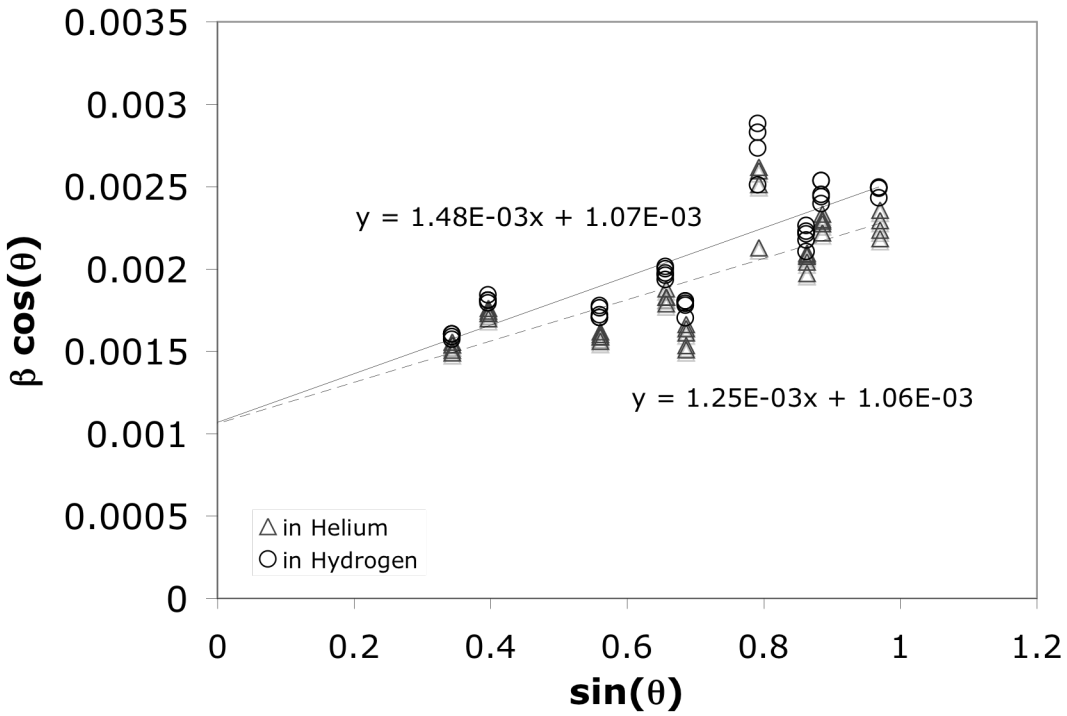

Figure 9-20 Microstrains in He and H_2 atmosphere for sample PH-4a pre-annealed in He at 400°C for one hour

As a consequence, an average microstrains value was estimated for the five H_2 lines and a second microstrains value was considered for the five He lines. As seen on Figure 9-20, the average microstrains (0.025%) in He atmosphere was smaller than in H_2 (0.029%) and both were very small compared to the initial microstrains present in the layer (0.29%).

Consequently, the heat-treatment of Pd thin films at 400ºC for one hour in He led to the irreversible release of microstrains. Once the microstrains were released, even by applying large stresses to the composite Pd-PH structure did not reintroduce microstrains. Microstrains only exist in freshly deposited samples.

9.4.6 Stress measurements in Pd-Cu –PH composite structures

The thermal stresses in composite Pd-Cu-PH were measured for the α phase and the β phase. Figure 9-21 shows the thermal stresses as a function of temperature for samples Pd-Cu-5 and Pd-Cu-6. The H_2 for pure Pd samples was also plotted for comparison purposes. Figure 9-21 shows that Pd-Cu layers on PH were subjected to higher tensile stresses in the 20-400ºC temperature range than Pd layers on PH. Higher tensile stresses in Pd-Cu alloys were consistent with the fact that Pd-Cu alloys have a larger thermal expansion coefficient than Pd. The thermal expansion coefficient of Pd-Cu alloys increases with Cu content, therefore, higher tensile stresses were expected for the Pd-Cu 40wt% (β phase) than for the Pd-Cu 10wt% alloy (α phase). Unfortunately, the thermal stresses on sample Pd-Cu-6 with the Pd-Cu α phase were measured with a low accuracy due to the low 2θ reflection considered. Figure 9-21 also indicates, by extrapolation to higher temperatures, that thermal stresses in the Pd-Cu layer were tensile at 500ºC if no stress release occurred.

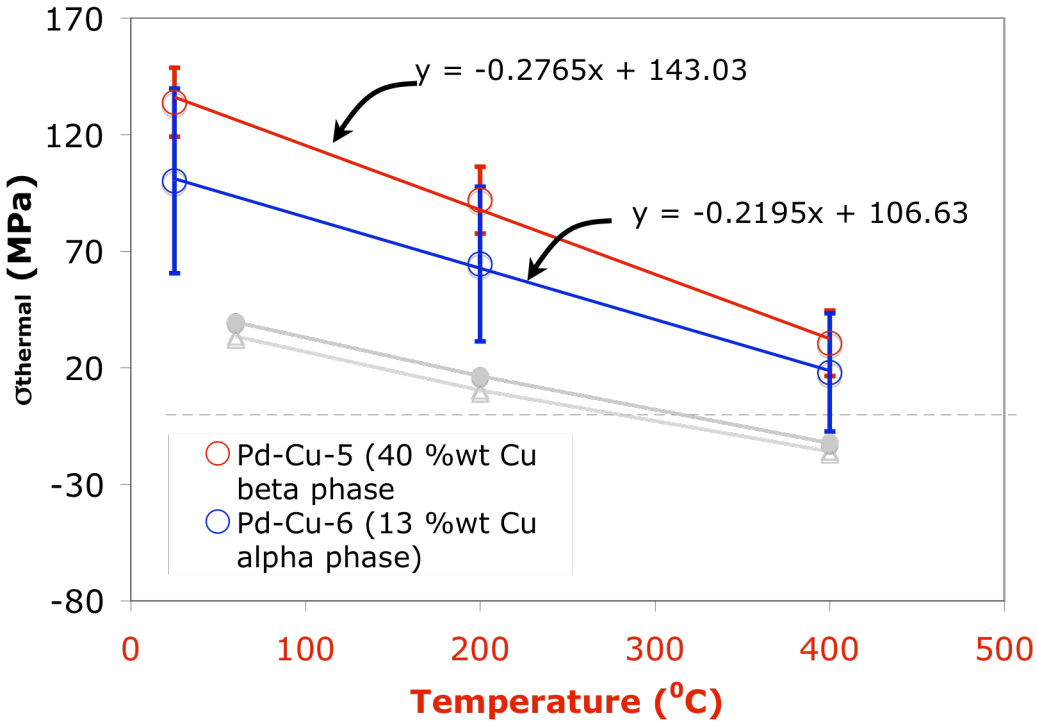

Figure 9-21 Thermal stresses as a function of temperature for the β phase (open circles) and the α phase (open diamonds)

The H_2 solubility in Pd-Cu alloys is very low. For instance, for the same H_2 pressure and temperature, the H_2 solubility is 100 times lower in Pd-Cu 40wt% than in pure Pd (Völkl and Alefeld, 1978). Therefore, H_2 stresses in a composite Pd-Cu 40wt% – PH structure should be 100 times lower than H_2 stresses in a composite Pd-PH structures. The maximum H_2 stress in a composite Pd-PH structures (at T=250ºC and P=4.5 bar) was estimated to be equal to 300MPA, therefore in a composite Pd-Cu 40wt% – PH structure the maximum H_2 stress would be equal to 3MPa. In fact, in composite Pd-Cu-PH structures H_2 stresses are negligible and the total stress equals the thermal stress. Hence, composite Pd-Cu 40wt% – PH structures are subjected to tensile stresses in the 20-400ºC temperature range regardless of the atmosphere. At temperatures higher than 400ºC, thermal stresses may become compressive with further stress release.

9.5 Conclusions

Freshly prepared composite Pd-PH structures were characterized by small Pd grains (50-100nm), an initial tensile intrinsic stress of 104.7MPa and an initial microstrains value of 0.29%. Initial microstrains and stress were released by heat-treatment in He at 400ºC for one hour with no visible change in microstructure. After annealing at 400ºC, thermal stresses were found to be a linear function of temperature in the 20-400ºC elasticity region in agreement with the literature. At temperatures higher than 400ºC stress relaxation occurred with visible changes in microstructure. Pd lattice parameter and H_2 stresses were found to be linear functions of H_2 concentration n (H/Pd) also in agreement with previous works. Stress estimations for pre-treated composite Pd membranes at 400ºC showed that the Pd thin films were always under compressive stresses. During membrane characterization the maximum compressive stress was reached at 250ºC and a

pressure of 5 bar and equaled 265 MPa. In addition stress did not play an important role in leak formation.

10 Leak growth mechanism in composite Pd membranes

10.1 Introduction

Membranes Ma-32b/34b/42 showed that the selectivity (H_2/He) decreased as a function of time when the membrane was held at 500ºC in H_2 atmosphere (see Section 0 and Table 6-2). Thermal and hydrogen stresses were found to play a small role in leak formation since holding a composite Pd membrane at low temperatures, when compressive stresses were the highest, did not lead to leak formation. Indeed, all membranes showed high (>1000) H_2 permselectivities at temperatures lower than 400ºC (see Figure 6-10). However, it was very interesting to note that thermal stress release started to occur at 400ºC when the energy barrier for diffusion was overcome and that selectivity started to decrease at temperatures close to 400-450ºC (see Figure 6-10).

The main objective of this part of the thesis was to investigate the process taking place at temperatures close to 400-450ºC that led to leak growth. The shape and size of defects were also studied. Also, the leak distribution on the surface was examined to determine whether leakage in composite Pd membranes was a localized phenomenon or a process taking place over the entire surface of the membrane. In addition, the rate at which the He leak of composite Pd membranes increased as a function of time was measured at different temperatures to estimate the activation energy of the rate of increase of the leak. The

order of magnitude of the activation energy would provide information on the mechanism underlying the leak formation and leak growth.

10.2 Experimental

10.2.1 Membrane preparation

The composite Pd membranes studied in this chapter are listed in Table 10-1. C01-F11/11b membranes were prepared on graded PSS supports and Ma-32b/34b/41/42 membranes were prepared on graded PH supports. All membranes were prepared according to the experimental procedure described in Chapter 3. Composite Pd membranes were characterized in the set-up described in Section 3.2.1.

10.2.2 Membrane characterization procedures

The characterization of membranes C01-F11a/b was described in detailed in Section 5.4.4.

Membrane Ma-32b was heated up to 500ºC in He atmosphere at a rate of 0.5ºC/min and then H_2 was introduced. The membrane was kept in H_2 atmosphere (ΔP=1 bar) at 500ºC for a period of 1,100 hr. The He leak of the membrane was measured frequently by switching from H_2 to He atmosphere at a constant pressure difference of 1 bar.

The characterization procedure of membrane Ma-34b needs to be described in detail since it deviated considerably from the characterization procedure described in Sections 3.2.2 and 3.2.3. Membrane Ma-34b was first characterized in H_2 atmosphere at 250, 300, 350 and 400ºC. It was then removed from the characterization set-up and stored at atmospheric conditions for more than a month. The membrane was characterized for a second time at 400, 450, 500, 550 and 600ºC. The H_2 permeance at 400ºC before and af-

ter storage at atmospheric conditions was the same indicating that the membrane did not deteriorate during storage. After checking that the H_2 permeance and the He leak at 400ºC were the same before and after storage, Ma-34b was heated to 450ºC. At 450ºC, membrane Ma-34b was held in He atmosphere and the He leak was monitored for 200 hr. H_2 was then introduced at 450ºC and the H_2 permeance monitored for 500 hr.

Table 10-1 Characteristics of composite Pd membranes considered in this chapter

Membrane	Support type	Grade (μm)	Ox. Temp	Thickness (μm)	Permeance at 500ºC	Final selectivity (H_2/He)
C01-F11	PSS	0.1	500	17	21	683
C01-F11b	C01-F11	0.1	500	19	23.5	478
Ma-32b	PH	0.1 medium	700	10	42	280
Ma-34b	Ma-34	0.1 coarse	700	8	24 (450ºC)	86
Ma-41	PH	0.1 coarse	700	10	30 (450ºC)	857
Ma-42	PH	0.1 medium	700	5.6	38.8	818

During the 500 hr-period the membrane was in H_2 atmosphere, the He leak was determined by switching from a pure H_2 feed to a feed containing 99%H_2-1%He. The composition of the permeate was analyzed by a on-line GC to obtain the ideal separation factor, or selectivity, (H_2/He). After 500 hr in H_2, the He leak of Ma-34b was measured in He atmosphere in order to determine if the He measurements with the GC were in agreement with the He leak measurements performed in He atmosphere as described in Section 3.3.1. The temperature was then raised up to 500ºC. The membrane was held at 500ºC in He atmosphere for 1500 hr and the He leak was measured regularly as described in Section 3.3.1. After 1500 hr in He atmosphere, H_2 was introduced at 500ºC and the H_2 permeance and leak were monitored for an additional 500 hr. At 500ºC, leaks were measured by switching from H_2 to He atmosphere. The remaining steps of the characterization

of membrane Ma-34b consisted of holding for 100 hr in H_2 atmosphere at 550 and 600ºC. At each temperature, the He leak was measured 3 or 4 times by switching from H_2 to He.

Membrane Ma-41, a composite Pd-Cu membrane, was characterized at 250, 300, 350 and 400ºC according to the procedure described in Sections 3.2.2 and 3.2.3. At 450ºC Ma-41 was held for 500 hr in H_2 atmosphere; the leak was determined by switching from pure H_2 to a 99%H_2-1%He mixture and measuring the permeate gas composition with an on-line GC. After 500 hr at 450ºC, He was introduced and the leak was measured in He atmosphere to corroborate the GC leak measurements previously taken. The temperature was then raised to 500ºC and H_2 was introduced. Ma-41 was not held at 500ºC in He atmosphere as was the case for Ma-34b. Ma-41 was held for 280 hr in H_2 atmosphere and the He leak was measured 3 or 4 times by switching from H_2 to He. Finally membrane Ma-42, was characterized as described in Sections 3.2.2 and 3.2.3

10.2.3 The activation energy for the rate of increase of leaks in composite Pd membranes

At a given temperature, leaks in composite Pd membranes were assumed to increase linearly with time, which turned out to be a good approximation at temperatures equal to or higher than 450ºC. The behavior of leaks at temperatures lower than 450ºC was difficult to study since they grew at a very slow rate. At temperatures higher than 450ºC, the leak was measured several times at a given temperature. Therefore, the rate at which the leak increased was determined relatively accurately. Yet, in cases, especially at low temperatures, only one leak measurement was performed. When only one leak measurement was available the rate at which the leak increased was calculated using the following procedure.

Figure 10-1 depicts the H_2 permeance as a function of time for an hypothetical membrane. At *t1* He was introduced and the He leak at 450ºC was measured. At *t2* the temperature was changed from 450ºC to 500ºC at a rate of 1ºC/min and *t3* was the time at which the He leak at 500ºC was measured.

Based on experimental observations, the He leak did not change during the 50 minutes that were necessary to bring the temperature up by 50ºC (e.g. from 450 to 500ºC). Therefore, the He leak at point *t2* was equal to the He leak at point *t1* plus the increase in He leak that occurred at 450ºC during the time $\Delta t = t2 - t1$. The rate of increase for the leak at 500ºC was then given by Equation (10-1)

$$rHe_{500} = \frac{He(t3) - \left\{He(t1) + rHe_{450} \cdot (t2 - t1)\right\}}{t3 - t2} \qquad (10\text{-}1)$$

where, $He(ti)$ is the He leak at the time ti (i=1, 2, 3, etc.) and rHe_{temp} is the rate of increase for the He leak at the temperature denoted in the subscript (*temp*). t_i corresponded to the time at which He leaks were measured and temperatures were changed as shown in Figure 10-1.

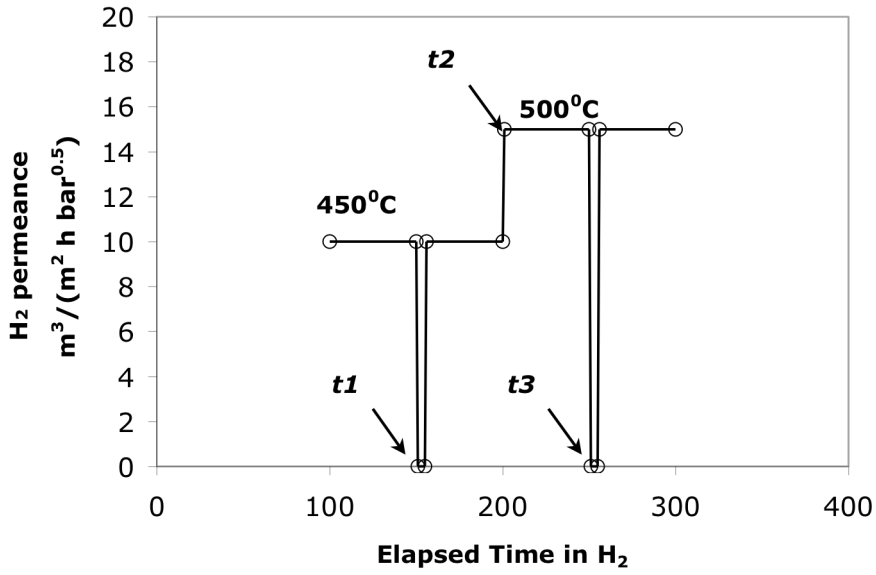

Figure 10-1 Schematic H_2 vs. time plot for a composite Pd membrane.

10.3 Results and discussion

10.3.1 Pinhole size, pinhole formation

10.3.1.1 Size characterization of pinholes

This section aimed at the study of defects already formed in a composite Pd membrane. The calculations are only shown for membrane Ma-41 at 450ºC although the same calculations were performed for all membranes.

The diffusion of gases through the defects in a Pd layer can be approximately given by the sum of a Knudsen term and a viscous term (slip-flow) as shown in Equation (10-2).

As already stated in Section 5.4.2, the flux of inert gases through defects was modeled as the flux of gases through a porous media with a very small porosity (Mardilovich et al., 1998). The flux of gases through defects was in general very small, therefore, leaks were not affected by mass transfer within the porous support. That is, when looking at Figure 5-1, the pressure P_2 is equal to pressure P_3.

$$\frac{J}{\Delta P} = \alpha + \beta \cdot P_{ave} = \frac{2}{6}\sqrt{\frac{8}{\pi}}\frac{\varepsilon \mu_k d}{L_{Pd}\sqrt{RTM}} + \frac{1}{32}\frac{\varepsilon \mu_v d^2}{L_{Pd}\eta RT}\cdot P_{ave} \qquad (10\text{-}2)$$

where $\alpha \cdot \Delta P$ is the Knudsen flow and $\beta \cdot \Delta P \cdot P_{ave}$ is the viscous flow. Equation (10-2) assumes that surface diffusion is negligible. Plotting gas permeance ($J/\Delta P$) as a function of the trans-membrane average pressure led to a straight line for every gas (He, N_2, Ar etc…) with α as the y-intercept and β as the slope. Figure 10-2 shows the permeance of He and Ar through Ma-41 as a function of the average trans-membranes pressure. Equation (10-2) also assumes that the defects of composite Pd membranes were pinholes within the Pd layer with an average diameter d. The average diameter d can be estimated from the β/α ratio after having assumed μ_k is equal to μ_v. After simplification, the β/α ratio is given by Equation (10-3)

$$\frac{\beta}{\alpha} = \theta \cdot \frac{3}{32}\cdot\sqrt{\frac{\pi}{8}}\cdot\frac{1}{\sqrt{RT}}\cdot\frac{\sqrt{M}}{\eta}d \qquad (10\text{-}3)$$

In fact μ_v is equal to $1/\tau$ and μ_k is equal $1/(\tau\ \theta_k)$ with θ_k the reflection factor. The reflection factor is proportional to the roughness of the pore walls. Smooth walls are characterized by a θ_k value equal to 1 while rough surfaces have reflection factors greater than 1. Therefore, assuming μ_k is equal to μ_v is equivalent to assume θ_k equal to 1 and that pinhole walls were smooth, which was close to the reality.

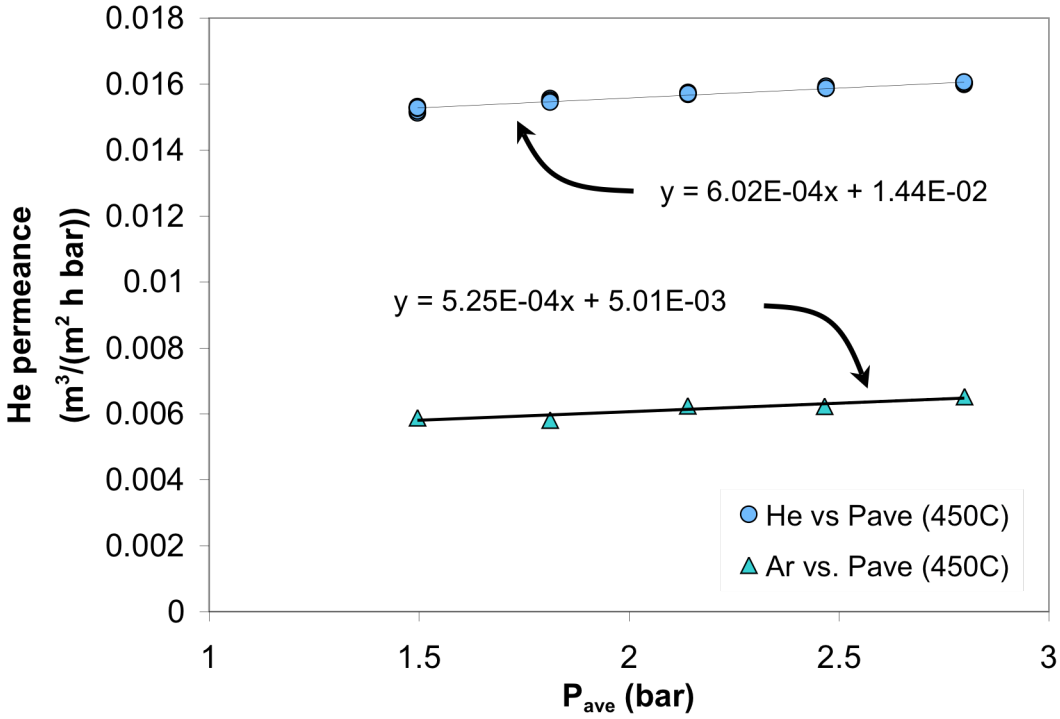

Figure 10-2 He and Ar permeance of Ma-41 as a function of average pressure across the membrane.

The β/α ratio of all gases can then be plotted as a function of $\sqrt{M}/\eta$ and be fitted with a straight line forced through the origin. Figure 10-3 shows the β/α ratio plotted as a function of $\sqrt{M}/\eta$ for He and Ar. The precision achieved on the determination of the diameter depended on the precision with which the β/α ratio was measured. The precision on the β/α ratio was estimated to be 1-2% when digital mass flow meters (MFM) were used. When bubble flow meters (BFM) were used for the measurement of the He permeance the precision on the β/α ratio dropped to 10-15%. He leak data from MFM were used when the He fluxes measured in the 0-4.5 bar (see Section 3.3.1) lay within the range of the mass flow meter (0-50sccm). The pinhole diameter was estimated with a 2-5% precision when data from MFM were used. The average pinhole size for Ma-41 was estimated to be 0.16 μm at 450ºC.

Table 10-2 summarizes the He leak and selectivity shown by all membranes after they were kept at the maximum temperature for the time listed in the Table. It became apparent that all composite Pd membranes suffered from selectivity reduction. Table 10-2 also lists the average pinhole size determined on each membrane. Membranes having a high selectivity (>800), Ma-41/42 were characterized by a very small average pinhole size equal to 0.16-0.17 μm. Membranes having a low selectivity (<100) were characterized by an average pinhole size larger than a micron.

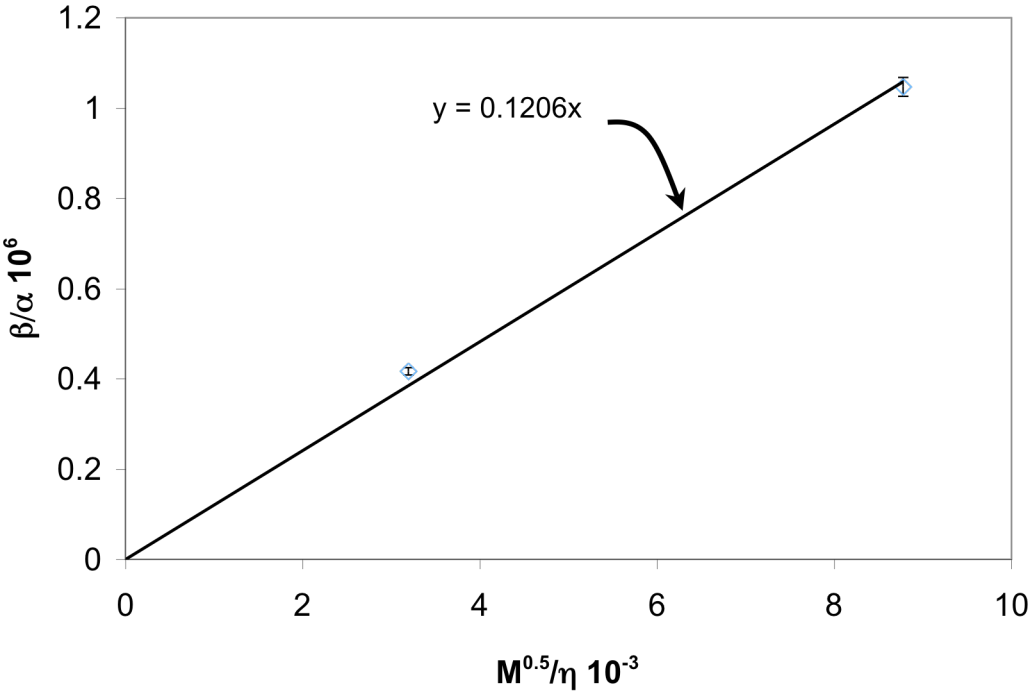

Figure 10-3 β/α ratio as a function of $M^{0.5}/\eta$ for He and Ar.

Table 10-2 He leak and selectivity of membranes considered in this chapter

membrane	Thick. (Weight gain) (μm)	Temp. (ºC)	Time spent at max Temp. (hr)	H_2 permeance at Temp. (col. 2) (m^3/m^2-h-$bar^{0.5}$)	He leak. (m^3/m^2-h-bar)	Selectivity at ΔP=1bar (H_2/He)	Average pinhole diameter (μm)
C01-F03	32	500	35	4.3	0.0148 (at RT) (BFM)	120	1.7 (at RT, He)
C01-F05	33	500	100	10.3	0.00766	587	n.d.
C01-F07	23	500	76	8	0.0763 (at RT) (BFM)	43	0.34 (at RT, He)
C01-F11	15	500	319	20.6	0.0125	683	0.83 (He)
C01-F11b	17	500	179	23.5	0.0214	478	0.47 (He)
C01-F11b	17	550	93	28.3	0.234 (at RT) (BFM)	52	0.34 (at RT, He and N_2)
Ma-32	7.7	500	52	50	0.485	42	n.d.
Ma-32b	10	500	1100	41	0.0651	280	n. d.
Ma-32c	12	500	556	38	1.101 (at RT) (BFM)	14	1.3 (at RT, He)
Ma-34b	8	500	552	20	0.0957	86	0.92 (He)
Ma-41	10	450	500	30	0.0145	857	0.16-0.17 (He and Ar)
Ma-42	5.6	500	111	39	0.0165	980	0.04 (He)
Ma-42	5.6	500	185	39	0.019	818	0.16 (He)

n.d. = not determined

10.3.1.2 The formation of pinholes at high temperatures

The morphology changes of Pd deposits formed by the electroless deposition method were studied by heating pieces of Ma-32c membrane at 500, 550, 600 and 650ºC for 48 hr in H_2 atmosphere. Figure 10-4(a), (b), (c) and (d) show the morphology of Ma-32c after the H_2 characterization at 500ºC, after the heat-treatment at 550, 600 and 650ºC respectively. No pinholes were readily seen on the surface of membrane Ma-32c after H_2 characterization at 500ºC. Figure 10-4(b) shows that the heat-treatment at 550ºC led to the growth of Pd clusters, yet pinholes were still not readily visible on a random region of the surface of the Pd layer. The heat-treatment at 600 and 650ºC led to the formation of a large number of pinholes, which were visible on random regions of Ma-32c surface. The number of pinholes per unit area was larger in the 650ºC annealed sample than in the 600ºC annealed sample.

Since high temperatures (600-650ºC) led to the formation of numerous and large (5μm in diameter) pinholes, and since few and small (1μm in diameter) pinholes were found at 500ºC, leak formation and growth might start at low temperatures 400-450ºC by the formation of small pinholes and leaks might grow at higher temperatures by the formation of new pinholes and growth of already formed pinholes. Section 10.3.1.3 aimed at the elucidation of the formation and growth of pinholes at moderate temperatures (450-550ºC).

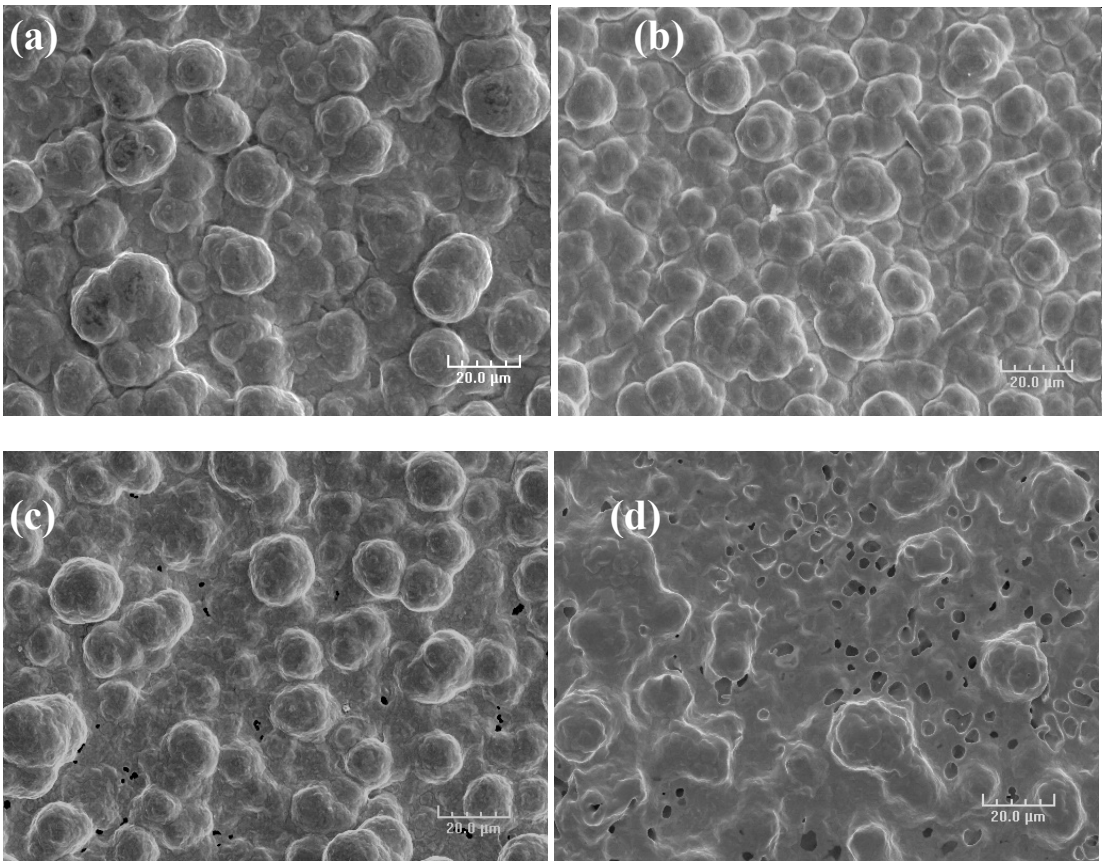

Figure 10-4 Ma-32c surface morphology after annealing in H_2 at (a) 500, (b) 550, (c) 600 and (d) 650ºC for 48 hr (Mag 1500)

10.3.1.3 The formation and growth of pinholes

This section aimed at the elucidation of the formation and growth of pinholes at the temperature at which leaks appeared in all composite Pd membranes, which was 450ºC (see Figure 6-10), and also at high temperatures (500 and 550ºC).

In order to investigate the formation and growth of pinholes at 450, 500 and 550ºC, the He permeance, the total pinhole surface, the pinhole diameter and the number of pinholes were determined as a function of time at 450 and 500ºC for membrane Ma-41 and at 500 and 550ºC for membrane Ma-34b. Figure 10-5 shows the He leak vs. average pressure at different times during the characterization of Ma-34b. In order to determine the He permeance, the total pinhole surface, the pinhole diameter and the number of pinholes were determined as a function of time, the He flux was measured at several pressures (see Section 3.2.3) and also at different times for a given temperature. As an example Figure 10-5 shows the raw data taken for membrane Ma-34b. The same type of data was also collected for Ma-41. The He permeance was measured after 1500 hr in He (circles in Figure 10-5), which was taken to be the zero time for the next H_2 characterization step. The He permeance of Ma-34b was also measured after 200, 400 and 550 hr after switching from H_2 to He atmosphere (Figure 10-5). The temperature was increased to 550ºC and the He permeance was measured after 60 hr. Figure 10-5 shows that for the first four lines (He permeance vs. P_{ave}) the ratio β/α increased, indicating an increase of the average pinhole diameter according to Equation (10-3) as the membrane was held at 500ºC in H_2. The straight line fitted through the experimental data taken at 550ºC clearly shows a lower β/α ratio indicative of a smaller average pinhole diameter at 550ºC.

The number of pinholes in the Pd layer can be estimated by first calculating the porosity ε of the Pd layer (Mardilovich et al., 1998) using Equation (10-4)b

$$\varepsilon_\beta = 8 \cdot L \cdot \eta \cdot \tau \cdot RT \cdot \beta \cdot \frac{4}{d^2} \qquad (10\text{-}4)a$$

$$\varepsilon_\alpha = \frac{3}{2}\sqrt{\frac{\pi}{8}} \cdot L \cdot \sqrt{RTM} \cdot \tau \cdot \alpha \cdot \frac{2}{d} \qquad (10\text{-}4)b$$

The tortuosity value τ was taken to be equal to 3.5, which is a general tortuosity value found in many pore systems.

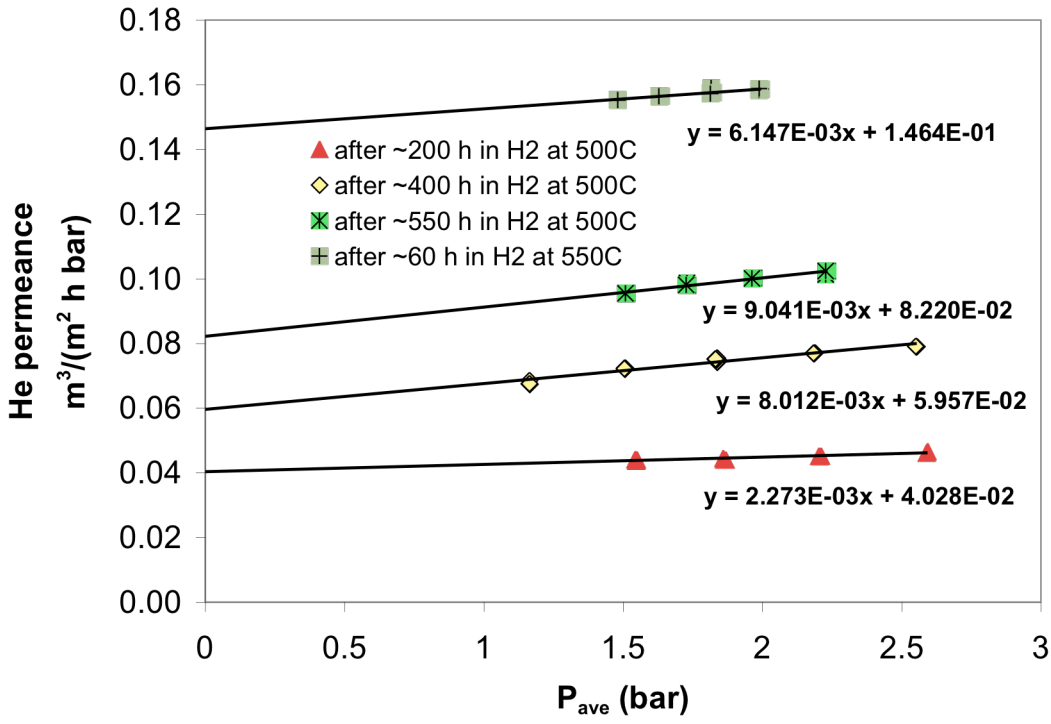

Figure 10-5 He permeance vs. average pressure at 500ºC at time t=0, 200, 400 and 550 hr and t=60 hr at 550ºC.

A greater precision was achieved using α than using β, which was due to somewhat larger errors on the determination of β. Therefore, porosity calculations based on α had a better precision. The number of pinholes per unit area can then be calculated from Equation (10-5)

$$N = 4 \cdot \frac{\varepsilon \cdot S}{\pi d^2} \qquad (10\text{-}5)$$

where N is the number of pinholes/m^2 and S the total surface of the composite Pd membrane. Since N is based on the porosity, a better estimation is found using ε based on α. ε·S is the total pinhole area.

Figure 10-6 shows the He permeance and the total pinhole area for membrane Ma-41 as a function of time at 450 and 500ºC. the total pinhole area (ε_α·S) as a function of time was calculated using experimental data similar to the one in Figure 10-5 and Equations (10-3) to (10-5). At 500ºC, both the leak rate and the total pinhole area increased linearly with time. Figure 10-7 shows the average pinhole diameter and the total number of pinholes in the 120 cm^2 of membrane Ma-41 as a function of time at 450ºC and 500ºC. The average pinhole diameter and the total number of the pinholes was also estimated using Equations (10-3), (10-4b) and (10-5). The average pinhole diameter decreased as a function of time from 0.42 to 0.25 μm at 500ºC. The number of pinholes slowly increased from around 1000 to around 6500. Therefore, it appeared that the He leak grew at 500ºC by the continuous formation of small pinholes.

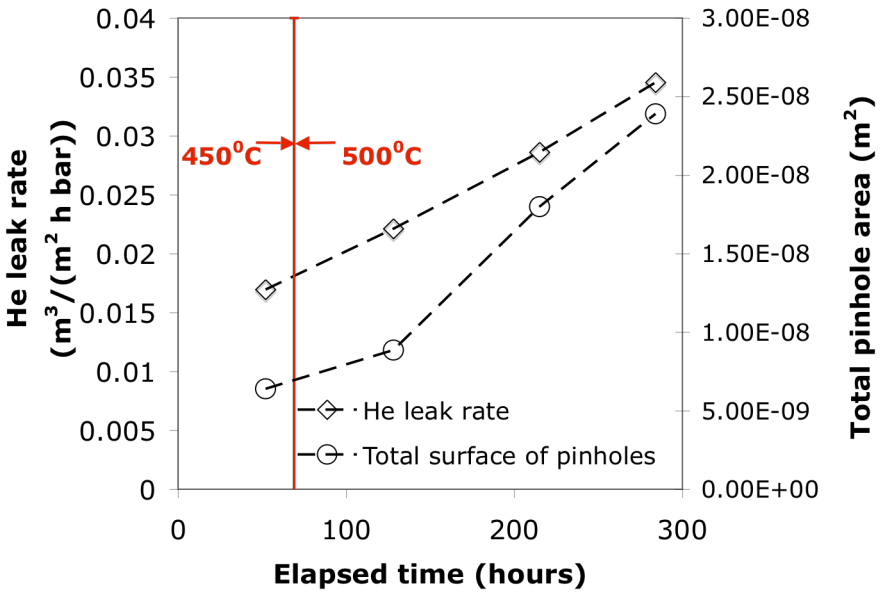

Figure 10-6 He leak rate vs. time at 450ºC and 500ºC for membrane Ma-41. The total pinhole area ($\varepsilon_\alpha \cdot S$) as function of time at 500ºC and 550ºC was also plotted.

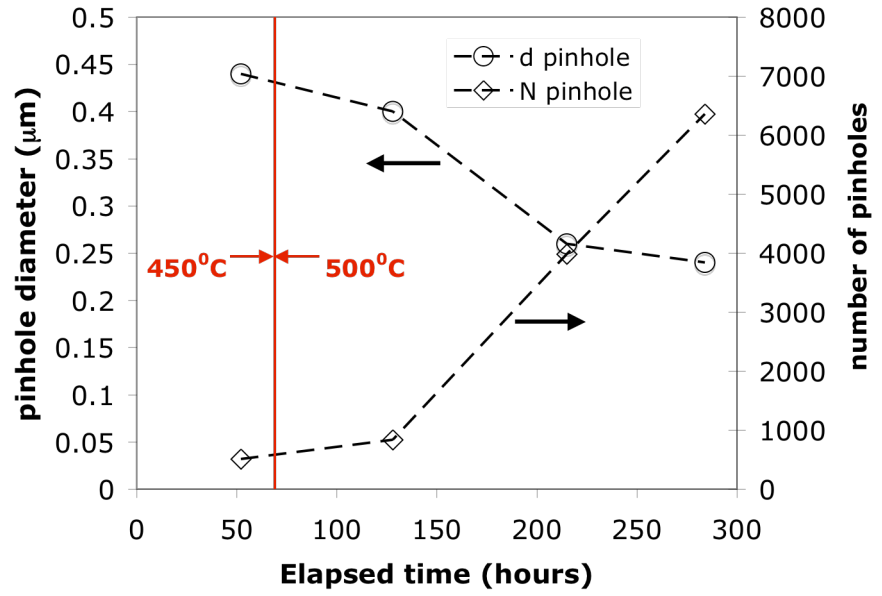

Figure 10-7 Pinhole diameter and number of pinholes as a function of time at 450ºC and 500ºC.

Figure 10-8 shows the He permeance and the total pinhole area for membrane Ma-34b as a function of time at 500 and 550ºC. the total pinhole area ($\varepsilon_\alpha \cdot S$) as a function of time was calculated using the data in Figure 10-5 and Equations (10-3) to (10-5). At 500ºC the leak rate increased linearly with time yet the total pinhole area appeared to be constant.

At 550ºC both the leak rate and the total pinhole area rapidly increased. Figure 10-9 shows the average pinhole diameter and the total number of pinholes in the 120 cm^2 of membrane Ma-34b as a function of time at 500ºC and 550ºC. The average pinhole diameter and the total number of pinholes were also estimated using data in Figure 10-5 and Equations (10-3), (10-4b) and (10-5). The average pinhole diameter increased as a function of time. It appeared then that at 500ºC the increase in He permeance was only due to an increase in pinhole size since the total pinhole surface and also the total number of pinholes were relatively constant. When the temperature was raised to 550ºC, the total number of pinholes increased from 100 to 8000. Also, the average pinhole size decreased from 0.8-1 μm to 0.4 μm. Therefore, The increase of the leak at 550ºC occurred by the formation of a large number of new pinholes with an average diameter of 0.35 μm.

In both membranes, Ma-34b and Ma-41, the average pinhole size decreased while the total number of pinholes increased when a temperature change was performed (450-500ºC or 500-550ºC) indicating the formation of new and small pinholes. The main difference between the two membranes was that in the case of Ma-41, the increase in total pinhole number was slow, while for membrane Ma-34b the total pinhole number increased by a factor of a 1000 in only 60 hr. In addition, Figure 10-6 suggests that at 500ºC formation and growth of pinholes occurred at the same time.

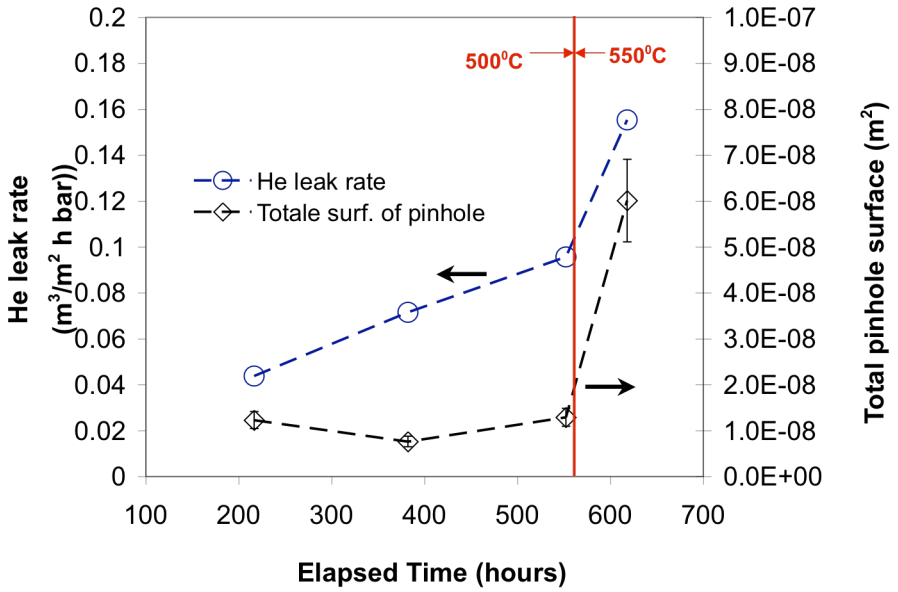

Figure 10-8 He leak rate vs. time at 500ºC and 550ºC for membrane Ma-34b. The total pinhole area ($\varepsilon_\alpha \cdot S$) as function of time at 500ºC and 550ºC was also plotted.

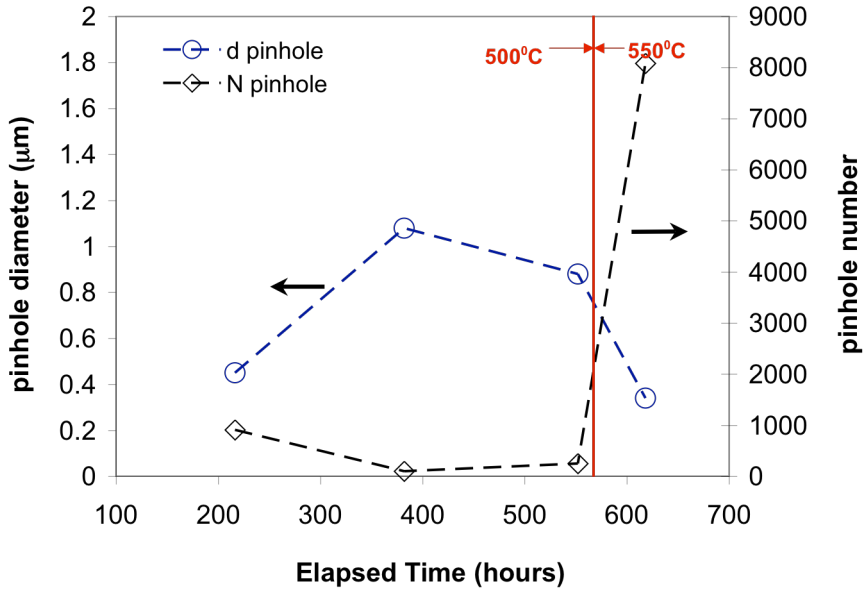

Figure 10-9 Pinhole diameter and number of pinhole as a function of time at 450ºC and 500ºC.

10.3.1.4 Distribution of defects in composite Pd membranes

Knowing the leak distribution in the membrane was an important piece of information to understand whether the He leak was due to localized imperfections or due to a process affecting the entire surface of the membrane.

In order to locate the He leak of Ma-32b and Ma-32c a rising "water test" was performed after cooling the membrane down to room temperature. The rising "water test" was performed according to the procedure described in Section 3.3.2. The normalized He leak for Ma-32b and Ma-32c were plotted in Figure 10-10 as a function of the water level. The He leak of Ma-32b/32c membranes decreased rather uniformly as the water level was increased, indicating that the He leak of both membranes was distributed uniformly across the surface. Therefore, the process leading to the leak formation and leak growth affected the entire Pd layer. The uniformity character of this process suggested that the leak formation was an internal phenomenon related to the nature of Pd metal.

10.3.2 Kinetics of leak increase in H_2 atmosphere

It is of great interest to determine the temperature at which leaks appeared. The temperature at which the He leak started shed some light on the mechanism of the leak formation. Figure 10-11 shows the He leak of membranes C01-F11a/11b, Ma-41 and Ma-42. For all membranes, the first large increase in He leak was measured at 450ºC, which fell within the range of 0.2-0.4 of the Pd melting point[1] in Kelvin.

[1] Pd melting point: 1552ºC

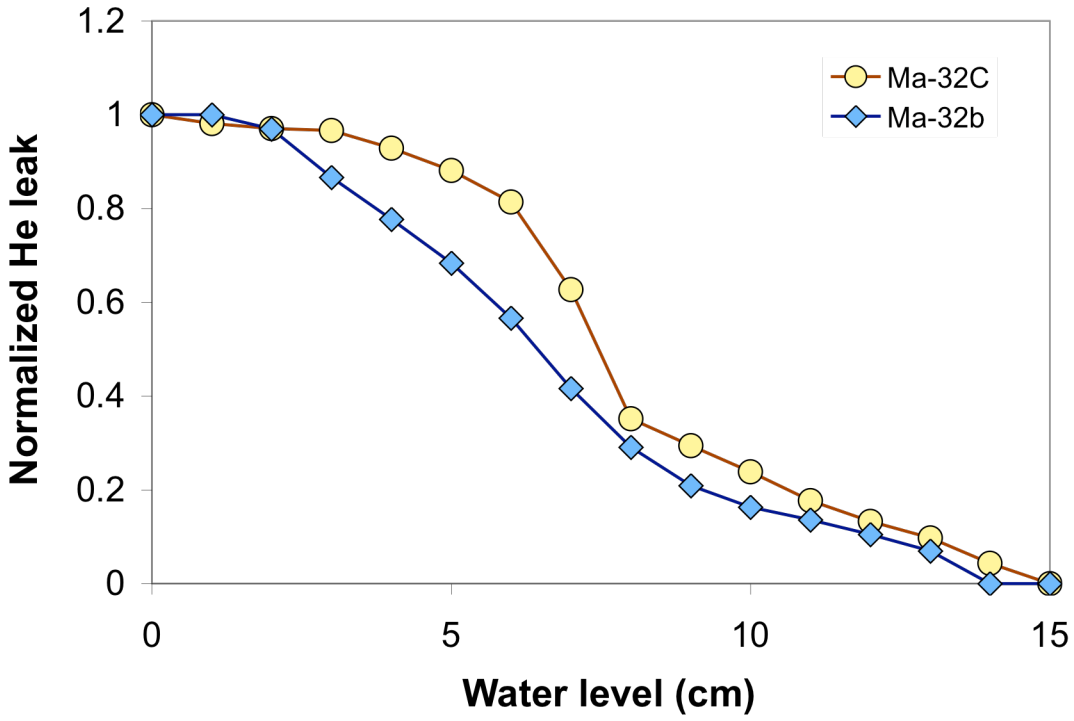

Figure 10-10 He leak as a function of water level for membrane Ma-32b/32c. The "0" mark corresponds to the lower weld and the "15" mark corresponds to the upper weld.

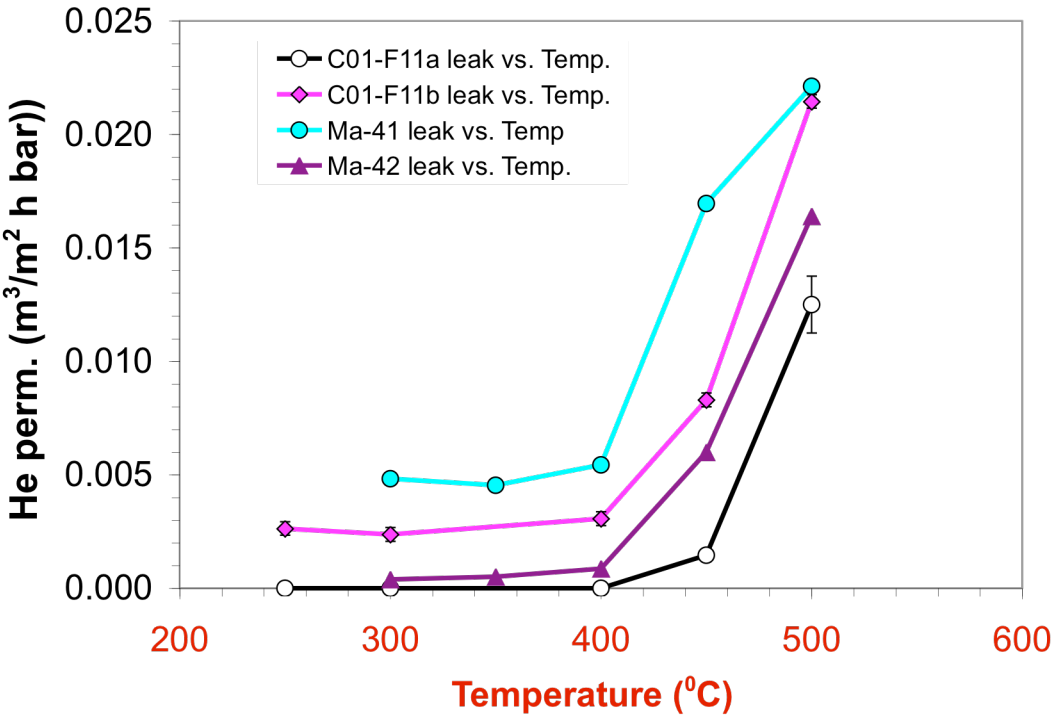

Figure 10-11 He leak of membranes C01-F11/11b and membrane Ma-41 and Ma-42 as a function of temperature.

It has been shown that sintering in nanocrystalline metals starts at 0.2-0.4 of the melting point (Koch, 2002). Therefore, leak formation and leak growth are related to the sintering of Pd grains and Pd clusters.

When plotting the He leak as a function of temperature, it is implicitly assumed that the He leak did not grow with time at a given temperature, which was valid at temperatures lower than 450ºC where the rate of increase of the He leak was very slow. However, at temperatures equal to or higher than 450ºC, the He leak increased faster, and the leak was followed as a function of time at a given temperature. As a consequence, the time for which each membrane was held at each temperature in Figure 10-11 needed to be considered. In fact, the He leak vs. temperature plot shown in Figure 10-11 lacks the "time" variable. The He leak at 450ºC for membrane Ma-41 was almost equal to the He leak at 500ºC because the times at which measurements were taken were not the same. The leak at 450ºC was taken after 500 hr in H_2 while the leak at 500ºC was measured after only 60 hr in H_2 at 500ºC.

Figure 10-12 shows the He leak- He leak$_0$[1] increase in H_2 atmosphere as a function of time for membrane Ma-34b at 450, 500 and 550ºC. The He leak increase was linear as a function of time and the rate of increase for the He leak was determined from the slope at each temperature. A similar approach was used for all composite Pd membranes, when the He leak was measured several times at a given temperature (Ma-32b, Ma-34b and Ma-41).

[1] He leak$_0$ corresponds to the He leak at the time t=0.

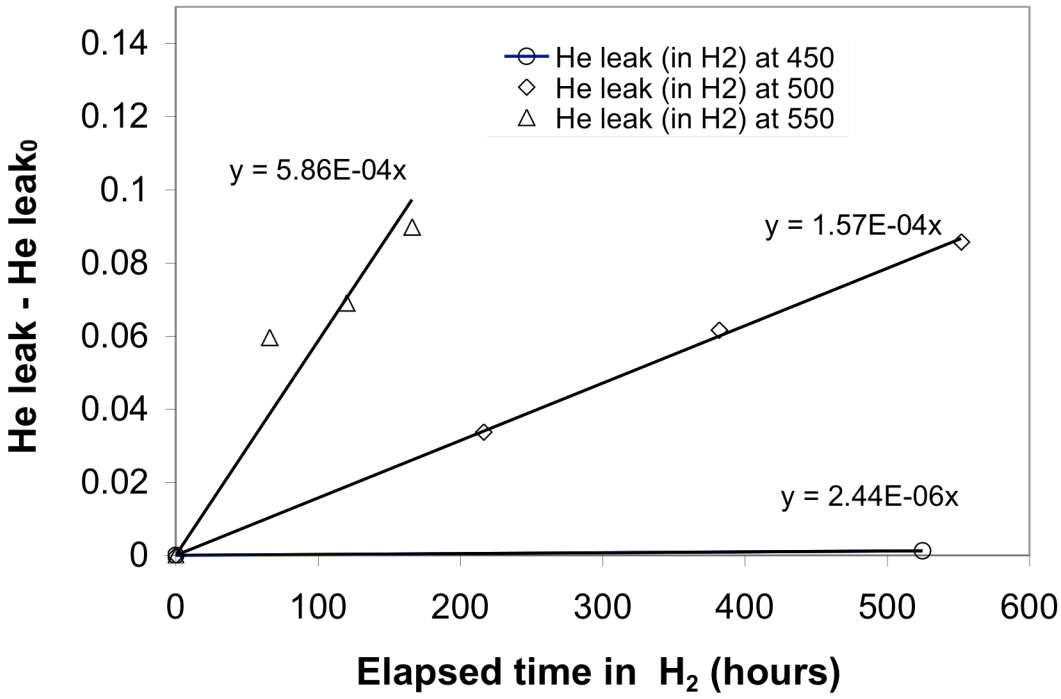

Figure 10-12 He leak rate increase in H_2 atmosphere at 450, 500 and 550ºC for membrane Ma-34b.

The rate of increase for the He leak of membrane C01-F11a/11b and Ma-42 was estimated as described in Section 10.2.3 since only one He leak measurement was performed at each temperature. The natural logarithm of the rate of increase for the leak was then plotted as a function of inverse temperature (Arrhenius plot) in order to estimate the activation energy of the mechanism underlying the leak increase in composite Pd membranes. The Arrhenius plot of leak rate growth for membranes C01-F11a/11b and membranes Ma-32b, Ma-34b, Ma-41 and Ma-42 is shown in Figure 10-13.

Figure 10-13 clearly shows that the rate of increase for the He leak in the 250-400ºC temperature range was very slow and that significant leaks began to develop at 450ºC. Moreover, the rate at which the He leak increased at 500ºC in pure H_2 was similar for all membranes with an average value of $9.1 \cdot 10^{-5}$ $m^3/(m^2\ h\ bar)/h$. Since leaks hardly grew in the 250-400ºC temperature range, the activation energy for leak growth was only estimated in the 450-550ºC temperature range using the rate at which the leak increased for membranes C01-F11a/11b and Ma-32b, Ma-34b and Ma-42. The data of membrane Ma-41, composite Pd-Cu membrane, were omitted for the calculation of the activation energy, as well as the average rate at which the He leak increased at 500ºC. Data for membrane Ma-41 was plotted in Figure 10-11 and Figure 10-13 for comparison purposes only and for later discussions.

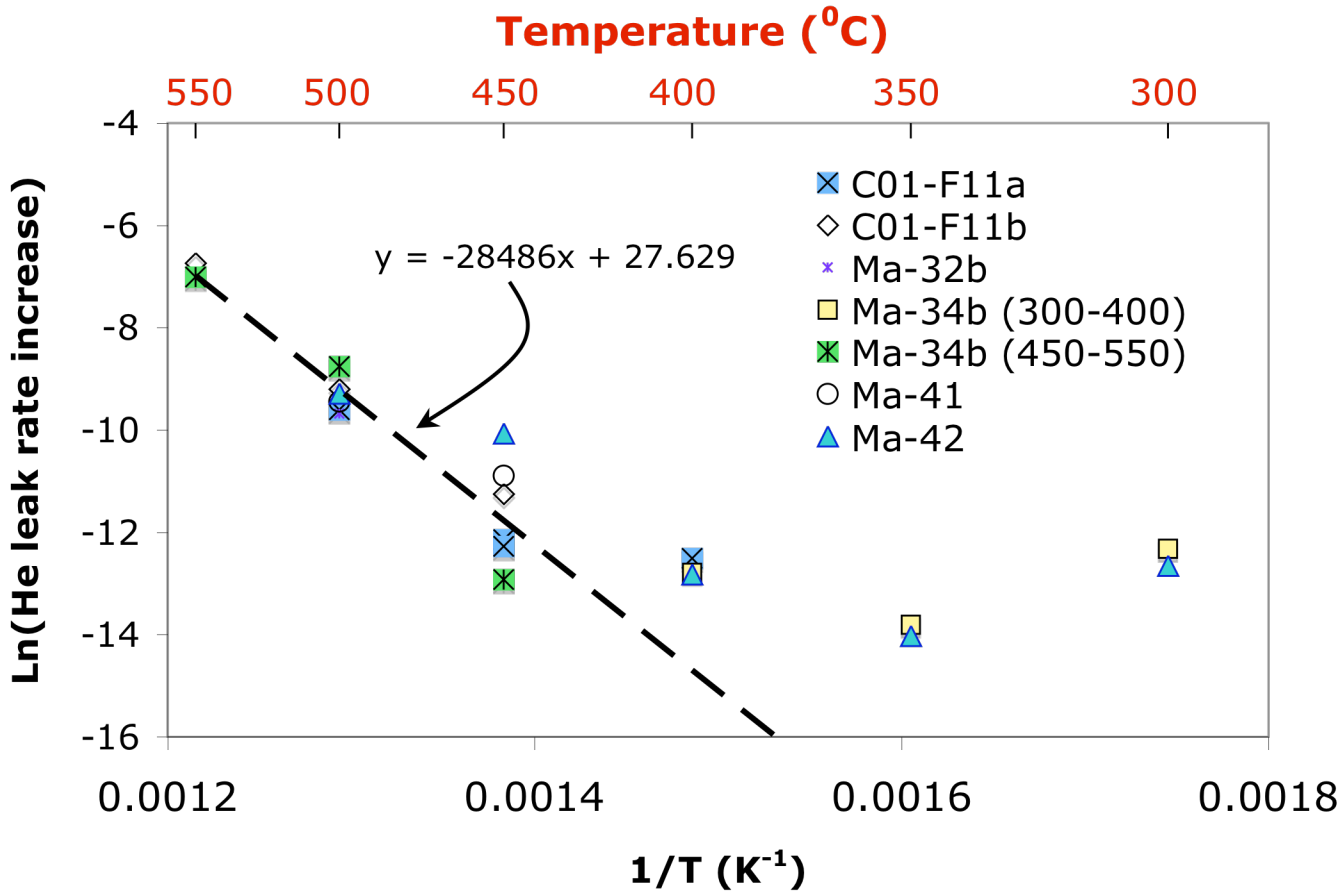

Figure 10-13 Arrhenius plot for membranes C01-F11a/11b and membranes Ma-32b, Ma-34b, Ma-41 and Ma-42. The activation energy was estimated in the 450-550°C temperature range.

The activation energy for the rate of increase was estimated to be 237 kJ·mol^{-1}, which closely matched the activation energy of Pd self diffusion coefficient of 266 kJmol^{-1}. Hence, leak growth was a diffusion-limited process, which required the diffusion of Pd atoms.

10.3.3 Leak growth in He atmosphere

In order to investigate the leak behavior of composite Pd membranes in H_2 and He, the He leak of membrane Ma-34b was measured as a function of time at 500ºC in both He and H_2 atmospheres. After storage and after 500 hr in H_2 at 450ºC, the He leak was measured (0.00285 m^3/(m^2 h bar)). The 450-500ºC temperature change was performed in He atmosphere (ΔP=1 bar) at a rate of 1ºC/min. The He leak did not grow during the temperature change. Therefore, at zero time at 500ºC, the He leak also equaled 0.00285 m^3/(m^2 h bar). After the temperature change, membrane Ma-34b was held in He atmosphere at 500ºC for 1,500 hr and the leak was monitored as a function of time. After 1,500 hr in He, H_2 was introduced for 500 hr. The leak which developed in H_2 atmosphere was measured three times by switching briefly back to He atmosphere. A similar procedure was used at 550ºC to measure the rate of increase in the He leak at 550ºC. The H_2 permeance of membrane Ma-34b at 450ºC was 24 m^3/(m^2 h bar$^{0.5}$) and was expected to be 28 m^3/(m^2 h bar$^{0.5}$) at 500ºC. However, after 1,500 hr in He at 500ºC the H_2 permeance was only 10 m^3/(m^2 h bar$^{0.5}$) and increased to 20 m^3/(m^2 h bar$^{0.5}$) after 350 hr in H_2 at 500ºC.

Industrial He contains some impurities (O_2, CO, CO_2) that were adsorbed on the surface of the Pd layer during the time the membrane was kept at 500ºC in He resulting in a very low H_2 permeance at 500ºC. The process was partially reversible since part of the

expected H_2 permeance (28 $m^3/(m^2\ h\ bar^{0.5})$) was recovered by holding the membrane in pure H_2 at 500ºC.

Figure 10-14 shows the He leak –He $leak_0$ of membrane Ma-34b at 500ºC in He atmosphere. The He leak started to increase after 300 hr following an "S" curve, characteristic of nucleation and growth processes. After 900-1000 hr the He leak reached a steady value equal to 0.0093 $m^3/(m^2\ h\ bar)$. After 1500 hr, H_2 was introduced and the He leak did not show the same pattern as in He atmosphere. The leak in H_2 atmosphere increased linearly ($1.57\ 10^{-4}\ m^3/(m^2\ h^2\ bar)$) and, assuming a linear rate increase in He atmosphere for he first 1000 hr, the leak increased 27 times faster in H_2 atmosphere than in He atmosphere ($5.85\ 10^{-6}\ m^3/(m^2\ h^2\ bar)$). The He leak of membrane Ma-32b as a function of time at 500ºC in H_2 atmosphere was also plotted for comparison purposes. The leak of membrane Ma-32b as a function of time follows a polynomial trend and was characterized by a short induction time of 100 hr.

After the induction time, the rate of increase in the He leak of membrane Ma-32b was considered as linear (last three data points) with a value equal to $8.73\ 10^{-5}\ m^3/(m^2\ h^2\ bar)$, which is close to the He leak increase of membrane Ma-34b at 500ºC in H_2 atmosphere. Therefore, the He leak was considered as linear in both He and H_2 atmosphere, after a short induction time in H_2 (100 hr) and longer induction time in He (300 hr). In He atmosphere, some process inhibited the growth of the leak while in H_2 atmosphere the leak grew continually.

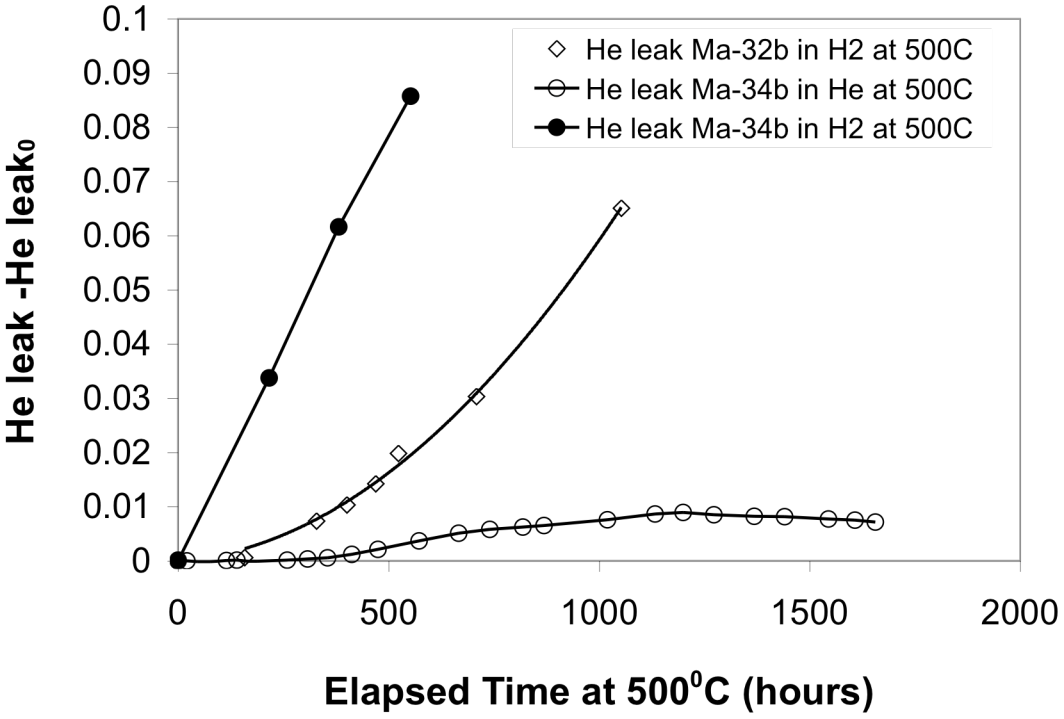

Figure 10-14 He leak increase at 500ºC of membrane Ma-34b in He atmosphere (circles) and in H_2 atmosphere (filled circles). The He leak increase of membrane Ma-32c at 500ºC in H_2 atmosphere was also plotted for comparison purposes.

10.3.4 Leaks in Pd-Cu membranes: the case of Ma-41

As already explained in Sections 2.1 and 7.1, one of the main purposes of alloying Pd with Cu is that the solubility of H_2 in Pd-Cu is very low, therefore, Pd-Cu are less prone to hydrogen stress problems and Pd-Cu alloys would develop less leaks than Pd membranes. It was of great interest to determine the leak stability of membrane Ma-41 at low temperatures (250-400ºC) and especially the leak behavior as a function of time at 450ºC and 500ºC in H_2 atmosphere to compare with composite Pd membranes. The He leak in He atmosphere at 300ºC was equal to 0.0048 $m^3/(m^2$ h bar) (selectivity H_2/He = 1050) after exposure to H_2 at 300ºC. After measuring H_2 permeance at 350 and 400ºC the He leak was measured at 400ºC in He atmosphere and equaled 0.0054 $m^3/(m^2$ h bar) (selectivity H_2/He = 1760). Since the He leak was almost unchanged up to 400ºC it appeared that the membrane microstructure did not change as the temperature was raised i.e. no changes in defects occurred at temperatures between 250 and 400ºC, which was consistent with the fact that the microstructure of composite Pd-PH structures did not change at temperatures lower than 400ºC (Sections 9.4.2.1 and Section 10.3.2). The initial He leak at 450ºC, determined with a GC analysis, equaled 0.0046 $m^3/(m^2$ h bar), which was equal to the He leak at 400ºC within experimental error. That is, the He leak did not increase during the 50 minutes (1ºC/min) of the temperature change. Figure 10-15 shows the He leak rate and selectivity (H_2/He) as a function of time at 450ºC and 500ºC in H_2. The selectivity steadily decreased as a function of time at 450 and 500ºC in H_2.

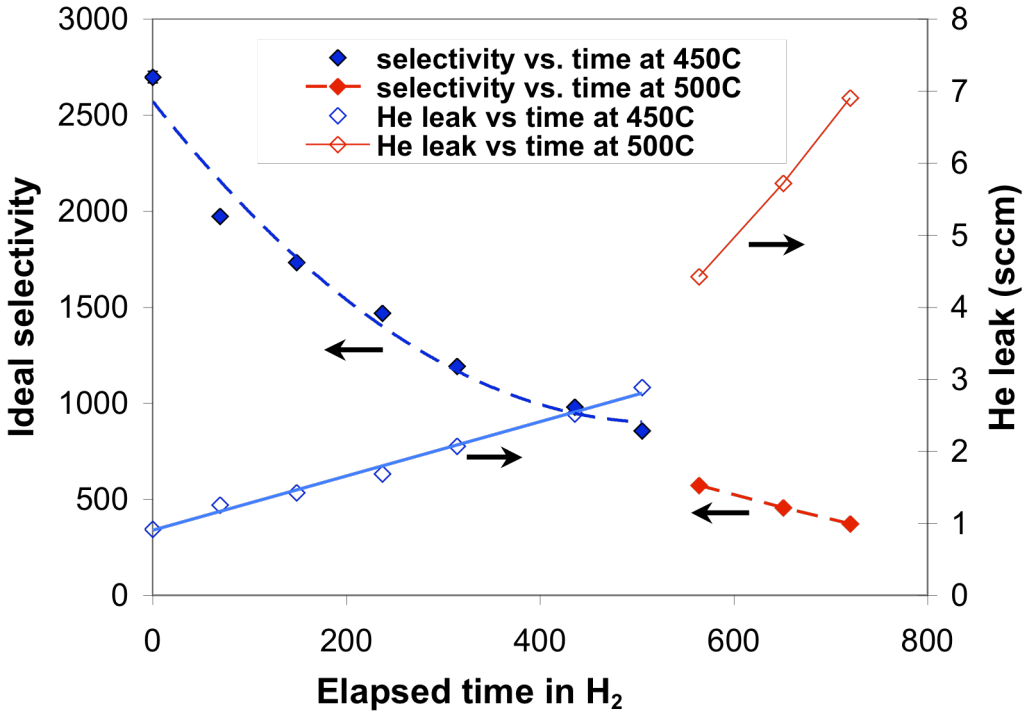

Figure 10-15 Ideal selectivity (H_2/He) and He leak (sccm[1]) as a function of time exhibited by the Pd-6.8wt% Cu membrane at 450°C in H_2 atmosphere

[1] sccm= standard cm^3 per minute

The rate at which the He leak increased was determined and plotted, as already seen, in Figure 10-13. The rate at which the He leak increased in Ma-41 was similar to the rate at which the He leak increased in membranes C01-F11a/11b, Ma-32b/34b/42. It is particularly interesting to note that at 450ºC, composite Pd membranes were under a compressive stress of magnitude around 10 MPa in H_2 atmosphere (see Figure 9-9) and that composite Pd-Cu membranes were most probably under a tensile stress of magnitude around 19 MPa at same conditions (see Figure 9-21). Apparently, the nature of the stress did not have large influences on the rate at which the leak developed in both type of composite membranes. That is due to the fact that stress do not play an important role in leak formation. That is, even though it was possible to lower the magnitude of the compressive stress at 450ºC for the Pd-Cu alloy, leaks still develop and at a similar rate than in Pd membranes. Hence, the reasons for leaks is the sintering of Pd clusters.

10.3.5 The formation of leaks in composite Pd membranes prepared by the electroless deposition technique

All materials keep excess energy in many ways such as stresses, surface energy in grain boundaries and metastable phases. Lower energy states are thermodynamically favorable. Many energy release mechanisms (sintering, dislocations, recrystallization) are diffusion-controlled mechanisms. Since diffusion is slow at low temperatures, materials kept at low temperatures will not undergo structural changes due to kinetics limitations (diffusion). At higher temperatures, when the activation energy for nucleation is overcome, diffusion is fast and the transformations occur. Fresh electroless Pd deposits were also characterized by an excess of energy since they were slightly porous and included a

significant number of Pd clusters (0.5μm) each one of which composed of thousands of 100nm Pd crystallites.

Moreover, fresh electroless Pd deposits are characterized by initial "intrinsic" tensile stresses and extrinsic stresses due to H_2 loading and Pd/support thermal coefficient mis-match. Therefore, electroless Pd deposits will undergo structural modifications at high temperatures i.e. at temperatures close to the Tamman temperature of Pd (m.p./2 in K), where Pd atoms acquire sufficient mobility. Section 9.4.2.3 showed that the temperature at which stress relaxation occurred was close to 400-450ºC and Section 0 showed that leaks started to develop at 400-450ºC. Section 10.3.2 showed that the leak development was a diffusion limited process with a high activation energy. Since the leak formation is a diffusion-limited process, any parameter affecting the diffusion of Pd atoms will have an impact on leak formation.

The Pd self-diffusion is a substitutional diffusion mechanism, that is, in order for a Pd atom to diffuse it needs first to overcome an activation barrier. Figure 10-16(a) depicts the jump of a Pd atom into a vacancy in a plane and Figure 10-16(b) depicts the jump of a Pd atom in a fcc cell (Porter and Easterling, 1981). In both cases, the jump of a Pd atom into a vacancy requires the stretch of other Pd atoms in between the Pd atom of interest and the vacancy. The absorption of H_2 leads to expansion of the Pd lattice cell, therefore the energy the Pd atom needs to overcome to jump into the vacancy is lower when H is dissolved in Pd. Indeed, Pd atoms 1 and 2 in Figure 10-16(a) are already stretched in H_2 atmosphere. Moreover, H_2 absorption leads to the increase of vacancies in Pd. Therefore, Pd self-diffusion coefficient is increased in H_2 atmosphere causing a faster leak growth in H_2 atmosphere than in He atmosphere as experimentally seen (see Figure 10-14)

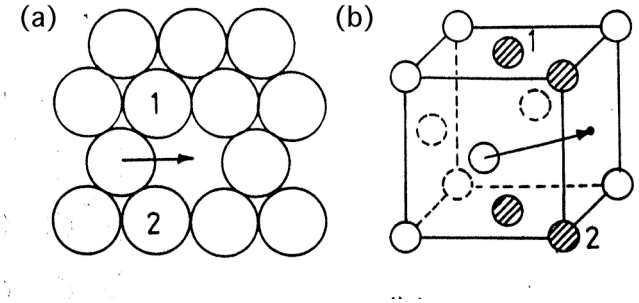

Figure 10-16 Jump into a vacant site. (a) Atoms 1 and 2 need to stretch. (b) The four dashed atoms need to stretch in the fcc cell (Porter and Easterling, 1981).

The process leading to the growth of Pd crystallites (see Figure 9-3(e)(f)) is sintering. The *sintering rate* is equal to the product of *mobility* and *stress* or *driving force,* which for sintering is defined as the surface energy times the surface curvature and is given by Equation (10-6)

$$\sigma_l = \gamma \cdot g \cdot (\frac{1}{R_1} + \frac{1}{R_2}) \qquad (10\text{-}6)$$

where γ is the interfacial energy, g a geometric constant, R_1 and R_2 are the curvature radii at the surface. For spherical particles R_1 and R_2 are equal and g equals to 1. Hence, smaller particles lead to higher stresses and faster sintering rates. Mobility refers to the speed of the process involved during sintering. Processes may be: surface diffusion (predominant at low temperatures), volume diffusion, grain boundary diffusion, plastic flow (when microstructure is highly curved) and dislocation climb. Electroless Pd deposits are characterized by a relatively high driving force for sintering due to their fine grain structure (100 nm Pd crystallites). The release of stresses at 400-450ºC (Section 9.4.2.3) and Figure 9-4 indicated that sintering started at 400-450ºC.

Sintering can occur coherently and incoherently (Skorokhod, 2003). Coherent sintering leads to a homogenous and high-density (close to or equal to the bulk material) material. However, incoherent sintering leads to evolution of pores and microholes due to local densification or differential shrinkage. Differential shrinkage is characteristic of sintering in ultra-fine materials. Coherent and incoherent sintering are depicted in Figure 10-17 from simulations performed by Skorokhod (2003).

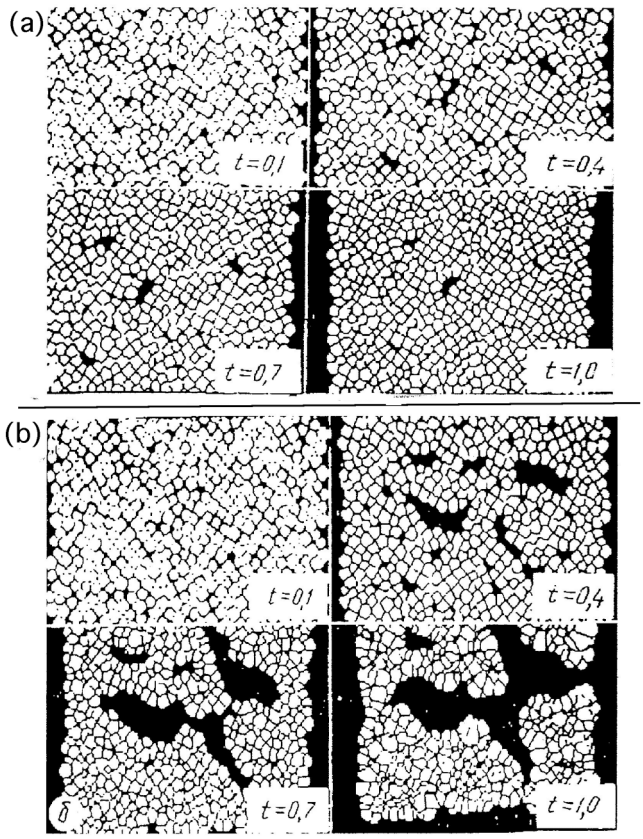

Figure 10-17 Mathematical simulation of (a) coherent sintering and (b) incoherent sintering (Skorokhod, 2003)

Figure 10-17(a) shows a simulation of the coherent sintering of small particles at different times. Figure 10-17(b) shows a simulation of the incoherent sintering of small particles at different times. Incoherent sintering leads to the formation of local voids.

It is known that the sintering process of metals depends on the sintering atmosphere. Indeed, faster densification was obtained for martensic steels in a 60%H_2-40%N_2 mixture than in pure N_2 (Blaine et al., 2003). H_2 reduced surface oxides formed at the grain boundaries increasing grain boundary mobility and therefore decreasing sintering time. It was possible that a thin oxide film at the Pd grain boundaries inhibited the grain growth or Pd cluster sintering in He atmosphere. However, the thin oxide layer was reduced in the presence of H_2 leading to incoherent sintering, leak formation and leak growth.

10.4 Conclusions

Raising water tests on Ma-32 showed that leaks in Pd membranes were uniformly distributed on the surface. Pinhole formation was faster at 550ºC than at 500ºC. The leak growth was found to be to diffusion-limited process with an activation energy equal to 237 kJ mol^{-1}, which corresponded to the activation energy of Pd self-diffusion coefficient. The fact that the leak growth was a diffusion-limited process was in agreement with the finding that leaks grew faster in H_2 atmosphere. Indeed, absorbed H in the Pd increases the self-diffusion coefficient of Pd. Pinhole formation at temperatures higher than 450ºC was due to incoherent sintering of the small (100nm) Pd crystallites.

.

11 Conclusions

- A new technique using pre-activated Al_2O_3 particles of different sizes was developed to grade the porous metal supports to obtain a very smooth surface with a narrow pore size distribution. The composite Pd membranes achieved on graded porous metal supports were as thin as 5.6 μm.
- The H_2 permeance of composite Pd and membranes prepared on graded PH supports was as high as 50 $m^3/(m^2\ h\ bar^{0.5})$. H_2 permeances as high as 93 $m^3/(m^2\ h\ bar^{0.5})$ were expected however, the presence of mass transfer within the porous support strongly affected the H_2 permeance.
- The H_2 permeance of composite Pd membranes prepared on graded PH supports was stable over 1100 hr at 500ºC in H_2 atmosphere.
- The H_2 permeance was enhanced by the oxidation of the membrane surface at 350ºC for 48 hr.
- The selectivity (H_2/He) of composite Pd membranes prepared on graded supports was higher than 300 for periods of time over 1100 hr at 500ºC in H_2 atmosphere. The selectivity of all membranes at temperatures lower than 400ºC was as high as 1000.
- Pd-Cu membranes prepared on graded supports showed permeances as high as 30 $m^3/(m^2\ h\ bar^{0.5})$ at 450ºC with a selectivity (H_2/He) equal to 900.

- The ordering transformation fcc→bcc occurred with the fastest rate at 400-450ºC with a 50% conversion after only 60 seconds.
- Thin Pd films deposited with the electroless deposition method were characterized by a nanocrystalline structure with Pd crystallites of 50-100 nm.
- It was found that, at low temperatures, part of the H_2 permeating through the composite Pd membranes, diffused through Pd grain boundaries.
- Microstrains and initial intrinsic stresses release occurred at 400ºC without visible sintering of Pd clusters. The release of microstrains and initial intrinsic stresses did not affect membrane selectivity.
- At temperatures higher than 400ºC, the energy was sufficient for thermal stresses to be released, which occurred with significant sintering of Pd grains and clusters.
- PH supports were more suited for the preparation of composite Pd membranes. The presence of a thick Cr_2O_3 layer drastically inhibited intermetallic diffusion at 500ºC. The Cr_2O_3 layer was not reduced in H_2 atmosphere and high temperatures (600ºC). All PH supports had a large mass transfer resistance.
- A model was developed to predict the effect of mass transfer resistance within the porous support of composite Pd membranes on the H_2 permeation mechanism. The activation energy for H_2 permeation data of all membranes were in good agreement with the mass transfer model.
- For the first time, the kinetics of H_2 flux decline were measured and showed that, at temperatures lower than 500ºC intermetallic diffusion occurred by the diffusion of Fe through Pd grain boundaries. At temperature higher than

500ºC, intermetallic diffusion took place by the diffusion of Fe through the Pd lattice.

- For the first time, the kinetics of selectivity decline were measured and showed that, leak growth was a diffusion-limited process and was attributed to the in-coherent sintering of Pd nano-crystallites.
- Thermal stresses and hydrogen stresses had no influence on selectivity decline.

12 Recommendations

In order to achieve composite Pd membranes with higher H_2 permeance and even better long-term stability, further research should focus on:

- The use of porous metal supports having a larger He permeance than PH supports in order to avoid mass transfer limitations.
- Develop thinner and more stable barriers for the inhibition of the intermetallic diffusion phenomena. The formation or deposition of the barrier should not lead to a large decrease of the He permeance of the bare support to avoid mass transfer limitations.
- The study of other smoothing techniques such as deposition of γ-alumina by the sol gel method. very smooth surfaces can be achieved by first grading the support with pre-activated Al_2O_3 particles followed by a thin (0.2-0.4 μm) of a sol gel layer.
- A further study on Pd surface modification is needed. The deposition of a thin layer of Pd black may lead to the increase of the H_2 permeance. If so, investigate the reasons for the increase in H_2 permeance.
- The study of the sintering mechanism of electroless thin Pd deposits by in-situ electron microscopic techniques. This experiment will further substantiate the incoherent sintering mechanism.

- The synthesis of Pd-Cu membranes having 40-42 wt% Cu on engineered surfaces.
- The study of the ordering/disordering transformation in a composite Pd -40 wt% Cu membrane on the leak stability of the membrane.

To avoid the sintering of Pd nano-crytsallites two approaches can lead to similar results: start from the beginning with a membrane having large Pd grains (no surface excess energy) or, freeze the initial microstructure. The following experiments are of great importance

- Study a composite Pd membrane with no excess energy to avoid incoherent sintering. A composite Pd membrane with no excess energy can be prepared by sputtering deposition (or CVD) and by heating the support at a temperature of 450ºC during deposition. The leak of this composite Pd membrane should not grow.
- Harden Pd with refractory metals to reduce the mobility of grain boundaries thereby, decreasing the sintering rate. This idea is based on the Zenner pinning effect of grain boundaries, which is commonly seen in metallographic studies.

References

Abys, J. A. (1964). U.S patent 4,424,241.

Aggarwal, S., A. P. Monga, S. R. Perusse, R. Ramesh, V. Ballarotto, E. D. Williams, B. R. Chalamala, Y. Wei and R. H. Reuss (2000). "Spontaneous ordering of oxide nanostructures." *Science* 287.

Akis, B. C., E. E. Engwall, P. I. Mardilovich and Y. H. Ma (2003). "Effects of the in-situ formation of an intermetallic diffusion barrier layer on the properties of composite palladium membranes." *American Chemical Society, Preprints* 48(1): 337-338.

Ali, J. K., E. J. Newson and D. W. T. Rippin (1994). "Deactivation and regeneration of Pd-Ag membranes for dehydrogenation reactions." *Journal of Membrane Science* 89(1-2): 171.

Athayde, A. L., R. W. Baker and P. Nguyen (1994). "Metal composite membranes for hydrogen separation." *Journal of Membrane Science* 94(1): 299.

Babanov, Y. A., L. A. Blaginina, I. V. Golovshchikova, T. Haubold, F. Boscherini and S. Mobilio (1997). "Defects in nanocrystalline palladium." *The physics of metals and metallography* 83(4): 444-451.

Balovnev, Y. A. (1974). "Diffusion of hydrogen in palladium." *Russian Journal of Physical Chemistry* 48(3): 409-410.

Baranowski, B., S. Majchrzak and T. B. Flanagan (1971). "The volume increase of fcc metals and alloys due to interstitial hydrogen over a wide range of hydrogen contents." *j. Phys. F: Metal Phys.* 1: 258-261.

Bartlett, A. A. (2000). "An analysis of U.S and world oil production patterns using Hubbert style curves." *Mathematical Geology* 32(1).

Blaine, D. C., Y. Wu, C. E. Schlaefer, B. Marx and R. M. German (2003). "Sintering shrinkage and microstructure evolution during densification of a martensitic stainless steel."

Bogdanov, S. V., E. M. Moroz and S. V. Tsylbulya (1984). "Investigation of substructure of catalysts by x-ray diffractions methods." *Kinetics and Catalysis* 25(5): 1028-1032.

Brandes, E. A. and G. B. Brook (1998). *Smithells Metals Reference Book (7th Edition)*, Elsevier.

Brodowsky, H. and E. Poeschel (1965). *Z. phys. Chem. N.F* 44: 143.

Bryden, K. J. and J. Y. Ying (2002). "Nanostructured palladium-iron membranes for hydrogen separation and membrane hydrogenation reactions." *Journal of Membrane Science* 203: 29-42.

Campbell, J. C. and J. H. Laherrere (1998). "The end of cheap oil." *Scientific American* 278(3): 78-83.

Checchetto, R., N. Bazzanella, B. Patton and A. Miotello (2004). "Palladium membranes prepared by r.f. magnetron sputtering for hydrogen purification." *Surface and Coatings Technology* 177-178: 73-79.

Cheng, Y. S., M. A. Pena, J. L. Fierro, D. C. W. Hui and K. L. Yeung (2002). "Performance of alumina, zeolite, palladium, Pd-Ag alloy membranes for hydrogen separation from Towngas mixture." *Journal of Membrane Science* 204(1-2): 329.

Cheng, Y. S. and K. L. Yeung (2001). "Effects of electroless plating chemistry on the synthesis of palladium membranes." *Journal of Membrane Science* 182(1-2): 195.

Collins, J. P. and J. D. Way (1993). "Preparation and characterization of a composite Palladium-ceramic membrane." *Ind. Eng. Chem. Res.* 32: 3006-3013.

Collins, S. R. (1998). "Stainless steel for semi-conductor applications." *Mechanical working and steel processing conference proceedings*(35): 607-619.

Cullity, B. D. and S. R. Stock (2001). *Elements of x-ray diffraction*. Upper Saddle River, NJ, Prentice Hall, Edition: 3rd ed.

Davis, W. (1954). *USAEC Report KAPL-1227, U. S. Atomic Energy Commission*.

Dirks, A. G. (1977). "Columnar microstructure in vapor-deposited thin films." *Thin Solid Films* 49: 219.

Duncan, R. C. and W. Youngquist (1999). "Encircling the peak of world oil production." *Natural Resources Research* 8(3): 219-232.

Eastman, J. A., L. J. Thompson and B. J. Kestel (1993). "Narrowing of the palladium-hydrogen miscibility gap in nanocrystalline palladium." *Physical Review B* 48(1): 84-92.

Edlund, D. J. and J. McCarthy (1995). "The relationship between intermetallic diffusion and flux decline in composite-metal membranes: implications for achieving long membrane lifetime." *Journal of Membrane Science* 107(1-2): 147.

Edlund, D. J. and W. A. Pledger (1993). "Thermolysis of hydrogen sulfide in a metal-membrane reactor." *Journal of Membrane Science* 77(2-3): 255.

Edlund, D. J. and W. A. Pledger (1994). "Catalytic platinum-based membrane reactor for removal of H_2S from natural gas streams." *Journal of Membrane Science* 94(1): 111.

Edwards, J. D. (1997). "Crude oil and alternative energy forecasts of the twenty-first century. The end of hydrocarbon era." *American Association of Petroleum Geologists Bulletin* 81: 1292-1305.

Farias, D., M. Patting and K. H. Rieder (1997). "Helium diffraction investigations of the transition of chemisorbed hydrogen into subsurfaces sites on palladium surfaces." *Phys. stat. sol. (a)* 159: 255-262.

Farr, J. P. G. and I. R. Harris (1973). U.S. patent 3,713,270.

Fazle Kibria, A. K. M. and Y. Sakamoto (2000). "The effect of alloying of palladium with silver and rhodium on the hydrogen solubility, miscibility gap and hysteresis." *International Journal of Hydrogen Energy* 25(9): 853.

Flanagan, T. B., G. Gross and J. D. Clewley (1977). "Absorption and diffusion of hydrogen in palladium/iron alloys." *Hydrogen in metals: Proceedings of the 2nd international congress, Paris, 6-10 june, 1977*.

Floro, J. A., S. J. Hearne, J. A. Hunter, P. Kotula, E. Chason, S. C. Seel and C. V. Thompson (2001). "The dynamic competition between stress generation and relaxation mechanisms during coalescence of Volmer-Weber thin films." *Journal of applied physics.* 89(9): 4886-4897.

Fort, D., J. P. G. Farr and I. R. Harris (1975). *Journal of less common metals* 39(2): 293.

Frieske, H. and E. Wicke (1973). "Magnetic susceptibility and equilibrium diagram of PdH_n." *Ber. Bunsenges. Physik. Chem.* 77: 48-52.

Galuszka, J., R. N. Pandey and S. Ahmed (1998). "Methane conversion to syngas in a palladium membrane reactor." *Catalysis Today* 46(2-3): 83.

Gao, H., J. Y. S. Lin, Y. Li and B. Zhang (2005). "Electroless plating synthesis, characterization and permeation properties of Pd-Cu membranes supported on ZrO2 modified porous stainless steel." *Journal of Membrane Science* 265(1-2): 142.

Gillespie, L. J. and L. S. Galstaun (1936). "The palladium-hydrogen equilibrium and new palladium hydrides." *Journal of the American Chemical Society* 58: 2565-2573.

Gillespie, L. J. and F. P. Hall (1926). "The palladium-hydrogen equilibrium and palladium hydride." *Journal of the American Chemical Society* 48: 1207-1219.

Graham, T. (1869a). *Proc. R. Soc.* 17: 212.

Graham, T. (1869b). *Proc. R. Soc.* 17: 500.

Gryaznov, V. (2000). "Metal containing membranes for the production of ultrapure hydrogen and the recovery of hydrogen isotopes." *separation and Purification Methods* 29(2).

Gryaznov, V. M., O. S. Serebyannikova and Y. M. Serov (1993). " Preparation and catalysis over palladium composite membranes." *Applied Catalysis A: General* 96: 15-23.

Guazzone, F., M. E. Ayturk and Y. H. Ma (2004). *Effect of intermetallic diffusion barrier on the stability of composite Pd/PSS membranes at high temperatures*. Annual international Pittsburgh Coal Conference, 21st, Japan, Pittsburgh Coal Conference.

Han, J., I.-S. Kim and K.-S. Choi (2002). "High purity hydrogen generator for on-site hydrogen production." *International Journal of Hydrogen Energy* 27(10): 1043.

Han, J., G. Zhu, D. Y. Zemlyanov and F. H. Ribeiro (2004). "Increase of Pd surface area by treatment in dioxygen." *Journal of Catalysis* 225(1): 7.

Hoang, H. T., H. D. Tong, F. C. Gielens, H. V. Jansen and M. C. Elwenspoek (2004). "Fabrication and characterization of dual sputtered Pd-Cu alloy films for hydrogen separation membranes." *Materials Letters* 58(3-4): 525.

Holleck, G. L. (1970). "Diffusion and solubility of hydrogen in palladium and palladium-silver alloys." *The journal of Physical Chemistry* 74(3): 503-511.

Hough, W. V., J. L. Little and K. V. Warheit (1981). U.S patent 4,255,194.

Howard, B. H., R. P. Killmeyer, K. S. Rothenberger, A. V. Cugini, B. D. Morreale, R. M. Enick and F. Bustamante (2004). "Hydrogen permeance of palladium-copper alloy membranes over a wide range of temperatures and pressures." *Journal of Membrane Science* 241(2): 207.

Hunter, J. B. (1960). "A new hydrogen purification process." *Plat. Met. Rev.* 4: 130-131.

IEA (1997). "International Energy Agency. “World energy prospect to 2020”." *Paper prepared for the G8 energy ministers’ meeting Moscow March 31 - April 1*.

Itoh, N., Y. Kaneko and A. Igarashi (2002). "Efficient hydrogen production via methanol steam reforming by preventing back-permeation of hydrogen in a palladium membrane reactor." *Ind. Eng. Chem. Res.* 41(19): 4702-4706.

Itoh, N., S. Niwa, F. Mizukami, T. Inoue, A. Igarashi and T. Namba (2003). "Catalytic palladium membrane for reductive oxidation of benzene to phenol." *Catalysis Communications* 4(5): 243.

Janßen, S., H. Natter, R. Hempelmann, T. Striffler, U. Stuhr, H. Wipf, H. Hahn and J. C. Cook (1997). "Hydrogen diffusion in nanocrystalline Pd by means of quasielastic neutron scattering." *Nanostructured Materials* 9: 579-582.

Jayaraman, V. and Y. S. Lin (1995). "Synthesis and hydrogen permeation properties of ultrathin palladium-silver alloy membranes." *Journal of Membrane Science* 104(3): 251.

Jemaa, N., J. Shu, S. Kaliaguine and B. P. A. Grandjean (1996). "Thin Palladium Film Formation on Shot Peening Modified Porous Stainless Steel Substrates." *Ind. Eng. Chem. Res.* 35(3): 973-977.

Jun, C.-S. and K.-H. Lee (2000). "Palladium and palladium alloy composite membranes prepared by metal-organic chemical vapor deposition method (cold-wall)." *Journal of Membrane Science* 176(1): 121.

Kamakoti, P., B. D. Morreale, M. V. Ciocco, B. H. Howard, R. P. Killmeyer, A. V. Cugini and D. S. Sholl (2005). "Prediction of Hydrogen Flux Through Sulfur-Tolerant Binary Alloy Membranes." *Science* 307(5709): 569.

Kamakoti, P. and D. S. Sholl (2003). "A comparison of hydrogen diffusivities in Pd and CuPd alloys using density functional theory." *Journal of Membrane Science* 225(1-2): 145.

Karpova, R. A. and I. P. Tverdovskii (1959). *J. Scient. Instrum.* 33: 615.

Kawagoshi, S. (1977). Japanese patent (Kokai Tokkyo Koho) 77-733.

Keuler, J. N. and L. Lorenzen (2002). "Developing a heating procedure to optimize hydrogen permeance through Pd-Ag membranes of thickness less than 2.2 mm." *Journal of Membrane Science* 195(2): 203.

Keuler, J. N., L. Lorenzen, R. N. Sanderson and V. Linkov (1977). "Optimizing palladium conversion in electroless palladium plating of alumina membranes." *Plating and surface finishing*: 34-40.

Kikuchi, E. (2000). "Membrane reactor application to hydrogen production." *Catalysis Today* 56(1-3): 97.

Kikuchi, E., Y. Nemoto, M. Kajiwara, S. Uemiya and T. Kojima (2000). "Steam reforming of methane in membrane reactors: comparison of electroless-plating and CVD membranes and catalyst packing modes." *Catalysis Today* 56(1-3): 75.

Klug, H. P., L. E. Alexander and joint author (1954). *X-ray diffraction procedures for polycrystalline and amorphous materials*, New York, Wiley.

Knapton, A. G. (1977). "Palladium alloys for hydrogen diffusion membranes-A review of high permeability materials." *Plat. Met. Rev.* 21: 44-50.

Koch, C. C. (2002). *Nanostructured Materials - Processing, Properties and Potential Applications*, William Andrew Publishing/Noyes.

Koch, R. (1994). "The intrinsic stress of polycrystalline and epitaxial thin metal films." *j. Phys.: Condens. Matter*(6): 9519-9550.

Koffler, S. A., J. B. Hudson and G. S. Ansell (1969). "Hydrogen permeation through alpha-palladium." *Transactions of the Metallurgical Society of AIME* 245: 1735-1740.

Kurman, P. V., I. P. Mardilovich and A. I. Trokhimets (1990). "Behavior of absorbed hydrogen in the Pd/g-Al_2O_3 system." *Russian Journal of Physical Chemistry* 64(3).

Lafferty, E. J., D. J. Macauley, P. V. Kelly and G. M. Crean (1997). "Atomic force microscopy investigation of the morphology of a UV photodefined palladium activation layer on alumina ceramic and the nucleation of electroless copper at the activated sites." *Mat. Res. Soc. Symp. Proc.* 441: 329-334.

Lee, D.-W., Y.-G. Lee, S.-E. Nam, S.-K. Ihm and K.-H. Lee (2003). "Study on the variation of morphology and separation behavior of the stainless steel supported membranes at high temperature." *Journal of Membrane Science* 220(1-2): 137.

Levine, P. L. and K. E. Weale (1960). "The palladium + hydrogen equilibrium at high pressures and temperatures." *Transactions Faraday Society* 56: 357-362.

Lewis, F. A. (1967). *The palladium hydrogen system*, London, New York, Academic Press.

Li, A., W. Liang and R. Hughes (1998). "Characterization and permeation of palladium/stainless steel composite membranes." *Journal of Membrane Science* 149: 259-268.

Li, A., G. Xiong, J. Gu and L. Zheng (1996). "Preparation of Pd/ceramic composite membrane 1. Improvement of the conventional preparation technique." *Journal of Membrane Science* 110(2): 257.

Li, Y. and Y.-T. Cheng (1996). "Hydrogen diffusion and solubility in palladium thin films." *International Journal of Hydrogen Energy* 21(4): 281-291.

Li, Z. Y., H. Maeda, K. Kusakabe, S. Morooka, H. Anzai and S. Akiyama (1993). "Preparation of palladium-silver membranes for hydrogen separation by the spray pyrolysis method." *Journal of Membrane Science* 78: 247-254.

Lin, Y.-M., G.-L. Lee and M.-H. Rei (1998). "An integrated purification and production of hydrogen with a palladium membrane-catalytic reactor." *Catalysis Today* 44(1-4): 343.

Lin, Y.-M. and M.-H. Rei (2000). "Process development for generating high purity hydrogen by using supported palladium membrane reactor as steam reformer." *International Journal of Hydrogen Energy* 25(3): 211.

Lin, Y.-M. and M.-H. Rei (2001). "Study on the hydrogen production from methanol steam reforming in supported palladium membrane reactor." *Catalysis Today* 67(1-3): 77.

Ma, Y. H., B. C. Akis, M. E. Ayturk, F. Guazzone, E. E. Engwall and I. P. Mardilovich (2004). "Characterization of Intermetallic Diffusion Barrier and Alloy Formation for Pd/Cu and Pd/Ag Porous Stainless Steel Composite Membranes." *Ind. Eng. Chem. Res.* 43(12): 2936-2945.

Ma, Y. H. and F. Guazzone (2004). 1021.2013-000 pending.

Ma, Y. H., I. P. Mardilovich and P. P. Mardilovich (2001). "Effects of porosity and pore size distribution of the porous stainless steel on the thickness and hydrogen flux of palladium membranes." *Journal of the American Chemical Society* 46(2).

Ma, Y. H., P. P. Mardilovich and Y. She (1998). *Stability of hydrogen flux through Pd/Porous Stainlees Steel Composite Membranes, Extended abstract*. The Fifth International Conference on Inorganic Membranes, Nagoya, Japan June 22-26.

Ma, Y. H., P. P. Mardilovich and Y. She (2000). Hydrogen gas-extraction module and method of fabrication. U. S. A. 6,152,987.

Mardilovich, P. P., Y. She, Y. H. Ma and M.-H. Rei (1998). "Defect-Free Palladium Membranes on Porous Stainless-Steel Support." *AIChe journal* 44(2): 310.

Marigliano, G., G. Barbieri and E. Drioli (2003). "Equilibrium conversion for a Pd-based membrane reactor. Dependence on the temperature and pressure." *Chemical engineering and processing* 42: 231-236.

Matzakos, A. N., S. L. Wellington, T. Mikus and J. M. Ward (2003). Integrated flameless distributed combustion/steam reforming membrane reactor for hydrogen production and use thereof in zero emissions hybrid power system. U. S. US 2003/0068269 A1.

McCool, B. A. and Y. S. Lin (2001). "Nanostructured thin Palladium-Silver membranes: effects of grain size on gas permeation properties." *Journal of Material Science* 36: 3221-3227.

McKinley, D. L. (1967). U.S patent 3,350,845.

McKinley, D. L. (1969). U.S patent 3,439,474.

Mitacek, P., Jr. and J. G. Aston (1963). "The thermodynamic properties of pure palladium and its alloys with hydrogen between 30 and 300°K." *Journal of the American Chemical Society* 85(2): 137-141.

Mizumoto, S., H. Nawabune, M. Haga and K. Tsuji (1986). *Extended abstracts of papers presented at the 73rd Tech. Conf., Metal Finish. Soc. Japan, 27B-8*: 116.

Morreale, B. D., M. V. Ciocco, R. M. Enick, B. I. Morsi, B. H. Howard, A. V. Cugini and K. S. Rothenberger (2003). "The permeability of hydrogen in bulk palladium at elevated temperatures and pressures." *Journal of Membrane Science* 212(1-2): 87.

Morreale, B. D., M. V. Ciocco, B. H. Howard, R. P. Killmeyer, A. V. Cugini and R. M. Enick (2004). "Effect of hydrogen-sulfide on the hydrogen permeance of palladium-copper alloys at elevated temperatures." *Journal of Membrane Science* 241(2): 219.

Murakami, M. (1991). "Deformation in thin films by thermal strain." *Journal of Vacuum Science and Technology A* 9(4): 2469-2476.

Müller, K. H. (1985). *J. Appl. Physics* 58: 2573.

Mütschele, T. and R. Kirchheim (1987). "Segregation and diffusion of hydrogen in grain boundaries of palladium." *Scripta metallurgica* 21: 135-140.

Nam, S.-E. and K.-H. Lee (2000). "A study on the palladium/nickel composite membrane by vacuum electrodeposition." *Journal of Membrane Science* 170(1): 91.

Nam, S.-E. and K.-H. Lee (2001). "Hydrogen separation by Pd alloy composite membranes: introduction of diffusion barrier." *Journal of Membrane Science* 192(1-2): 177.

Nam, S.-E., S.-H. Lee and K.-H. Lee (1999). "Preparation of a palladium alloy composite membrane supported in a porous stainless steel by vacuum electrodeposition." *Journal of Membrane Science* 153(2): 163.

Nam, S. E. and K. H. Lee (2005). "Preparation and Characterization of Palladium Alloy Composite Membranes with a Diffusion Barrier for Hydrogen Separation." *Ind. Eng. Chem. Res.* 44(1): 100-105.

Ohno, I., O. Wakabayashih and S. Haruyama (1985). "Anodic oxidation of reductants in electroless plating." *J. Electrochem. Soc.: electrochemical science and technology* 132(10): 2323-2330.

Pearlstein, F. and R. F. Weightman (1969). *Plating* 56(10): 1158.

Porter, D. A. and K. E. Easterling (1981). *Phase transformations in metals and alloys*, Van Nostrand Reinhold Company Ltd.

Radzhabov, T. D., L. Y. Alimova, E. Y. Zhukova and F. S. Melkumyan (1980). "Effect of thin-film coatings on the hydrogen permeability of metals." *Russian Journal of Physical Chemistry* 54(11): 1605-1606.

Ragaini, V., R. Giannantonio, P. Magni, L. Lucarelli and G. Leofanti (1994). "Dispersion measurement by the single introduction method coupled with the back-sorption procedure: a chemisorption and TPD study on the different chemisorbed hydrogen species." *Journal of Catalysis* 146: 116-125.

Rajamani, A., B. W. Sheldon, E. Chason and A. F. Bower (2002). "Intrinsic tensile stress and grain boundary formation during Volmer-Weber film growth." *Applied Physics Letters* 81(7).

Reimann, K. and R. Wurschum (1997). "Distribution of internal strains in nanocrystalline Pd studied by x-ray diffraction." *Journal of applied physics.* 81(11).

Reva, O. V. and T. N. Vorob'eva (2002). "Oxidation, Hydrolysis, and Colloid Formation in Storage of SnCl2 Aqueous Solutions." *Russian Journal of Applied Chemistry* 75(5): 700-705.

Rhoda, R. N. (1959a). *Trans. Inst. Metal Finish.* 36: 82.

Rhoda, R. N. (1959b). U.S patent 2,915,406.

Roa, F. and J. D. Way (2005). "The effect of air exposure on palladium-copper composite membranes." *Applied Surface Science* 240(1-4): 85.

Roa, F., J. D. Way, R. L. McCormick and S. N. Paglieri (2003). "Preparation and characterization of Pd-Cu composite membranes for hydrogen separation." *Chemical Engineering Journal* 93(1): 11.

Roshan, N. R., A. P. Mishchenko, V. P. Polyakova, N. I. Parfenova, E. M. Savitsky, E. A. Voitekhova, V. M. Gryaznov and M. E. Sarylova (1983). "The effect of the surface state on the hydrogen permeability and the catalytic activity of palladium alloy membranes." *Journal of less common metals* 89: 423-428.

Rothenberger, K. S., A. V. Cugini, B. H. Howard, R. P. Killmeyer, M. V. Ciocco, B. D. Morreale, R. M. Enick, F. Bustamante, I. P. Mardilovich and Y. H. Ma (2004). "High pressure hydrogen permeance of porous stainless steel coated with a thin palladium film via electroless plating." *Journal of Membrane Science* 244(1-2): 55.

Sanders, P. G., J. A. Eastman and J. R. Weertman (1998). "Pore distributions in nanocrystalline metals from small-angle neutron scattering." *Acta Materialia* 46(12): 4195.

Sanders, P. G., A. B. Whitney, J. R. Weertman, R. Z. Valiev and R. W. Siegel (1995). *Mater. Sci. Eng. A* 204: 7.

Sergienko, A. (1968). U. S. patent 3,418,143.

She, Y. (2000). Composite palladium membranes: synthesis, separation and reaction. Chemical Engineering. Worcester, Worcester Polytechnic Institute. PhD.

Shirasaki, Y. O., Y. Ohta, K. Kobayashi and K. Kuroda (1997). "Development of a hydrogen separation reformer." *Proceedings of the 27th annual meeting of Japan petroleum institute*: 247.

Shu, J., A. Adnot, B. P. A. Grandjean and S. Kaliaguine (1996). "Structurally stable composite Pd-Ag alloy membranes: Introduction of a diffusion barrier." *Thin Solid Films* 286: 72-79.

Shu, J., B. P. A. Grandjean, A. Van Neste and S. Kaliaguine (1991). "Catalytic palladium-based membrane reactors; a review." *The canadian journal of chemical engineering* 69: 1036-1060.

Shukla, S., S. Seal, J. Akesson, R. Oder, R. Carter and Z. Rahman (2001). "Study of mechanism of electroless copper coating of fly-ash cenosphere particles." *Applied Surface Science* 181: 35-50.

Sieverts, A., E. Jurisch and A. Metz (1915). *Z. anorg. allg. Chem.* 92: 329.

Skorokhod, V. V. (2003). *SURFACE RELAXATION AND LOCAL DENSIFICATION IN NANOSIZED SYSTEMS AT ISOTHERMAL SINTERING*. Sintering 2003: An International Conference on the Science, Technology & Applications of Sintering, https://www.mri.psu.edu/conferences/sint03/pdf/Skorokhod_1_3.pdf.

Souleimanova, R. S., A. S. Mukasyan and A. Varma (2000). "Effects of osmosis on microstructure of Pd-composite membranes synthesized by electroless plating technique." *Journal of Membrane Science* 166(2): 249.

Souleimanova, R. S., A. S. Mukasyan and A. Varma (2002). "Pd membranes formed by electroless plating with osmosis: H_2 permeation studies." *AIChe journal* 48(2): 262-268.

Souleimanova, R. S., M. A. S. and A. Varma (2001). "Pd-composite membranes prepared by electroless plating and osmosis: synthesis, characterization and properties." *Separation and Purification Technology* 25(1-3): 79-86.

Su, C., T. Jin, K. Kuraoka, Y. Matsumura and T. Yazawa (2005). "Thin Palladium Film Supported on SiO_2-Modified Porous Stainless Steel for a High-Hydrogen-Flux Membrane." *Ind. Eng. Chem. Res.* 44(9): 3053-3058.

Subramanian, P. R. and D. E. Laughlin (1991). "Cu-Pd (Copper-Palladium)." *Journal of Phase Equilibria* 12(2).

Swansiger, W. A., J. H. Swisher, J. P. Darginis and C. W. Schoenfelder (1976). "Hydrogen permeation palladium-chromium alloys." *The journal of Physical Chemistry* 80(3): 308-312.

Takasu, S., R. Unwin, B. Tesche and A. M. Bradshaw (1978). *Surface Science* 77: 219.

Thomas, S., R. Schafer, J. Caro and A. Seidel-Morgenstern (2001). "Investigation of mass transfer through inorganic membranes with several layers." *Catalysis Today* 67: 205-216.

Thornton, J. A. (1974). "Influence of apparatus geometry and deposition conditions on the structure and topography of thick sputtered coatings." *Journal of vacuum Science and Technology* 11: 666.

Toda, G. (1958). *J. Res. Inst. Catalysis Hokkaido Univ.* 6: 13.

Tong, J., Y. Kashima, R. Shirai, H. Suda and Y. Matsumura (2005a). "Thin Defect-Free Pd Membrane Deposited on Asymmetric Porous Stainless Steel Substrate." *Ind. Eng. Chem. Res.* 44(21): 8025-8032.

Tong, J., Y. Matsumura, H. Suda and K. Haraya (2005b). "Thin and dense Pd/CeO2/MPSS composite membrane for hydrogen separation and steam reforming of methane." *Separation and Purification Technology* 46(1-2): 1.

Tong, J., H. Suda, K. Haraya and Y. Matsumura (2005c). "A novel method for the preparation of thin dense Pd membrane on macroporous stainless steel tube filter." *Journal of Membrane Science* 260(1-2): 10.

Tosti, S. (2003). "Supported and laminated Pd-based metallic membranes." *International Journal of Hydrogen Energy* 28(12): 1445.

Tosti, S., L. Bettinali, S. Castelli, F. Sarto, S. Scaglione and V. Violante (2002). "Sputtered, electroless, and rolled palladium-ceramic membranes." *Journal of Membrane Science* 196(2): 241.

Tosti, S., L. Bettinali and V. Violante (2000). "Rolled thin Pd and Pd-Ag membranes for hydrogen separation and production." *International Journal of Hydrogen Energy* 25(4): 319.

Touloukian, Y. S., R. K. Kriby, R. E. Taylor and P. D. Desai (1977). "Thermal expansion: metallic elements and alloys." *Thermophysical Properties of Matter* 12: 298.

Uemiya, S., I. Koike and E. Kikuchi (1991a). "Promotion of the conversion of propane to aromatics by use of a palladium membrane." *Applied Catalysis* 76(2): 171.

Uemiya, S., T. Matsuda and E. Kikuchi (1991b). "Hydrogen permeable palladium-silver alloy membrane supported on porous ceramics." *Journal of Membrane Science* 56(3): 315.

Uemiya, S., N. Sato, H. Ando, Y. Kude, T. Matsuda and E. Kikuchi (1991c). "Separation of hydrogen through palladium thin film supported on a porous glass tube." *Journal of Membrane Science* 56(3): 303.

Uemiya, S., N. Sato, H. Ando, K. Y., T. Matsuda and E. Kikuchi (1991d). "Separation of hydrogen through palladium thin film supported on a porous glass tube." *Journal of Membrane Science* 56: 303-313.

Vereshchinskii, S. Y., S. B. Kalmykova and N. V. Korovin (1973). *Zashch. Metal.* 9(1): 117.

Vook, R. W. and F. Witt (1965). "Thermally induced strains in evaporated films." *Journal of Applied Physics* 36(7): 2169-2171.

Völkl, J. and G. Alefeld (1978). *Diffusion of hydrogen in metals. Hydrogen in metals, Vol I. Vol 28 of Topics in applied physics*.

Wang, D., J. Tong, H. Xu and Y. Matsumura (2004). "Preparation of palladium membrane over porous stainless steel tube modified with zirconium oxide." *Catalysis Today* 93-95: 689.

Ward, T. L. and T. Dao (1999). "Model of hydrogen permeation behavior in palladium membranes." *Journal of Membrane Science* 153(2): 211.

Warren, B. E. and B. L. Averbach (1950). *X-ray diffraction studies of cold work in metals: solid solutions and grain boundaries*. Cambridge, MA, Massachusetts Institute of Technology, [Dept. of Metallurgy].

Weissmuller, J., J. Loffler and M. Kleber (1995). "Atomic structure of nanocrystalline metals studied by diffraction techniques and EXAFS." *Nanostructured Materials* 6(1-4): 105.

Wellington, S. L., A. N. Matzakos, T. Mikus and J. M. Ward (2003). Integrated flameless distributed combustion/membrane steam reforming reactor and zero emissions hybrid power system. U. S. US 2003/0068260 A1.

Wicke, E. and G. H. Nernst (1964). "Phase diagram and thermodynamic behavior of the system Pd/H_2 and Pd/D_2 at normal temperatures; H/D separations effects." *Ber. Bunsenges. Physik. Chem.* 68: 224-235.

Wieland, I. S., I. T. Melin and I. A. Lamm (2002). "Membrane reactors for hydrogen production." *Chemical Engineering Science* 57(9): 1571.

Williamson, G. K. and W. H. Hall (1953). "X-ray line broadening from filed aluminum and wolfram." *Acta metallurgica* 1: 22-31.

Witt, F. and R. W. Vook (1968). "Thermally induced strains in cubic metal films." *Journal of applied physics.* 39(6): 2773-2776.

Wolf, R. J., M. W. Lee and J. R. Ray (1994). "Pressure-composition of nanocrystalline palladium hydride." *Physical Review Letters* 73(4): 557-560.

Wu, L. Q., N. Xu and J. Shi (2000). "Preparation of a Palladium Composite Membrane by an Improved Electroless Plating Technique." *Ind. Eng. Chem. Res.* 39(2): 342-348.

Yamakawa, K., M. Ege, B. Ludescher and M. Hirscher (2003). "Surface adsorbed atoms suppressing hydrogen permeation of Pd membranes." *Journal of Alloys and Compounds* 352(1-2): 57.

Yan, S., H. Maeda, K. Kusakabe and S. Morooka (1994). "Thin palladium membrane formed in support pores by metal-organic chemical vapor deposition method and application to hydrogen separation." *Ind. Eng. Chem. Res.* 33: 616-622.

Yang, R. P., X. Cai and Q. L. Chen (2001). "Mechanism of hydrogen desorption during palladium brush-plating." *Surface and Coatings Technology* 141(2-3): 283.

Yepes, D., L. M. Cornaglia, S. Irusta and E. A. Lombardo "Different oxides used as diffusion barriers in composite hydrogen permeable membranes." *Journal of Membrane Science* In Press, Corrected Proof.

Yeung, K. L., J. M. Sebastian and A. Varma (1995). "Novel preparation of Pd/Vycor composite membranes." *Catalysis Today* 25: 231-236.

Zabel, H. and B. Hjorvarsson (2001). Hydrogen in thin films and multilayers. *Progress in hydrogen treatment of materials*. V. A. Goltsov**:** 119-146.

Zayats, A. I., I. A. Stepanowa and A. V. Gorodyskii (1973). *Zahch. Metals.* 9(1): 116.

Zhang, J. Y., S. L. King, I. W. Boyd and Q. Fang (1997). "UV light-induced decomposition of palladium acetate films for electroless copper plating." *Applied Surface Science* 109/110: 487.

Zhao, H. and G. Xiong (1999). "Preparation and characterization of Pd-Ag alloy composite membrane with magnetron sputtering." *Science in China (Serie B)* 42(6): 581-588.

Zhao, H. B., K. Pflanz, J. H. Gu, A. W. Li, N. Stroh, H. Brunner and G. X. Xiong (1998). "Preparation of palladium composite membranes by modified electroless plating procedure." *Journal of Membrane Science* 142(2): 147.

Nomenclature

Ea	Activation energy for H_2 absorption reaction (J mol^{-1} or kJ mol^{-1})
Ed	Activation energy for H_2 desorption reaction (J mol^{-1} or kJ mol^{-1})
Ep	Activation energy for H_2 permeation (J mol^{-1} or kJ mol^{-1})
F_{H2}	H_2 permeance derived from the H_2 flux at ΔP = 1bar (2:1) (m^3 m^{-2} h^{-1} $bar^{-0.5}$)
$F_{0.5}$	H_2 permeance derived from least square analysis assuming n=0.5 (m^3 m^{-2} h^{-1} $bar^{-0.5}$)
F_n	H_2 permeance derived from least square analysis adjusting the n-exponent (m^3 m^{-2} h^{-1} bar^{-n})
J	Gas molar flux (mol m^{-2} s^{-1} or m^3 m^{-2} h^{-1})
K	*Sieverts' constant ($bar^{0.5}$, $Torr^{0.5}$)*
K'	*Proportionality constant when the n-exponent is different than 0.5 ($bar^{n\text{-}exponent}$, $Torr^{n\text{-}exponent}$)*
L	Porous support wall thickness (m or μm)
L_{Pd}	Pd membrane thickness (m or μm)
M_i	Molecular weight for *i* compound (kg mol^{-1})
n-exponent	n-exponent or H_2 pressure exponent (-)
n(H/Pd)	Amount of hydrogen dissolved in the bulk of Pd (mol H/ mol Pd)

P_{H2hp}	H_2 partial pressure in retentate, shell or high pressure side (Pa or bars), also noted as P_{shell}
P_{H2lp}	H_2 partial pressure in permeate, tube or low pressure side (Pa or bars), also noted as P_{tube} or P_0
P_{max}	H_2 pressure at which the maximum solubility in the Pd-H a-phase (a-max) is reached (atm)
Q_0	H_2 Pd permeability pre-exponential factor (m^3 m^1 m^{-2} h^{-1} $bar^{0.5}$)
r	Percentage of the leak permeating according to a Knudsen mechanism. $r=\alpha/(\alpha+\beta \cdot P_{ave})$
R	Universal gas constant (8.314 J mol^{-1} K^{-1})
T	Membrane temperature (at the permeate side) K or ^0C

Greek symbols

α	He leak Knudsen component coefficient (m^3 m^{-2} h^{-1} bar^{-1})
β	He leak viscous component coefficient (m^3 m^{-2} h^{-1} bar^{-2})
ε	Porosity of the Pd layer or the porous support
η_i	Viscosity of gas i (Pa s^{-1})

Appendix A: Error analysis on H_2 permeance

It was of great importance in this work to determine confidence intervals for all fitted parameters: H_2 permeance assuming the Sieverts' law, H_2 permeance and n-exponent from non-linear fit. Specially, great care was taken to measure errors on the n-exponent. Confidence intervals of any given measurement are based on the standard deviation and were determined using Equation A.1

$$\mu = \mu^{ave} \pm t(s/\sqrt{A}) \qquad \text{A.1}$$

where μ is the considered quantity, μ^{ave} is the average value of the data set, A is the number of times that the μ quantity was measured, t is a tabulated number depending on the number of degrees of freedom (equal to A-1) and the degree of confidence required. s is the standard deviation. The standard deviation of the H_2 permeance and n-exponent determined from a non-linear fit and the standard deviation of the H_2 permeance determined from a linear fit were estimated by taking the H_2 flux of membrane C01-F05 as a function of $\Delta P^{0.5}$ ten times during steady state at 250ºC. H_2 permeance measurements were spaced in 24-hr intervals. Figure A.1 shows the H_2 permeance and the n-exponent (from non-linear fit) and the H_2 permeance assuming the Sieverts' law (linear fit) as function of time. The standard deviation of H_2 permeance assuming the Sieverts' law was determined to be 0.02 $m^3/(m^2\ h\ bar^{0.5})$, see Table A.1, attesting to the very good precision achieved in the experimental measurements.

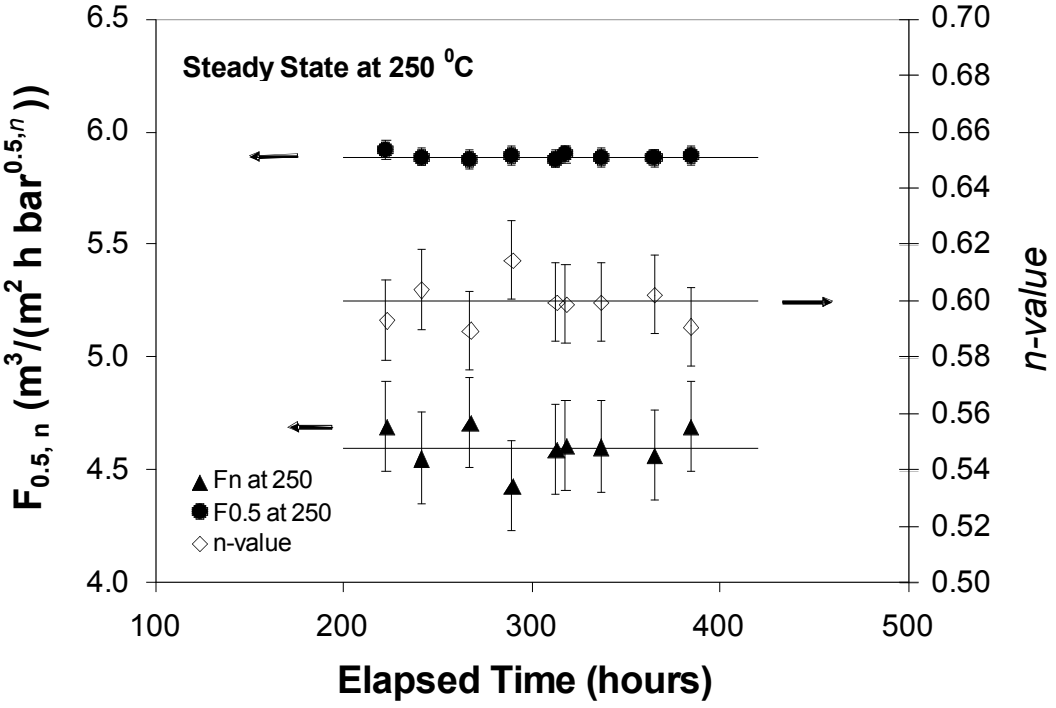

Figure A.1 $F_{0.5}$, F_n and n-exponent at 250ºC of membrane C01-F05. Ten measurements were used to compute standard deviations and estimate confidence intervals of $F_{0.5}$, F_n and n-exponent

Table A.1 Statistical analyses on permeance and n-exponent at 250ºC, membrane C01-F05

	n-exponent	H_2 Permeance ($m^3/(m^2\ h\ bar^n)$)	H_2 Permeance (n=0.5) ($m^3/(m^2\ h\ bar^{0.5})$)
Average	0.60	4.60	5.89
Calculated standard dev.	0.007	0.09	0.02
Considered standard dev.	0.014	0.2	0.04
Confidence interval (99%)	0.014	0.2	0.04

The high precision in data collection was achieved in this work by using digital mass flow meters, pressure transducers and continuously logging data.

The standard deviation of the H_2 permeance determined from a non-linear fit was 0.09 $m^3/(m^2\ h\ bar^{0.6})$, which was slightly larger than the permeance determined by assuming the Sieverts' law. Indeed, even though the non-linear fit of the experimental data was better than the linear fit (assuming *n* equal to 0.5), the nature of the mathematical expression involved in the fitting procedure (an exponential function of *n*) rendered the calculated H_2 permeance very sensitive to the n-exponent. The standard deviation of the n-exponent, also listed in Table A.1, was found to be equal to 0.007. Figure A.1 clearly shows the high standard deviation of F_n and the n-exponent resulting from the calculated H_2 permeance being extremely sensitive to the n-exponent fitting parameter. Moreover, the standard deviation calculated from any data set containing ten measurements could be as far as 60% from the real standard deviation. More than 100 measurements would be needed to determine a more accurate standard deviation, yet the time needed to collect such an enormous amount of data was prohibitive in this case. Therefore, the actual standard deviation of H_2 permeance determined assuming the Sieverts' law could be as high as 0.04 $m^3/(m^2\ h\ bar^{0.5})$ and as high as 0.014 for the n-exponent. Considering 0.014 as the

standard deviation of the n-exponent, the standard deviation of F_n was calculated to be 0.2 $m^3/(m^2\ h\ bar^{0.5})$. Calculated standard deviations, adjusted standard deviations due to insufficient number of measurements and confidence intervals are given in Table A.1 and were assumed to be the same at all temperatures.